



THE UNIVERSITY *of* EDINBURGH

This thesis has been submitted in fulfilment of the requirements for a postgraduate degree (e.g. PhD, MPhil, DClinPsychol) at the University of Edinburgh. Please note the following terms and conditions of use:

This work is protected by copyright and other intellectual property rights, which are retained by the thesis author, unless otherwise stated.

A copy can be downloaded for personal non-commercial research or study, without prior permission or charge.

This thesis cannot be reproduced or quoted extensively from without first obtaining permission in writing from the author.

The content must not be changed in any way or sold commercially in any format or medium without the formal permission of the author.

When referring to this work, full bibliographic details including the author, title, awarding institution and date of the thesis must be given.

**SELECTIVE EXHAUST GAS RECIRCULATION IN
COMBINED CYCLE GAS TURBINE POWER PLANTS
WITH POST-COMBUSTION CARBON CAPTURE**

Laura Herraiz Palomino



THE UNIVERSITY
of EDINBURGH

Ph. D. Thesis

School of Engineering

University of Edinburgh

2016

Lay Summary

Gas-fired power plants with Carbon Capture and Storage (CCS) are expected to play a significant role to reduce carbon dioxide (CO₂) emissions from the power generation sector. They can provide dispatchable low-carbon electricity to maintain the flexibility required in an electricity system with high penetration of renewables.

The low CO₂ concentration and large volumes of flue gas generated in natural gas-fired power plants make CO₂ separation with post-combustion capture technologies more challenging, compared to coal-fired power plants.

This thesis investigates options for increasing CO₂ concentration upstream of the capture system by selectively transferring CO₂ from a flue gas stream into an air stream used for natural gas combustion. Other components in the flue gas are not recirculated back to the inlet of the gas turbine system and a large excess of air is maintained. Strategies to enhance capture should aim to introduce minimal modification in the gas turbine engine, as current gas turbine technology presents high efficiency and plays an important role in achieving high combined cycle net power output.

Process simulations in a linked model of a natural gas combined cycle plant with a carbon capture and compression system conducted in this thesis show that high CO₂ levels at the exhaust of the gas turbine can be achieved maintaining levels of oxygen for efficient combustion, and that existing class of gas turbine engines can be operated with Selective Exhaust Gas Recirculation (S-EGR). For capture technologies using amine solvents, a reduction in equipment size and energy requirements are achieved.

A novel system for selective CO₂ transfer between a flue gas stream and an air stream is proposed consisting on rotary physical adsorption. A conceptual design assessment shows that a step change in the performance of adsorbent materials is necessary before this novel system can be commercially deployed.

Finally, a novel contribution is made to show that the availability of cooling might not necessarily constitute a limitation for the full scale deployment of CCS, particularly in regions with increasingly restricted access to cooling water and limited availability of fresh or sea water abstraction licences. Process simulations showed that cooling and process water demand can be drastically reduced in natural gas-fired power plants with carbon capture by using dry cooling systems consisting of rotary gas/gas heat exchangers with ambient air as the cooling fluid.

Abstract

Selective Exhaust Gas Recirculation (S-EGR) consists of selectively transferring CO₂ from the exhaust gas stream of a gas-fired power plant into the air stream entering the gas turbine compressor. Unlike in “non-selective” Exhaust Gas Recirculation (EGR) technology, recirculation of, principally, nitrogen does not occur, and the gas turbine still operates with a large excess of air.

Two configurations are proposed: one with the CO₂ transfer system operating in parallel to the post-combustion carbon capture (PCC) unit; the other with the CO₂ transfer system operating downstream of, and in series to, the PCC unit. S-EGR allows for higher CO₂ concentrations in the flue gas of approximately 13-14 vol%, compared to 6.6 vol% with EGR at 35% recirculation ratio. The oxygen levels in the combustor are approximately 19 vol%, well above the minimum limit of 16 vol% with 35% EGR reported in literature.

At these operating conditions, process model simulations show that the current class of gas turbine engines can operate without a significant deviation in the compressor and the turbine performance from the design conditions. Compressor inlet temperature and CO₂ concentration in the working fluid are critical parameters in the assessment of the effect on the gas turbine net power output and efficiency. A higher turbine exhaust temperature allows the generation of additional steam which results in a marginal increase in the combined cycle net power output of 5% and 2% in the investigated configurations with S-EGR in parallel and S-EGR in series, respectively. With aqueous monoethanolamine scrubbing technology, S-EGR leads to operation and cost benefits. S-EGR in parallel operating at 70% recirculation, 97% selective CO₂ transfer efficiency and 96% PCC efficiency results in a reduction of 46% in packing volume and 5% in specific reboiler duty, compared to air-based combustion CCGT with PCC, and of 10% in packing volume and 2% in specific reboiler duty, compared to 35% EGR. S-EGR in series operating at 95% selective CO₂ transfer efficiency and 32% PCC efficiency results in a reduction of 64% in packing volume and 7% in specific reboiler duty, compared to air-based, and of 40% in packing volume and 4% in specific reboiler duty, compared to 35% EGR.

An analysis of key performance indicators for selective CO₂ transfer proposes physical adsorption in rotary wheel systems as an alternative to selective CO₂ membrane systems. A conceptual design assessment with two commercially available adsorbent materials, activated carbon and Zeolite X13, shows that it is possible to regenerate the adsorbent with air at near ambient temperature and pressure. Yet, a significant step change in adsorbent materials is necessary to design rotary adsorption systems with dimensions comparable to the largest rotary gas/gas heat exchanger used in coal-fired power plants, i.e. approximately 24 m diameter and 2 m height. An optimisation study provides guidelines on the equilibrium parameters for the development of materials.

Finally, a technical feasibility study of configuration options with rotary gas/gas heat exchangers shows that cooling water demand around the post-combustion CO₂ capture system can be drastically reduced using dry cooling systems where gas/gas heat exchangers use ambient air as the cooling fluid. Hybrid cooling configurations reduce cooling and process water demand in the direct contact cooler of a wet cooling system by 67% and 35% respectively, and dry cooling configurations eliminate the use of process and cooling water and achieve adequate gas temperature entering the absorber.

Acknowledgment

This thesis is the result of work done after generous opportunity given by Dr. Mathieu Lucquiaud, Prof. Jon Gibbins and Dr. Hannah Chalmers. Thanks to my supervisor Dr. Mathieu Lucquiaud for his essential support to get this Ph.D. completed and for keeping me interested in the “broader picture” of CCS and in the essential role of collaboration between academy and industry for CCS to happen.

Special tanks to Dr. Eva Sánchez Fernández for her guidance and advice, stimulating discussions and fruitful exchange of ideas. Thanks to Dr. María Sanchez del Río Sáez and Ms. Olivia Errey. This Ph.D. would not have been possible without their help.

I also thank my colleagues in the Power Plant Engineering & CCS group at the University of Edinburgh. In particular, I would like to thank Dr. Bill Bulchle, Dr. Ignacio Trabadela, Dr. Abigail Gonzalez, Dr. Alasdair Bruce, Dr. Juan Riaza, Mr. Paul Tait, Ms. Erika Palfi, Mr. Thomas Spitz and Mr. Gordon Paterson for their support and unforgettable time spent together. Special thanks to Dr. Atul Agarwal and Dr. Siraj Sabihuddin for their support, encouragement and friendship.

This project has also given me the opportunity to work with excellent people outside of academia. I would like to thank Mr. Dougal Hogg, Mr. Jim Cooper and Mr. Richard Smith from Howden UK, Glasgow, for their extremely valuable input and technical advice on rotary heat exchangers. I would also like to thanks Ms. Meron Reid for giving me the opportunity to attend the Howden Academy.

Financial support for this research was provided by the Doctoral Training Account of School of Engineering of the School of Engineering at the University of Edinburgh, funded by the UK Engineering and Physical Science Research Council (EPSRC) and Howden Group (Glasgow, Scotland). Support from the GAS-FACTS project funded by the EPSRC (EP/J020788/1) is gratefully acknowledged. Thanks to the UK Carbon Capture and Storage Research Centre (UKCCSRC)

I sincerely appreciate the time and efforts of my examination committee members, Dr. Hannah Chalmers and Dr. Richard Marsh. Thank you for sharing your experience and advice with me as well as being kind in your assessment of this work.

Finally, I am grateful to my family because they have always encouraged me to pursue this project and follow my dreams, helping me along the way.

Declaration of originality

The work included in this Ph.D. thesis, except when referenced, is the results of the effort of years that has been done by the author alone under the guidance of her supervisor Dr. Mathieu Lucquiaud. The author acknowledges essential contributions by others in the acknowledgment section of this thesis and in further sections of the work where required. This Ph.D. thesis has not been submitted for any other degree or professional qualifications in the UK or elsewhere. The author recommends referencing this thesis as follows:

Herraiz, L. (2016), *Selective Exhaust Gas Recirculation in Combined Cycle Gas Turbine Power Plants with Post-combustion Carbon Capture*, Ph.D. Thesis, School of Engineering, University of Edinburgh, United Kingdom of Great Britain and Northern Ireland (UK).

Laura Herraiz Palomino

List of publications

The work described in this thesis has been reported in the following publications:

Journal publications

Herraiz, L., Hogg, D., Cooper, J., Gibbins, J. and Lucquiaud, M. 2015. *Reducing water usage with rotary regenerative gas/gas heat exchangers in natural gas-fired power plants with post combustion carbon capture*. Energy, vol. 90 Part 2, pp. 1994-2005.

Conference publications

Herraiz, L., Hogg, D., Cooper, J., Gibbins, J. and Lucquiaud, M. 2014. *On the use of rotary gas/gas heat exchangers as a novel integration option for heat and water management in exhaust gas recycling gas turbine plants*. Energy Procedia, vol. 63, pp. 559-571.

Oral presentations

Herraiz, L., Gibbins, J. and Lucquiaud, 2012. *Impact Assessment of Transition Engineering and Capture Ready Options for New-build Natural Gas-fired power plants*. UKCCSC Early Career Annual Meeting, Leeds, The UK.

Herraiz, L., Sánchez Fernández, E., Palfi, E. and Lucquiaud, 2015. *Selective Exhaust Gas Recirculation in Combined Cycle Gas Turbine power plants with Post-combustion Carbon Capture*. 14th Annual Conference on Carbon Capture Utilization and Storage (CCUS), Pittsburgh, Pennsylvania, U.S.A.

Herraiz, L., Sánchez Fernández, E., Palfi, E. and Lucquiaud, 2015. *Selective Exhaust Gas Recirculation in Combined Cycle Gas Turbine power plants with Post-combustion Carbon Capture*. 8th Trondheim Conference on CO₂ Capture Transport and Storage, Trondheim, Norway.

Herraiz, L., Sánchez Fernández, E., Palfi, E. and Lucquiaud, 2016. *Selective Exhaust Gas Recirculation in Combined Cycle Gas Turbine power plants with Post-combustion Carbon Capture*. The 3rd University of Texas Conference on Carbon Capture and Storage (UTCCS3), The University of Texas, Austin, United States.

Poster presentation

Herraiz, L., Hogg, D., Cooper, J., Gibbins, J. and Lucquiaud, M. 2014. *On the use of rotary gas/gas heat exchangers as a novel integration option for heat and water management in exhaust gas recycling gas turbine plants*. 12th International Conference on Greenhouse Gas Control Technologies, GHGT 2014; University of Texas, Austin, United States.

Contents

Lay Summary	i
Abstract	ii
Acknowledgements	iii
Declaration of originality	iv
List of publications	v
Contents	vii
List of Figures	xiii
List of Tables	xxi
Nomenclature	xxiii
List of Symbols	xxv
1. Introduction	1
1.1. Background	1
1.2. Global Status of Carbon Capture and Storage	5
1.3. Water demand for cooling in a Combine Cycle Gas Turbine power plant with Post-combustion Carbon Capture systems	8
1.4. Research Objectives	9
1.5. Original contribution	10
1.6. Thesis overview	10
2. State of Combined Cycle Gas Turbine Power Plants with Post-Combustion CO₂ Capture	13
2.1. Post-combustion CO ₂ capture in Combined Cycle Gas Turbine plants: Current Challenges	13
2.2. Strategies to increase CO ₂ concentration in the exhaust flue gas from Combined Cycle Gas Turbine power plants	14
2.2.1. Exhaust Gas Recirculation	14
2.2.2. Gas turbine humidification	18
2.2.3. Supplementary fired combined cycle	19
2.2.4. Selective Exhaust Gas Recirculation	22

2.3.	Effects of CO ₂ concentration on the PCC performance: EGR and S-EGR options.....	27
2.4.	Strategies to reduce water requirements in CCGT power plants with PCC	29
2.5.	Novel application for adsorption systems in S-EGR	31
	2.5.1. Adsorbents for CO ₂ capture from CCGT exhaust flue gas.....	32
	2.5.2. Adsorption in rotary systems	35
2.6.	Current state and gaps in knowledge	37
3.	System Design and Performance Modelling	43
3.1.	Introduction	43
3.2.	Combined cycle gas turbine power plant	45
	3.2.1. Gas Turbine	47
	3.2.2. Compressor and turbine performance	58
	3.2.3. Gas turbine off-design performance	63
	3.2.4. Steam cycle	68
	3.2.5. Thermal integration of the post-combustion CO ₂ capture and the power generation systems.....	73
	3.2.6. Technical and operation parameters for the reference CCGT plant	74
3.3.	Post-combustion CO ₂ capture and compression systems.....	77
	3.3.1. CO ₂ capture plant description.....	77
	3.3.2. CO ₂ capture process modelling	80
	3.3.3. Absorber sizing	81
	3.3.4. Reboiler duty optimisation	82
	3.3.5. CO ₂ compression.....	85
	3.3.6. Technical and operation parameters of the CO ₂ capture and compression systems for the reference plant	86
3.4.	Rotary gas/gas heat exchangers for water and heat management.....	88
	3.4.1. Rotary gas/gas heat exchangers technology	88
	3.4.2. Methodology for the selection, sizing and thermal performance analysis of rotary gas/gas heat exchangers	89

3.5.	Rotary adsorber for selective CO ₂ transfer.....	94
3.5.1.	<i>Problem description.....</i>	94
3.5.2.	<i>Performance modelling for a conceptual design.....</i>	95
4.	Strategies to increase CO₂ concentration in Gas Turbines Exhaust Flue Gas .	101
4.1.	Introduction	101
4.2.	Exhaust Gas Recirculation	103
4.2.1.	<i>Description of the configuration.....</i>	103
4.2.2.	<i>Flue gas CO₂ concentration and limitations to the recirculation ratio ...</i>	105
4.2.3.	<i>Effects on the Gas Turbine.....</i>	106
4.2.4.	<i>Effects on the Steam Cycle.....</i>	109
4.2.5.	<i>Effects on the Post combustion capture unit.....</i>	110
4.2.6.	<i>Sensitivity analysis to the recycled flue gas temperature</i>	113
4.3.	Selective Exhaust Gas Recirculation in Parallel.....	115
4.3.1.	<i>Description of the configuration.....</i>	115
4.3.2.	<i>Operating framework.....</i>	118
4.3.3.	<i>Effects on the Gas Turbine.....</i>	121
4.3.4.	<i>Effects on the Steam Cycle.....</i>	124
4.3.5.	<i>Effects on the Post-combustion Carbon Capture unit.....</i>	125
4.3.6.	<i>Sensitivity analysis</i>	126
4.4.	Selective Exhaust Gas Recirculation in Series	131
4.4.1.	<i>Description of the configuration.....</i>	131
4.4.2.	<i>Operating framework.....</i>	134
4.4.3.	<i>Effects on the Gas Turbine.....</i>	137
4.4.4.	<i>Effects on the Steam Cycle.....</i>	139
4.4.5.	<i>Effects on the Post-combustion Carbon Capture unit.....</i>	140
4.4.6.	<i>Sensitivity analysis</i>	143
4.5.	Comparison and discussion of the results.....	147
4.5.1.	<i>Overall effect on the post-combustion CO₂ capture system</i>	148
4.5.2.	<i>Overall effect on the CCGT power plant</i>	153

5.	Rotary Adsorption for Selective Exhaust Gas Recirculation	159
5.1.	Introduction	159
5.2.	Description of adsorption process and parameters used in conceptual design assessment	162
5.2.1.	<i>Adsorbent material</i>	163
5.2.2.	<i>Adsorbent structure</i>	166
5.2.3.	<i>Rotary wheel</i>	167
5.3.	Conceptual design assessment.....	167
5.3.1.	<i>Boundaries within the CCGT power plant and the PCC system integrated model</i>	168
5.3.2.	<i>Estimations of adsorption design parameters</i>	170
5.4.	Performance and operating profiles.....	172
5.4.1.	<i>Flue gas and air: CO₂ concentration and temperature profiles</i>	173
5.4.2.	<i>Adsorbent: CO₂ adsorbed and temperature profiles</i>	177
5.5.	Feasibility and discussion	182
5.5.1.	<i>Sensitivity analysis to the solid properties</i>	183
5.5.2.	<i>Sensitivity analysis to the operating conditions</i>	187
5.6.	Key findings and recommendations.....	189
6.	Options for Heat and Water Management.....	193
6.1.	Introduction	193
6.2.	Novel integration options for heat and water management in CCGT power plant with PCC	195
6.2.1.	<i>Wet cooling system with a direct contact cooler (base case)</i>	197
6.2.2.	<i>Hybrid system with a gas/gas heat exchangers and a direct contact cooler in series</i>	197
6.2.3.	<i>Dry system with a gas/gas and an air/gas heat exchangers in series</i> ..	197
6.2.4.	<i>Dry systems with a trisector gas/gas/air heat exchanger</i>	198

6.3.	Thermal performance analysis of the rotary gas/gas heat exchangers	198
6.3.1.	<i>CCGT with air-based combustion gas turbine</i>	201
6.3.2.	<i>CCGT with EGR: effect of the recirculation ratio</i>	203
6.3.3.	<i>Effect of the ambient air temperature on the performance of dry cooling systems</i>	206
6.4.	Booster fan implications: power requirements and leakage control	207
7.	Conclusions	211
7.1.	Effect of S-EGR on the CCGT plant with PCC	211
7.2.	Practical feasibility of rotary adsorption for S-EGR	213
7.3.	Dry cooling options for CCGT plants with PCC	215
7.4.	Limitations and recommendations for future work.....	216
7.5.	Original contribution addressing knowledge gaps	219
	References	223
	Appendix A. Technical data of the Reference Power Plant.	233
	Appendix B. Process Flow Diagrams.....	237
	Appendix C. Technical data for the reference CCGT plant for water management assessment.....	239

List of Figures

Figure 1.1.- Energy system model trajectories for the UK’s power sector (CCC 2015)	2
Figure 1.2.- Actual and expected operation dates for large-scale CCS projects in the Operate, Execute and Define stages by region and project lifecycle stage (Global CCS Institute 2015).....	6
Figure 2.1.- Block flow diagrams of a CCGT plant with exhaust gas recirculation and post-combustion capture.....	15
Figure 2.2.- Block flow diagrams of a CCGT plant with (a) Supplementary firing and (b) Sequential supplementary firing.....	21
Figure 2.3.- Block flow diagrams for the flue gas CO ₂ enriching strategies of (a) S-EGR in parallel and (b) S-EGR in series.....	23
Figure 2.4.- VeloxoTherm™ process (InvenTys 2016) (a) and schematic diagram of the CO ₂ separation process (b).....	36
Figure 3.1.- Diagram of the linked model of a CCGT power plant, developed in gPROMS, and the carbon capture system, developed in Aspen Plus, indicating the input/output variables to each model.....	44
Figure 3.2.- Process flow diagram of the power system in the reference case: air- based combustion CCGT with PCC.	46
Figure 3.3.- Variation of temperature (enthalpy), velocity and pressure through an axial-flow compressor (Boyce 2006).....	49
Figure 3.4.- Stage velocity triangles for an axial-flow compressor (Dixon and Hall 1998).	50
Figure 3.5.- Temperature-Entropy diagram in a single compressor stage	51
Figure 3.6.- Dry Low NO _x (DLN-2) combustion system with diffusion and premixed fuel lines (General Electric, Davis and Black 2000).	52
Figure 3.7.- Enthalpy – entropy diagram for the Brayton cycle showing the method used to model turbine cooling modelling (Jonshagen 2011)	54
Figure 3.8.- Schematic of axial-flow turbine flow (Boyce 2006).	55
Figure 3.9.- Stage velocity diagram in an axial-flow turbine (Dixon and Hall 1998)	56
Figure 3.10.- Temperature-Entropy diagram in a single turbine stage	56
Figure 3.11.- Air-cooled first stage nozzle in GE F class gas turbine technology (Brooks 2000).....	57
Figure 3.12.- Axial compressor performance curve (Saravanamuttoo and Maclsaac 1983) .	63

Figure 3.13.- GE F class gas turbine (Chacartegui et al. 2012).....	68
Figure 3.14.- Temperature versus heat flux/thermal power diagram for the heat recovery steam generator for the air-based combustion CCGT configuration.	71
Figure 3.15.- Process flow diagram of the post-combustion CO ₂ capture system with amine-based chemical absorption technology.	79
Figure 3.16.- Sensitivity of the rich solvent CO ₂ loading and the specific reboiler duty to the absorber packing height for the reference case: air-based combustion CCGT with PCC.....	82
Figure 3.17.- (a) Illustrative example of reboiler duty minimisation as a function of the absorber liquid/gas flow rate ratio and (b) contributions to the specific reboiler heat duty (Freguia and Rochelle 2003).....	84
Figure 3.18.- Sensitivity of the specific reboiler duty to the liquid/gas flow rates ratio and the corresponding lean solvent CO ₂ loading for the reference case: air-based combustion CCGT with PCC.	85
Figure 3.19.- Process flow diagram of the CO ₂ compression train.	86
Figure 3.20.- Example of a typical rotary regenerative heat exchanger used in coal-fired power plants (Kitto and Stultz 1992).....	89
Figure 3.21.- Heat and mass transfer of water for rotary heat exchangers operated below the flue gas dew point (Herraiz et al. 2015).....	90
Figure 3.22.- Schematic diagram of the rotary adsorber for selective CO ₂ transfer.....	94
Figure 3.23.- Performance model of the rotary adsorber (a) division of the equilibrium model into cells, (b) cross-flow arrangement, (c) stage equilibrium, (d) operation and equilibrium curves.	96
Figure 4.1.- Process flow diagram for a Combined Cycle Gas Turbine plant with Exhaust Gas Recirculation and Post-combustion CO ₂ Capture.....	104
Figure 4.2.- Sensitivity of CO ₂ concentration and flue gas mass flow rate at the post-combustion capture unit (absorber) inlet, O ₂ concentration at the combustor to the exhaust gas recirculation ratio. Configuration: CCGT with EGR and PCC.	105
Figure 4.3.- Sensitivity of the deviation of the working fluid properties from the reference configuration with air combustion at ISO conditions to the working fluid CO ₂ concentration at the compressor inlet. Configuration: CCGT with PCC and EGR.	108
Figure 4.4.- Dimensionless parameter groups constituting the compressor performance curve for a range of EGR ratios from 0% to 50%. Normalised values for the design operating point with air combustion at ISO conditions. The compressor efficiency is indicated at each recirculation ratio. Configuration: CCGT with PCC and EGR.	108

Figure 4.5.- Sensitivity of the gas turbine exhaust gas mass flow rate and temperature to the CO ₂ concentration in the flue gas. Configuration: CCGT with PCC and EGR.	109
Figure 4.6.- Heat transfer – temperature diagram for EGR configuration at 35% recirculation ratio, compared to air-based combustion configuration.	110
Figure 4.7.- Sensitivity of the rich solvent CO ₂ loading and the specific reboiler duty to the packing volume required to achieve 90% CO ₂ capture efficiency for the conventional exhaust gas recirculation configuration. The reference case is an air-based combustion configuration.	112
Figure 4.8.- CO ₂ partial pressure as function of loading for H ₂ O-MEA-CO ₂ system with a 30 mass% MEA aqueous solution, experimental data at equilibrium for ○, 40°C; ◇, 60°C; □, 80°C; Δ, 100°C; x, 120°C (Fang-Yuan et al. 1994; Ma'mun et al. 2005; Hilliard 2008; Dugas 2009; Aronu et al. 2011).	113
Figure 4.9.- Sensitivity analysis of the GT and CCGT power output, mass flow rate and compressor inlet temperature to the recirculated flue gas temperature. Configuration: exhaust gas recirculation at 35% recirculation ratio.	114
Figure 4.10.- Process flow diagram for a Combined Cycle Gas Turbine power plant with Selective Exhaust Gas Recirculation in parallel to the Post-combustion CO ₂ Capture process.	117
Figure 4.11.- Sensitivity of CO ₂ concentration in the exhaust flue gas at the post-combustion capture unit inlet and O ₂ concentration in the CO ₂ -enriched combustion air to the selective exhaust gas recirculation ratio, for a selective CO ₂ transfer efficiencies of 90 and 97%. Configuration in parallel with an overall CO ₂ capture level of 90%.	120
Figure 4.12.- Sensitivity of the post-combustion CO ₂ capture efficiency to the selective exhaust gas recirculation ratio for a range of selective CO ₂ transfer efficiencies. Configuration in parallel with an overall CO ₂ capture level of 90%.	120
Figure 4.13.- Sensitivity of the deviation of the working fluid properties from the reference configuration with air combustion at ISO conditions as function of the working fluid CO ₂ concentration at the compressor inlet. Configuration: CCGT with PCC and S-EGR in parallel.	122
Figure 4.14.- Dimensionless parameter groups constituting the compressor performance curve for a range of S-EGR ratios from 30% to 70%. Normalised values for the design operating point with air combustion at ISO conditions. The compressor efficiency is indicated at each recirculation ratio. Configuration: CCGT with PCC and S-EGR in parallel.	123
Figure 4.15.- Sensitivity of the gas turbine exhaust gas mass flow rate and temperature to the flue gas CO ₂ concentration, for a range of S-EGR ratios from 0 to 80%, increments of 10%. Configuration: CCGT with PCC and S-EGR in parallel.	123
Figure 4.16.- Heat transfer – temperature diagram for S-EGR configuration in parallel at 70% recirculation ratio, 97% selective CO ₂ transfer efficiency and 96% post-	

combustion CO ₂ capture efficiency, compared to air-based combustion and EGR at 35% recirculation ratio configurations.....	124
Figure 4.17.- Sensitivity of the rich solvent CO ₂ loading and the specific reboiler duty to the packing volume for S-EGR in parallel at 70% recirculation ratio and 96% post-combustion CO ₂ capture efficiency. Compared to air-based combustion configuration and EGR at 35% recirculation ratio and 90% post-combustion CO ₂ capture efficiency.....	126
Figure 4.18.- Sensitivity of the flue gas CO ₂ concentration and the comburent O ₂ concentration to the O ₂ transfer level from the air into the flue gas, for a range of water vapour transfer levels from the flue gas into the air. Configuration: S-EGR in parallel with a recirculation ratio of 70%, a selective CO ₂ transfer efficiency of 97% and a post-combustion capture efficiency of 96.7%.	128
Figure 4.19.- Sensitivity of the gas turbine power output and thermal efficiency to the CO ₂ -enriched air temperature at the inlet of the compressor. Configuration: parallel S-EGR with a recirculation ratio of 70%, a selective transfer efficiency of 97% and a post-combustion capture efficiency of 96.7%.	129
Figure 4.20.- Sensitivity of the gas turbine power output and air fan power consumption to the pressure drop in the air side of the selective CO ₂ transfer device for the configuration in parallel with and without an air fan. Configuration: parallel S-EGR with a recirculation ratio of 70%, a selective transfer efficiency of 97% and a post-combustion capture efficiency of 96.7	130
Figure 4.21.- Process flow diagram for a Combined Cycle Gas Turbine power plant with Selective Exhaust Gas Recirculation in series to the Post-combustion CO ₂ Capture process.....	133
Figure 4.22.- Sensitivity of CO ₂ concentration in the exhaust flue gas, at the inlet of the post-combustion capture unit and the selective CO ₂ transfer unit, and O ₂ concentration in the CO ₂ -enriched combustion air to the selective CO ₂ transfer efficiency. Configuration S-EGR in series with an overall CO ₂ capture level of 90%	136
Figure 4.23.- Sensitivity of the post-combustion CO ₂ capture efficiency to the selective CO ₂ transfer efficiency. Configuration S-EGR in series with an overall CO ₂ capture level of 90%.....	136
Figure 4.24.- Sensitivity of the deviation of the working fluid properties from the reference configuration with air combustion at ISO conditions, to the working fluid CO ₂ concentration at the compressor inlet. Configuration: CCGT with PCC and S-EGR in series, for 85%, 90% and 95% selective CO ₂ transfer efficiency.	138
Figure 4.25.- Dimensionless parameter groups constituting the compressor performance curve for the configurations of S-EGR in series with 85%, 90% and 95% selective CO ₂ transfer efficiency. Normalised values for the design operating point with air combustion at ISO conditions. Configuration: CCGT with PCC and S-EGR in series	138

Figure 4.26.- Sensitivity of the gas turbine exhaust gas mass flow rate and temperature to the CO ₂ concentration in the flue gas. Configuration: CCGT with PCC and S-EGR in series, for 85%, 90% and 95% selective CO ₂ transfer efficiency.....	139
Figure 4.27.- Heat transfer – temperature diagram for S-EGR in series configuration, with 95% selective CO ₂ transfer efficiency and 32% post-combustion CO ₂ capture efficiency, compared to air-based combustion and EGR at 35% recirculation ratio diagrams.	140
Figure 4.28.- Sensitivity of the rich solvent CO ₂ loading and the specific reboiler duty to the packing volume for S-EGR in series for the configurations operating at 32%, 48% and 58% CO ₂ capture efficiency. Compared to air-based combustion configuration and EGR at 35% recirculation ratio for 90% CO ₂ capture efficiency.	142
Figure 4.29.- Sensitivity of CO ₂ concentration in flue gas at PCC unit inlet and the O ₂ concentration in the comburent to the O ₂ transfer level from the air into the flue gas, for a range of water vapour transfer levels from the flue gas into the air. Configuration: S-EGR in series operating at 95% selective CO ₂ transfer efficiency and 32% post-combustion capture efficiency.	144
Figure 4.30.- Sensitivity of the gas turbine power output and thermal efficiency to the CO ₂ -enriched air temperature at the inlet of the compressor. Configuration: S-EGR in series with a selective transfer efficiency of 95%, post-combustion capture efficiency of 32%.	145
Figure 4.31.- Sensitivity of the gas turbine power output and air fan power consumption to the pressure drop in the air side of the selective CO ₂ transfer device for the configuration in parallel with and without an air fan. Configuration in series with selective transfer efficiency of 95% and post-combustion capture efficiency of 32%.	146
Figure 4.33.- Specific reboiler duty and packing volume reduction for a CCGT plant with Post-combustion Carbon Capture for the configurations: 30% exhaust gas recirculation, selective exhaust gas recirculation in parallel and in series, compared to the reference case: air-based combustion CCGT with PCC.	149
Figure 4.34.- Temperature profile of the gas phase (continuous and dashed lines) and the liquid phase (dotted lines) in the absorber for the configurations with: air-based combustion with 90% CO ₂ absorption efficiency, 35% EGR with 90% CO ₂ absorption efficiency, S-EGR in parallel at 70% recirculation ratio and 96% CO ₂ absorption efficiency, and for S-EGR in at 32%, 48% and 58% CO ₂ absorption efficiencies.	152
Figure 4.34.- CCGT net power output and net thermal efficiency variation with post-combustion carbon capture (PCC) and the operational strategies of conventional EGR, selective EGR in parallel and in series, compared to the reference case: air-based combustion CCGT with PCC.	157
Figure 5.1.- Schematic diagram of the rotary adsorber for selective CO ₂ transfer.	162

- Figure 5.2.- Sensitivity to temperature of CO₂ and water vapour concentrations and mass flow rate of the flue gas stream prior to CO₂ transfer. Configuration S-EGR in parallel at 70% recirculation ratio, 97% selective CO₂ transfer efficiency and 96% post-combustion CO₂ capture efficiency. 169
- Figure 5.3.- Sensitivity to temperature of CO₂ and water vapour concentrations and mass flow rate of the inlet flue gas stream prior to CO₂ transfer. Configuration S-EGR in parallel at 70% recirculation ratio, 97% selective CO₂ transfer efficiency and 96% post-combustion CO₂ capture efficiency. 170
- Figure 5.4.- (a) Longitudinal sections (vertical slices) representing the flue gas and air profiles and (b) horizontal slices representing the profiles of the adsorbent contained in the rotor. 173
- Figure 5.5.- CO₂ partial pressure profiles of (a) the flue gas (adsorption) and (b) the air (desorption) in longitudinal direction for each vertical slide. Configuration: S-EGR in parallel at 70% recirculation ratio. Adsorbent: Activated Carbon..... 175
- Figure 5.6.- Temperature profiles of (a) the flue gas (adsorption) and (b) the air (desorption) in longitudinal direction for each vertical slide. Configuration: S-EGR in parallel at 70% recirculation ratio. Adsorbent: Activated Carbon..... 176
- Figure 5.7.- CO₂ adsorbed profile for adsorption (a) and desorption (b) for several cross sections (horizontal slides). Rotation speed of 1 rpm. Configuration: parallel S-EGR at 70% recirculation ratio. Adsorbent: Activated Carbon..... 179
- Figure 5.8.- Solid temperature profile in adsorption (a) and desorption (b) for several cross sections (horizontal slides). Rotation speed of 1 rpm. Configuration: parallel S-EGR at 70% recirculation ratio. Adsorbent: Activated Carbon..... 180
- Figure 5.9.- Working cycle capacity of the adsorbent along the longitudinal direction. Configuration: parallel S-EGR at 70% recirculation ratio. Adsorbent: Activated Carbon..... 181
- Figure 5.10.- Sensitivity of adsorbent mass and working cycle capacity to the adsorbed saturation capacity. Configuration parallel S-EGR at 70% recirculation ratio, 97% selective CO₂ transfer efficiency and 96% post-combustion CO₂ capture efficiency. 183
- Figure 5.11.- Sensitivity of adsorbent mass to the enthalpy of adsorption and the pre-exponential factor of the equilibrium constant, for a adsorbed saturated capacity of (a) $q_s = 3.08$ mol/kg, (b) $q_s = 6.17$ mol/kg, (c) $q_s = 12.34$ mol/kg. Configuration: S-EGR in parallel at 70% recirculation ratio, 97% selective CO₂ transfer efficiency 185
- Figure 5.12.- Surface/contours of the sensitivity of adsorbent mass to the enthalpy of adsorption and the pre-exponential factor of the equilibrium constant, for a adsorbed saturated capacity of (a) $q_s = 3.08$ mol/kg, (b) $q_s = 6.17$ mol/kg, (c) $q_s = 12.34$ mol/kg. Configuration: S-EGR in parallel at 70% recirculation ratio, 97% selective CO₂ transfer efficiency. 186

Figure 5.13.- Effect of the air inlet temperature on (a) the CO ₂ -enriched air and the solid temperatures and (b) the adsorbent mass and the working cycle capacity. Configuration: parallel S-EGR at 70% recirculation ratio.	188
Figure 5.14.- Effect of the air inlet temperature on the selective CO ₂ transfer for a given solid mass of 326.21 t. Configuration: parallel S-EGR at 70% recirculation ratio.	188
Figure 5.15.- Effect of the flue gas inlet temperature on (a) the air and flue gas outlet temperatures and (b) the adsorbent mass and the working cycle capacity. Configuration: parallel S-EGR at 70% recirculation ratio	189
Figure 6.1.- Block flow diagrams of rotary heat exchangers configurations for a conventional (air-based combustion) combined cycle gas turbine plant with post-combustion capture.	196
Figure 6.2.- Block flow diagrams of rotary heat exchangers configurations for a combined cycle gas turbine plant with post-combustion carbon capture and exhaust gas recirculation.....	196
Figure 6.3.- Direction of the flow in a trisector rotary gas/gas/air heat exchanger.....	198
Figure 6.4.- A comparison of the cooling water, recirculating process water and cooling air mass flow rates per gas turbine train in a convectional (air-based combustion) combined cycle gas turbine plant and a plant with an exhaust gas recirculation ratio of 40%, both with post-combustion capture technology.....	199
Figure 6.5.- Heat and mass transfer of water for rotary regenerative heat exchangers operated below the dew point.	202
Figure 6.6.- Dry cooling configuration with two rotary heat exchangers in series: Sensitivity analysis of flue gas and air temperature to the recirculation ratio and the mass flow rate of cooling air.	205
Figure 6.7.- Dry cooling configuration with a trisector gas/gas/air heat exchangers: Sensitivity analysis of flue gas and air temperature to the recirculation ratio and the mass flow rate of cooling air.	205
Figure 6.8.- Sensitivity to the ambient air temperature of the performance of a dry cooling configuration with two rotary heat exchangers in series for a conventional CCGT plant (without exhaust gas recirculation). Heating surface area 45868 m ²	207
Figure 6.9.- Sensitivity of the overall CO ₂ removal ratio to leakage level from the untreated flue gas into the CO ₂ -depleted gas	209
Figure 6.10.- Booster fan, air fan, cooling and process water pumps power consumption per gas turbine train for convectional (air-based combustion) combined cycle gas turbine plant and a plant with 40% exhaust gas recirculation ratio, both with post-combustion capture technology.....	209

Figure B.1- Process flow diagram for an air-based combustion Combined Cycle Gas Turbine plant with Post-combustion CO₂ Capture..... 237

Figure B.2- Process flow diagram for a Combined Cycle Gas Turbine plant with Exhaust Gas Recirculation and Post-combustion CO₂ Capture. 237

Figure B.3- Process flow diagram for a Combined Cycle Gas Turbine power plant with Selective Exhaust Gas Recirculation in parallel to the Post-combustion CO₂ Capture process. 237

Figure B.4- Process flow diagram for a Combined Cycle Gas Turbine power plant with Selective Exhaust Gas Recirculation in series to the Post-combustion CO₂ Capture process. 237

Figure B.5- Process flow diagram for the post-combustion CO₂ capture plant with aqueous monoethanolamine scrubbing technology and the CO₂ compression train. 237

Figure B.6- Block diagram for process model simulations: gPROMS and Aspen Plus linked model..... 237

List of Tables

Table 2.1.- Comparison of strategies to increase CO ₂ concentration in the exhaust flue gas from a gas turbine, from the power plant point of view.....	25
Table 2.2.- Comparison of physical adsorbents for CO ₂ capture (Ben-Mansour et al. 2016)	35
Table 2.3.- Key concepts for CCS on CCGT power plants, level of understanding and gaps in knowledge.....	39
Table 3.1.- Combined cycle gas turbine power and thermal efficiency.....	75
Table 3.2.- Gas turbine engine technical and operation parameters per GT-HRSG train.....	75
Table 3.3.- Heat recovery steam generator technical and operation parameters per GT-HRSG train.....	76
Table 3.4.- Steam turbines technical and operation parameters for the two GT-HRSG trains	76
Table 3.5.- Technical and operational parameters of the CO ₂ capture plant for the reference case: Air based combustion CCGT with PCC per GT-HRSG train.....	87
Table 4.1.- Operating parameters and concentrations of the investigated configurations ...	147
Table 4.2.- Technical parameters and operational variables of the CO ₂ capture process with chemical absorption using 30 wt% MEA aqueous solution.....	150
Table 4.3.- Working fluid properties at compressor inlet, turbine inlet and turbine outlet for the investigated configurations	155
Table 4.4.- Dimensionless parameter groups constituting the compressor and turbine performance curves for the investigated configurations.	155
Table 4.5.- Exhaust flue gas stream variables.....	156
Table 4.6.- Power and thermal efficiencies for a CCGT power plant with PCC and strategies to increase exhaust gas CO ₂ concentration.	156
Table 5.1.- Material properties and structural parameters for rotary adsorption process modelling	163
Table 5.2.- Properties of the solids and Extended Langmuir equation parameters.....	166
Table 5.3.- Adsorbent requirements and preliminary dimensions of the rotary adsorber....	172

Table 6.1.- Summary of the results: Rotary heat exchangers basic design and operational parameters (per GT-HSRG-absorber train).....	200
Table 7.1.- Key concepts for CCS on CCGT power plants: novelty and contribution to knowledge.....	220
Table A.1.- Ambient conditions	233
Table A.3.- Natural gas supply specifications.....	233
Table A.4.- Technical parameters for the steam cycle of the CCGT plant	234
Table A.6.- Technical parameters for the CO ₂ capture plant and compression train	236
Table C.1.- Exhaust flue gas stream information at HRSG outlet at different recirculation ratios (per GT-HSRG-absorber train).....	240
Table C.2.- CO ₂ -depleted gas stream information at absorber outlet, at different recirculation ratios (per GT-HSRG- absorber train).....	240
Table C.3.- Assumptions	241

Nomenclature

Acronyms

CAPEX	Capital expenditures
CCC	Committee on Climate Change
CCGT	Combined cycle gas turbine
CCS	Carbon capture and storage
CO	Carbon monoxide
CO ₂	Carbon dioxide
COT	Combustor outlet temperature
DCC	Direct contact cooler
ECO	Economiser
EGR	Exhaust gas recirculation
EVA	Evaporator
FGD	Flue gas desulphuration
GE	General Electric
GT	Gas turbine
H ₂ O	Water
HHV	Higher heating value
HP	High pressure
HRSG	Heat recovery steam generator
IEA	International Energy Agency
IEAGHG	IEA Greenhouse Gas R&D Programme
IP	Intermediate pressure
IPCC	Intergovernmental Panel on Climate Change
LHV	Lower heating value
LP	Low pressure
MEA	Monoethanolamine
NGCC	Natural gas combined cycle
O ₂	Oxygen
OPEX	Operational expenditures
PC	Pulverized coal
PCC	Post-combustion CO ₂ capture
S-EGR	Selective exhaust gas recirculation
SH	Superheater
SO ₂	Sulphur dioxide

ST	Steam turbine
TIT	Turbine inlet temperature
UHC	Unburned hydrocarbons

List of Symbols

Symbols

A	Cross section (m^2)
C	Absolute fluid velocity in the turbomachinery blades (m s^{-1})
C_p	Specific heat at constant pressure ($\text{J kg}^{-1} \text{K}^{-1}$)
C_v	Specific heat at constant volume ($\text{J kg}^{-1} \text{K}^{-1}$)
C_x	Axial component of the absolute velocity (m s^{-1})
C_θ	Tangential component of the absolute velocity (m s^{-1})
D	Diameter or characteristic dimension (m)
\dot{G}	Gas molar flow rate (mol s^{-1})
g_c	Gravitational constant ($1 \text{ kg m N}^{-1} \text{ s}^{-2}$)
\dot{m}	Mass flow rate (kg s^{-1})
h	Specific enthalpy (J kg^{-1})
ΔH_{ads}	Enthalpy of adsorption (kJ mol^{-1})
L	Number of sectors in the axial/longitudinal direction (--)
MW	Molar mass (kg mol^{-1})
Ma	Mach number (--)
N	Rotor angular speed (rpm) or number of sectors
P	Pressure (bar)
ΔP	Pressure difference (bar)
PR	Pressure ratio (Pa/Pa)
\dot{Q}	Heat flow rate (J/s)
R_u	Universal gas constant ($8.314 \text{ J mol}^{-1} \text{K}^{-1}$)
\dot{S}	Solid mass flow rate (kg s^{-1})
S	Number of sectors in the angular direction (--)
T	Temperature (K)
U	Rotor linear speed (m s^{-1})
V_{solid}	Volume of the adsorbent (m^3)
V_{wheel}	Volume of the rotor in a gas/gas heat exchanger (m^3)
V_{BED}	Volume of the solid structure for selective CO_2 transfer (m^3)
W	Relative fluid velocity in the turbomachinery blades (m s^{-1})
W_x	Axial component of the relative velocity (m s^{-1})
W_θ	Tangential component of the relative velocity (m s^{-1})

\dot{W}	Electric power (MW)
w	Absolute humidity ($\text{kg}_{\text{water}}/\text{kg}_{\text{dry gas}}$)

Greek letters

ε_{bulk}	Bulk void fraction ($\text{m}^3 \text{m}^{-3}$)
ε_p	Particle porosity ($\text{m}^3 \text{m}^{-3}$)
$\eta_{Rankine}$	Efficiency of the Rankine cycle
η_{SC}	Net electric efficiency of a steam cycle with either combustion or heat recovery
ρ_p	Particle density ($\text{kg}_{\text{solid}} \text{m}^{-3}_{\text{particle}}$)
ρ_s	Solid density ($\text{kg}_{\text{solid}} \text{m}^{-3}_{\text{solid}}$)
γ	Specific heat ratio, $\gamma = C_p/C_v$
ξ	Friction coefficient
ρ	Density (kg m^{-3})
χ	Efficiency of the heat recovery
ω	Angular speed (rpm)
τ	Torque or angular momentum

Superscripts

*	Equilibrium
---	-------------

Subscripts

c	Compressor
des	Design
g	Gas
in	Inlet
l	Liquid
out	Outlet
r	Radial direction measured outwards from the shaft
s	Solid or steam or isentropic conditions
t	Turbine
x	Axial direction, measured along the axis of rotation
θ	Angle of rotation or angle turned by the blades
0	Stagnation or total properties

Introduction

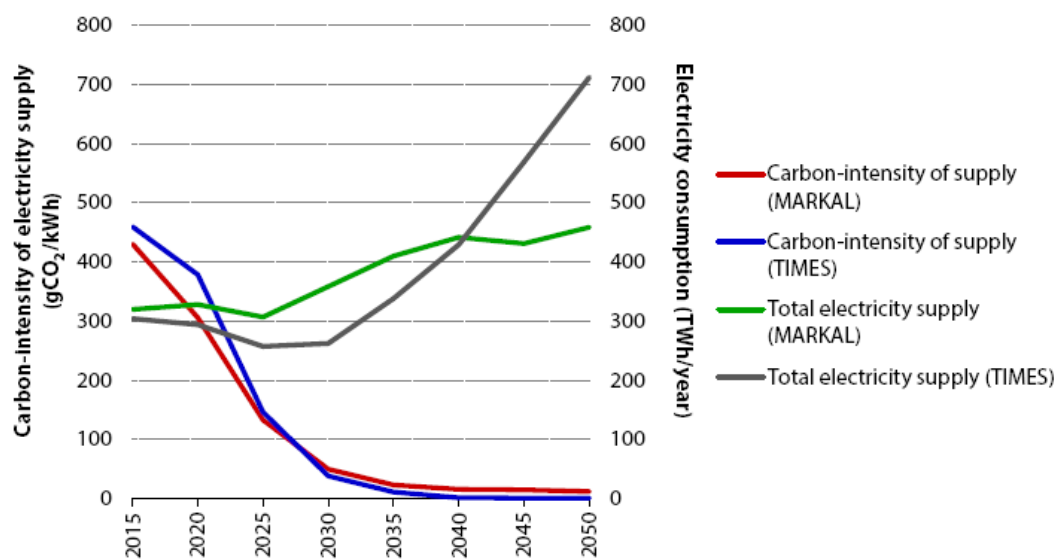
1.1. Background

Greenhouse gas (GHG) emissions need to be substantially reduced over the next few decades to reduce the risk and mitigate the effects of climate change by limiting global warming. Tackling climate change requires a coordinate action by nations around the world. All countries members of the United Nations Framework Convention on Climate Change (UNFCCC) agreed to adopt a new global climate protocol and legal instruments during the 21st United Nations Conference of Parties (COP21), December 2015. Furthermore, some industrialised countries committed to reduce its GHG emissions to limit global temperature increase to 2 °C above pre-industrial levels by 2050. For this purpose, net anthropogenic GHG emissions should be progressively and drastically reduced during the second half of the 21st century (IPCC 2014).

The European Union (EU) actions to tackle climate change include setting out targets on GHG emissions, using energy more efficiently and increasing the share of renewable energy in the energy mix. The Energy Roadmap developed by the European Commission proposes several possible scenarios for a sustainable and competitive low-carbon transition to a secure energy system with a reduction in GHG emissions by 80-95% below 1990 levels by 2050 (European Commission 2011). In the pathways towards a low-carbon economy transition, a contribution from all sectors, e.g. power generation, industry, transport, building, construction and agriculture, is necessary. Reducing emissions from power generation has a key role, due to the fact that this sector is the major source of GHG emissions, primary carbon dioxide (CO₂), and the possibility of extending low-carbon electricity to other energy sources, e.g. replacing fossil fuel in transport and heating. Particularly in the UK, CO₂ emissions from the power sector were around a quarter of total GHG emissions in 2014 (CCC 2015). The EU Energy Roadmap aims to almost eliminate CO₂ emissions from the power generation sector by 2050 (European Commission 2011).

The UK has also developed national legislation and has established an economically feasible and competitive framework to develop emissions reduction paths. The Climate Energy Act established a statutory carbon target for 2050 to reduce CO₂ emissions across the economy by at least 80% from 1990 levels (UK Gov 2008). In order to meet the 2050 target, the

Committee on Climate Change (CCC) suggests the development of policy approaches consistent with reducing the carbon intensity of the power sector from levels of approximately 450 gCO₂/kWh in 2014 to levels within 50-100 gCO₂/kWh in 2030, as illustrated in Figure 1.1, the upper limit accounts for delays in nuclear and carbon capture and storage (CCS) projects. Beyond 2030 a substantial reduction of the direct emissions from the power sector to below 50 gCO₂/kWh become necessary, along with a considerable mitigation of direct emissions from energy use, power heat and transport. A decarbonised power sector can therefore provide the low-carbon energy sources. This reduction could be delivery by a range of different mixes of low-carbon generation to reach a total share of approximately 75% of generation by 2030 (CCC 2015).



Source: MARKAL modelling by University College London for the CCC (2010); UK TIMES modelling for the CCC by DECC (2015)

Notes: Carbon-intensity calculations exclude 'negative emissions' benefits of using biomass in conjunction with CCS.

Figure 1.1.- Energy system model trajectories for the UK's power sector (CCC 2015)

Low-carbon electricity can be supplied from renewable sources, e.g. biomass, wind power, solar power, hydropower and geothermal energy, and other low-carbon sources, e.g. nuclear power plant or fossil fuel power plants equipped with carbon capture and storage (CCS) technology. The energy mix will vary widely among individual countries, reflecting local conditions and opportunities.

The International Energy Agency's Energy Technology Perspectives (ETP 2012) towards a maximum 2 °C temperature rise suggests that CCS is likely to contribute by 17% to CO₂

emissions reduction required in the energy sector by 2050, and by 14% to the cumulative emissions reduction between 2015 and 2050 (IEA 2013).

In the European context, the European Commission has emphasised that “CCS may be the only option available to reduce direct emissions from industrial processes at large scale needed in the long term” (European Commission 2014).

In the UK, the Committee on Climate Change (CCC) and the Energy Technology Institute (ETI) suggest that a cost-competitive option should include CCS equipped fossil fuel power plants in the UK electricity system. CCS provides additional value since, in addition to its role in power generation, CCS can capture emissions from many heavy industrial applications at low cost, e.g. iron, steel and cement production, and chemical processes, can provide flexible low-carbon energy for industry, road transport and heat in buildings, and provide other routes to reduce emissions (e.g. based on hydrogen, using CCS in combination with bioenergy to offset emissions or deliver negative emissions). The Energy Technology Institute (ETI) estimates that the cost of meeting the UK’s 2050 targets would increase by over 100% in the absence of CCS deployment. Without CCS it may be necessary to find potentially more expensive carbon reduction options to meet the UK statutory targets set out in the Climate Change Act as well as the more recent commitment set out at the Paris climate summit (ETI 2015; CCC 2016; Oxburgh 2016).

In order to facilitate CCS to play this vital role in the UK decarbonisation, it will be required to install around 10 GW of capacity by 2030. This high CCS deployment level is consistent with DECC’s Electricity Market Reform (EMR) delivery plan, which includes up to 13 GW of CCS by 2030, and with the CCC’s scenarios to reduce power sector emissions below 50 gCO₂/kWh by 2030 (ETI 2015).

The CCC’s scenarios, along with the decarbonisation of installed capacity, foresee a need to invest in new low-carbon electricity generation, e.g. approximately 30-40 GW of new capacity is likely to be required in the decade from 2020, to supply predicted demand growth and replace coal and nuclear fleet which will be forced to close over the next decades (CCC 2015). Unabated coal-fired power plants are likely to be closed by 2025 and coal generation is likely to be progressively taken out of the UK electricity system (DECC 2015).

Large-size combined cycle gas turbines (CCGT) capacity is expected to increase due to their relatively low investment cost and short construction time, lower CO₂ emissions per unit of electricity and competitive price of electricity (DECC 2015). Particularly in the UK, over 20 GW of new generation capacity with new-build natural gas-fired power plants has been permitted since 2007 (AEA, 2010) and is expected to contribute to the UK fossil fleet that

will be used to fill the gap between the demanded electricity and renewable and nuclear output to ensure security of supply. Approximately 30-35 GW of natural gas-fired power plants are likely to be on the system by 2020 (CCC 2015).

Unabated natural gas-fired power plants could help to reduce emissions in the short term, yet they still produce on average 400 gCO₂/ kWh. Carbon intensity targets by 2030 requires CCS technology to be integrated in almost all natural gas-fired power plants to provide dispatchable low-carbon electricity, and reserve services to ensure security of supply while maintaining operational flexibility required in the electricity system. Other low-carbon options are inflexible, e.g. nuclear, or intermittent, e.g. wind and solar. The power system in the 2030s is likely to be characterised by increasing levels of intermittent generation and more variable demand, implying a great need for flexibility.

A portion of new-build plants, as well as existing ones, may implement CCS between 2020 and 2030, as result of future legislation and policy incentives, aiming to drastically reduce CO₂ emissions from the UK fossil fuel sector and achieve 2050's GHG targets.

CCS is currently at the demonstration stage, with uncertainty over potential costs, which is compounded by uncertainty over future gas prices. However, the CCC anticipates that, over a range of gas prices it is likely that low carbon electricity with CCS would be competitive with coal with CCS and most renewable sources. CCGT plants with CCS may be able to access a higher value funding regime and/or achieve higher running hours, and thus higher load factors, to maximize revenues, compared to unabated CCGT plants under current proposal for EMR (Grant and Skillings 2009).

Considering the current commercially available gas turbine technologies, CCGT with post-combustion capture systems have been reported to have higher thermal efficiencies, and appears likely to give low total electricity costs and incurs lower capital costs, when compared with pre-combustion capture from IGCC plants and oxy-fuel technology (Gibbins & Chalmers 2008; IEA 2011; ETI 2016). The most commercially advanced methods uses wet scrubbing with aqueous amine solutions; a well-established technology which has been demonstrated in commercial plants to separate CO₂ from natural gas at gas fields and to produce CO₂, mainly for enhanced oil recovery (EOR) and the chemical industry.

Flue gases from natural gas-fired power plants raise particular challenges for post-combustion capture technologies due to the relatively low CO₂ concentration and high oxygen content, when compared with flue gas from coal-fired power plants. The large excess of air, for the purpose of nitrogen oxides (NO_x) emissions control and cooling, leads to large volumes of exhaust gases to be treated in the capture plant, increasing the size of the

plant and auxiliary equipment and, thus capital costs. Capturing CO₂ from a CCGT plants incurs additional capital cost (CAPEX), similar to the cost of the original power plant and may use up to 20% of the power generation output (ETI 2016).

It is worthy to emphasize that low energy consumption of the capture process is a key factor in power plants to guarantee the lowest cost of electricity generation possible for base-load plants. ETI reports that every 10% reduction in the capture plant CAPEX or 10% reduction in the energy penalty reduces the electricity cost by 1.2 – 2%. However, if a reduction of the load factor for fossil fuel power plants occurs, as expected if the installed renewable energy capacity increases, the contribution of capital cost to the electricity prices in NGCC with CCS increases, and its reduction becomes an important issue to post-combustion CCS development and commercialization (ETI 2016).

1.2. Global Status of Carbon Capture and Storage

Given the long-term importance in reducing emissions across the economy and the vital role in driving down the costs, the effort needs to be focused on the large-scale integration of the components constituting the CCS chain and on the transition from demonstration on the path towards commercialisation and deployment (IEA 2013).

In terms of the scale of CCS deployment, out of forty five CCS projects identified by the Global CCS Institute, illustrated in Figure 1.2, there are fifteen large-scale projects currently in operation across many industrial sectors around the world, and seven are due to become operational (currently at execute stage) in 2016 and 2017, with a total CO₂ capture capacity of around 40 million tonnes per annum (Global CCS Institute 2015).

In the power sector, the Boundary Dam Integrated CCS Project is the world first large scale project. Located at SaskPower's existing Boundary Dam coal-fired power station in Saskatchewan, Canada, the project was started in October 2014 and has demonstrated the feasibility of post-combustion carbon (PCC) with amine-based scrubbing technology for commercial scale operation. The capture unit removes 90% of the CO₂ from the flue gas generated in one coal-fired unit with a net power output of 139 MWe, using chemical absorption with a dedicated solvent developed by Shell Cansolv (Stéphenne 2014).

Key learning and experiences in the development and the early operation of first generation demonstration projects constitute valuable information to decrease uncertainty in the cost of design, construction and operation of future generation CCS projects, conduct R&D efforts on specific aspects, reduce the risk and reinforce investors and stakeholder's confidence.

Outcomes from Boundary Dam CCS project are likely to reduce cost of up to 30% for the next generation of projects (Global CCS Institute 2015).

Two more large-scale projects are at execution stage and expected to start operation in 2016: The Kemper Country Energy Facility in Mississippi, United States, which consists of a new build integrated gasification combined cycle (IGCC), and the Petra Nova Carbon CCS Project at the W.A. Parish power plant in Texas, United States, which is based on post-combustion capture retrofitting in a pulverized coal power plant.

The most advanced CCS projected planned in Europe is the Rotterdam Opslag en Afvang Demonstratie (ROAD), presently on hold, and involves the retrofit of a 250 MWe equivalent post-combustion carbon capture and compressor unit to a new ultra-supercritical power plant located in at Maasvlakte power plant, Rotterdam, The Netherlands.

The majority of the defined and identified CCS projects consider retrofitting post-combustion capture technology (PCC) to existing pulverized coal fired power plants, mainly due to the larger emission intensity and the more strictly legislation, compared to gas-fired power plants.

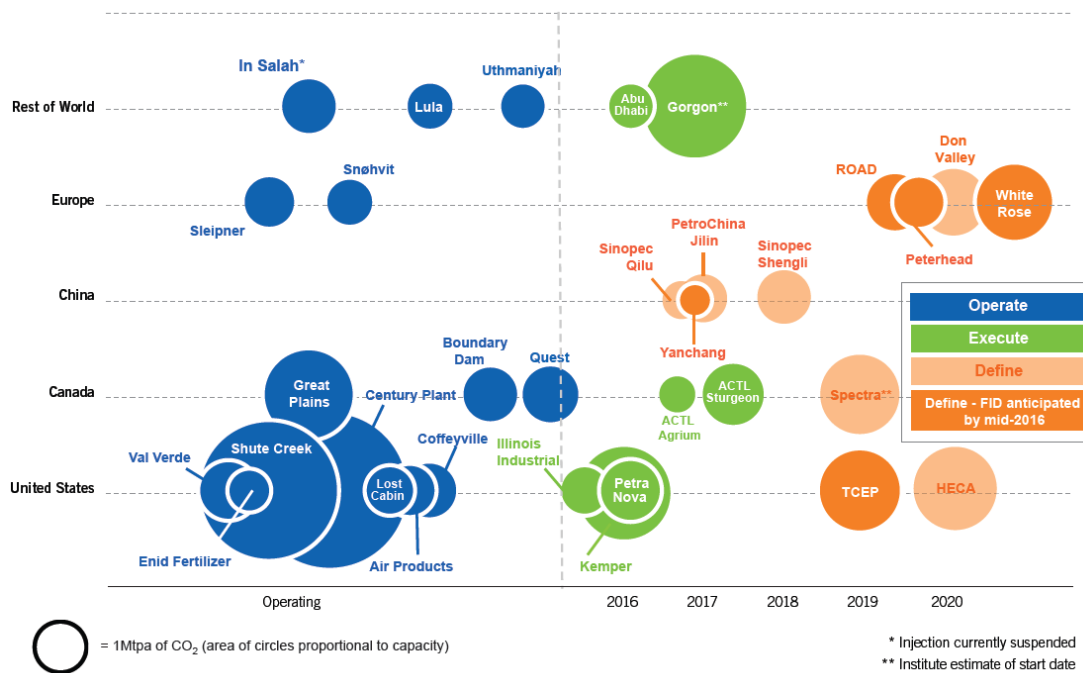


Figure 1.2.- Actual and expected operation dates for large-scale CCS projects in the Operate, Execute and Define stages by region and project lifecycle stage (Global CCS Institute 2015)

Carbon capture from industrial scale gas-fired power plant is also necessary, in order to drastically reduce GHG emissions and meet the 2050 targets in many countries and to reduce the cost of CCS to a level where it will be more competitive with other forms of low carbon

energy generation. A full-scale demonstration project has been defined at Peterhead power station. Under the UK CCS commercialization program, the Peterhead CCS project was the results of a partnership between Shell UK Limited, SSE Generation Limited and the UK Government. The project was one of the two bidders in the UK Government's CCS Commercialisation Programme, yet it was announced to be cancelled in November 2015. At the stage of front end engineering and design (FEED) study, the Peterhead CCS project is proposed to capture CO₂ emissions at one of the three existing 385 MWe combined cycle gas turbines at Peterhead Power Station in Aberdeenshire, Scotland, and then it will be transported by pipeline and stored offshore in the depleted Goldeneye gas reservoir, at the North Sea. The CO₂ capture system consists on flue gas scrubbing technology using the amine-based solvent developed by Shell Cansolv, similar to Boundary Dam but with a more simple flow sheet, e.g. without absorber intercooling, since this process modification results in a marginal benefit for gas fired-plants (Kvamsdal et al. 2011). With a dedicated steam cycle, the steam generated from the heat recovery steam generator associated to the gas turbine would be used to drive a new steam turbine and provide steam for solvent regeneration (Spence et al. 2014).

The portfolio of large-scale CCS projects is complemented by pilot projects across the world. The most recent work which can be considered as an independently verified baseline of a non-proprietary post-combustion amine-based solvent system has been conducted at a semi-industrial scale plant facility, located at CO₂ Technology Centre Mongstad (TCM DA) in Norway (Thimsen et al. 2014; Hamborg et al. 2014). The base-case test campaign employed an aqueous 30 wt% monoethanolamine solvent system to capture CO₂ from a flue gas slipstream from a natural gas-fired combined heat and power (CHP) plant, with a flow rate of approximately 47000 sm³/ hr and a CO₂ concentration of approximately 3.5 vol%, operating at 90% CO₂ capture rate. In addition to provide valuable information regarding key performance parameters and assess a generic CO₂ capture testing methodology, environmental issues of great concern are also addressed, e.g. emissions of MEA are very low and MEA related degradation products are all below detection levels, within the emissions limits set by the Norwegian environmental authorities (Thimsen et al. 2014; Hamborg et al. 2014).

1.3. Water demand for cooling in a Combine Cycle Gas Turbine power plant with Post-combustion Carbon Capture systems

An environmental impact associated to carbon capture systems and addressed in this thesis is the additional cooling and process water demand in natural gas-fired power plants with CCS (IEAGHG 2011). This is particularly important in post-combustion capture with gas scrubbing technologies. Water is becoming a scarce natural resource and fresh water and marine environments are under increasing pressure, mainly because of growing populations, changing socioeconomics conditions and climate change (Byers et al. 2014). Moreover, water demand is expected to rise further in places due to electrification with new-build thermal power plants and, even more, if decarbonisation of electricity generation takes place with higher contribution of carbon capture and storage technologies in fossil fuel-fired plants.

The availability of cooling water might therefore constitute a limitation for the full scale deployment of carbon capture and storage, particularly in regions with increasingly restricted access to cooling water and limited availability of fresh or sea water abstraction licences (Byers et al. 2014, Schakel et al. 2015). Restricted access to water is notably likely to be the result of growing concerns to protect inland water resources and minimise marine ecological impact, or simply seasonality change in cooling water availability and fresh water shortages. In periods of low flow, thermal plants may be required to shut down.

Novel engineering solutions are therefore necessary to limit the additional water abstraction and water consumption of power plants with CCS (IEAGHG 2011). Electricity production in thermal power plants requires the use of significant quantities of water, primarily for the purpose of cooling the steam in the condenser of the steam turbines. The cooling capacity is mostly provided by water diverted from surface or ground water sources such as, rivers, tidal estuaries and coasts. This is generally referred to as water abstraction or water withdrawal. In industrialised countries, water abstraction for thermal power generation can constitute up to around 40% of the total abstraction from fresh water sources. This is notably the case in Europe (EEA 2010; Cormos et al. 2013; Schakel et al. 2015) and the United States (Zhai and Rubin 2010; Zhai et al. 2011). The fraction of water abstracted that is permanently withdrawn from its source is referred to as water consumption, i.e. water evaporated to the atmosphere when wet cooling water towers are used.

1.4. Research Objectives

Commercial-scale deployment of natural gas-fired combined cycle power plants equipped with CCS requires to investigate options to reduce capital and operational costs, equipment size and electricity output penalty. In this context:

- Strategies to increase CO₂ concentration in the exhaust flue gas of a CCGT power plant are investigated in this thesis. The benefits of Selective Exhaust Gas Recirculation (S-EGR), i.e. a technology option consisting of selectively transferring CO₂ from a flue gas stream into an air stream used as comburent in a gas turbine, are evaluated and compared to the benefits of “non-selective” Exhaust Gas Recirculation (EGR), where a fraction of a flue gas stream is recirculated back to gas turbine inlet. For this purpose it is important to develop a rigorous model of a CCGT power plant with post-combustion capture systems (PCC).

PCC technologies aim to introduce minimal modifications in the CCGT power plant and, particularly, in the gas turbine engine, as current gas turbine technology presents a high efficiency and plays an important role in achieving a high combined cycle net power output.

In this context:

- The effects of S-EGR on the performance of a CCGT power plant with PCC systems is assessed and quantified.

The operation and cost benefits of S-EGR on the PCC system need to be compared to the cost and operation of introducing an additional system for selective CO₂ transfer. In this context:

- Technology options for the application of S-EGR are considered and adsorption in a rotary wheel is further investigated at the stage of concept development.

Regarding environmental impacts and limiting factors for full scale deployment of CCS, the water demand associated to PCC technologies using solvent scrubbing technology needs to be minimised. In this context:

- Dry cooling options using ambient air as the cooling fluid are investigated using rotary gas/gas heat exchangers to manage heat and water demand around the post-combustion carbon capture process.

1.5. Original contribution

The following results can be considered an original contribution to knowledge:

- The definition of an operating framework for CCGT plants with post-combustion carbon capture (PCC) and Selective Exhaust Gas Recirculation (S-EGR) and the identification of a range of CO₂ concentrations possible in the exhaust flue gas and operating conditions in the combustor of the gas turbine.
- The technical assessment of the effect of S-EGR on the performance of a CCGT power plant, by evaluating deviations on the performance of the compressor, the turbine and the steam cycle from the design point. The identification of key operation parameters with a critical role on the operation of a CCGT plant with S-EGR, in order to establish minimum requirements for potential technologies for S-EGR application
- The technical assessment of the effect of S-EGR on PCC systems with amine based scrubbing technology, by quantitatively evaluating the reduction in equipment size and energy requirements. The technical comparison with previously investigated options of “non-selective” Exhaust Gas Recirculation (EGR).
- A conceptual design assessment of the use of existing carbon capture technologies, particularly, adsorption with structured adsorbent materials in a rotary wheel configuration, for the application of selective CO₂ transfer in CCGT plants with PCC and S-EGR. An optimisation study is also included to propose a step change in adsorbents technology for practical feasibility of S-EGR application.
- The technical feasibility study of novel options using a range of configurations of rotary regenerative gas/gas heat exchangers to manage cooling and process water demand around the capture system in CCGT plants equipped with amine-based scrubbing technology. This work is presented on Herraiz *et al.* (2015).

1.6. Thesis overview

This thesis is composed of seven chapters whose contents are summarised below.

- Chapter 2 presents an overview of the technologies proposed in literature to increase the CO₂ concentration in the flue gas from natural gas combined cycle plants. The level of knowledge on the effect of the previous technologies on the power cycle and the capture systems is summarised, with special attention on exhaust gas recirculation and selective exhaust gas recirculation. This chapter identifies possible technologies for selective exhaust gas recirculation applications. A review of adsorbent materials

investigated for CO₂ capture and of applications using structured adsorbents in rotary wheel configurations is also presented. Finally, this chapter highlights the importance of reducing water demand in carbon capture processes and the strategies for water management and integration previously investigated in literature. A summary of the level of understanding and gaps in knowledge of the key concepts investigated in this thesis is included.

- Chapter 3 describes the fundamental principles considered in the process modelling of the Combined Cycle Gas Turbine plant and the methodology followed to investigate the performance of the plant at off-design conditions, when exhaust gas recirculation and selective exhaust gas recirculation are implemented. This chapter describes the thermal integration with the carbon capture system and the optimisation procedure followed to evaluate operating and design parameters. The fundamental principles and performance of rotary gas/gas heat exchangers the methodology followed to conduct the thermal performance analysis and sizing are also presented in this Chapter. Finally, the equilibrium model of the rotary adsorption system for selective exhaust gas recirculation is described.
- Chapter 4 presents a technical assessment of the performance of natural gas combined cycle plants with current class gas turbine engines when the strategies of exhaust gas recirculation and selective exhaust gas recirculation are implemented. The effect of enriching the gas turbine compressor inlet stream with CO₂ on the CO₂ capture system is quantitatively evaluated. Finally this chapter performs a sensitivity analysis of the effect of the key parameters associated to the selective CO₂ transfer system on the performance of a gas turbine combined cycle plant with post-combustion capture systems.
- A conceptual design assessment of rotary adsorption systems for selective exhaust gas recirculation applications is conducted in Chapter 5. In a first step, the technical feasibility of applying rotary adsorption for S-EGR is investigated for best class commercially available adsorbents. In a second step, starting with the size of a large rotary system, optimal properties of the adsorbent and process conditions are identified for S-EGR application.
- Chapter 6 presents a technical feasibility study of novel options with rotary regenerative gas/gas heat exchangers for the management of water demand around post-combustion carbon capture process integrated with CCGT plants with and without exhaust gas recirculation. Hybrid and dry cooling systems, where gas/gas heat exchangers use air as the cooling fluid, are proposed to reduce or mitigate cooling and

process water required in the pre-treatment of the flue gas upstream of the capture system. The sensitivity of the performance of dry-cooling systems to ambient temperature is investigated. Consideration to minimise pressure drop and manage leakages from high CO₂ concentration stream to stream with lower concentration are described. This chapter is based on Herraiz *et al.* (2015).

- Chapter 7 discusses the conclusions and suggests recommendations and improvements for future work.

State of Combined Cycle Gas Turbine Power Plants with Post-Combustion CO₂ Capture

2.1. Post-combustion CO₂ capture in Combined Cycle Gas Turbine plants: Current Challenges

Post-combustion CO₂ capture technologies, e.g. absorption, adsorption, membrane-based separation processes, rely on the gradient of partial pressure of CO₂ as the driving force for CO₂ separation. Compared to coal-fired power plants, natural gas-fired combined cycle power plants produce a significantly larger volume of flue gas with lower CO₂ concentration, i.e. 3-4 vol% compared to 12-14 vol%, and higher O₂ concentration, i.e. 12-13 vol% compared to 3-4 vol% (EBTF 2011). This will provide significant challenges for CO₂ separation processes likely resulting in larger separation equipment size requirements. A theoretical stoichiometric combustion of natural gas would result in a CO₂ concentration in combustion gases of approximately 10 vol%. Yet, a large amount of excess air is necessary in gas turbine engines for the purpose of reducing the flame temperature for NO_x emissions control and further cooling the gas turbine components in contact with the high temperature combustion gases. The highest temperature in the cycle defines the amount of excess air and it is limited by NO_x formation and by metallurgical constraints of the materials (Davis and Black 2000; Brooks 2000; Pavri and Moore 2001).

A higher CO₂ concentration in the gas phase enhances the amount of CO₂ chemically/physically bounded to the solid material or liquid solvent or the permeation rates in membrane-based processes. Particularly for chemical absorption technologies, increasing the CO₂ concentration in the flue gas from a gas turbine has been proposed as an effective method to reduce the energy penalty of the CO₂ capture process and equipment size, improving the net thermal efficiency and capital cost (CAPEX) and cost of electricity (COE) and CO₂ avoidance cost, in the short, medium and long time (Li, Ditaranto, et al. 2011a).

This work is focused on the strategies to increase CO₂ concentration in the flue gas from natural gas combined cycles.

2.2. Strategies to increase CO₂ concentration in the exhaust flue gas from Combined Cycle Gas Turbine power plants

Options for increasing the CO₂ concentration in the exhaust flue gas from gas turbine systems have been investigated following two principles. The first consists of replacing some of the excess of air by either recirculation of the flue gas, injection of steam or vaporization of water, with the purpose of controlling the flame temperature and the combustion gas temperature downstream of the combustion chamber. The second principle considers burning additional fuel using as comburent the excess of oxygen in the flue gas (Bolland and Saether 1992; Li, Ditaranto, et al. 2011a).

A comparative study of four strategies, including exhaust gas recirculation (EGR), gas turbine humidification or evaporative gas turbines (EvGT), supplementary firing combustion (SFC) and external firing combustor (EFC), has been conducted by Li and co-workers (Li, Ditaranto, et al. 2011a). In their work, an integrated model of a CCGT power plant with PCC systems using aqueous monoethanolamine scrubbing technology is developed to evaluate the energy efficiency penalty when these strategies are implemented and identify advantages, challenges and key parameters in each configuration. While PCC technologies fitted to CCGT plants do not affect the performance of the gas turbine engine, strategies to increase CO₂ concentration in the exhaust flue gas will have an effect on the power plant performance and this requires further investigation.

A review of the state of options previously proposed in literature is included in this section with particular attention given first to the effect of the technology option on the gas turbine system and the steam cycle, and then to the capital and operation benefits of the technology options for use with post-combustion systems with amine-based scrubbing technology. Finally, a more recent technology known as selective exhaust gas recirculation (S-EGR) is considered using the same methodology.

2.2.1. Exhaust Gas Recirculation

Exhaust gas recirculation (EGR) was originally proposed as a compressor anti-icing method, since the flue gas is recirculated at a higher temperature than the ambient air, and as a strategy to reduce NO_x emissions, since the rate of thermal NO_x formation decreases with decreasing fuel-to-air ratio or firing temperature (Pavri & Moore 2001). Moreover, recycling minor species, e.g. NO and CO, into the combustion zone results in a reduction of their concentration through the reburning mechanism (Li, Ditaranto, et al. 2011).

EGR consists of recycling a portion of the exhaust flue gas leaving the heat recovery steam generator (HRSG) back to the compressor inlet. A block flow diagram of the EGR process is included in Figure 2.1. The recycled flue gas replaces part of the intake air and the gas turbine operates with a lower excess of air. This strategy results in an increase of the CO₂ concentration and a decrease of the flow rate of the non-diverted flue gas stream to be treated in the PCC unit depending on the recirculation ratio. The exhaust gas recirculation ratio is defined as the flow rate of the diverted flue gas over the total amount of the flue gas leaving the gas turbine, before cooling and condensation of the excess of humidity, as indicated in Equation [2.1].

$$\text{EGR ratio} = \frac{\text{mass flow of recirculated exhaust flue gas}}{\text{mass flow of exhaust flue gas}} \Bigg|_{\text{HRGS outlet}} \quad [2.1]$$

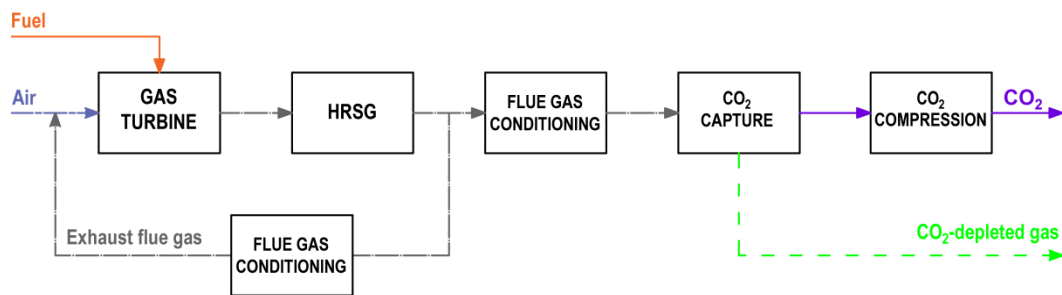


Figure 2.1.- Block flow diagrams of a CCGT plant with exhaust gas recirculation and post-combustion capture.

Since the oxygen concentration in the flue gas stream is smaller than in the ambient air, the oxygen available for combustion decreases with increase of EGR ratio. The maximum recirculation ratio and, thus, the highest CO₂ concentration achievable are limited by the oxygen level in the combustor. The theoretical minimum oxygen is defined as the stoichiometric amount of oxygen required for complete combustion of natural gas. In practice, however, the oxygen concentration must be high enough to ensure ignition, flame stability and complete combustion, with low levels of CO and unburned hydrocarbons (UHCs) in the exhaust flue gas that achieve environmental compliance with local environmental regulations. This is particularly important in gas turbine combustors which are characterised by a high flame velocity and a low residence time (Li, Ditaranto, et al. 2011).

Experimental investigations of the combustion process indicate that “a low oxygen concentration reduce the reaction rates, allowing for combustion to spread over a large region and to reduce the peak flame temperature, which is not in favour of the oxidation of

CO to CO₂. On the contrary, reduction in the oxygen level combined with supplementary CO₂ in the comburent leads to changes in the heat release process via CO₂ dissociation” (ElKady et al. 2009). CO emissions are therefore expected to rise for a particular engine operation with increasing the recirculation ratio and decreasing the oxygen concentration in the comburent. Yet, CO emission levels are dependent on the type of burner, the combustion chamber configuration and the quality of the mixing (Burdet et al. 2010).

Experimental work by Røkke and Hustad, conducted in a 65 kW combustor operating in a pre-mixed flame mode, indicates that the blow out limit occurs with an oxygen concentration in the comburent below 13-14 vol% (Røkke and Hustad 2005). The blowout limit is defined as “the point at which a premixed fuel and air mixture is unable to self-sustain” (Davis and Black 2000). ElKady and co-workers however reports that a higher minimum oxygen concentration of 16-17 vol% is necessary for good combustion efficiency with acceptable low levels of CO and UHCs (ElKady et al. 2009; Evulet et al. 2009), according to the results from combustion tests performed on a bench-scale lean pre-mixed burner used in Dry Low-NO_x (DLN) combustor systems, currently employed in General Electric (GE) F-class gas turbine technology. Tests were conducted at 10 bar, which is lower than the typical operating pressure of approximately 18 bar, and for a range of temperatures up to 1630 °C. They also suggest that lowering the oxygen level below 16 vol% might be possible with minor modifications of the combustion system, e.g. in the premix, injection and control systems or optimisation of the pilot, or at larger operating pressures while complying with CO emissions. Experimental test were also conducted by Jansohn and co-workers (Jansohn et al. 2011) in a high pressure test rig up to 20 bar, without providing details of the burner type or combustion mode.

Achieving an oxygen concentration of 16 vol% in the combustor would require a recirculation ratio of 35% for an excess of air of 150% used in GE F-class gas turbines. This results in a corresponding CO₂ and O₂ concentrations of approximately 8 vol% and 4.5 vol% respectively at the combustor outlet, and 6 vol% and 7.5 vol% at the turbine exhaust, after mixing with cooling air. There is also an advantage for lower NO_x emissions, which may decrease more than 50% with 35% EGR ratio (ElKady et al. 2009). Yet, for a given oxygen concentration in the combustor, the recirculation ratio depends on the design turbine inlet temperature (TIT), since this parameter defines the required excess of air, and on the amount of cooling air which is extracted from the compressor last stages and by-passes the combustor. A lower TIT allows for higher recirculation ratios but acts on detriment of the gas turbine thermal efficiency. The TIT depends on the materials of construction and the cooling system of the blades, the vanes and the rotor in the expansion section.

EGR has also been investigated for the sequential combustion system employed in Alstom GT26/GT24 engines, which consists of, first, a generic lean premix dry low-NO_x burner followed by reheat burner, with a high pressure expansion stage in between. The feasibility of operating Alstom reheat engines under high EGR ratios is investigated in literature with numerical simulation and experimental combustion tests. Numerical simulations of the combustion process using detailed chemistry were performed for the two burners (Guethe et al. 2009), and high pressure combustion tests were conducted using both, a full-sized industrial lean premix burner, reproducing standard gas turbine flow conditions within the combustor, e.g. pressure up to 16 bar and temperatures up to 550 °C (Burdet et al. 2010), and a single burner reheat combustion test rig (Guethe et al. 2011). The main advantage of this configuration is that the two main limiting factors for operation with EGR, flame stability and CO emissions, can be decoupled and controlled in the two separate combustor systems. Moreover, the pressure ratio and the combustor inlet temperature in the Alstom gas turbine engine are higher, compared to other manufacturers, e.g. GE or Siemens. The premix burner flame was sustained and stable at high EGR ratios, corresponding to O₂ concentrations in the combustion gas within a range from 2 to 5 vol% (Burdet et al. 2010; Sander et al. 2011), with a lower end smaller than the previously reported 4.5 vol% for the GE F-class turbine. Although CO emissions increase with increasing the EGR level, they are lowered in the reheat burner. Moreover, lower O₂ inlet values are feasible for the reheat combustor as it runs stable in auto ignition mode due to its high inlet temperature and it is not affected by lean blow out problems (Guethe et al. 2011). For a higher inlet burner pressure and, thus, inlet burner temperature, the increase in CO emissions due to EGR is smaller. The operation at high EGR ratios results in CO₂ concentrations within a range from 6 to 9 vol% (Burdet et al. 2010).

A higher EGR ratio could increase further the CO₂ concentration and reduce the mass flow rate of the flue gas treated in the PCC unit. In order to reduce the impacts on combustion, an oxygen enrichment of the comburent has been proposed, which would only be possible integrating a low purity oxygen air separation unit or introducing oxygen membranes technology (Bolland & Mathieu 1998; Kvamsdal et al. 2007; Amann et al. 2009), as the amount of transferred oxygen would be limited by the additional energy consumption.

In addition to the effect on the combustion process, EGR also results in different compressor inlet temperature and pressure and different working fluid composition, compared to the turbomachinery design point, which is defined for ambient air at ISO ambient conditions, i.e. 15 °C, 1.013 bar and 60% relative humidity.

Less attention has been paid in the literature to the investigation of the effect of EGR on the gas turbine performance. Jonshagen and co-workers (2011) have developed a rigorous model of a state-of-the-art CCGT power plant equipped with GE Class F gas turbine technology to evaluate the deviation of the dimensionless parameter groups, typically used to describe the compressor and the turbine performance at off-design conditions from their design point. It is concluded that a minimum deviation is expected and the gas turbine engine may operate at recirculation ratios of 40% (Jonshagen et al. 2011). EGR has also been investigated by Sander and co-workers (2011) with Alstom reheat GT26 gas turbine technology. The work is focused on evaluating temperature and pressure through the gas turbine (Sander et al. 2011).

The effect on the gas turbine performance of a higher temperature of the recycled flue gas stream, compared to the design compressor inlet temperature, i.e. 15 °C, is similar to the predicted behaviour when the ambient temperature increases. A smaller mass flow rate is then swallowed by the compressor at higher compressor inlet temperatures, derating the gas turbine (Botero et al. 2009).

The strategy of EGR has been experimentally tested at pilot scale in microgas turbines. Microgas turbines are small scale combined heat and power (CHP) applications with a power output typically within the range 50-500 kW_e. The engine control maintains the electric power output constant at a constant turbine inlet temperature (TIT) by changing the shaft speed and the fuel flow rate, in order to maintain a high electric efficiency (De Paepe et al. 2012; Akram et al. 2016). Tests conducted at the Vrije Universiteit Brussel (VUB, Belgium) showed unsteady operation of the microgas turbine with EGR due to the large effect of the high temperature of the recycled gas on the microgas turbine performance. Due to changes in the temperature, the intake mass flow rate fluctuates and the control system rapidly responds increasing the rotational speed to restore the power output. Results cannot therefore be extended to predict the behaviour of an axial flow heavy duty gas turbine engine operating at constant rotation speed.

2.2.2. Gas turbine humidification

Gas turbine humidification systems are usually divided into two categories: inlet air cooling systems and combustion chamber injection systems. In the former, the ambient air stream evaporates water increasing the absolute humidity up to a value limited by the ambient air saturation temperature, i.e. the wet bulb temperature. Combustion chamber injection systems consist of either direct steam injection (STIG) or water injection by evaporation in a humidification tower with a recirculation water loop, also known as evaporative gas turbines

(EvGT). These systems were originally proposed with the purpose of preventing the reduction in the gas turbine power output due to high ambient temperatures or low ambient pressures (i.e. at high elevations), and reducing NO_x emissions (Bianchi et al. 2010).

In humidified gas turbine, water or steam therefore replace part of the excess of air used for cooling. Since the water vapour can easily be separated from the flue gas by condensation, a higher CO₂ concentration in the flue gas is achieved compared to conventional gas turbines. The highest possible CO₂ concentration depends on the water to air ratio (WAR) and the cooled temperature of flue gas prior to entering the PCC plant, and therefore on the humidification system and the heat rejection system of the power plant.

The combustion process with gas turbine humidification is affected by the reduction in the oxygen concentration, since the excess of air is partially replaced, and the presence of high water vapour levels in the combustor. State-of-the-art heavy duty gas turbines typically operate with Dry Low-NO_x burners and so achieving high gas turbine efficiency with wet burners can be considered a technical risk.

A flue gas CO₂ concentration above 5.2 vol% in a dehydrated flue gas is possible with a ratio of water to air mass flow rates higher than 15%. At this operating conditions, the oxygen level in the combustor is approximately 16.5 vol% (Li, Ditaranto, et al. 2011). A significantly higher exhaust flue gas flow rate with smaller CO₂ concentration is treated in the PCC process, compared to EGR at 35% recirculation ratio.

A drawback for STIG and EvGT technologies implemented in CCGT power plants is the significant reduction in the thermal efficiency of the cycle. The available heat in the exhaust flue gas is partially used to generate the steam or to heat the water up to the saturation temperature. Less heat is therefore available to generate the steam that will be used in the steam turbines, with the subsequent reduction in the net power output (Li and Yan 2009). This option is, therefore, generally used as a power augmentation technology in a gas turbine operating in open cycle, i.e. without heat recovery steam generator.

2.2.3. Supplementary fired combined cycle

Supplementary fired combined cycle (SFCC) can increase the CO₂ concentration of the flue gas treated in the PCC unit by burning additional fuel in a secondary combustor using the remaining excess of oxygen. The secondary combustor, known as in-duct burner, is located downstream of the gas turbine and upstream of the heat transfer banks in the HRSG. The considerably high gas turbine exhaust temperature helps to stabilize the flame, despite the

relatively low oxygen concentration of approximately 11-12 vol%, compared to 21 vol% in ambient air.

The block flow diagram for a CCGT system with SFCC is shown in Figure 2.2 (a). Unlike EGR and EvGT options, SFCC technology does not affect the turbomachinery performance or the combustion process. The thermal efficiency of the CCGT power plant with supplementary firing however decreases with respect to an unfired CCGT power plant. This technology was therefore traditionally proposed to increase the power output in response to high electricity prices at peaks demand times or to supply additional steam at cogeneration facilities because this allows for independent control of electrical and thermal outputs (Kehlhofer et al. 2009)

Modifications to the system have been proposed in order to reduce the efficiency penalty, by increasing the efficiency of either the gas turbine (Brayton cycle) or the steam cycle (Rankine cycle). The reheated gas turbine concept was proposed to increase the gas turbine efficiency and consists of burning additional fuel in a secondary burner after the flue gas partial expansion in a high pressure stage and, then, the reheated flue gas is expanded in low pressure stages, e.g. Alstom GT26/24 (Güthe et al. 2009). The high flue gas temperature and the diffusion mode operation help to the flame stabilization in low oxygen content. The second option consists of recovering extra heat from the reheated flue gas in a supercritical HRSG. A supercritical steam cycle operates at pressure and temperature above the critical point and results in considerably higher steam turbine power output, compared to a subcritical steam cycle (Li et al. 2012; Gonzalez Diaz et al. 2014).

The highest flue gas CO₂ concentration that can be achieved is restricted by the largest amount of additional fuel that can be burnt, which is limited by the maximum allowable flue gas temperature in the HRSG. This temperature is approximately 800 °C using conventional materials according to metallurgical constrains, and results to a CO₂ concentration of approximately 6-7 vol% (Li, Ditaranto, et al. 2011).

The flue gas CO₂ concentration can be further increased with sequential supplementary fired combined cycle (SSFCC). The block flow diagram is shown in Figure 2.2 (b). This technology consists of burning additional fuel sequentially in several stages in between the heat transfer banks along the HRSG, without surpassing the flue gas temperature constrain in any of the stages. The amount of additional fuel is then constrained by the minimum excess of oxygen in the combustion gas that ensures complete combustion, which is typically of the order of 3 vol% (Kitto & Stultz 1992). The flue gas CO₂ concentration can be increased from approximately 4 vol%, in an unfired CCGT plant, up to approximately 9.4 vol% with SSFCC

provided that an excess oxygen level of 1 vol% at the exit of the HRSG is possible (Gonzalez Diaz et al. 2014).

In order to evaluate the effect on the carbon capture process, SSFCC results in an increase of the CO₂ concentration and a significant reduction of the flue gas flow rate entering the PCC system. For instance, in a supercritical CCGT power plant, only one GT-HRSG train is required to maintain the same power output as in a standard CCGT with two GT-HRSG trains (Gonzalez Diaz et al. 2014). This is due to the significant increase in the steam flow rate and the steam turbines power output. However, the process also causes a significant reduction in the thermal efficiency of approximately 5 %points, from 53% to 48%, and it makes SSFCC as an attractive option exclusively under the context of deploying CCS along with enhance oil recovery (EGR) and a certain range of prices for natural gas (operational cost) and CO₂ (additional revenue).

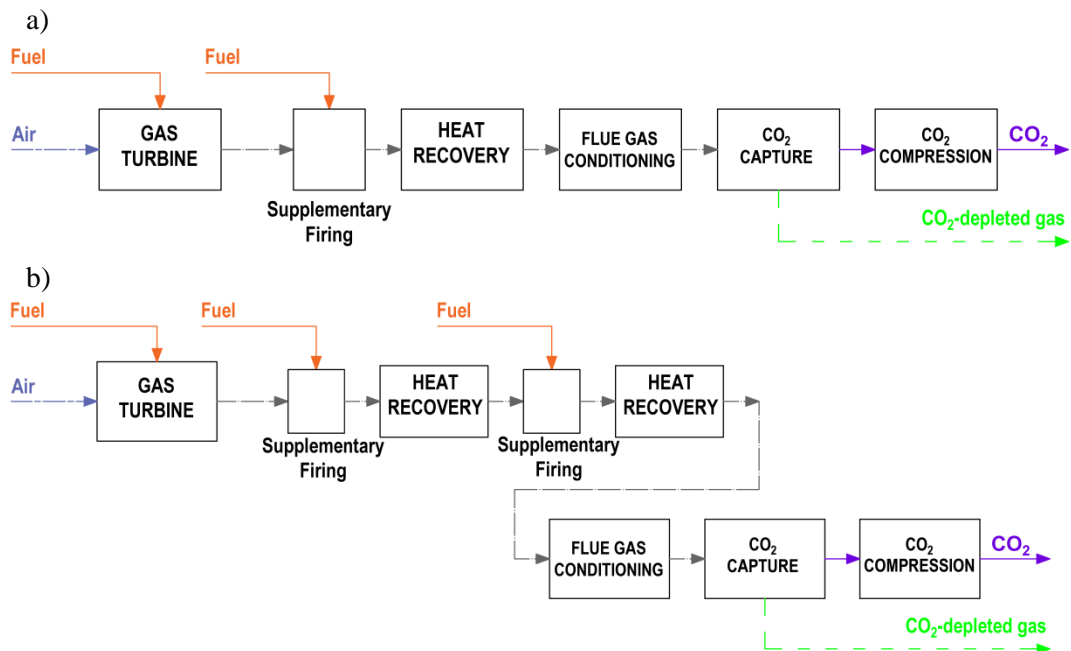


Figure 2.2.- Block flow diagrams of a CCGT plant with (a) Supplementary firing and (b) Sequential supplementary firing.

Externally fired gas turbine cycles are also proposed to burn natural gas or other fuels in an external combustor with a lower excess of air, since cooling air for the turbine blades is not required. The combustion gases do not pass through the turbine and the heat is transferred to the compressed air through indirect contact heat exchangers. This option has a minimum impact on the turbomachinery. The need for ceramic materials that withstand the combustion high temperature and the heat losses make however this option not suitable for power generation with currently available gas turbine technology.

An option combining the technologies of SFCC and EGR at 35% recirculation ratio to a CCGT power plant (Biliyok & Yeung 2013) would not be feasible due to the significant reduction in the oxygen concentration in the combustor, as the oxygen content in recycling flue gas drops significantly after the additional natural gas combustion in in-duct burners.

2.2.4. Selective Exhaust Gas Recirculation

Selective exhaust gas recirculation (S-EGR) has recently been proposed as an alternative to further increase the CO₂ concentration in the exhaust flue gas above the maximum value that can be achieved with “non-selective” EGR, with a small reduction in the oxygen level in the gas turbine combustor. This strategy consists of selectively transferring CO₂ from the flue gas stream into the air stream entering the gas turbine compressor. Since other components in the flue gas, mainly nitrogen and water vapour, are not recirculated, less amount of excess air is replaced and the oxygen concentration in the combustor remains above the limiting value of 17 % vol, reported for EGR, for a wide range of CO₂ concentrations in the flue gas.

Merkel and co-workers propose two configurations to implement S-EGR in CCGT power plants with post-combustion capture systems (Baker et al. 2011; Wijmans et al. 2011; Wijmans, Merkel and Baker 2012; Merkel et al. 2013):

- A configuration consisting of diverting a fraction of the exhaust of the HRSG into a device transferring CO₂ into the inlet air stream of the gas turbine compressor. The selective CO₂ transfer unit operates “in parallel” to the post-combustion capture process.
- A configuration consisting of a selective CO₂ transfer unit operated downstream of, and “in series” to, the post-combustion capture process.

The block flow diagram for a CCGT with S-EGR in parallel and S-EGR in series is illustrated in Figure 2.3(a) and Figure 2.3(b), respectively.

Alternative configurations combine S-EGR either in series or in parallel with “non-selective” EGR (Wijmans et al. 2012a; Wijmans et al. 2012b). For steady state operation, these configurations result in a lower CO₂ concentration in the flue gas at a given oxygen concentration in the combustor. They are however interesting to be investigated for the start-up of a CCGT plant with PCC and S-EGR. Merkel and co-workers claim that CO₂ concentrations of approximately 19 vol% and 14 vol% are possible in the flue gas feed to the PCC unit, with S-EGR in parallel and S-EGR in series, respectively, maintaining the oxygen level in the gas turbine combustor at 16 vol%. In order to achieve these concentration, it is necessary to operate at a large selective recirculation ratio and considerably high efficiencies in both the post-combustion capture unit and the selective CO₂ transfer device (Merkel et al.

2013). The selective exhaust gas recirculation ratio is defined as the flow rate of the diverted flue gas to the selective CO₂ transfer unit over the flow rate of the flue gas leaving the gas turbine, before cooling and condensation of the excess of humidity, Equation [2.2].

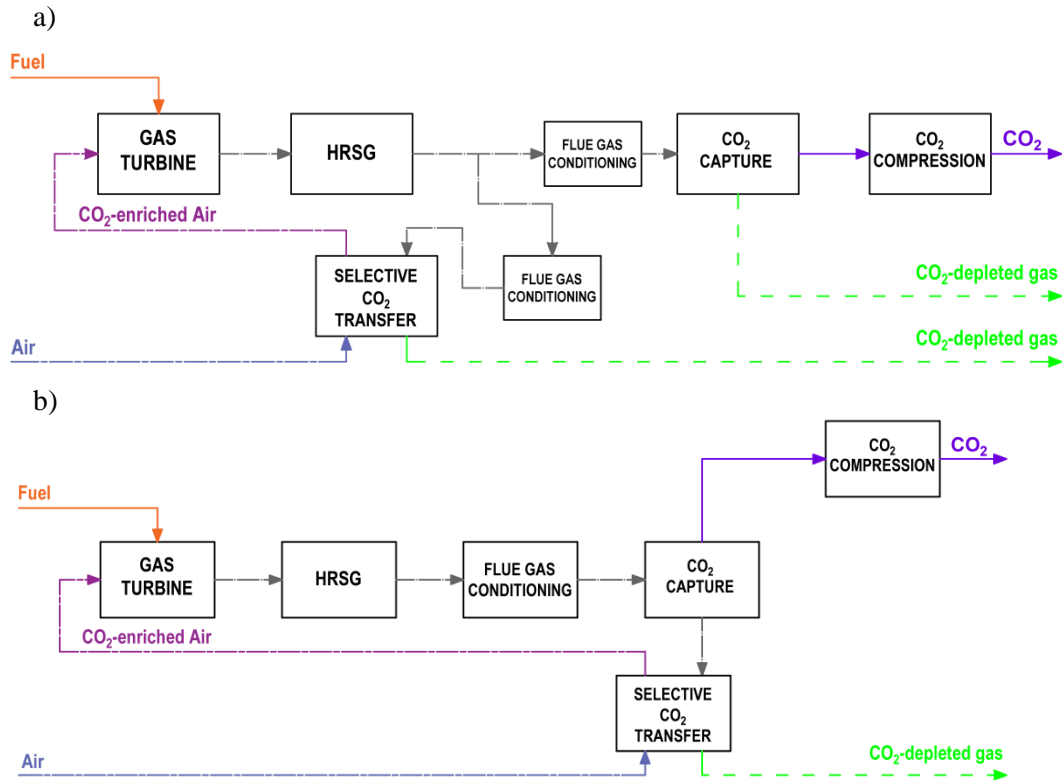


Figure 2.3.- Block flow diagrams for the flue gas CO₂ enriching strategies of (a) S-EGR in parallel and (b) S-EGR in series.

$$S - EGR \text{ ratio} = \frac{\text{mass flow of flue gas to selective CO}_2 \text{ transfer system}}{\text{mass flow of exhaust flue gas}} \Bigg|_{\text{HRGS outlet}} \quad [2.2]$$

This thesis provides a broader overview of the integrated process of a CCGT with S-EGR in parallel and S-EGR in series, in order to define an operating framework for each configuration that identifies the range of CO₂ potentially achievable in the flue gas and the minimum requirements for both the CO₂ capture system and the selective CO₂ transfer system, within which S-EGR presents advantages compared to EGR operating at 35% recirculation ratio.

Little detailed information is provided concerning the effect of S-EGR on the gas turbine performance, and practical limitations, e.g. minimum oxygen in the comburent or cooling air bypass in the combustor, are not taken into account in previous publications. Similar to EGR, the strategy of S-EGR results in different inlet conditions at the gas turbine compressor and

different working fluid composition and properties, compared to operation at design point. The effect on the compressor and turbine performance of S-EGR and, thus, of a significantly higher CO₂ concentration in the working fluid, need to be investigated in more detail. This work extends the procedure followed by Jonshagen and co-workers (Jonshagen et al. 2011) to investigate the gas turbine performance with S-EGR.

The combustion effects associated with S-EGR are, similarly to EGR, changes in operability, flame stability, combustion efficiency, CO, UHCs and NO_x emissions. The chemistry of CO₂ replacement of N₂ in air for natural gas/CH₄ combustion on premixed (Liu et al. 2003; Min et al. 2011) and non-premixed (Masri & Barlow 1992) flames has been investigated for oxy-fuel combustion. It is concluded that CO₂ does not only act as diluent but also participate in the combustion reaction mechanism, increasing CO emissions, and varies the transport and thermal properties of the fuel-comburent mixture. Operating conditions in previous work, e.g. high CO₂ concentrations above 30 vol% and atmospheric pressures, are however different from the conditions in the combustor with S-EGR application and there is a clear need of more experimental investigation. This is outside of the scope of this thesis and it is currently being investigated within the scope of the EPSRC project “Selective Exhaust Gas Recirculation for Carbon Capture with Gas Turbines: Integration, Intensification, Scale-up and Optimisation” (SELECT 2014). The combustion behaviour of premixed CH₄/Oxyfuel flames have also been investigated concluded that the O₂ concentration in CO₂ has to be larger than the 21 vol% in air for the stabilization of the flame, due to the larger heat capacity of CO₂ compared to nitrogen which result in lower combustion temperature and lower laminar flame speed (Kutne et al. 2011).

A summary of the strategies to increase the CO₂ concentration in the flue gas explained in this section is included in Table 2. Exhaust Gas Recirculation and Selective Exhaust Gas Recirculation are the options considered in this thesis base on the ease of integration with current state of CCGT power plants, the relatively small penalty in the thermal efficiency of the combined cycle and the range of CO₂ concentrations that could potentially be achieved in the flue gas.

Table 2.1.- Comparison of strategies to increase CO₂ concentration in the exhaust flue gas from a gas turbine, from the power plant point of view.

<i>Key challenges:</i>		<i>Strategy:</i>					
		Exhaust gas recirculation	Evaporative Gas Turbines	Supplementary fuel combustion	Sequential supplementary fuel combustion	Selective Exhaust Gas Recirculation in Parallel	Selective Exhaust Gas Recirculation in Series
<i>Impact on combustion</i>	<i>Comburent composition compared to air-combustion</i>	Low O ₂ conc. ≈ 16-17 vol% and moderately high CO ₂ conc. ≈ 2-3 vol%	Low O ₂ conc. and high H ₂ O conc.	Low O ₂ conc. ≈ 12 vol% in secondary combustor	Low O ₂ conc. < 12 vol% in secondary combustors	Low O ₂ conc. ≈ 18 %vol and considerably high CO ₂ conc. ≈ 10 vol%	Low O ₂ conc. ≈ 18 %vol and considerably high CO ₂ conc. ≈ 10 vol%
	<i>Potential problems</i>	Flame stability, CO and UHC emissions, soot formation	Flame stability, CO and UHC emissions, soot formation	Combustion in in-duct burners benefits from high flue gas temperature	Combustion in in-duct burners benefits from high flue gas temperature	Flame stability, CO and UHC emissions, soot formation	Flame stability, CO and UHC emissions, soot formation
	<i>NO_x reduction</i>	yes	yes	yes	yes	yes	yes
<i>Impact on compressor and turbine</i>	<i>Deviations from design operation point due to:</i>	Compressor inlet conditions and working fluid composition	Increase in turbine mass flow affects pressure ratio and working fluid composition	None	None	Compressor inlet conditions and working fluid composition	Compressor inlet conditions and working fluid composition
<i>Impact on CCGT efficiency</i>	<i>Compared to conventional CCGT with PCC</i>	Small increase	Moderate reduction in combined cycle	Significant reduction of several percentage points	Significant reduction of several percentage points	Not investigated/ not available	Not investigated/ not available
	<i>Main effect</i>	Increase in compressor inlet temperature	Lower heat available in HRSG or steam extraction for injection	Reheated flue gas only generates work in the steam cycle	Reheated flue gas only generates work in the steam cycle		
<i>Impact on the CO₂ capture process</i>	<i>Max. CO₂ conc. achievable</i>	Up to 6 vol%	Up to 6 vol%	Up to 6 vol%	Up to 9 vol%.	Up to 18-20 vol%	Up to 18-20 vol%
	<i>Flue gas flow rate reduction</i>	Up to 35%	Moderate	Moderate	Up to 50%	Up to 70%	None

Table 2.1.-Comparison of strategies to increase CO₂ concentration in the exhaust flue gas from a gas turbine, from the power plant point of view (cont.)

<i>Operating variable to increase CO₂</i>	Recirculation ratio	Water to Air ratio	Additional natural gas fired	Additional natural gas fired	Recirculation ratio and selective CO ₂ transfer efficiency	Selective CO ₂ transfer efficiency
<i>Limiting factor</i>	Min. O ₂ level in the combustor	Min. O ₂ level in the combustor and water/steam injection system	Max. temperature limited by metallurgical constraints in the HRSG	Min. O ₂ excess in flue gas for complete combustion of the fuel in in-duct burners	Max. practical efficiencies in PCC and selective CO ₂ transfer process. Max. CO ₂ level in the combustor for operating O ₂ conc.	Max. practical efficiencies in PCC and selective CO ₂ transfer process. Max. CO ₂ level in the combustor for operating O ₂ conc.
<i>Technology readiness</i>	Experimental work reach industrial scale burners	Process modelling. Further development of the burners required for combustion efficiency.	Commercially available	Process modelling	Process modelling	Process modelling

2.3. Effects of CO₂ concentration on the PCC performance: EGR and S-EGR options

Increasing CO₂ concentration in the exhaust flue gas from natural gas-fired power plants has been identified as an effective method to decrease the equipment size and the energy consumption for CO₂ capture. This would result in a reduction of capital and operation cost and the power output and efficiency penalty associated to the CO₂ capture system (Li, Haugen, et al. 2011).

The operation and cost benefits of implementing EGR and S-EGR in CCGT power plants is investigated in literature with two post-combustion CO₂ capture technologies: chemical absorption with amine-based aqueous solvents (Aboudheir and ElMoudir 2009; Li, Ditaranto, et al. 2011a; Sipöcz and Tobiesen 2012; Biliyok and Yeung 2013; Vaccarelli et al. 2014), and CO₂ selective membrane system (Belaissaoui et al. 2013; Merkel et al. 2013; Voleno et al. 2014; Swisher and Bhowan 2014).

For chemical absorption with a 30 wt% aqueous solution of monoethanolamine (MEA), process model simulations and experimental tests have been conducted to quantitatively determine the reduction in the specific reboiler duty and the size of the absorber column with increasing the flue gas CO₂ concentration. The specific reboiler duty is defined as the thermal energy required to regenerate the solvent per unit of mass of CO₂ recovered, as shown in Equation [2.3],

$$\text{Specific Reboiler Duty} = \frac{\text{Thermal energy rate}}{\text{CO}_2 \text{ mass flow}} ; \left[\frac{\text{MJ}}{\text{kgCO}_2} \right] \quad [2.3]$$

Process modelling of the integrated process showed that a significant decrease in the specific reboiler duty occurs when the flue gas CO₂ concentration increases up to 6 vol%. Beyond this concentration, the specific reboiler duty continues to decrease, but at a considerably lower rate. Li and co-workers reported that EGR operating at 50% recirculation ratio leads to a reduction in the flue gas mass flow rate entering the absorber of 51% with an increase in the CO₂ concentration from 3.8 vol% to 7.9 vol%. This results in a 8% reduction of the thermal energy consumption, from 4 to 3.7 MJ/kg_{CO2} (Li, Haugen, et al. 2011a).

The simulations performed at SINTEF/NTNU demonstrated the possibility to decrease both the thermal energy requirements and the dimensions of the CO₂ capture plant with EGR, attenuating the overall thermal efficiency penalty (Sipöcz and Tobiesen 2012). At 40% EGR ratio, the higher CO₂ concentration of 7.8 vol%, compared to 4.4 vol% without EGR, in a

saturated flue gas entering the absorber at 42 °C results in a decrease in the reboiler duty of 9%, from 3.97 to 3.64 MJ/kg_{CO2}. The reduction in the packing volume in the absorber is approximately equal to the fraction of EGR, slightly below 40%.

The model developed by Biliyok and Yeung suggests that, operating at 40% EGR ratio, an increase in the CO₂ concentration from 4 vol% to 6.6 vol% in a saturated flue gas fed the absorber at 40 °C, decreases the reboiler duty by 7.5%, from 4 to 3.72 MJ/kg_{CO2} (Biliyok and Yeung 2013).

An additional advantage of EGR is that the smaller O₂ concentration in the flue gas may reduce the rate of amine solvent chemical degradation compared to conventional configurations, which lowers operational costs (Li, Haugen, et al. 2011).

For an accurate and consistent quantitative evaluation of the reduction in the thermal energy consumption with EGR, it is important to define a common base case for the power system and the capture plant. Design parameters, such as the temperatures in the gas turbine, determine the increase in the flue gas CO₂ concentration for a given recirculation ratio. Moreover, the optimisation criteria for sizing the absorption and evaluation the optimum CO₂ loading in the regenerated solvent determines the energy reduction.

The effect of increasing the flue gas CO₂ concentration has been experimentally investigated at pilot plant scale with 30 wt% aqueous MEA scrubbing technology. The absorber feed stream consists of either synthetic flue gas (Notz et al. 2012) or exhaust flue gas from a natural gas-fired microturbine (Akram et al. 2016). Since microturbines typically operate at lean combustion conditions, additional CO₂ injection was required to achieve different CO₂ concentration within a range of EGR ratios.

Results from an experimental campaign carried out at the Pilot-scale Advance Capture Technology (PACT) facilities at the UK Carbon Capture and Storage Research Centre (UKCCSRC) shows a reduction in the specific reboiler duty of around 7.1% relative per unit vol% increase in CO₂ concentration (Akram et al. 2016), while the largest drop in the reboiler duty being observed from 7.1 to 5.3 MJ/kgCO₂ when the CO₂ concentration is increased from 5.5 to 9.9 vol%. This reduction in reboiler duty highly dependent to the pilot plant dimensions and the operational conditions, and neither the absorber packing height nor the solvent flow rate were optimised to the minimum reboiler duty for the reference case.

S-EGR allows for a significantly higher flue gas CO₂ concentration compared to EGR. Typical concentrations of 13-14 vol% in flue gas from coal-fired power plants are possible at

certain operating conditions with S-EGR. Yet, operating parameters in the capture process, such as the ratio of solvent to flue gas mass flow rate in the absorber, may differ.

The effect of S-EGR on the CO₂ capture plant with aqueous MEA scrubbing technology is investigated by Merkel and co-workers. A sensitivity analysis of the effect of a higher CO₂ concentration in the flue gas on the energy consumption is investigated for a range of concentrations up to 30 vol%, and evaluated in terms of the ideal minimum energy for CO₂ separation, compressor and liquefaction. The minimum energy thermodynamic analysis corresponds to the difference between the Gibbs free energy between two states, i.e. the flue gas at the PCC inlet and the CO₂ after compression and liquefaction. They reported that, for 90% capture, the ideal minimum energy of separation is reduced by 42% with the configuration of S-EGR in parallel when the flue gas CO₂ concentration increases from 4 vol% to 19 vol% (Merkel et al. 2013). In this thesis, a rigorous quantitative analysis is conducted to investigate the effect of S-EGR on the CO₂ capture process for the configurations with S-EGR operating in parallel and in series.

2.4. Strategies to reduce water requirements in CCGT power plants with PCC

Post-combustion carbon capture systems based on chemical absorption with amine-based solvents require additional cooling capacity for the exhaust flue gas entering the absorber column, water wash system, absorber intercooler, lean solvent cooler, reflux reboiler condenser and CO₂ compressor interstage coolers. The cooling water demand will therefore drastically increase if CCS technology is added to thermal power plants with either one-through cooling systems or a recirculating cooling system with evaporative cooling towers, unless dry cooling systems are used. Recent publications reported an increase in cooling water usage from 50 to 90% when post-combustion carbon capture with chemical absorption technology is integrated in a natural gas-fired power plant, comparing to an unabated natural gas-fired plant of similar capacity (Zhai & Rubin 2010; Zhai et al. 2011; Macknick et al. 2012; Cormos et al. 2013; Byers et al. 2014; Schakel et al. 2015).

In CCGT plants without CO₂ capture, flue gas typically leaves the heat recovery steam generator (HRSG) at a temperature ranging from 80 to 150 °C. The exhaust flue gas temperature is sufficiently high to rise through the stack by buoyancy effects and meet the regulatory requirements of stack plume visibility that exists in some jurisdictions. When CO₂ capture with amine-based chemical absorption is implemented, the temperature of the flue

gas entering the absorber has to be adapted to the specific solvent. The exhaust flue gas is typically cooled down by means of a direct contact cooler (DCC) to an optimal temperature, which is a trade-off between kinetic reaction rate and enhanced thermodynamic capacity. Temperatures ranging from 35 °C (NETL 2011; IEA 2012) to 45 °C (Kvamsdal et al. 2010; Plaza et al. 2010; Sanchez Fernandez et al. 2014) have been reported for an aqueous solution of monoethanolamine. Temperatures as high as 50 °C have also been presented in pilot plant data (Notz et al. 2012). A large volume of process and cooling water is therefore required in the direct contact cooler.

At the outlet of the absorber, the CO₂-depleted gas typically leaves at a temperature similar to the inlet flue gas. A water wash section is located at the top of the absorber to avoid solvent losses into the atmosphere and to maintain the water balance of the system. The CO₂-depleted gas is then either directly released into the atmosphere through a wet stack, e.g. in (Huizeling and Van der Weijde 2011), or is reheated to increase the buoyancy of the gas to ensure dispersion and avoid plume visibility in a dry stack design, e.g. in (IEA 2012). The temperature of the gas stream entering the stack depends on the requirements for plume rise and dispersion, driven by the national/regional legislation and geographical location of the plant.

Process water integration options to reduce make-up process water requirements and waste water production have been investigated for PCC systems with a DCC upstream of the absorber. Kvamsdal and co-workers (Kvamsdal et al. 2010) focused their study in natural gas-fired units with PCC for offshore operations, where access to fresh water constitute a limiting factor and yet there is not restriction on sea water abstraction. These options consist of producing process water from the flue gas in the DCC, by cooling the gas down to a temperature lower than dew point, at the expense of increasing the cooling duty. The produced process water, along with a fraction of the reflux water in the stripper column condenser and some condensed water from the knock-out drums in the compression section, are used as a source for make-up water, e.g. for the absorber water wash section, maintaining a close to neutral water balance.

With the purpose of reducing or eliminating both process and cooling water requirements in the DCC upstream of the CO₂ absorber, and ensuring that the flue gas reaches an appropriate temperature at the stack, this work proposes a heat integration option transferring heat from the gas stream entering the absorber to the gas stream leaving the absorber. This can be achieved with the use of rotary regenerative gas/gas heat exchangers; a technology widely used in coal fired power plants to increase boiler efficiency. A thermal performance analysis

and sizing of the rotary heat exchanger is conducted for two configurations of natural gas-fired power plants:

- A conventional (air-based combustion) CCGT power plant with post-combustion capture
- A CCGT power plant with post-combustion capture using Exhaust Gas Recirculation.

In a CCGT with EGR, the recirculated gas stream is typically cooled down before it is mixed with ambient air, as lower inlet temperature favours compressor and increases gas turbine power output. Due to the higher water content in the gas turbine exhaust with EGR, cooling water requirements increase (Aboudheir and ElMoudir 2009). In previous work, little consideration has been given to optimising heat and water management of the flue gas loop. The same cooling equipment is typically used for both streams (IEAGHG 2004; Jordal et al. 2012). Recent studies have, however, proposed the recycling of exhaust gas at lower temperatures, with two direct contact coolers of smaller size introduced to the process (IEAGHG 2012).

2.5. Novel application for adsorption systems in Selective Exhaust Gas Recirculation

The technology proposed for S-EGR in recent work consists of CO₂ selective polymeric membranes (Merkel et al. 2013) and solvent supported membranes (Voleno et al. 2014; Swisher and Bhowan 2014; Zhang et al. 2016). Merkel and co-workers report a good performance of a specifically developed membrane at laboratory scale with a low energy input, operating with a moderate ratio of feed pressure to permeate pressure, compared to the pressure ratio that is required when membranes are used to separate the CO₂ for final capture and sequestration, which is typically higher than 4 bar (Voleno et al. 2014). In S-EGR application, the flue gas is compressed to overcome the pressure drop through the membrane system, to approximately 100 mbar. The reason is that a higher CO₂ permeance at the expense of a lower CO₂/N₂ selectivity is acceptable for this application and, thus, it is possible to operate with a moderate difference between the CO₂ partial pressure in the flue gas and in the air, i.e. pressure-ratio limited region, (Baker 2004). This explains the smaller power consumption and size of the compressor, used mainly to overcome the pressure drop through the membrane system, in comparison to the compressors used in a membrane system for CO₂ capture (Merkel et al. 2013).

In principle, any technology relying on the difference of CO₂ partial pressure between flue gas and ambient air streams as the driving force for selective CO₂ transfer, and using an air

stream as the sweep stream for selective CO₂ recycle can potentially be used for S-EGR application. There is therefore an opportunity for existing or new technologies to be adapted or developed for this application.

Adsorption with CO₂ selective porous materials is proposed in this thesis as an alternative to selective CO₂ membrane systems. The relatively low CO₂ partial pressure in the exhaust flue gas from natural gas-fired power plants also raise difficulties for CO₂ capture with adsorption systems. Extensive research work has been focused on improving solid materials by increasing surface area, improving pore structure and/or introducing chemical modifications on the surface to increase the working capacity and CO₂ selectivity over nitrogen and oxygen (Mangano et al. 2013; Abanades et al. 2015). Recent adsorbent materials present strong physical or chemical interactions with CO₂ molecules and, thus, the regeneration of the material is conducted by decreasing the pressure (pressure swing adsorption) or increasing the temperature (temperature swing adsorption). Yet an important aspect for S-EGR applications is balancing the affinity for CO₂ and the energy requirements for regeneration (Ben-Mansour et al. 2016).

S-EGR implies that the regeneration of the adsorbent is conducted with ambient air at near ambient temperature and pressure so that a CO₂-enriched air stream is recycled back to the gas turbine compressor. Physical adsorption appears therefore as an interesting option, since CO₂ is adhered to the adsorbent surface by means of van der Waals forces. The relatively weak interaction requires reduced amount of energy for regeneration, compared to chemisorption that implies new covalent bonds formed between the sorbate and the sorbents. Although a weak adsorbent-adsorbate interaction is detrimental to the CO₂/N₂ selectivity (Dantas et al. 2011), the difference in nitrogen partial pressure between a flue gas and an air streams is small and low nitrogen transfer rate is expected in S-EGR applications.

The selection of the material usually precedes the process design. An overview of existing materials is presented Section 2.5.1, and a description of the possible configurations is included in Section 2.5.2.

2.5.1. Adsorbents for CO₂ capture from CCGT exhaust flue gas

Several types of adsorbent materials have been proposed for CO₂ capture from diluted gas streams and extensive review work has been conducted (Samanta et al. 2012; Hedin et al. 2013; Abanades et al. 2015; Ben-Mansour et al. 2016). In this thesis, commercially available physical adsorbents are considered to investigate the concept of selective CO₂ transfer. A comparison of three classes of adsorbent materials: zeolites, metal-organic frameworks

(MOFs) and activated carbon, is included in Table 2.2. Based on their commercial availability and cost, zeolite and activated carbon are selected.

Carbon based materials, such as activated carbon, have been extensively investigated for CO₂ capture due to their wide availability and low cost, as they can be produced from numerous carbon-based naturally existing or spent materials (Ben-Mansour et al. 2016). Their advantages are the high thermal stability and the low sensitivity to moisture, due to the hydrophobic or non-polar nature (Marx et al. 2013; Xu et al. 2013). Activated carbon present moderate selectivity for CO₂/N₂, yet low adsorption capacity for CO₂ at low pressures, e.g. typically less than 0.5 mol/kg at 0.1 bar and 40 °C (Abanades et al. 2015). This is due to relatively uniform electric potential on the surface, which also results in a lower enthalpy of adsorption for CO₂. Their high surface area, however, leads to a great adsorption capacities at high pressures. An advantage for S-EGR is that due to the relatively small heat of adsorption for CO₂, activated carbon generally requires a relatively lower regeneration temperature, compared to zeolites or metal-organic frameworks (MOFs).

The introduction of surface modifications or localised charges, i.e. cations in zeolites or open metal sites in metal-organic frameworks, allows to increase the selectivity for CO₂ and the absolute amount of CO₂ adsorbed can reach values of 2 mol/kg at 0.1 bar and 40 °C. The main drawback is that Zeolites and MOFs are hydrophilic adsorbents and their actual adsorption capacity is significantly reduced in the presence of moisture in the gas. On polar adsorbents, water adsorption is much stronger and can displace adsorbed CO₂.

Zeolites are crystalline microporous aluminosilicates with large internal specific surface area and porous volume. The synthetic zeolites 5A (CaA) and 13X (NaX) have been widely investigated for CO₂ capture. They present a moderate capacity for CO₂ adsorption but a low CO₂ selectivity. The adsorption capacity varies with its composition and structure, which can be modified by changing the ratio of silica to alumina (SiO₂/Al₂O₃) and by the presence of cations. The alumina gives the framework a negative charge that is balanced by cations such as Na⁺. Zeolites with a high Si-to-Al ratio of the order of 7-10 are more hydrophobic but present a smaller capacity for CO₂ adsorption compared to zeolites with a lower Si-to-Al ratio, typically 1.3 for Zeolite X (Xu et al. 2013).

Metal-organic frameworks (MOFs) have recently attracted significant interest due to their high surface area and pore size which results in a considerably high adsorption capacity and good diffusional properties, compared to zeolites and carbon based materials. Moreover, they present adjustable pore size, structure and surface properties, which can be modified by

changing either the metallic cluster or the organic ligand. MOFs are however generally instable in the presence of moisture (Ben-Mansour et al. 2016).

At laboratory scale, novel adsorbent materials, specifically designed for CO₂ capture from flue gas in natural gas-fired power plants, are being synthesized and characterized as part of the EPSRC project “Innovative Gas Separation for Carbon Capture” (IGSCC 2012), which is a UK research consortium aiming to develop novel materials for absorption, adsorption and membrane separation processes (Mangano et al. 2013; Gibson et al. 2016).

Research on stable adsorbent materials under moisture conditions is also being conducted, along with options to remove the water from the flue gas prior entering into contact with hydrophilic adsorbents such as:

- The use of a “water guard” section in the absorber column made of a suitable material that can be easily regenerated, e.g. alumina or silica gel, in order to prevent water front from moving into the CO₂ adsorption section of zeolite (Xu et al. 2013).
- The addition of flue gas dehydration system to process, which consist of a direct contact cooler followed by a unit operation which consists of either refrigeration, compression and cooling, membranes separation or TEG (triethylene glycol) absorption (Hasan et al. 2012). The water content in the flue gas can be reduced to 0.1 %vol from saturation conditions in the direct contact cooler, however this additional equipment introduces further capital and running costs, therefore economic analysis is required.

Table 2.2.- Comparison of physical adsorbents for CO₂ capture (Ben-Mansour et al. 2016)

Material/ Specifications	Zeolites	Carbon-based materials	MOFs
<i>Major application</i>	H ₂ production	High pressure CO ₂ adsorption flue gas	CO ₂ separation
<i>Capacity</i>	Moderate	Lower than Zeolites at low pressure and gets higher at high pressures	High
<i>CO₂/N₂ selectivity</i>	Low	Moderate	High
<i>Energy for regeneration</i>	Significant	Lower temperature for regeneration compared to zeolites. Better energy efficiency compared to metal oxide	Limited by low temperatures for regeneration, but still low economic efficiency
<i>Stability under moisture conditions</i>	Reduced capacity	No decreased capacity under moist conditions	Mainly unstable: improvement under research.
<i>Cost</i>	Low production cost	Reasonable cost	Expensive
<i>Advantages</i>	- Large micropores/ mesopores - Medium CO ₂ adsorption at ambient conditions	- High thermal and chemical stabilities - Light weight with high surface areas as well as large pore volumes - Low energy consumption	- Possibility of tuning the pore size - Large surface area
<i>Disadvantages</i>	- Adsorb water, so CO ₂ adsorption is reduced at presence of moisture - High energy for regeneration	- Low CO ₂ adsorption capacity compared to some types of Zeolites and MOFs	- Synthesis is tedious and complicated - Low economy efficiency - Need further investigation at large scale applications

2.5.2. Adsorption in rotary systems

Adsorption separation processes typically use packed bed columns or circulating fluidised bed columns. Pressure/vacuum swing adsorption (PSA/VSA) is most suitable for packed bed (Dantas et al. 2011; Delgado et al. 2011), while thermal swing adsorption (TSA) can be performed in either packed bed (Serna-Guerrero et al. 2010) or circulating fluidized bed (Veneman et al. 2012) configurations.

The concept of rotary adsorption has been employed for air dehumidification systems (Kodama et al. 2001; Ge et al. 2008) and volatile organic compounds (VOCs) abatement systems (Yamauchi et al. 2007). In rotary adsorption, structured adsorbents are used in the form of adsorbent sheets or monoliths. The regeneration of the solid material is performed by increasing the temperature. Monolithic adsorbent offer practical advantages over traditional packed adsorbent columns for applications due to their low pressure, which has a significant economic impact (Brandani et al. 2004; Rezaei et al. 2010).

Thermal swing adsorption in a rotary wheel configuration for the application of CO₂ capture has been described in several patents developed by InvenTys (Boulet and Khiavi 2015) and has been investigated by experimental and modelling approach in the “Next Generation CCS

Technology” project (NGCT2 2016), which is a consortium of three engineering companies, InvenTys Thermal Technologies, Howden Group and Doosan Power Systems, and is based on using InvenTys patented Veloxotherm™ technology (Inventys 2016). A schematic diagram of the CO₂ separation process is illustrated in Figure 2.4. In this application, the rotary wheel configuration offers the advantage of a rapid response to thermal swing and a hot stream of vapour and/or air can be used for the regeneration of the adsorbent (Boulet and Khiavi 2015). The process of rotary adsorption for CO₂ capture has also been investigated and tested in a laboratory scale prototype in the EPSRC project “Adsorption Materials and Processes for carbon capture from Gas-fired power plants” (AMPGas 2012) at the University of Edinburgh. The objectives of this project are to develop advance adsorbents capable to capture CO₂ from diluted flue gas in natural gas-fired power plants and to optimise rapid thermal swing regeneration using rotary wheel adsorbers (Gibson et al. 2016).

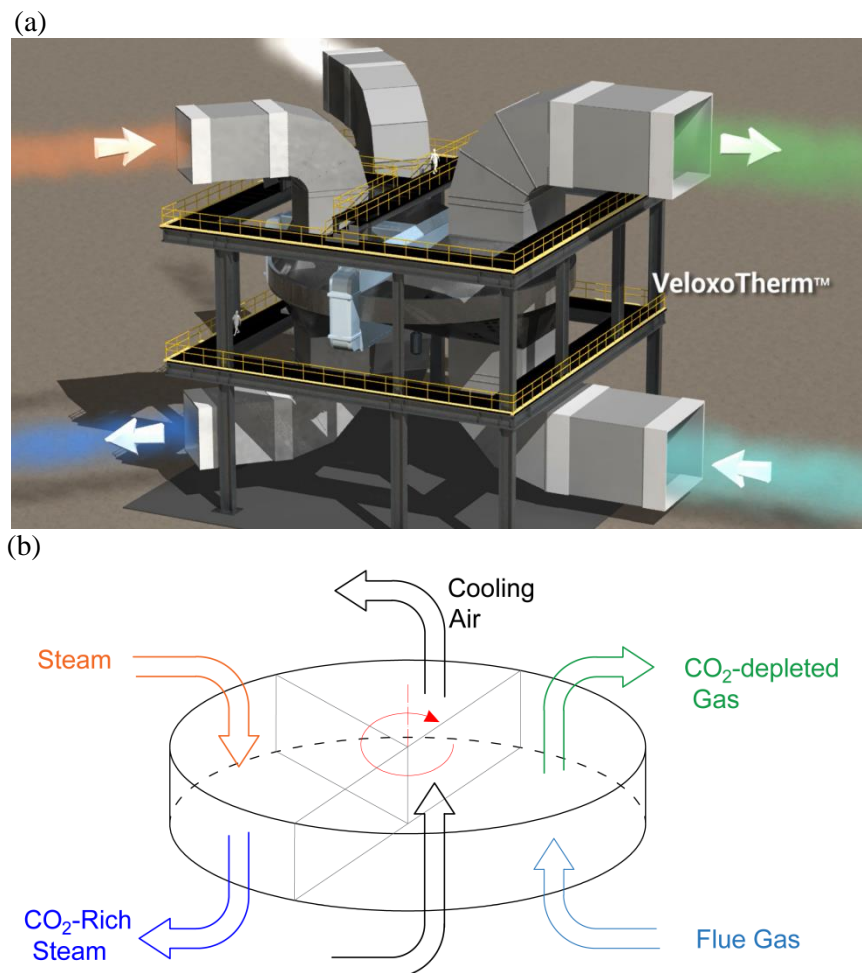


Figure 2.4.- VeloxoTherm™ process (InvenTys 2016) (a) and schematic diagram of the CO₂ separation process (b).

For large-scale industrial applications, rotary wheel equipment have been dimensioned, implemented and operated in heat exchange applications for large volume of flue gas typically generated in thermal power plans, e.g. regenerative rotary gas/gas heat exchangers typically used in coal-fired power plants, as explained in Section 2.4. This suggests that the scale-up of this technology is likely to be possible from a structural point view.

The objective of this work is to investigate physical adsorption in rotary wheel configurations is for the application of S-EGR. Since rotary systems constitute a relatively simple structure to perform the cycle of adsorption/desorption and offers the advantage of relatively fast heat transfer and the possibility of cooling the material while it is being regenerated with ambient air. Additionally, structure adsorbents present a relatively small pressure drop and the relatively simplicity of the process may lower the capital costs, compared to conventional systems (Boulet and Khiavi 2015). For this purpose, a conceptual design is developed to assess the practicability and feasibility of using rotary adsorption for the novel application of selective CO₂ transfer. This sets the basis to further evaluate the advantages of S-EGR to reduce energy consumption and/or capital and operational costs in CCGT power plants with PCC.

2.6. Current state and gaps in knowledge

Key concepts and current level of understanding for the three aspects in gas CCS, investigated in this thesis and explained in more detail in the literature review conducted in previous sections, are summarised in Table 2.3. Gaps in knowledge have been identified to define the research objectives described in Section 1.4.

- Exhaust gas recirculation (EGR) has been widely investigated as a technology to increase CO₂ concentration in gas turbine exhaust flue gases. Process model simulations have been conducted to investigate the effect on the performance of the power plant and the benefits in the post-combustion CO₂ capture system with chemical absorption using MEA based. Experimental work has been focused on the combustion system. Experimental work is therefore still required on the power plant performance and the capture process. EGR is investigated here in process simulations to set a common framework to assess the benefits of S-EGR over EGR.
- Selective Exhaust Gas Recirculation (S-EGR) has to be further investigated in process simulations using a rigorous model of a CCGT power plant and CO₂ capture system

with chemical absorption. An operating framework needs to be first identified to assess the possible range of CO₂ concentrations in the flue gas. S-EGR needs to be investigated in process simulations in a rigorous model of a CCGT power plant with CO₂ capture systems using solvent chemical absorption, in order to investigate the performance of currently available gas turbine engines with S-EGR and to quantify the operation and cost benefits of S-EGR. Process model simulations are conducted in this work, an economic analysis is however out of the scope of this work.

- S-EGR has been investigated for selective CO₂ membrane systems. Yet membrane systems require further investigation for industrial scale application. Alternatively, there is an opportunity for new technologies to be developed for this application, aiming to minimise capital and operational costs associated with the overall post-combustion CO₂ capture system. At the stage of concept development, the technical feasibility and practicality of rotary adsorption is investigated in this thesis. New adsorbent materials are likely to be required for S-EGR, and this work aims to provide guidelines for material developers as results of a parametric study.
- Options for heat and water management in post-combustion CO₂ capture systems with amine-based solvent need further investigation to minimise cooling and process water consumption. Dry-cooling options using rotary gas/gas heat exchangers with ambient air as the cooling fluid are investigated in this thesis to manage heat and water around the PCC process. Options to reduce water demand within the boundaries of the PCC process are out of the scope of this thesis.

Table 2.3.- Key concepts for CCS on CCGT power plants, level of understanding and gaps in knowledge

Key concepts for CCS on CCGT power plants	Level of knowledge / understanding	Gaps in knowledge
1.1.- Options for CO₂ enriching flue gas : Exhaust Gas Recirculation		
<i>Integration with the CCGT power plant: effect on the components of the power plant</i>		
<ul style="list-style-type: none"> • Compressor and turbine 	<p>Process model simulation of GE F-class [1](*) and Alstom reheat GT26 engines [2]gas turbine engines show:</p> <ul style="list-style-type: none"> ○ Small deviation of the compressor and turbine performance from the design point at 40% EGR. ○ Gas turbine performance is highly sensitive to the temperature of the recirculated flue gas stream. A higher temperature, compared to ambient temperature, reduces power output and efficiency [1, 2]. ○ Different working fluid thermodynamic properties (due to a high CO₂ and H₂O concentrations) results in an increase of the Gas Turbine (GT) exhaust temperature. 	<p>Experimental work still required at pilot plant scale (at least)</p>
<ul style="list-style-type: none"> • Combustion 	<p>Combustion process investigated in experimental tests in bench-scale lean premixed burner of the Dry Low-NOx combustor system employed in GE F-class [3, 4] and reheat combustion system of Alstom GT26 [2, 5].</p> <ul style="list-style-type: none"> ○ In GE F-class gas turbines combustor, 16-17 O₂ % vol required to ensure flame stability and acceptable CO and UHC emissions. It corresponds to 35% EGR ratio. 40% EGR ratio possible with minor modifications in the combustor system. ○ In Alstom GT26 lower O₂ levels are possible, as the reheated burner adds operational flexibility. 	<p>Experimental work required for combustion process at high pressure to investigate the effect on the minimum oxygen level possible in the combustor.</p>
<ul style="list-style-type: none"> • Steam cycle 	<p>Process model simulations shows that EGR results in a higher steam mass flow rate in the HRSG and steam turbines (ST) power output [1, 2], due to an increase in the GT exhaust temperature.</p>	
<i>Integration with the steam cycle: thermal energy supply</i>		
<i>Effect on post-combustion capture process</i>		
	<p>Process model simulation of the capture plant with 30 wt% aqueous MEA solvent and with a rate-based absorber model concluded [6, 7, 8] concluded that:</p> <ul style="list-style-type: none"> ○ An increase in CO₂ conc. from approx. 4 % vol to approx. 8 vol% at 40% EGR ratio results in a 8% approx. reduction in specific reboiler duty and 40% reduction of the absorber packing vol. 	<p>Common framework to in process model simulation is required for a consistent comparison of the effect on the PCC process</p>
	<p>Experimental work in pilot plant at PACT facilities (UKCCSRC) report a significant reduction in reboiler duty for a CO₂ conc. increase from 5 to 9 vol%. [9]</p>	<p>Experimental work required in a dedicated pilot plant designed for a typical CO₂ conc. in gas-fired power plants</p>
<p>* Key references are provided at the end of the table</p>		

Table 2.3.- Key concepts for CCS on CCGT power plants, level of understanding and gaps in knowledge (**cont.**)

Key concepts for CCS on CCGT power plants	Level of knowledge / understanding	Gaps in knowledge
1.2.- Options for CO₂ enriching flue gas : Selective Exhaust Gas Recirculation		
<i>Integration with the CCGT power plant: effect on the gas turbine component</i>		
<ul style="list-style-type: none"> Compressor and turbine performance 	No investigated/ no information available in literature	Effect of S-EGR on compressor and turbine performance requires further investigation, since S-EGR significantly increases CO ₂ conc. in working fluid and water is not transferred
<ul style="list-style-type: none"> Combustion 	Combustion tests performed for oxy-fuel combustion experimental conditions to evaluate the effect on flame stability [24, 25, 26] (*).	Combustion process at high CO ₂ conc. of approx. 10 vol%, maintaining O ₂ conc. at approx. 18 vol% needs to be experimentally investigated at high pressure and temperature
<ul style="list-style-type: none"> Steam cycle 	No investigated/ no information available in literature	Effect of S-EGR on heat available and steam production in the steam cycle needs to be investigated
<i>Integration with the steam cycle: thermal energy supply</i>		
Similar grade of integration as in air-based combustion CCGT power plant with PCC		
<i>Effect on post-combustion capture process</i>	<ul style="list-style-type: none"> For amine based chemical absorption: Investigated using the concept of minimum energy thermodynamic analysis for CO₂ separation, compression and liquefaction [10]. S-EGR using selective membranes for both selective CO₂ transfer and CO₂ capture has been investigated in more detail [10]. 	Further investigation of the effect of S-EGR on the PCC process based on chemical absorption, with a rate-base model for absorption
<i>Integration with selective CO₂ transfer system</i>		Parametric analysis to identify key operating parameters of the S-EGR system with a large effect on the CCGT plant performance with PCC
* Key references are provided at the end of the table		

Table 2.3.- Key concepts for CCS on CCGT power plants, level of understanding and gaps in knowledge (cont.)

Key concepts for CCS on CCGT power plants	Level of knowledge / understanding	Gaps in knowledge
2.- Technology for Selective CO₂ transfer process		
<i>Selective CO₂ membrane systems</i>	Process model simulations and lab scale experimental tests [10, 11, 12] (*) suggest good performance of specifically developed membranes. Trade-off between selectivity and permeance reduces the pressure ratio and power consumption. The estimated pressure drop of approx. 100 mbar is still high.	Further investigation to reduce capital and operational costs in industrial scale applications large scale applications. Technology options with small pressure drop.
<i>Physical adsorption in a rotary wheel configuration</i>	Adsorbent material development focused on CO ₂ capture process for Pressure/Vacuum or Thermal swing adsorption processes- with the aim of augmenting working capacity, affinity and selectivity for CO ₂ [13, 14, 15, 16].	Adsorbent materials needs to be developed for the specific application of CO ₂ transfer
	Rotary adsorption in a wheel for CO ₂ capture investigated in process model simulations and experimental tests at pilot plant scale, using chemical adsorbents and thermal swing regeneration [17, 18 19]	The concept of CO ₂ transfer from flue gas into air stream needs further investigation with process modelling and experimental work.
	Rotary wheels manufactured, implemented and operated at industrial scale for gas/gas heat transfer in coal-fired power plants [23]	Technology still needs to be adapted for rotary adsorption
3.- Water and heat management in Gas CCS with amine based CO₂ capture systems		
<i>Process water integration options in the CO₂ capture system</i>	Process model simulations performed to investigate process water integration options. The objective is to reduce water make-up in the CO ₂ capture system with amine based solvents[20]	Options to reduce cooling water demand in addition to the reduction in process water requirement need to be investigated
<i>Dry cooling options in power plant</i>	Air-cooled systems for steam turbines condensate and cooling water. Higher investment cost and lower performance compared to one-through cooling systems or recirculating cooling systems with wet cooling towers [21]	Options to reduce or completely eliminate cooling and process water requirements
<i>Reheat of the CO₂-depleted gas to the stack</i>	Heat supplied by the steam cycle, e.g. condensate return from the reboiler of the PCC system [22]	Heat integration options for heat transfer between gas streams need to be investigated
* KEY REFERENCES: [1] Jonshagen et al 2011; [2] Sander et al. 2011; [3] EIKady et al 2009; [4] Evulet et al 2009; [5] Burdet et al 2010; [6] Li, Haugen, et al 2011; [7] Sipöcz and Tobiesen 2012; [8] Biliyok and Yeung 2013; [9] Akram et al. 2016; [10] Merkel et al 2013; [11] Voleno et al 2014; [12] Swisher and Bhowan 2014; [13] Dantas et al 2011; [14] Delgado et al. 2011; [15] Serna-Guerrero et al. 2010; [16] Veneman et al. 2012; [17] Boulet and Khiavi 2015; [18] NGCT2 2016; [19] AMPGas 2012; [20] Kvamsdal et al. 2010; [21] IEAGHG 2010; [22] IEAGHG 2012; [23] Howden Group, 2016; [24] Liu et al. 2003; [25]Min et al. 2011; [26] Masri & Barlow 1992.		

System Design and Performance Modelling

3.1. Introduction

The assessment of the performance of the Combined Cycle Gas Turbine (CCGT) power plant integrated with Post-combustion Carbon Capture (PCC) systems and the CO₂-enriching technologies of Exhaust Gas Recirculation (EGR) and Selective Exhaust Gas Recirculation (S-EGR), requires developing a rigorous model of the power plant and the capture system. The linked model of the power plant and the capture system is illustrated in Figure 3.1, where the software used and the variables connecting the models are specified.

The model of the CCGT power plant is developed in gPROMS Model Builder (PSE 2016), as it is a process modelling software that allows creating customized models for each unitary operation. The process flow diagram as set up in gPROMS is shown in Figure 3.2. The fundamental principles and the equations used in building the models of each component constituting the power cycle are described in Section 3.2. A detailed description of the performance of each component is required to explain the methodology used in predicting the behaviour of the gas turbine at off-design conditions when either EGR or S-EGR are implemented. The gas turbine in the reference CCGT power plant is a General Electric F-class engines, since this engine has been widely used in literature (IEAGHG 2012) and a large amount of information is available. Exhaust flue gas composition and flow rate in the reference configuration and in the configurations with EGR and S-EGR are specific to the gas turbine engine, since design parameters, such as the turbine inlet temperature, define the excess of air, yet the assessment of the gas turbine performance is based on a non-dimensional analysis and, therefore, results would be valid for other gas turbine technology.

The post-combustion CO₂ capture plant use chemical absorption technology with an aqueous solution of monoethanolamine (MEA) and is modelled in Aspen Plus (Aspen Tech 2016). The process flow diagram for a conventional MEA based chemical absorption process, as set up in Aspen Plus, is illustrated in Figure 3.15. The capture plant configuration, the process modelling technical parameters and the design optimization procedure are described in Section 3.3.

The investigation of heat integration options for water demand reduction with regenerative rotary heat exchangers requires to conduct thermal performance analysis and to evaluate the

dimensions of the heat exchangers to assess the technical feasibility. A proprietary software developed by Howden Group, a global equipment manufacturer of balance of plant equipment (Howden Group 2016), is used for this purpose following a methodology specifically developed for this novel application, as described in Section 3.4.

An analogous configuration to rotary heat exchangers is considered for the rotary adsorber used for transferring CO₂ from a flue gas stream to air for the purpose of S-EGR. The selective CO₂ transfer system is initially considered as a “grey box” in the CCGT power plant and PCC linked model, where key operating parameters with a larger effect on the performance of the power and capture plants are input variables. Yet the rotary adsorption process is further developed in Section 3.5 through a conceptual design, in order to assess the technical feasibility of a proof of concept. The rotary adsorber model is developed in gPROMS Model Builder (PSE 2016).

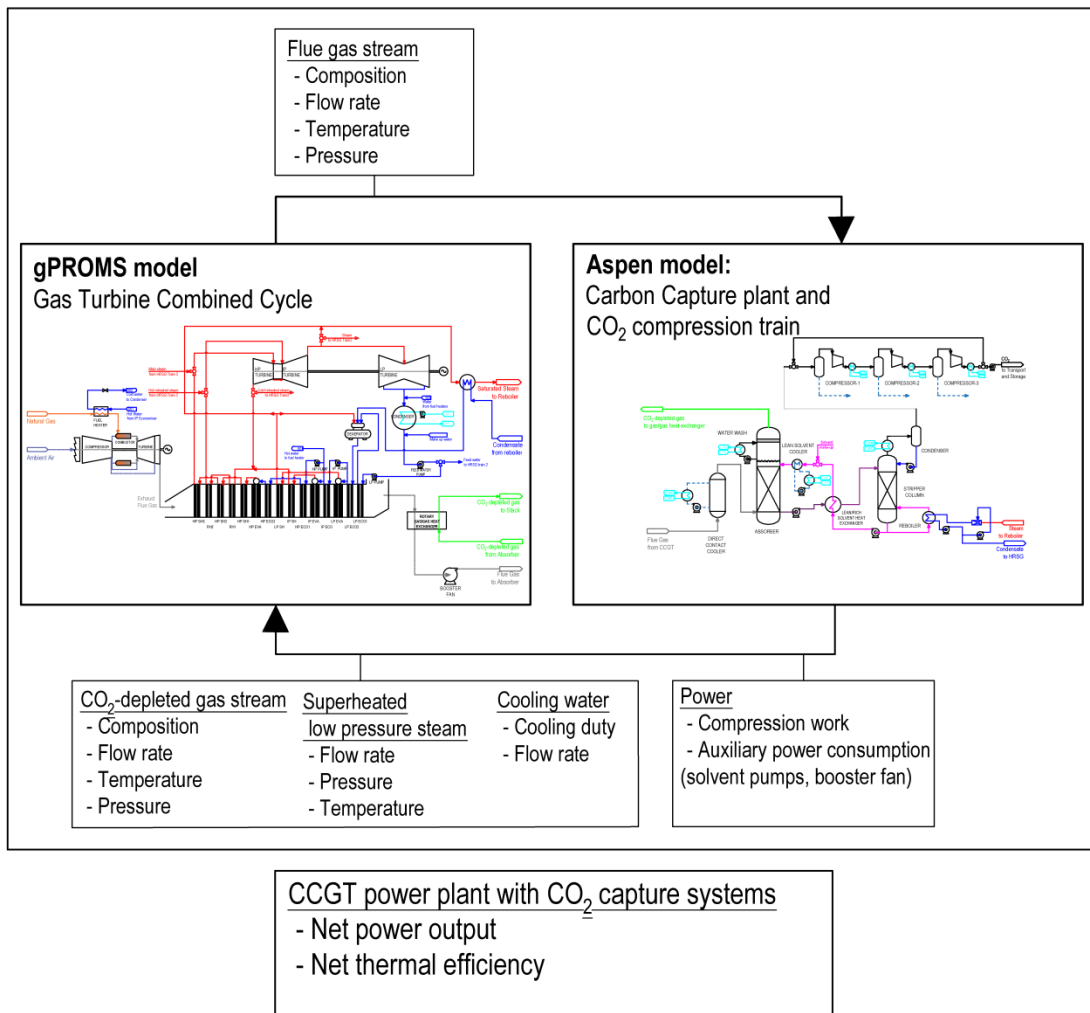


Figure 3.1.- Diagram of the linked model of a CCGT power plant, developed in gPROMS, and the carbon capture system, developed in Aspen Plus, indicating the input/output variables to each model.

3.2. Combined cycle gas turbine power plant

A combined cycle gas turbine (CCGT) power plant combines a topping cycle, which is a gas turbine (GT) operating as an open Brayton cycle, and a bottoming cycle, which combines a heat recovery steam generator (HRSG) and a steam turbine (ST). The bottoming cycle is an ordinary Rankine cycle using water as the working medium.

Large CCGT plants for power generation with a net power output of the order of 800 MWe commonly have a 2-in-1 configuration, in which two gas turbines run in parallel and generate exhaust gas for each of the two HRSG. The steam generated in each GT+HRSG train is combined and used in a large steam turbine. This configuration gives extra flexibility and better part-load performance (IEAGHG 2012).

The CCGT gross power output is the sum of electrical power at each of the generator terminals. The CCGT net power output deducts the auxiliary plant power consumption in the cooling and process water pumps, the fans and the natural gas compressor. The CCGT net power output ($\dot{W}_{\text{CCGT,net}}$) the auxiliary plant losses (\dot{W}_{aux}), the thermal efficiency ($\eta_{th,CC}$) referred to the natural gas low heating value (LHV) and the heat input ($\dot{Q}_{in,LHV}$) are evaluated according to Equations [3.1], [3.2], [3.3] and [3.4], respectively, where \dot{W}_{GT} is the gas turbine power output, \dot{W}_{ST} is the steam turbine power output, $\eta_{\text{generator}}$ is the efficiency of the generator and \dot{m}_{fuel} the fuel mass flow rate.

$$\dot{W}_{\text{CCGT,net}} = (\dot{W}_{\text{GT}} + \dot{W}_{\text{ST}} - \dot{W}_{\text{aux}}) \cdot \eta_{\text{generator}} \quad [3.1]$$

$$\begin{aligned} \dot{W}_{\text{aux}} = & \dot{W}_{\text{water pumps}} + \dot{W}_{\text{fans}} + \dot{W}_{\text{fuel compressor}} \\ & + \dot{W}_{\text{aux PCC}} + \dot{W}_{\text{CO2compression train}} \end{aligned} \quad [3.2]$$

$$\eta_{th,CCGT} = \frac{\dot{W}_{\text{CCGT,net}}}{\dot{Q}_{in,LHV}} \quad [3.3]$$

$$\dot{Q}_{in,LHV} = \dot{m}_{\text{fuel}} \cdot LHV \quad [3.4]$$

The process flow diagram of the CCGT plant for the reference case with an air-based combustion CCGT with post-combustion capture system is illustrated in Figure 3.2.

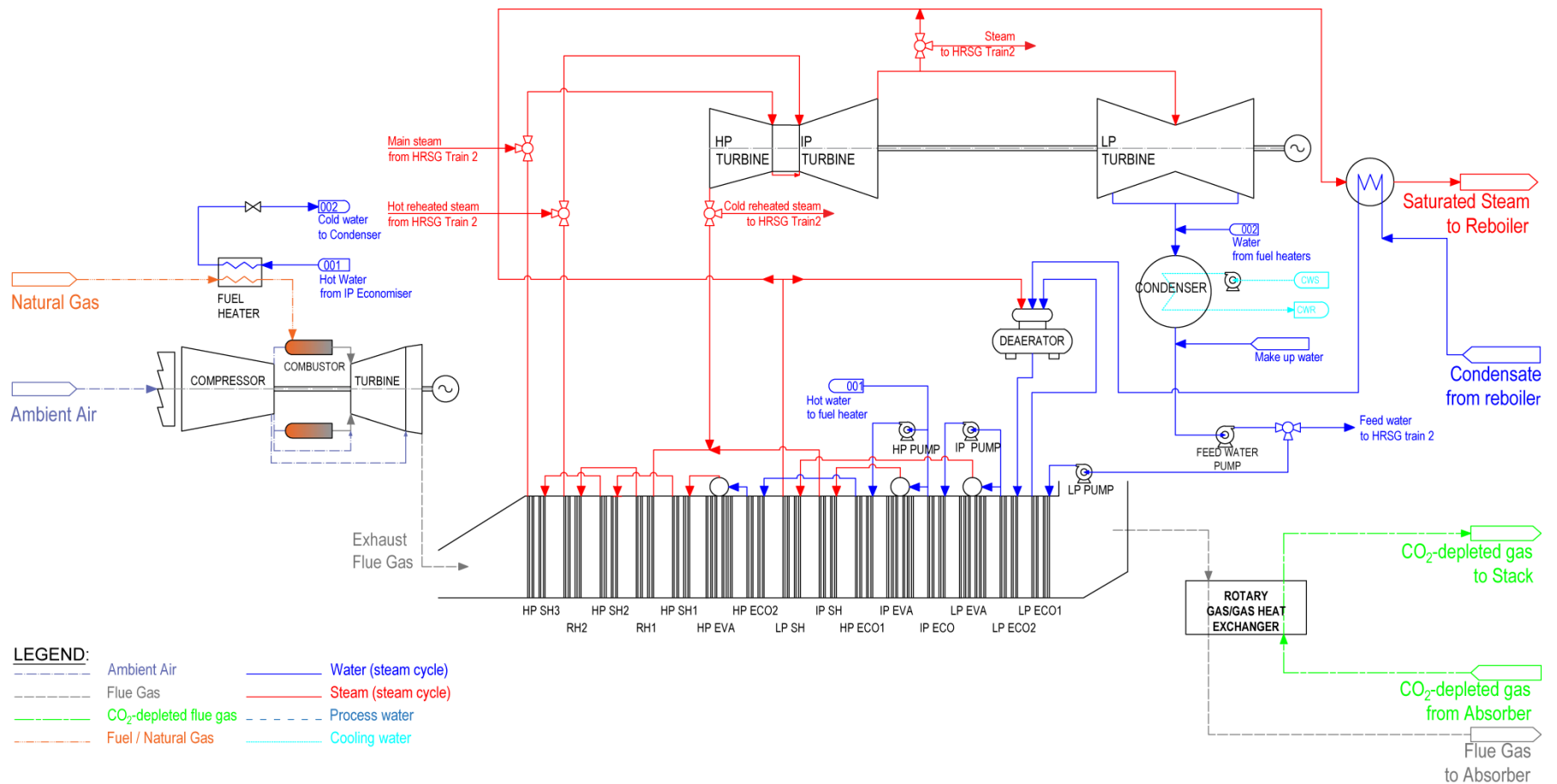


Figure 3.2.- Process flow diagram of the power system in the reference case: air- based combustion CCGT with PCC.

The fundamental principles and the equations used to develop the models of the gas turbine components are described in Section 3.2.1. They provide the basis for the understanding of the fundamental principles on which the turbomachinery performance maps are based, as described in Section 3.2.2. Section 3.2.3 describes the methodology and the modelling procedure followed in the assessment of the performance of an existing gas turbine technology at off-design conditions when CO₂ enriching strategies are added to the power cycle. The configuration of the bottoming cycle is described in Section 3.2.4. Section 3.2.5 describes the thermal integration of the power cycle and the PCC plant.

3.2.1. Gas Turbine

The gas turbine is modelled considering the unitary operations of compression of the intake air, combustion of the fuel in lean conditions at approximately constant pressure, and expansion of combustion gases (Brayton cycle). Mixing of the combustion gas with the cooling air diverted from the compressor and the pressure drop through the inlet duct and combustion chamber are also considered. The gas turbine power output ($\dot{W}_{GT,net}$) is evaluated according to Equation [3.5], where \dot{W}_t is the turbine power output, \dot{W}_c is the compressor power consumption and η_{mech} is the mechanical efficiency of the compressor. The gas turbine thermal efficiency ($\eta_{th,GT}$) is evaluated as shown in Equation [3.6]. Unless otherwise specified, the equations are based on fundamental principles and are general for gas turbine modelling.

$$\dot{W}_{GT,net} = \left(\dot{W}_t - \frac{\dot{W}_c}{\eta_{mech}} \right) \quad [3.5]$$

$$\eta_{th,GT} = \frac{\dot{W}_{GT,net}}{\dot{Q}_{in,LHV}} \quad [3.6]$$

3.2.1.1 Inlet system

The ambient air is first filtered in the filter system to eliminate particles and droplets of condensate moisture suspended in the air, which might cause erosion in the compressor blades. This process has a pressure drop associated, which is constantly monitored due to the potential risk of filter icing or blockage causing damage to the compressor.

3.2.1.2 Compressor

The compressor increases the total pressure of the fluid to that required in the cycle while absorbing the minimum shaft power possible (Walsh & Fletcher 2004). The compressor

work (\dot{W}_c) is evaluated as the difference in the stagnation enthalpy of the working fluid as it is compressed to achieve the design pressure ratio, according to Equation [3.7]. Since the turbomachine are essentially adiabatic systems and, thus, the ideal process is isentropic, the isentropic efficiency (η_c) is considered to evaluate the actual compressor work, as indicated in Equation [3.8].

The working fluid is ambient air, in the reference case with an air-based combustion CCGT plant, or CO₂-enriched air, in the configuration with a CCGT plant equipped with PCC and EGR or S-EGR. For the reference case, the isentropic efficiency is calculated to match gas turbine gross power output reported in technical specifications for General Electric (GE) F-class engine (General Electric Power Generation 2016). Data from previous publications using the same class gas turbine engine, i.e. GE F-class are also considered (Sánchez et al. 2010, Jordal et al. 2012, Chacartegui et al. 2012, International Energy Agency 2012).

$$\dot{W}_c = \dot{m}_{\text{air}} \cdot \frac{h_{0 \text{ air, out isentropic}} - h_{0 \text{ air, in}}}{\eta_c} \quad [3.7]$$

$$\eta_c = \frac{h_{0 \text{ air, out isentropic}} - h_{0 \text{ air, in}}}{h_{0 \text{ air, out actual}} - h_{0 \text{ air, in}}} \quad [3.8]$$

Heavy-duty gas turbines use axial flow compressors, where the working fluid enters parallel to the axis of rotation. An axial compressor consists of a series of stages, each one comprising a row of rotating blades (rotor) followed by a row of stationary vanes (stator), as illustrated in Figure 3.3. An additional row of “inlet guide vanes” (IGV) is usually located before the first stage to ensure that the fluid enters the first rotor blades at a suitable flow angle. Many industrial units have “variable inlet guide vanes” (VIGV) permitting the flow angle to be adjusted to the correct position when the air mass flow rate varies due to changes in load or in the inlet conditions, pressure or temperature, improving the efficiency of the turbomachinery off-design performance (Walsh & Fletcher 2004).

The length of the blades and the annulus areas decreases through the length of the compressor to compensate for the increase in fluid density as it is compressed and, thus, the axial component of the absolute velocity, noted by C_x , can be assumed constant. The flow through the axial compressor is assumed to be two dimensional flow and the flow conditions at the mean radius represent the flow at all other radii (Boyce 2006).

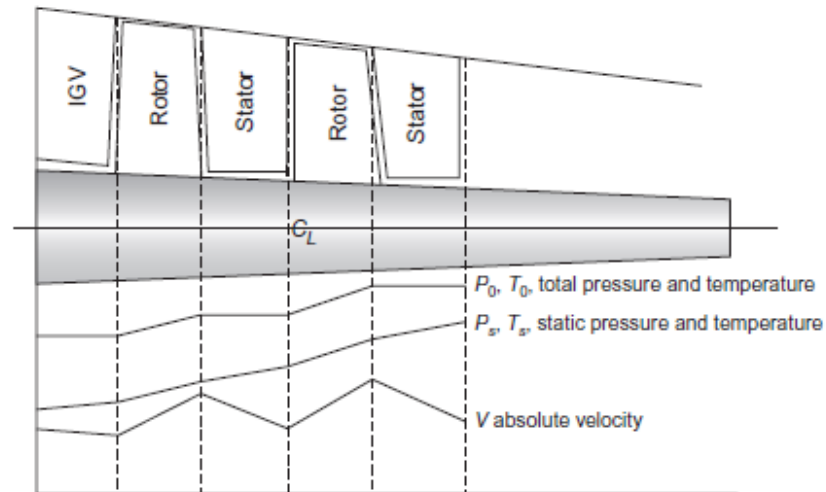


Figure 3.3.- Variation of temperature (enthalpy), velocity and pressure through an axial-flow compressor (Boyce 2006)

The compressor operates on the principle of adding work to the fluid to raise its pressure, by first acceleration in the rotor and then deceleration, or diffusion, in the stator. The diffusion in the stator converts the increase in kinetic energy gained in the rotor to a pressure increase.

Figure 3.4 describes the stage velocity diagram for a two dimensional flow in an axial compressor. The velocity and the angles in the absolute system are noted by C and α , and the velocity and the angles in the relative system are noted by W and β , respectively. Axial and tangential components of both absolute (C_x, C_θ) and relative velocities (W_x, W_θ) are represented in Figure 3.4. The fluid enters the rotor with an absolute velocity C_1 and an angle α_1 , which combines vectorially with the tangential velocity of the blade U to result in the relative velocity W_1 at an angle β_1 . The fluid flows through the passage (open area) in between the rotor blades and is given a relative velocity W_2 at an angle β_2 , which is smaller than α_2 . The relative velocity W_2 is smaller than W_1 due to an increase in the passage width as the blades become thinner towards the trailing edges. Some diffusion thus takes place in the rotor of the stage. The combination of the relative exit velocity and the blade velocity produce an absolute velocity C_2 at the exit of the rotor. The fluid then passes through the stator, where it is turned through an angle so that it is directed into the rotor of the next stage with a minimum incidence angle α_3 (Boyce 2006). The amount of diffusion in the rotor compared to the stator is known as “reaction stage”. It is normal practice to design for 50% reaction stage and then the diffusion is equal in the stator and the rotor (Bhargava et al. 2004). The process is repeated in multiple stages to achieve the required overall pressure ratio, typically between 18 and 30 bar in heavy-duty gas turbines. Each stage raises the pressure incrementally, with a pressure ratio of each compression stage from 1.1:1 to 1.4:1, which results in very high stages efficiencies.

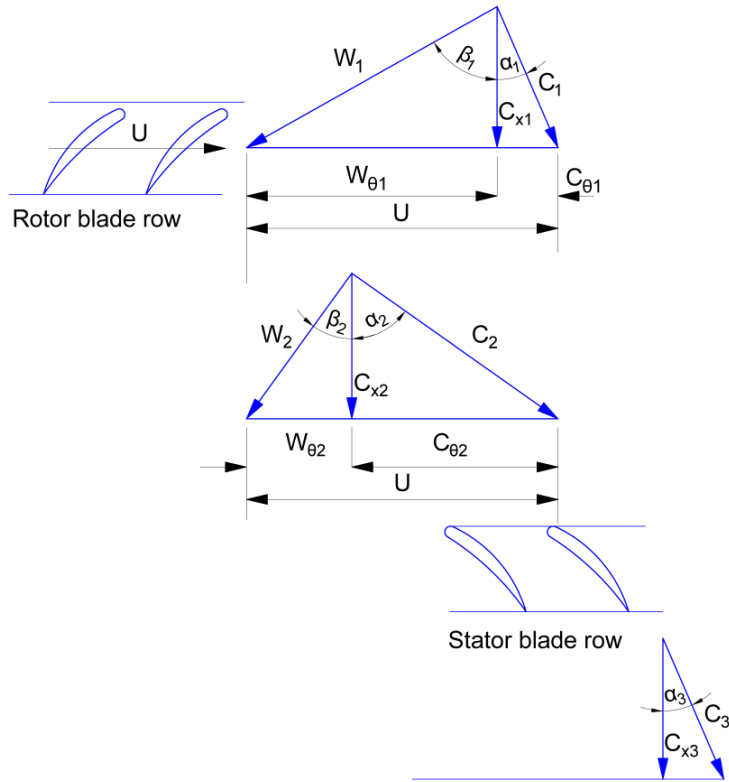


Figure 3.4.- Stage velocity triangles for an axial-flow compressor (Dixon and Hall 1998).

The fundamental law describing the conversion of mechanical energy into pressure in a turbomachine is Euler's law, which states that a compressor stage imparts energy on the fluid by increasing its angular momentum or torque ($\Delta\tau$). The torque is produced by increasing the swirl or tangential velocity the fluid (ΔC_θ).

The mathematical expression of Euler's law is given by Equation [3.9], where \dot{W} is the shaft power input per stage, ω is the angular velocity of the rotor, \dot{m}_{fluid} is the mass flow rate of the working fluid and r the average radius of the rotor blades. From Euler's equation, the specific absolute enthalpy rise per stage (Δh_0), assuming adiabatic compression process, can be evaluated as indicated in Equation [3.10], where U is the liner velocity of the rotor blades at the mean radius.

$$\dot{W} = \omega \cdot \Delta\tau = \omega \cdot \dot{m}_{\text{fluid}} \cdot \Delta(r \cdot C_\theta) = \omega \cdot \dot{m}_{\text{fluid}} \cdot (r_2 \cdot C_{\theta 2} - r_1 \cdot C_{\theta 1}) \quad [3.9]$$

$$\Delta h_0 = \frac{\dot{W}}{\dot{m}_{\text{fluid}}} = U \cdot C_x \cdot (\tan(\alpha_2) - \tan(\alpha_1)) \quad [3.10]$$

$$\Delta h_0 = h_{03} - h_{01} = h_{02} - h_{01} \quad [3.11]$$

The rotor blades convert the shaft power input into enthalpy in the form of increasing static temperature (T), absolute velocity (C) and hence total temperature (T_0), as indicated in Equation [3.11]. In the stator vanes there is no work or heat transfer and the total enthalpy remains constant ($h_{03} = h_{02}$). Figure 3.3 showed the variation of pressure, absolute velocity and temperature through several stages of the axial-flow compressor. These properties are qualitatively illustrated for one stage in an enthalpy vs. entropy diagram in Figure 3.5.

Equation [3.10] can be written in terms of the stage-loading coefficient (ψ) and the flow coefficient (ϕ), defined in Equation [3.13] and Equation [3.14] respectively, where α_1 is the outlet angle of the previous stage and β_2 the rotor outlet angle, which are determined by the geometry of the blades. For a fixed geometry and volumetric flow rate swallowed by the compressor, the stage-loading coefficient can be used to predict the compressor behaviour at off design conditions (Razak 2007).

$$\frac{\Delta h_0}{U^2} = 1 - \frac{C_x}{U} \cdot (\tan(\beta_2) + \tan(\alpha_1)) \quad [3.12]$$

$$\psi = \frac{\Delta h_0}{U^2} \quad [3.13]$$

$$\phi = \frac{C_x}{U} \quad [3.14]$$

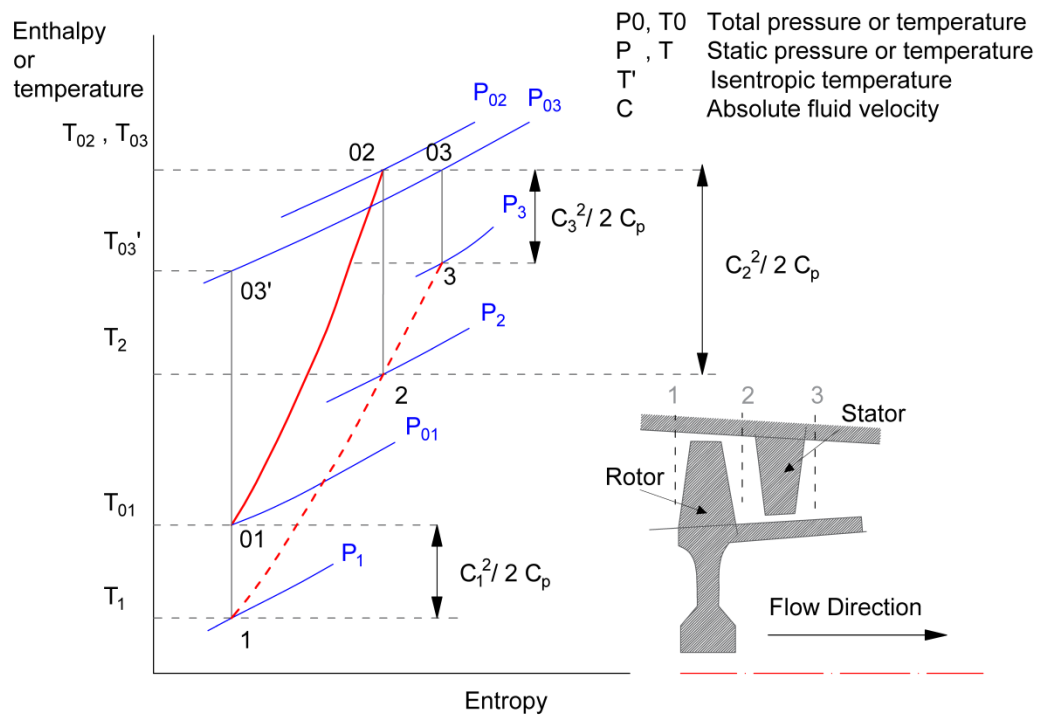


Figure 3.5.- Temperature-Entropy diagram in a single compressor stage

The understanding of Euler's equation and the stage velocity diagram is important to explain the dimensionless parameter groups that constitute the compressor performance curves, described in Section 3.2.2, and its behaviour at off-design conditions due to changes in the working fluid composition, inlet pressure and temperature, when EGR and S-EGR are added to the CCGT plant.

3.2.1.3 *Combustor*

Heavy-duty gas turbines typically employ lean pre-mixed Dry Low NO_x (DLN) combustion systems, specifically developed to operate at low levels of NO_x without any requirements for water. DLN-2 GE combustor operates in a diffusion model at low loads (typically < 50% load) and a pre-mixed model at high loads (typically > 50% load). In the premixed line, the fuel and the air are fully mixed and flow out the mixing tubes at high velocity to enter the burning zone where the lean combustion occurs. The use of air in the combustor is strictly controlled in order to have an optimal air-fuel ratio in the combustion zone. A portion of the compressor discharge air is introduced directly in the combustion-reaction zone to be mixed with the fuel and burned. The rest of the air quenches the flame prior to the combustor gas entering the turbine or cools the wall of the combustor, as shown in Figure 3.6 (Davis and Black 2000). The NO_x emissions are also controlled with fuel staging (Cohen et al. 1996). In low emissions operation, 90% of the gas fuel is injected through radial gas injection spokes in the pre-mixer tubes, and combustion air is mixed with fuel in tubes surrounding each of the five fuel nozzles

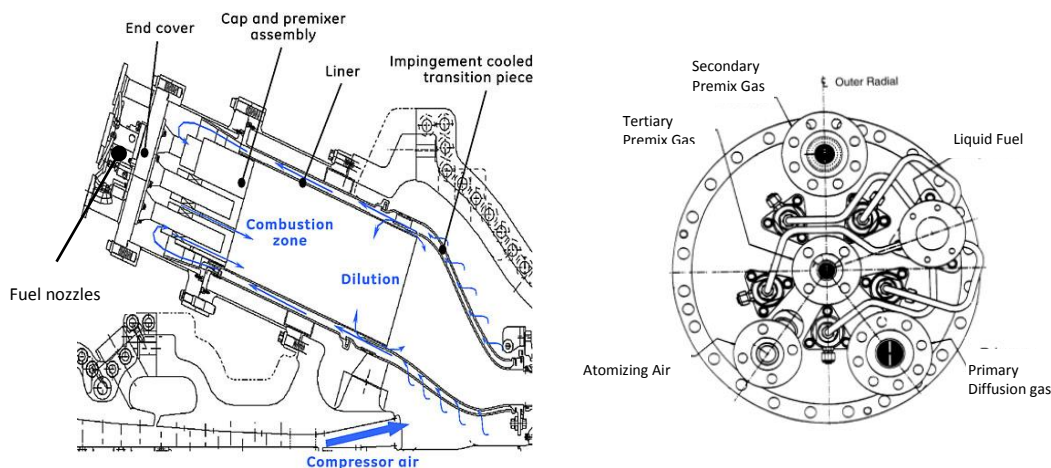


Figure 3.6.- Dry Low NO_x (DLN-2) combustion system with diffusion and premixed fuel lines (General Electric, Davis and Black 2000).

There are two important design parameters in the model of the gas turbine used in this work: the firing temperature or combustor outlet temperature (COT) and the turbine inlet temperature (TIT), qualitatively illustrated in an enthalpy entropy diagram in Figure 3.7. The

COT is obtained with an energy balance considering only the primary air used in the fuel combustion, according to Equation [3.15], where m_{air} is the air mass flow rate and m_{fuel} the gas fuel mass flow rate, usually expressed in terms of the air-to-fuel mass flow ratio (AFR), Equation [3.16]. The maximum allowable turbine inlet temperature (TIT) is usually provided by gas turbine original equipment manufacturers and refers to the resulting temperature after the combustion gas is mixed with the cooling air used to cold down the stator vanes in the turbine first stage. The energy balance is shown in Equation [3.17]. The TIT is therefore the highest temperature at which work is extracted. Air is also bled from the compressor outlet to cold down the shaft and other components and does not generate any mechanical work.

GE Frame 9 FB-class gas turbine engine, considered in this model, operates at a TIT of approximately 1370 °C, as reported in literature (Eldrid et al. 2001). In the reference case, the cooling air ($m_{cooling\ air}$) and bleed air (m_{bleed}) mass flow rates are evaluated to match the gas turbine gross power output and thermal efficiency at ISO conditions reported in General Electric technical specifications and data available in literature (International Energy Agency 2012; Jordal, Andreas, et al. 2012; Chacartegui et al. 2012; Sánchez et al. 2010)

The combustion efficiency ($\eta_{combustion}$) varies as a function of the combustor outlet temperature. In this work, a constant value of 99.8% is assumed. The exhaust flue gas composition is calculated assuming that the combustion is complete (Walsh & Fletcher 2004).

$$\begin{aligned} & (m_{air} - m_{cooling\ air} - m_{bleed}) \cdot (h_{air, T_{in}} - h_{air, T_{ref}}) + m_{fuel} \cdot \\ & (h_{fuel, T_{in}} - h_{fuel, T_{ref}}) + LHV \cdot m_{fuel} \cdot \eta_{combustion} = \\ & m_{EFG} \cdot (h_{EFG, T_{firing}} - h_{EFG, T_{ref}}) \end{aligned} \quad [3.15]$$

$$AFR = \frac{m_{comburent}}{m_{fuel}} \quad [3.16]$$

$$\begin{aligned} & (m_{air} - m_{bleed}) \cdot (h_{air, T_{in}} - h_{air, T_{ref}}) + m_{fuel} \cdot (h_{fuel, T_{in}} - h_{fuel, T_{ref}}) \\ & + LHV \cdot m_{fuel} \cdot \eta_{combustion} \\ & = m_{EFG} \cdot (h_{EFG, ISO\ TIT} - h_{EFG, T_{ref}}) \end{aligned} \quad [3.17]$$

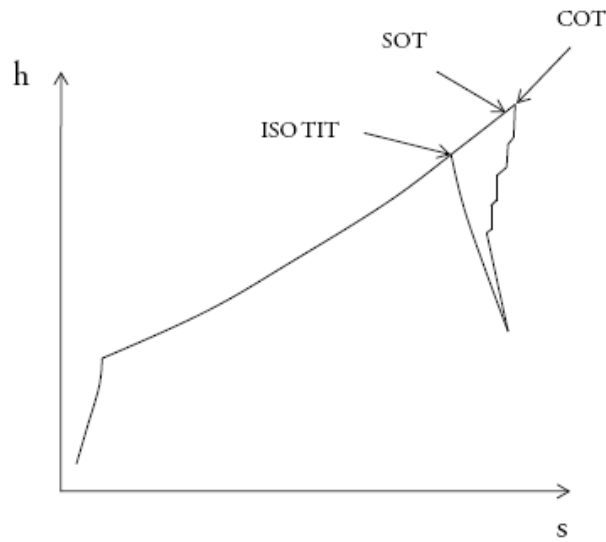


Figure 3.7.- Enthalpy – entropy diagram for the Brayton cycle showing the method used to model turbine cooling modelling (Jonshagen 2011)

3.2.1.4 *Turbine*

The combustion gases at high temperature and pressure enters axially the turbine section providing power needed to drive the compressor and the electrical generator (Walsh & Fletcher 2004).

The turbine work (\dot{W}_t) is evaluated as the difference in the stagnation enthalpy as the gases the flue gas expands to the discharge pressure, as indicated in Equation [3.19]. The turbine isentropic efficiency (η_t), given by Equation [3.18], allows the evaluation of the actual work and outlet temperature. For the reference case, the isentropic efficiency is estimated to reproduce the temperatures through the turbomachinery and match the gas turbine gross power output reported in the technical specifications (General Electric Power Generation 2016). Data from previous publications using the same class gas turbine engine, i.e. General Electric (GE) F-class are also considered (Sánchez et al. 2010, Jordal et al. 2012, Chacartegui et al. 2012, International Energy Agency 2012).

$$\eta_t = \frac{h_{EFG, out actual} - h_{EFG, in}}{h_{EFG, out isentropic} - h_{EFG, in}} \quad [3.18]$$

$$\dot{W}_t = \dot{m}_{EFG} \cdot (h_{EFG, out actual} - h_{EFG, in}) \quad [3.19]$$

An axial-flow turbine consists of a series of stages. Each stage is composed of a row of static guide vanes or nozzle vanes followed by a row of rotor blades, as illustrated in Figure 3.8. The gas enters axially the nozzle vanes and is deflected to enter the rotor at a suitable angle to minimise losses. The nozzle vanes accelerate and add swirl to the fluid. There is not work

or heat transfer in the nozzles and thus, the total temperature remains unchanged, except by the mixing with cooling air, while the static pressure and temperature reduce due to the acceleration. The small reduction in total pressure is due to friction and turbulent losses.

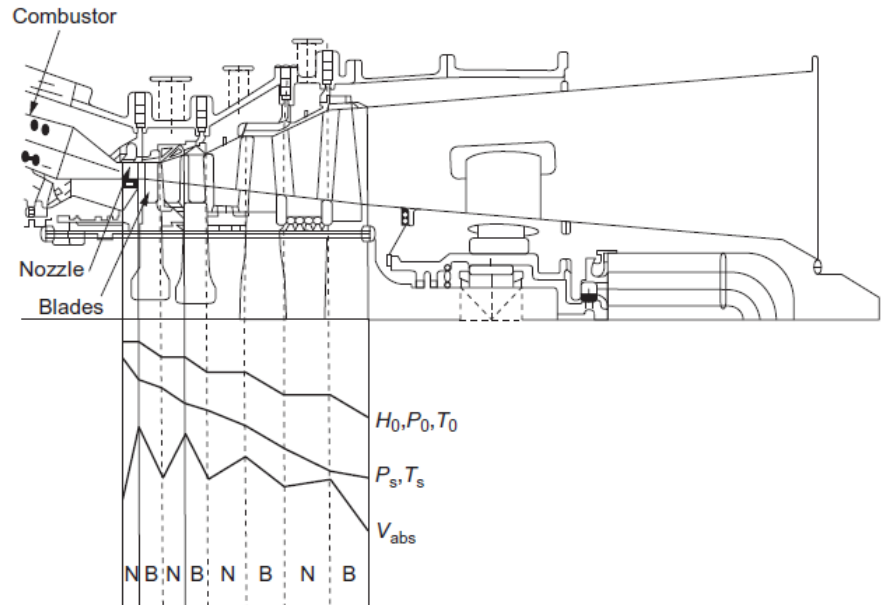


Figure 3.8.- Schematic of axial-flow turbine flow (Boyce 2006).

Figure 3.9 describes the velocity diagram in a single stage of an axial turbine for a two-dimensional flow. The velocity and the angles in the absolute system are noted by C and α , and the velocity and the angles in the relative system are noted by W and β , respectively. Axial and tangential components of both absolute (C_x, C_θ) and relative velocities (W_x, W_θ) are as indicated in Figure 3.4. Power is extracted across the rotor due to change in tangential velocity. As in the compressor, the Euler's equation evaluates the specific absolute enthalpy drop per stage (Δh_0) as indicated in Equation [3.20]

$$\Delta h_0 = \frac{\dot{W}}{\dot{m}_{\text{fluid}}} = U \cdot C_x \cdot (\tan(\alpha_3) + \tan(\alpha_2)) = U \cdot C_x \cdot (\tan(\beta_3) + \tan(\beta_2)) \quad [3.20]$$

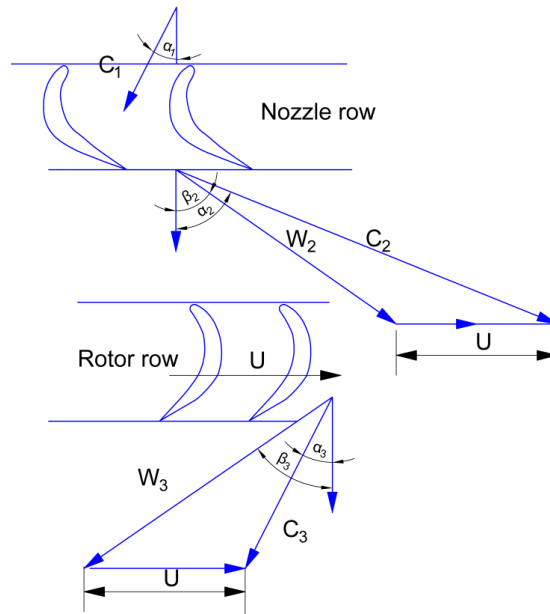


Figure 3.9.- Stage velocity diagram in an axial-flow turbine (Dixon and Hall 1998)

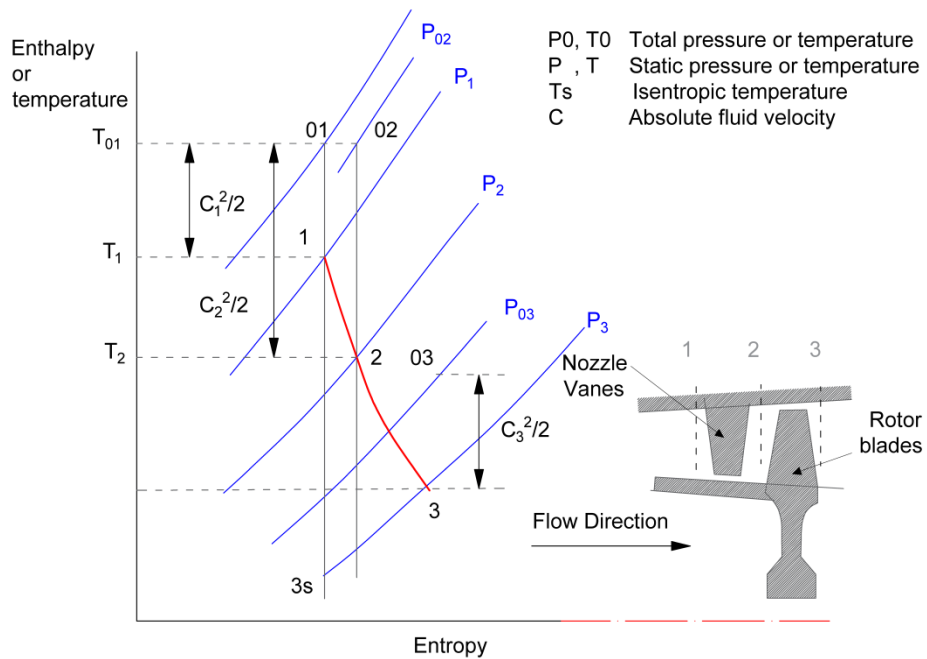


Figure 3.10.- Temperature-Entropy diagram in a single turbine stage

3.2.1.5 Turbine blade cooling

Cooling is required for the stator vanes and rotor blades of the first expansion stages which are in contact with the hot flue gas leaving the combustor, as well as other components such as the turbomachinery shaft. Cooling air is extracted from the intermediate and last stages of the compressor at a suitable pressure for its injection. A rigorous model including the air extraction requires the analysis of the actual expansion in each turbine stage and identifying the properties, pressure and temperature of the extracted air streams and the downstream injection points. The cooling air flow rate is evaluated as the fraction of the total inlet air flow rate required to cold the combustion gases down to the turbine inlet temperature, which is specified by gas turbine manufacturers according to the material of the blades and the cooling system. The open loop air-cooling system used in GE F-class turbines implies mixing cooling air with the flue gas to low its temperature for expansion (Brooks 2000), as shown in Figure 3.11.

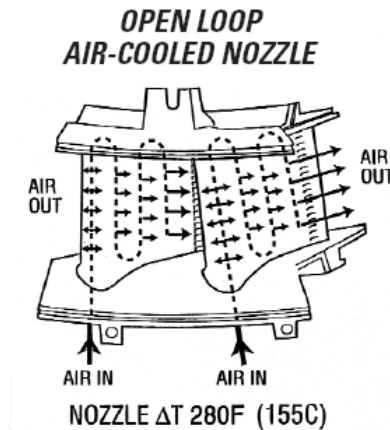


Figure 3.11.- Air-cooled first stage nozzle in GE F class gas turbine technology (Brooks 2000)

3.2.1.6 Pressure loss

Pressure losses in the system (e.g. in the gas turbine inlet system) are evaluated using Equation [3.21] and [3.22], in terms of velocity (C) and mass flow rate (\dot{m}) respectively. The pressure drop (ΔP) in a given component is proportional to the absolute velocity and density of the fluid (ρ_g) at the operational conditions. The friction coefficient (ξ) is assumed to be constant for a specific component and evaluated at design conditions, with the overall pressure drop expected as a fixed percentage of the inlet pressure. Any change in the temperature, pressure, mass flow rate and/or composition results in a different value of the pressure loss (ΔP) in a given component and is calculated with Equation [3.24], where P_{in} is the inlet pressure, M is the molar mass of the gas and R_u the universal or ideal gas constant.

$$\Delta P = \xi \cdot \frac{C^2}{2} \cdot \rho_g \quad [3.21]$$

$$\Delta P = \xi \cdot \left(\frac{\dot{m}}{A \rho_g} \right)^2 \cdot \rho_g \quad [3.22]$$

$$\frac{\Delta P}{(\Delta P)_{des}} = \frac{\left(\dot{m} / \sqrt{\rho_g} \right)_{in}^2}{\left(\dot{m} / \sqrt{\rho_g} \right)_{in,des}^2} \quad [3.23]$$

$$\frac{\Delta P / P_{in}}{(\Delta P / P_{in})_{des}} = \frac{\left(\dot{m} \sqrt{T} / P \right)_{in}^2 \cdot R_u / M}{\left(\dot{m} \sqrt{T} / P \right)_{in,des}^2 \cdot R_u / M_{des}} \quad [3.24]$$

The pressure drop in the combustion chamber is required to evaluate the turbine inlet pressure and hence the turbine swallowed capacity. Equation [3.25] (Walsh and Fletcher 2004) takes into account the cold pressure drop, associated to the air injected through the walls of the combustion chamber, and the hot pressure drop, due to the heat released in the combustion section of the flame. In the base case model at design conditions, a pressure drop of 5% of the combustion inlet is assumed, and the values of the coefficients, K_C and K_H , are calculated and used to evaluate the pressure drop when the gas turbine is operated off-design with a working fluid other than the resulting product of combustion in air, e.g. CO₂ enriched air for selective exhaust gas recirculation.

$$\frac{\Delta P_0}{P_{0, in}} = \left(\frac{\dot{m}_{gas}}{P_{0,in}} \cdot \sqrt{\frac{R_u / M \cdot T_{0,in}}{\gamma_{in}}} \right)^2 \left(K_C + K_H \cdot \left(\frac{T_{0, out}}{T_{0, in}} - 1 \right) \right) \quad [3.25]$$

3.2.2. Compressor and turbine performance

The behaviour of the compressor and the turbine depends on a large number of parameters. The analysis of their performance is commonly simplified by using dimensionless parameter groups which together fully describe the turbomachinery behaviour.

The dimensionless parameter groups can be derived using Buckingham's π theorem. This theorem states that the minimum number of dimensionless parameter groups, which fully characterise the behaviour of a system, can be determined as the difference between the

number of independent variables and the number of fundamental dimensions required to represent those variables (Dixon and Hall 1998).

The independent variables involved in the analysis of the compressor and turbine performance can be classified in three groups: control variables (mass flow rate, \dot{m} , and shat speed, N), geometrical variables (characteristic diameter, D) and fluid properties (density, ρ_0 , dynamic viscosity, μ , speed of sound, a_0 , and specific heat ratio, γ). The fundamental dimensions of the previous variables are mass, length and time. The dependent variables (isentropic enthalpy, $\Delta h_{0,s}$, efficiency, η , and power output, \dot{W}) can therefore be expressed as a function of four dimensionless parameter groups (mass, length, time), as shown in Equation [3.33]. The intermediate steps in the derivation of the set of dimensionless parameter groups are described from Equation [3.26] to Equation [3.32]. It is important to note that the choice of dimensionless parameters is not unique. A more physical derivation leading to the same set of equations is explained hereinafter with the assumption of ideal gas behaviour.

- Dependent variables: $\Delta h_{0,s}$, η , \dot{W}
- Independent variables: μ , N , D , \dot{m} , ρ_0 , a_0 , γ
- Fundamental dimensions: $[M]$, $[L]$, $[T]$

$$\Delta h_{0,s}, \eta, \dot{W} = f(\mu, N, D, \dot{m}, \rho_{0,in}, a_{0,in}, \gamma) \quad [3.26]$$

$$\frac{\Delta h_{0,s}}{N^2 \cdot D^2}, \eta, \frac{\dot{W}}{\rho_{0,in} \cdot N^3 \cdot D^5} = f\left(\frac{\dot{m}}{\rho_{0,in} \cdot N \cdot D^3}, \frac{\rho_0 \cdot N \cdot D^2}{\mu}, \frac{N \cdot D}{a_{0,in}}, \gamma\right) \quad [3.27]$$

$$\frac{\dot{m}}{\rho_{0,in} \cdot N \cdot D^3} = \frac{\dot{m} \cdot R_u / MW \cdot T_{0,in}}{P_{0,in} \cdot N \cdot D \cdot D^2} = \frac{\dot{m} \cdot \sqrt{R_u / MW \cdot T_{0,in}}}{P_{0,in} \cdot D^2 \cdot \sqrt{\gamma}} \quad [3.28]$$

$$\frac{N \cdot D}{a_{0,in}} = \frac{N \cdot D}{\sqrt{\gamma \cdot R_u / MW \cdot T_{0,in}}} \quad [3.29]$$

$$\frac{\rho_0 \cdot N \cdot D^2}{\mu} = Re \quad [3.30]$$

$$\frac{\Delta h_{0,s}}{N^2 \cdot D^2} = \frac{C_p \cdot T_{0,in} \cdot \left[\left(\frac{P_{0,out}}{P_{0,in}} \right)^{\frac{\gamma-1}{\gamma}} - 1 \right]}{a_{0,in}^2} = \frac{C_p \cdot T_{0,in} \cdot \left[\left(\frac{P_{0,out}}{P_{0,in}} \right)^{\frac{\gamma-1}{\gamma}} - 1 \right]}{\gamma \cdot R \cdot T_{0,in}} \quad [3.31]$$

$$= f \left(\frac{P_{0,out}}{P_{0,in}} \right)$$

$$\frac{\dot{W}}{\rho_{0,in} \cdot N^3 \cdot D^5} = \frac{\dot{m} \cdot C_p \cdot \Delta T_0}{\rho_{0,in} \cdot N \cdot D^3 \cdot (N \cdot D)^2} = \frac{C_p \cdot \Delta T_0}{\gamma \cdot R_u / MW \cdot T_{0,in}} = f \left(\frac{\Delta T_0}{T_{0,in}} \right) \quad [3.32]$$

$$\frac{P_{0,out}}{P_{0,in}}, \eta, \frac{\Delta T_0}{T_{0,in}} = f \left(\frac{\dot{m} \sqrt{T_{0,in} \cdot R_u / MW}}{D^2 \cdot P_{0,in} \sqrt{\gamma}}, Re, \frac{N \cdot D}{\sqrt{\gamma \cdot R_u / MW \cdot T_{0,in}}}, \gamma \right) \quad [3.33]$$

The dimensionless parameter groups for the mass flow, the pressure ratio and the rotational speed, shown in Equation [3.33], are used to generate the turbomachinery characteristic curve or performance map. In the turbine the pressure rise is taken as an independent variable and the dimensionless mass flow rate as a dependent variable.

The former dimensionless parameter groups can also be derived from the expressions of the Mach number for the vectors which constitute the velocity triangle in the blades as described in Jonshagen's work (Jonshagen 2011). The velocity diagram for two-dimensional fluid flow is defined by three components, as explained in Section 3.1.1. These components are the axial and tangential components for the absolute velocity of the fluid, C_x and C_θ , and the rotational shaft speed, N . The velocity diagram for a compressor stage is illustrated in Figure 3.4. A set of three dimensionless groups needs therefore to be derived in order to fully describe the velocity diagram in the blades based on Mach numbers. The fundamental principle is that if, under different operational conditions, the Mach numbers for all vectors in the velocity triangle are equal, the velocity diagrams are uniform and the Reynolds number is constant, a unique flow condition is obtained. Each point on the turbomachinery characteristic curve based on the dimensionless parameter groups should therefore represents a unique flow condition (Jonshagen 2011).

- Mass flow

The axial component of the absolute velocity (C_x) is included when forming the mass-flow group. The continuity equation is taken into account in the derivation of the Mach number expression for the axial component (Ma_{c_x}), showed in Equation [3.37]. In a two dimensional fluid flow analysis, the axial component of the absolute velocity can be assumed

constant along the longitudinal axis of the compressor as the blade height of each stage is sized so that the change in the cross section area (A) compensates the variation on the density (ρ), for a given constant mass flow rate.

$$\dot{m} = \rho \cdot A \cdot C_x \quad [3.34]$$

$$C_x = Ma_{c_x} \cdot \sqrt{\gamma \cdot T_0 \cdot R_u / MW} \quad [3.35]$$

$$\dot{m} = \frac{\pi}{4} \cdot D^2 \cdot \rho \cdot Ma_{c_x} \cdot \sqrt{\gamma \cdot T_0 \cdot R_u / MW} \quad [3.36]$$

$$Ma_{c_x} \propto \frac{\dot{m} \cdot \sqrt{T_0}}{D^2 \cdot P_0} \cdot \frac{\sqrt{R_u / MW}}{\sqrt{\gamma}} \quad [3.37]$$

- Rotor Speed

The rotational speed is included in the second dimensionless group, showed in Equation [3.40], which is referred to as the aerodynamic speed (Jonshagen 2011).

$$U = Ma_U \cdot \sqrt{\gamma \cdot T_0 \cdot R_u / MW} \quad [3.38]$$

$$U = N/60 \cdot D \cdot \pi \quad [3.39]$$

$$Ma_U = \frac{N/60 \cdot D \cdot \pi}{\sqrt{\gamma \cdot T_0 \cdot R_u / MW}} \propto \frac{N \cdot D}{\sqrt{\gamma \cdot T_0 \cdot R_u / MW}} \quad [3.40]$$

- Pressure ratio

The variation in the tangential component of the fluid velocity is related to the change in stagnation enthalpy according to Euler's law expression, Equation [3.41], (Jonshagen 2011).

$$\Delta h_0 = U \cdot \Delta C_\theta \quad [3.41]$$

$$U = Ma_U \cdot \sqrt{\gamma \cdot T_0 \cdot R_u / MW} \quad [3.42]$$

$$C_\theta = Ma_{c_\theta} \cdot \sqrt{\gamma \cdot T_0 \cdot R_u / MW} \quad [3.43]$$

$$Ma_U \cdot Ma_{c_\theta} = \frac{\Delta h_0}{\gamma \cdot T_0 \cdot R_u / MW} \quad [3.44]$$

The expression shown in Equation [3.44] is used as the third dimensionless group which constitute the turbomachinery performance map. Pressure ratio (PR) is, however, more

commonly used in the characteristic curves provided by gas turbine manufactures. The stagnation enthalpy variation is related to the pressure ratio in the turbomachine through the expression describing the adiabatic compression or expansion in the compressor or turbine respectively. Equation [3.45] shows the expression for the dimensionless parameter group in terms of the pressure ratio.

$$Ma_U \cdot Ma_{C_\theta} = \frac{\eta_s \cdot \left(PR^{\frac{\gamma-1}{\gamma}} - 1 \right)}{\gamma - 1} \quad [3.45]$$

The dimensionless parameter group constituting the turbomachinery performance maps, shown in Figure 3.12, are usually presented in the form of either corrected values by the design temperature and pressure or normalized by the corresponding values at the design conditions. The design point is the operation point corresponding at full load operation with air at ambient ISO conditions (15 °C, 1.013 bar and 60% relative humidity). In normalized turbomachinery performance maps, the design point corresponds to the coordinates (1,1,1) and changes in any variable will result in an off-design operation.

The compressor performance maps obtained for a specific gas turbine frame can be scaled up or down in order to predict the behaviour of a machine with different characteristic diameter, provided that the both machines present the same aerodynamic behaviour.

Using the extended expression of the dimensionless parameter groups, as showed in Equation [3.37], [3.40] and [3.45], the performance of the gas turbine with a different working fluid composition, physical and thermal properties can be investigated and the deviation from the design operational point evaluated. This procedure follows (Jonshagen et al. 2011) and makes use of the scaled up performance map for a GE Gas Turbine Frame 9 presented in Saravanamuttoo's work (Saravanamuttoo and Maclsaac 1983). It is included in Figure 3.12 for completeness.

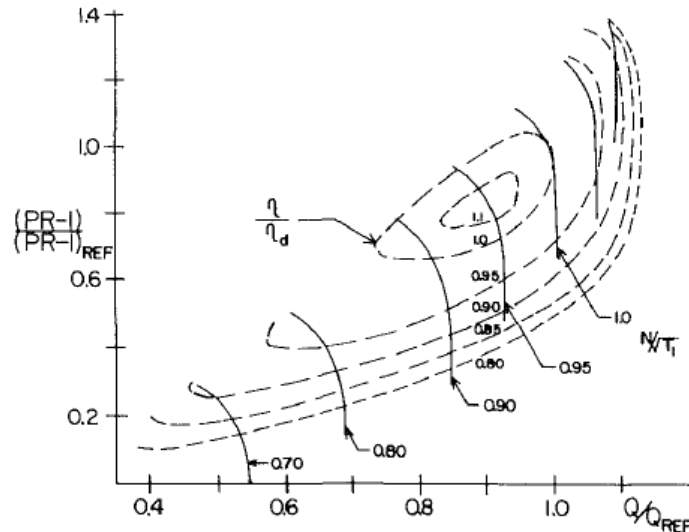


Figure 3.12.- Axial compressor performance curve (Saravanamuttoo and Maclsaac 1983)

3.2.3. Gas turbine off-design performance

A change in the operational conditions or the working fluid composition results in an off-design operation of the gas turbine system, in particular the compressor and the turbine. The methodology described hereinafter is followed to assess the performance of the gas turbine system when the strategies of EGR or S-EGR are added. Since the assessment is based in a dimensionless analysis, the methodology could be applied for any gas turbine technology.

The gas turbine compressor is well approximated as a constant volumetric flow rate machine when rotating at synchronous speed with a fixed angle of the variable inlet guide vanes (VIGV). The volumetric flow rate is mostly influenced by the VIGV angle and, thus, the mass flow rate swallowed by the compressor varies with changes in density of the working fluid, e.g. with inlet pressure or temperature.

Fixed compressor geometry is assumed with the position of the VIGV set at the corresponding angles for full load operation. The intake mass flow rate (\dot{m}) varies as a function of the CO_2 -enriched air density (ρ_g) at the compressor inlet conditions (composition, temperature and pressure) for a constant cross section area (A) and gas absolute velocity (C_x), Equation [3.46].

$$\dot{m}_{\text{Compressor inlet}} = \rho_g \cdot A \cdot C_x \Rightarrow \dot{m}_{\text{Compressor inlet}} = f(\rho_g) \quad [3.46]$$

In gas turbine performance analysis, a usual criterion for the gas turbine performance analysis is to assume that the gas turbine is choked when running at full load. The conditions of choked flow can then be applied for the throat of the nozzle constituted by two

consecutive blades forming the first ring of stator vanes and Equation [3.47] applies at the inlet section (Sánchez et al. 2010). A reorganization of Equation [3.47] with the invariable parameters on one side leads to Equation [3.48], which defines the turbine swallowing capacity (K_T). This parameter remains constant for a choked turbine and it is an important concept in turbomachinery off-design modelling (Cooke 1985)

$$\dot{m} = P_0 \cdot A \cdot \sqrt{\frac{\gamma \cdot MW}{Z \cdot R_u \cdot T_0} \left(\frac{2}{\gamma + 1}\right)^{\gamma+1/\gamma-1}} \quad [3.47]$$

$$K_T = \frac{\dot{m}}{P_0} \cdot \sqrt{\frac{Z \cdot T_0}{\gamma \cdot MW} \left(\frac{\gamma + 1}{2}\right)^{\gamma+1/\gamma-1}} \quad [3.48]$$

A change in the composition of the working fluid is considered by means of the fluid properties: molar mass (M), compressibility factor (Z) and specific heats ratio or isentropic factor (γ). The temperature in Equation [3.48] corresponds to the combustor outlet temperature (COT) prior to being mixed with the cooling air in the first expansion stage. It is desirable to maintain the COT at the design value since it results in the highest turbine inlet temperature (TIT) achievable and maximises mechanical work. The natural gas flow rate and the cooling air flow rate, extracted from the last compression stage, are evaluated to maintain the COT and TIT at the design value, respectively.

Equation [3.48] establishes the pressure at the turbine inlet (P_0) and, thus, the compressor discharge pressure and the pressure ratio through the turbomachinery for a given temperature and flue gas mass flow rate. The pressure drop through the inlet duct and in the combustor is also evaluated for the mass flow rate in each configuration.

Equation [3.48] can be derived from the expression describing an adiabatic steady state flow in a nozzle. According to the first law of thermodynamics for a nozzle where the fluid does not generate/produce any work and the potential energy variation is neglected, the stagnation enthalpy remains constant

$$h_{0, in} = h_{0, out} \quad [3.49]$$

The definition of the stagnation properties establishes a relationship between the stagnation and static enthalpy and the axial component of the absolute velocity of the fluid as shown in Equation [3.50]. Assuming that the fluid behaves as a thermally and calorically perfect gas, the velocity at any point through the nozzle is given by Equation [3.51].

$$h_0 = h + 1/2 \cdot C_x^2 \quad [3.50]$$

$$C_x = \sqrt{2(h_0 - h)} = \sqrt{2 \cdot C_p (T_0 - T)} \quad [3.51]$$

The relationship between stagnation and static properties for an isentropic process is shown in Equation [3.52] and [3.53]. Replacing these equations in the expression for the velocity and mass conservation in the nozzle, Equations [3.54] and [3.55] are obtained, respectively.

$$\frac{T}{T_0} = \left(\frac{P}{P_0}\right)^{\frac{\gamma-1}{\gamma}} \quad \text{where } \gamma = \frac{C_p}{C_v} \quad [3.52]$$

$$\frac{\rho}{\rho_0} = \left(\frac{P}{P_0}\right)^{\frac{1}{\gamma}} \quad [3.53]$$

$$C_x = \sqrt{2 \cdot C_p \cdot T_0 \left(1 - \left(\frac{P}{P_0}\right)^{\frac{\gamma-1}{\gamma}}\right)} \quad [3.54]$$

$$\dot{m} = A \cdot C_x \cdot \rho = A \cdot C_x \cdot \frac{P_0 \cdot MW}{R_u \cdot T_0} \cdot \left(\frac{P}{P_0}\right)^{\frac{1}{\gamma}} \quad [3.55]$$

An expression for the mass flow rate through a converging nozzle is shown in Equation [3.56] which results from the combination of Equations [3.54] and [3.55].

For a specific gas turbine geometry, the effective flow area is a constant and, therefore, the mass flow coefficient is a constant times the radical on the right in Equation [3.56], which is a function of the pressure ratio across the nozzle. This function presents a maximum at a pressure ratio PR^* , whose value is shown in Equation [3.58].

$$\dot{m} = A \cdot \frac{P_0}{\sqrt{T_0}} \cdot \sqrt{\frac{2 \cdot \gamma \cdot MW}{(\gamma - 1) \cdot R_u}} \sqrt{\left(\frac{P}{P_0}\right)^{\frac{2}{\gamma}} - \left(\frac{P}{P_0}\right)^{\frac{\gamma+1}{\gamma}}} \quad [3.56]$$

$$f(PR) = \left[\left(PR\right)^{\frac{2}{\gamma}} - \left(PR\right)^{\frac{\gamma+1}{\gamma}} \right]^{1/2} \quad [3.57]$$

$$\frac{d}{dPR} f(PR^*) = 0 \Rightarrow PR^* = \left(\frac{2}{\gamma + 1}\right)^{\frac{\gamma}{\gamma-1}} \quad [3.58]$$

Substituting the pressure ratio which maximised the function in Equation [3.56], the following expression is obtained.

$$\dot{m} = A \cdot \frac{P_0}{\sqrt{T_0}} \cdot \sqrt{\frac{2 \cdot \gamma \cdot MW}{(\gamma - 1) \cdot R_u}} \sqrt{\left(\frac{2}{\gamma + 1}\right)^{\frac{2}{\gamma - 1}} - \left(\frac{2}{\gamma + 1}\right)^{\frac{\gamma + 1}{\gamma - 1}}} \quad [3.59]$$

Considering now the stagnation properties in terms of Mach number for perfect gases shown in Equation [3.60], and substituting these equations into Equation [3.56], an expression for the mass flow rate through a converging nozzle in terms of the Mach number is obtained, Equation [3.61].

$$\frac{P_0}{P} = \left(1 + \frac{\gamma - 1}{2} \cdot Ma^2\right)^{\frac{\gamma}{\gamma - 1}} \quad [3.60]$$

$$\dot{m} = A \cdot \frac{P_0}{\sqrt{T_0}} \cdot \sqrt{\frac{\gamma \cdot MW}{R_u}} \left[\frac{Ma}{\left(1 + \frac{\gamma - 1}{2} \cdot Ma^2\right)^{\frac{\gamma + 1}{2(\gamma - 1)}}} \right] \quad [3.61]$$

At choked conditions at the throat of the nozzle, resulting in a Mach number equal to one, Equation [3.62] is obtained:

$$\dot{m} = A^* \cdot \frac{P_0}{\sqrt{T_0}} \cdot \sqrt{\frac{\gamma \cdot MW}{R_u}} \left(\frac{2}{\gamma + 1}\right)^{\frac{\gamma + 1}{2(\gamma - 1)}} \quad [3.62]$$

For a given geometry and, thus, constant cross section area, Equation [3.62] can be reorganised to obtain Equation [3.48], where the invariable parameters are included within a coefficient, K_T , representing the turbine capacity or swallow capacity of a gas turbine. The turbine swallow capacity will remain constant for a gas turbine operating at choked conditions.

Equation [3.48] establishes a relationship between the mass flow rate, pressure and temperature at the inlet of the first stage nozzle in the gas turbine, for a given flue gas composition at the design operational conditions. The effect of a change in the combustion gas composition on the thermodynamic properties, due to either a change in the fuel or in the comburent composition, is accounted for by the molar mass and the specific heat ratio.

The next step is to determine the dimensionless parameter groups for mass flow, pressure ratio and rotational speed for the compressor and gas turbine, according to Equation [3.37],

[3.40] and [3.45]. Since geometrical parameters of commercial gas turbine systems are not in the public domain, the deviation of the previous parameters with design operating conditions are evaluated, instead of determining absolute values.

The fundamental principle is that, if the Mach numbers for all the velocity vectors are the same, the velocity diagrams are uniform and the Reynolds number is constant, unique flow conditions are then obtained. Each point on the turbomachinery characteristic curve based on these dimensionless groups should therefore represent a unique flow conditions and the new operational point can be identify in a performance map developed for air combustion (Jonshagen et al. 2011).

The dimensionless parameter groups are therefore used to predict the behaviour of the compressor and turbine with a change in working fluid properties according to Equations [3.63], [3.64] and [3.65], which have been derived for the compressor.

$[Ma_{c_x}]_{\text{air}} = [Ma_{c_x}]_{\text{CO}_2\text{-enriched air}}$, then

$$FN_{\text{map}} = \frac{\dot{m} \cdot \sqrt{\frac{T_0}{T_{0\text{ref}}}}}{\frac{P}{P_{\text{ref}}} \cdot \sqrt{\frac{\gamma}{\gamma_{\text{air}}} \cdot \frac{R_{\text{air}}}{R}}} \quad [3.63]$$

$[Ma_U]_{\text{air}} = [Ma_U]_{\text{CO}_2\text{-enriched air}}$, then

$$N_{\text{map}} = \frac{N}{\sqrt{\gamma \cdot T_0 \cdot R}} \cdot \sqrt{\gamma_{\text{air}} \cdot T_{0\text{ref}} \cdot R_{\text{air}}} \quad [3.64]$$

$[Ma_U \cdot Ma_{c_\theta}]_{\text{air}} = [Ma_U \cdot Ma_{c_\theta}]_{\text{CO}_2\text{-enriched air}}$, then

$$PR_{\text{map}} = \frac{1}{PR_{\text{ref}}} \left[\frac{\left((PR)^{\frac{\gamma-1}{\gamma}} - 1 \right)}{\frac{\gamma-1}{\gamma_{\text{air}}-1}} + 1 \right]^{\gamma_{\text{air}}/(\gamma_{\text{air}}-1)} \quad [3.65]$$

A change in the compressor inlet conditions, pressure or temperature, or a change in the working fluid composition and properties results in a different operational point in the compressor and the turbine. The variation in the specific heat ratio changes the compressor and turbine outlet temperatures according to the expression for polytropic compression and expansion.

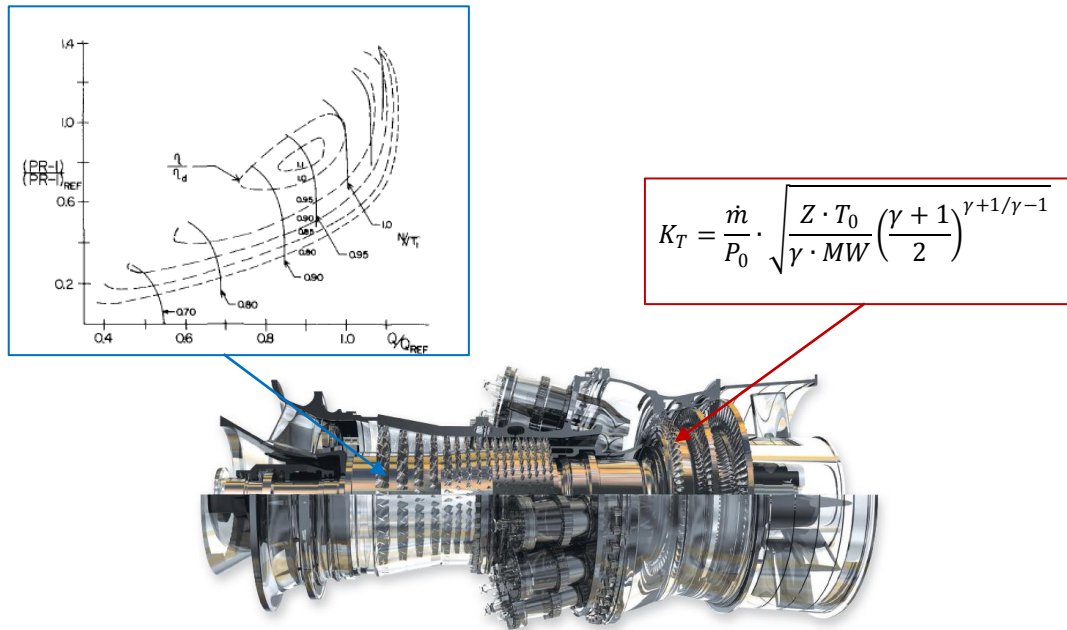


Figure 3.13.- GE F class gas turbine (Chacartegui et al. 2012)

3.2.4. Steam cycle

In a CCGT power plant, the heat available in the gas turbine exhaust flue gas is used in the heat recovery steam generator (HRSG) to generate steam at high pressure, which expands in a series of steam turbines increasing the power output and the efficiency of the plant.

The steam cycle is designed according to the configuration of a comprehensive report commissioned by the International Energy Agency Greenhouse Gas R&D programme (IEAGHG 2012). The configuration consists of a three pressure level HRSG with double reheat. The steam is sent to a turbine train with high, intermediate and low-pressure cylinders. The steam turbine is connected to a fixed-speed generator operated at a fixed speed of 50 Hz.

The components of the steam cycle and fundamental equations using in the modelling are described in this Section.

3.2.4.1 Heat recovery steam generator

The arrangement of the heat transfer banks and the design parameters, such as the pressure levels, the approach temperature difference at the superheater and reheater, the pinch temperature difference at each evaporator, the subcooling temperature difference at the exit of the economiser and the flue gas stack temperature, are sized according to the International

Energy Agency report (IEAGHG 2012) and are based on the following design criteria (Martelli et al. 2012):

- 1) The temperature for the superheated and hot reheated steam is fixed on the basis of the flue gas temperature at the high-pressure superheater and the steam turbines specifications. For the reference case, the minimum approach temperature difference (ΔT_{ap}) with the flue gas temperature is limited by the highest inlet temperature to the steam turbines, which is reported of 600 °C for advance steam turbines, e.g. the Siemens SST-6000 (Siemens Power Generation, 2016), GE ST-600 Series Reheat (General Electric Thermal Power Generation, 2016). For the investigated configurations that results in a different GT exhaust flue gas temperature, the steam turbines inlet temperature is fixed to 600 °C and the approach temperature difference is adjusted.
 - 2) The pinch point temperature difference (ΔT_{pp}) must be fixed to an optimum value given by a trade-off between the cost associated to the surface area for heat exchange and the steam cycle efficiency (η_{SC}), defined as the ratio of the net electric power output and the thermal power input to the steam cycle, shown in Equation [3.66]. For large combined cycle a common criteria is to fix this value at 3 to 8 K. A pinch temperature of 10 K is considered for all the configurations in this work based on the IEAGHG report (IEAGHG 2012).
 - 3) The subcooling temperature difference (ΔT_{ss}) and control valves are required at the hot end of the economizers to avoid steaming, which would cause vibrations and pressure oscillations. This however decreases the mass flow rate of steam raised in the economiser with a negative effect on the plant efficiency. The subcooling temperature difference is generally in the range of 2-6 K. A subcooling temperature difference of 3 K is considered in this work based on the IEAGHG report (IEAGHG 2012).
 - 4) The flue gas stack temperature must be kept above the acid and water dew point to avoid condensation in a dry stack design. Moreover, the temperature must be high enough to ensure high buoyancy forces to rise by natural convention and avoid plume visibility.
- The steam mass flow rates generated in the high pressure (HP), intermediate pressure (IP) and low pressure (LP) evaporators as well as the gas and the steam temperature profiles are evaluate according to energy balances in each banks along the HRSG, considering heat transfer by convection from the flue gas to the water/steam, according to Equations [3.67] and [3.68], where \dot{Q}_j is the heat flow rate.

$$\eta_{SC} = \chi \cdot \eta_{\text{Rankine}} = \chi \cdot \frac{\dot{W}_{\text{ST}}}{\dot{m}_{\text{gas}} (h_{\text{gas, HRSG in}} - h_{\text{gas, HRSG out}})} \quad [3.66]$$

$$\dot{Q}_j = \dot{m}_{\text{gas}} (h_{\text{gas, in}} - h_{\text{gas, out}}) \quad [3.67]$$

$$\dot{Q}_j = \dot{m}_{\text{steam/water}} (h_{\text{steam/water, in}} - h_{\text{steam/water, out}}) \quad [3.68]$$

$$\forall j \in 1 \dots \text{no banks}$$

The design of the HRSG is based on the first and the second law of thermodynamics, which implies that as much energy as possible should be recovered from the flue gas and that the water/steam should be as close as possible to the gas temperature. The smaller the temperature difference between the gas and water/steam across the HRSG, the lower the generated entropy in the process.

The heat transfer surface area (A) in each bank is evaluated with the overall heat transfer equation, Equation [3.69], where the overall heat transfer coefficient (U) is a function of the convection heat transfer coefficients for the gas and water/steam sides and thermal conductivity of the materials.

$$\dot{Q}_j = (U \cdot A)_j \cdot LMTD_j \quad \forall j \in 1 \dots \text{no banks} \quad [3.69]$$

The design of the steam cycle for the configurations with conventional EGR and S-EGR consider the same arrangement of the tube banks in the HRSG as in the reference case. The higher GT exhaust flue gas temperature results in a larger approach temperature difference between the superheated and reheated steam, as the maximum HP and IP steam turbines inlet temperature is limited to 600 °C. As the exhaust flue gas temperature does not exceed 780 °C it is possible to keep the same materials for all unfired HRSG (Martelli et al. 2012).

To illustrate the process a temperature – heat flux diagram is shown in Figure 3.14.

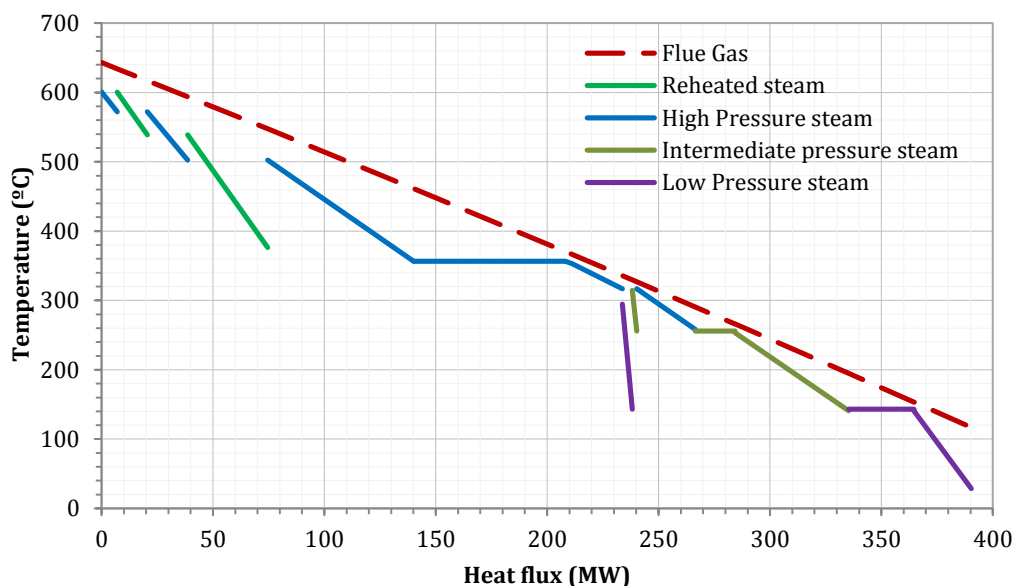


Figure 3.14.- Temperature versus heat flux/thermal power diagram for the heat recovery steam generator for the air-based combustion CCGT configuration.

3.2.4.2 *Deaerator*

Dissolved oxygen and other gases, i.e. carbon dioxide, are removed from the feed water in the deaerator in order to avoid corrosion in the system. Their presence is due to the low pressure at the end of the expansion and in the condenser below the atmospheric pressure, which results in air leaking into the system. The principle is based on the fact that the solubility of gases in saturated water drops to almost zero. The feed water is heated to saturation by adding low pressure steam in a closed tank. The steam and the gases will rise to the surface where they are cooled, and the gases and some steam are vented out of the system at the top of the deaerator. Although the deaeration can be performed in the low-pressure drum, a separate deaerator is considered (Jonshagen 2011).

3.2.4.3 *Steam turbines*

In the 2-in-1 configuration, the steam generated in the two HRSG is feed to one steam turbine train with high pressure (HP), intermediate pressure (IP) and low pressure (LP) cylinders. The design steam turbine inlet temperature is 600 °C for advance steam turbines technology and the admission and the discharge pressure are defined in accordance to the pressure levels in the HRSG, with a pressure drop through the steam ducts proportional to the steam/water mass flow rate. The design pressure in the IP-LP crossover and in the LP drum are selected according to the steam requirements in the reboiler of the post-combustion capture unit as explained in Section 3.2.5. The LP steam turbine capacity is set for the remaining steam mass flow rate after the steam extraction point.

The steam turbines have been modelled in terms of the isentropic efficiencies ($\eta_{\text{isentropic}}$) of the HP, IP and LP cylinders, with estimated values matching the operational conditions reported in the International Energy Agency report (IEAGHG 2012) according to Equation [3.70]. The steam cycle power output is evaluated as indicated in Equation [3.71].

$$\eta_{\text{isentropic}} = \frac{h_{\text{steam in}} - h_{\text{steam out}}}{h_{\text{steam in}} - h_{\text{steam out, isentropic}}} \quad [3.70]$$

$$\dot{W}_{ST} = \sum_j \dot{m}_{\text{steam},j} \cdot (h_{\text{steam in}} - h_{\text{steam out}})_j \quad [3.71]$$

$$\forall j \in \text{HP, IP, LP turbines}$$

3.2.4.4 Power plant heat rejection

A large majority of the CCGT power plants in Europe use recirculation or closed-loop evaporative cooling systems as heat rejection medium (IEAGHG 2012). The cooling water return (CWR) is cooled in a wet cooling tower by evaporation through contact with ambient air and then recirculated back to the main condenser and heat exchangers. This design relies mainly on the latent heat of water evaporation to create the cooling effect. With ambient air at ISO conditions (15 °C, 1.013 bar, 60% RH), the corresponding wet bulb temperature is 10.8 °C. Assuming a cooling tower pinch of 7.4 °C, the cooling water is supplied at 18.2 °C to the condenser and the coolers. For a maximum allowable temperature rise of 11 °C, the cooling water then returns to the cooling tower at 29.2 °C (EBTF 2011).

3.2.4.5 Condenser

The design of the condenser depends on the heat sink available (i.e. cooling water temperature and nature of the cooling medium) and on the exhaust mass flow rate of the low pressure turbine. For a cooling water return (CWR) temperature of 29.2 °C and a condenser pinch of 3 °C (EBTF 2011), the saturation temperature in the condenser is 32.2 °C, which corresponds to a saturation pressure of 48 mbar, as in Equation [3.72]. The steam expansion in the LP steam turbine and, thus, the steam turbines power output highly depends on the cooling water supply (CWS) temperature. The condenser pressure is assumed to be identical for all the configurations investigated.

$$P_{\text{condenser}} = P_{\text{sat}} \quad \text{at} \quad (T_{\text{CWR}} + \Delta T_{\text{condenser pinch}}) \quad [3.72]$$

3.2.5. Thermal integration of the post-combustion CO₂ capture and the power generation systems

The thermodynamic integration of the post-combustion CO₂ capture process using chemical absorption with amine-based solvent technology in the CCGT power plant requires the supply of thermal energy for the solvent regeneration and electrical energy for the CO₂ compression train and ancillary equipment, such as recirculation pumps and flue gas booster fans.

Thermal energy is supplied with steam. The quality of the steam extracted from the power plant steam cycle depends on the pressure and temperature required in the reboiler of the capture plant. CO₂ capture with aqueous monoethanolamine (MEA) solvent is a common benchmarking process widely used for performance comparison of post-combustion capture technology. It is typically operated with a reboiler designed for saturated steam at 3 bar.

Superheated steam is extracted from the LP superheater in the HRSG and from the steam turbine IP/LP crossover, as illustrated in Figure 3.1. The LP drum and the IP/LP crossover are designed for an operation pressure of 4 bar to overcome the pressure drop, estimated at approximately 1 bar along the pipe. The steam is then suitably conditioned for reboiler use. The superheated steam is cooled in a heat exchanger and brought to saturation conditions with sprayed nozzle desuperheater using part of the reboiler condensate return, as illustrated in Figure 3.15. By selecting the appropriate nozzle, the amount of residual superheat can be reduced to 3-5 °C (Spirax Sarco, 2016).

The condensate from the reboiler is pumped back to the steam cycle and it can be either mixed with the feed water (International Energy Agency 2012) or injected in the deaerator. Since the pressure and the temperature of the condensate return are suitable for the deaerator, this option is considered and proposed as an alternative to the configuration in the IEAGHG report (2012), used as the reference case. A new build steam cycle with dedicated steam extraction for the capture unit is considered in each of the investigated configurations. The steam turbines are sized for steam extraction at nominal conditions, operating at the design efficiency. The capture plant is integrated in the power plant cycle with the same degree of heat integration in all the configurations.

3.2.6. Technical and operation parameters for the reference CCGT plant

The reference plant is an air-based combustion CCGT with a 2-on-1 configuration: two GE F-class (GE9371FB) gas turbines with the flue gas exiting into two HRSGs, which jointly supply steam to a subcritical triple pressure steam cycle. The configuration of the reference plant is based on the International Energy Agency report of 2012 (IEA 2012). The net power output of the CCGT power plant equipped with PCC system is approximately 780 MWe and the net thermal efficiency is approximately 52 %, as indicated in Table 3.1.

The gas turbine operates at a turbine inlet temperature (TIT) of 1371 °C and air fuel ratio (AFR) of 40.5 on mass basis equivalent to an excess of air of 150%, at ISO atmospheric conditions and 100% load, with a power output at coupling of 285 MWe and thermal efficiency of 38.2%. Technical and operational parameters of the gas turbine engine of the reference plant are presented in Table 3.2 and have been obtained from General Electric technical specifications (General Electric Power Generation 2016) and information from previous publications using the same class gas turbine engine (Sánchez et al. 2010, Jordal et al. 2012, Jonshagen et al. 2011, Chacartegui et al. 2012).

The remaining heat contained in the exhaust flue gas is partially recovered to generate steam at three pressure levels in the HRSG. Technical and operation data of the HRSG are presented in Table 3.3. The steam from each GT-HRSG train is sent to a subcritical triple pressure steam turbine. Technical details of the steam turbines are presented in Table 3.4

Two post-combustion capture systems using CO₂ scrubbing technology are implemented at the tail-end, one per each GT-HRSG train. In each train, flue gas is cooled down before tendering the absorber. The capture process is explained in more detail in Section 3.3.

The rigorous model of the power plant is developed in gPROMS Model Builder (PSE 2016), as it is a process modelling software that allows creating customized models for each unitary operation, using the property methods of Peng-Robinson as equation of state for gas and the Steam Tables (IAPWS-95) for water/steam. Additional technical data and assumption to perform the simulations are included in Appendix A.

Table 3.1.- Combined cycle gas turbine power and thermal efficiency

Gas turbine net power per GT-HRSG train	MWe	285.8
Gas turbines net power	MWe	571.6
Open cycle thermal efficiency	% LHV	38.18
Steam turbine power	MWe	256.0
Fuel heat input per GT-HRSG train	MWth	748.0
CCGT gross power	MWe	827.6
CCGT gross thermal efficiency	% LHV	55.50
CCGT net power output	MWe	777.44
CCGT net thermal efficiency	%	51.94

Table 3.2.- Gas turbine engine technical and operation parameters per GT-HRSG train

Gas turbine		
Model	GE 9371FB	
Air mass flow rate	kg/s	641.81
Fuel mass flow rate	kg/s	16.10
Compressor		
No. stages	--	18
Inlet pressure drop	kPa	1
Pressure ratio (PR)	--	18.1
Compressor isentropic efficiency	%	79.5%
Combustor		
Pressure drop	%	5
Combustor efficiency	%	99.8%
P fuel in	bar	27.20
T fuel in	°C	117
Turbine		
No. stages	--	4
Turbine inlet temperature (TIT)	°C	1371
Turbine inlet temperature (TIT)	K	1644
Turbine back pressure	bar	1.039
Turbine isentropic efficiency	%	90.5%
Exhaust flue gas (EFG)		
Pressure	kPa	103.9
Temperature	°C	643.29
Exhaust flue gas flow rate	kg/s	657.92
Composition:		
	CO ₂	%vol 4.21%
	H ₂ O	%vol 8.82%
	N ₂	%vol 74.21%
	O ₂	%vol 11.87%
	Ar	%vol 0.89%
Molar mass	g/mol	28.38
GAS TURBINE PERFORMANCE		
Mechanical efficiency compressor	%	99.6
Net Power	MW	285.76
Net Thermal efficiency	%	38.18
Net Heat Rate	kJ/kWh	9428.07

Table 3.3.- Heat recovery steam generator technical and operation parameters per GT-HRSG train

Heat recovery steam generator		
Flue gas mass flow rate	kg/s	657.92
Gas Inlet temperature	°C	643.29
Gas Stack temperature	°C	117.87
Feed water temperature	°C	32.28
Gas inlet pressure	bar	1.039
Gas outlet pressure	bar	1.013
HRSG efficiency	%	99.7

Table 3.4.- Steam turbines technical and operation parameters for the two GT-HRSG trains

Steam turbine		
<i>HP STEAM TURBINE</i>		
Live steam molar flow	mol/s	9587
Live steam mass flow	tn/h	621
P in	bar	170
T in	°C	600
P out	bar	45.2
T out	°C	394
Isentropic efficiency	%	88.1%
<i>IP STEAM TURBINE</i>		
Hot reheated molar flow	mol/s	10445
Hot reheated mass flow	tn/h	677
P in	bar	40
T in	°C	600
P out	bar	3.75
T out	°C	266.8
Isentropic efficiency	%	92.4%
<i>LP STEAM TURBINE</i>		
Turbine exhaust molar flow	mol/s	5595
Turbine exhaust mass flow	tn/h	363
P in	bar	3.75
T in	°C	266.93
P out	bar	0.0481
Exhaust steam quality	%	91.9%
Isentropic efficiency	%	88.0%

3.3. Post-combustion CO₂ capture and compression systems

Strategies for increasing CO₂ concentration at the exhaust of CCGT power plants with EGR and S-EGR, and the associated reduction in flue gas flow rates in some of these configurations, have a wide range of benefits for post-combustion CO₂ capture technology. For the purpose of a performance assessment of these concepts, a model consisting of the power cycle of a CCGT, a wet scrubbing chemical absorption process with conventional aqueous 30 %wt. monoethanolamine (MEA) solvent and a CO₂ compression train is developed. The linked model is shown in Figure 3.1.

An aqueous 30 %wt. MEA solvent is used as a benchmark solvent to compare strategies for increasing CO₂ concentration at the exhaust of a reference CCGT power plant on a consistent basis. Aqueous MEA solutions have been widely studied in the literature and a large amount of experimental data at laboratory and pilot plant scale is available. It is, at the time of writing, a widely used benchmark technology used to compare other solvent technologies (Razi et al. 2013; Sanchez Fernandez et al. 2014) in terms of efficiency and costs.

Any other solvent processes and any other type of post-combustion capture technology, e.g. membranes or adsorption would likewise benefit from an increase in performance with EGR or S-EGR. Assessing the benefits to these technologies is outside the scope of this thesis, which concentrates instead on CCGT power plant systems and assesses configurations with a benchmark solvent process.

3.3.1. CO₂ capture plant description

The process flow diagram for the conventional MEA based chemical absorption process, as set up in Aspen Plus, is illustrated in Figure 3.15.

The flue gas temperature entering the absorber has to be adapted to the specific solvent. The selection is generally a trade-off between the kinetics and the thermodynamics. The reactions kinetic rate increase with increasing temperature, while a lower temperature displaces the thermodynamic equilibrium to a higher CO₂ loading and enhances the solvent capacity. Moreover, the flue gas typically enters the absorber saturated in moisture in order to minimise water evaporation from the solvent and possible solvent carry over. A temperature of 45 °C at the inlet of the absorber is considered for MEA (Kvamsdal et al. 2010). Unlike conventional process configurations where flue gas cooling is primarily achieved with a direct contact cooler, the reference configuration relies on cooling down the flue gas leaving the HRSG in a gas/gas rotary heat exchanger, with a further reduction of the temperature to saturation conditions achieved in a direct contact cooler. This is discussed in more detail in

Chapter 6. In the gas/gas heat exchanger, sensible heat from the flue gas is transferred to the CO₂-depleted gas, which typically leaves the absorber at a temperature similar to the inlet flue gas. The CO₂-depleted gas must then be reheated in order to increase buoyancy forces and avoid plume visibility in a dry stack design.

In the absorber, the flue gas is brought into direct contact with the solvent. The CO₂ is chemically bounded to the amine solvent and the CO₂ loaded solvent (rich solvent) leaves the column at the bottom. The CO₂-depleted gas is cooled down in the water wash section at the top of the absorber to avoid solvent vaporization and solvent losses into the atmosphere. The flue gas temperatures at the inlet and at the outlet of the absorber column are similar to maintain the water balance in the system (Kvamsdal et al. 2010).

The rich solvent is reheated in the lean-rich heat exchanger and enters the top of the stripper column where it is thermally regenerated. The steam generated in the reboiler strips off the CO₂ from the solvent. The vapour phase leaving the top of the stripper column is condensed at 40 °C. The condensed liquid is separated from the gas phase in a flash vessel and recycled back to the stripper at the top stage (reflux). The CO₂-rich gas, with a CO₂ concentration of around 95 vol%, is compressed, liquefied and pumped up to 110 bar for transport and storage. The regenerated solvent (lean solvent) returns to the absorber at the first stage, after being cooled down to 45 °C, first in the lean-rich heat exchanger and then in the lean solvent cooler.

As the reaction kinetics between CO₂ and MEA are relatively fast, the CO₂ mass transfer is the limiting step in the chemical absorption process. The rate of mass transfer depends on the overall mass transfer coefficient and on the available driving force, which is directly proportional to the CO₂ partial pressure in the gas phase. The overall mass transfer coefficient varies with process parameters, including gas flow rate, liquid flow rate, CO₂ partial pressure, MEA concentration, CO₂ loading and interfacial area (Razi et al. 2014). When the CO₂ absorption rate is limited by the rate of mass transfer, the solvent CO₂ loading is lower than the corresponding value in equilibrium with the actual CO₂ partial pressure in the gas, decreasing the solvent capacity. This fact has a negative impact on the specific reboiler duty since more solvent is required to capture the same amount of CO₂, and in the packing volume, since a larger surface contact area is required to achieve a certain CO₂ absorption efficiency. The resistance to mass transfer is taken into account by rigorously modelling the chemical absorption process using a rate-based model.

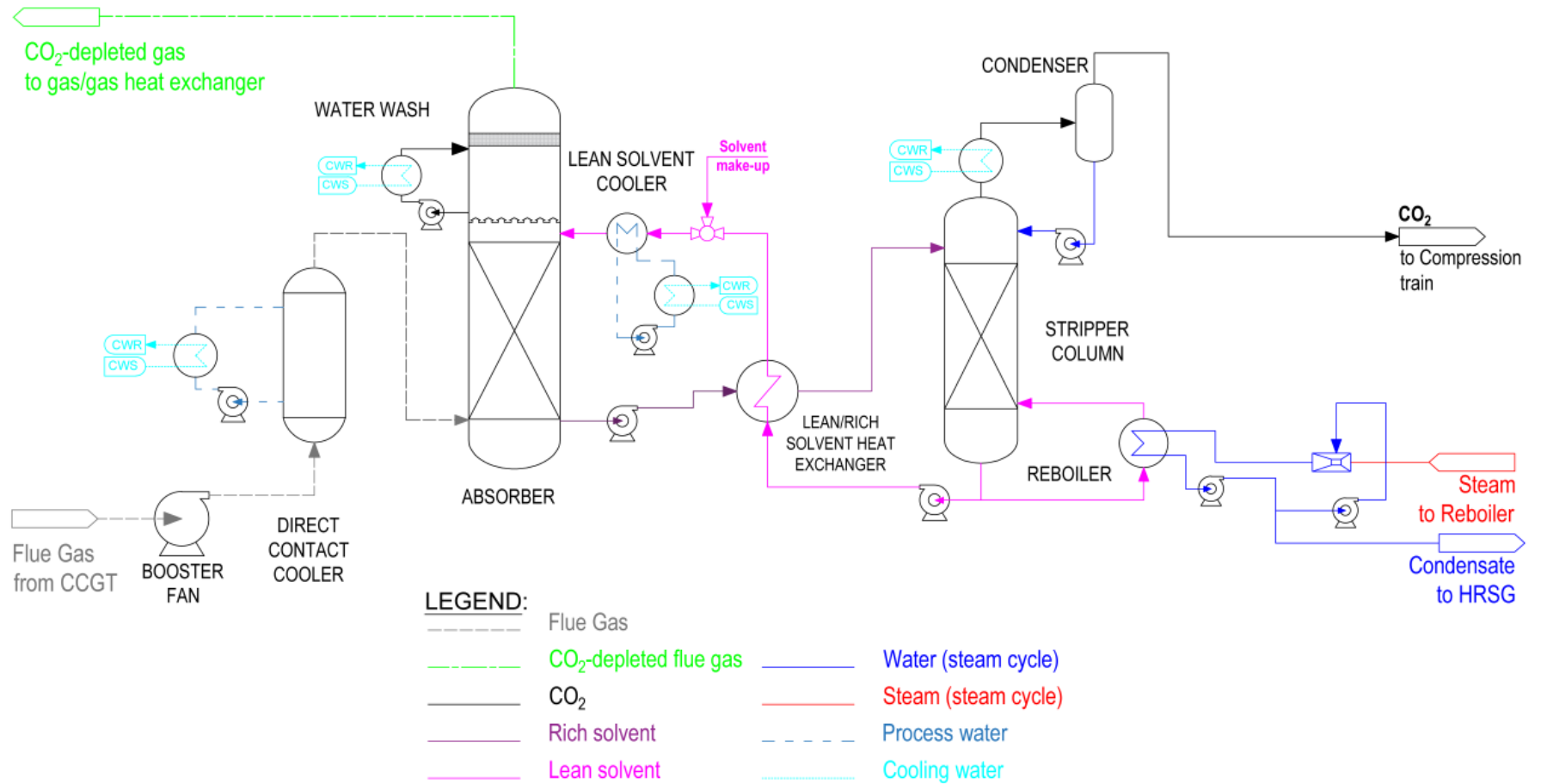


Figure 3.15.- Process flow diagram of the post-combustion CO₂ capture system with amine-based chemical absorption technology.

3.3.2. CO₂ capture process modelling

The capture process technical data and performance are determined by simulation using Aspen Plus commercial software (Aspen Tech). The electrolyte non-random two-liquid (E-RNRTL) thermodynamic package is used to predict the CO₂ solubility in aqueous MEA solution.

The absorption process is described with three unit operations: direct contact cooler, absorber and water wash section. The absorber is simulated as a rate-based model which includes reaction kinetics, thermodynamic equilibrium, mass transfer and heat transfer phenomena. The reactions between CO₂ and MEA are very fast and they take place in the liquid phase with no reaction in the gas phase (Razi et al. 2013). Mass and heat transfer rates between the contacting phases are therefore based on the combined diffusion-reaction process in the liquid phase, while phase equilibrium exists at the interface. For the gas phase only diffusional resistance is taken into account. Mass transfer coefficients and the interfacial area are evaluated according to correlations developed by Bravo et al. (Bravo et al. 1985, 1992) which are valid for structured packing Sulzer Mellapak 250Y, and heat transfer coefficients are predicted by the Chilton and Colburn analogy. The bulk properties are typically evaluated at the outlet conditions for the liquid phase, i.e. well-mixed flow model, and at average conditions for the vapor phase, i.e. plug flow model, (Abu Zahra 2009; Sánchez Fernández 2013; Bui et al. 2014). Flow type refers to how the bulk properties of the fluid are calculated. The plug flow model uses discretised partial differential equations in a distributed system, while the well-mixed model uses ordinary differential equations at one or more well-mixed nodes in a lumped system. These are an adequate assumptions in steady state models (Walters et al. 2016)

The kinetic model, describing the reaction rates between CO₂ and MEA, has significant impact on the simulation and scale up analysis of an absorber. A number of kinetic data for the CO₂-MEA-H₂O system are available in literature. The kinetic model considered in Aspen Plus is described in Razi's work, where results from the absorber model were in good agreement with experimental data sets from the Esbjerg CESAR (CO₂ Enhanced Separation and Recovery) pilot plant, for CO₂ capture with aqueous MEA solution at 30 wt% from a flue gas slip of a 400 MWe pulverized coal-fired power plant (Razi et al. 2013; Sanchez Fernandez et al. 2014). The modelling results for the reference case, a CCGT plant with PCC, are compared to data from a test campaign with 30 wt% MEA at the CO₂ Technology Centre, in Mongstad, Norway (Hamborg et al. 2014).

The lean-rich solvent heat exchanger is designed on the basis of a fixed overall heat transfer coefficient and a temperature approach of 8 °C (cold out- hot in approach).

The stripper is simulated with an equilibrium model. Due to the high operation temperature, the kinetic of the reactions is fast and the process is thermodynamically controlled. Moreover, a high temperature enhances the mass transfer and mass transfer resistance is neither the limiting step. The stripper is designed to achieve a fixed molar CO₂ recovery ratio and the number of equilibrium stages is consequently defined. The CO₂ recovery ratio is set to control the lean solvent CO₂ loading at which the stripper column operates and its value is selected to bring the specific heat consumption to a minimum.

3.3.3. Absorber sizing

Technical parameters in the CO₂ capture system are evaluated following the procedure described in Freguia's work (Freguia and Rochelle 2003) to achieve the required post-combustion CO₂ capture in the absorber that results in a 90% overall CO₂ capture level. The overall CO₂ capture level and the post-combustion CO₂ capture efficiency are defined according to Equations [3.73] and [3.74], respectively.

$$\text{Overall CO}_2\text{ capture level} = \frac{|\text{mol CO}_2|_{\text{to transport and storage}}}{|\text{mol CO}_2|_{\text{generated in natural gas combustion}}} \quad [3.73]$$

$$\text{PCC efficiency} = 1 - \frac{|\text{mol CO}_2|_{\text{absorber outlet}}}{|\text{mol CO}_2|_{\text{absorber inlet}}} \quad [3.74]$$

The absorber diameter is determined for a flue gas velocity that corresponds to 85% of the velocity at the flood-point (Oexmann et al. 2008). The absorber packing height is then increased for a constant diameter. A larger packing volume results in a larger contact surface area and a longer residence time, which enhances the CO₂ absorption rate and, thus, the CO₂ loading of the solvent at the bottom of the absorber (rich solvent). The maximum achievable CO₂ loading is the corresponding value in equilibrium with the CO₂ partial pressure in the flue gas. For a constant lean solvent CO₂ loading, it results in an increased solvent capacity and, thus, less amount of solvent is required to achieve certain CO₂ capture efficiency in the absorber. With a smaller solvent flow rate, the specific reboiler duty decreases. The absorber packing height is augmented up to a value at which a further increase results in a marginal gain in the rich solvent CO₂ loading (<0.2% of the previous value) and in a marginal reduction of the reboiler duty.

The optimisation of the absorber packing height in the reference case, i.e. an air-based combustion CCGT plant with PCC system, is illustrated in Figure 3.16.

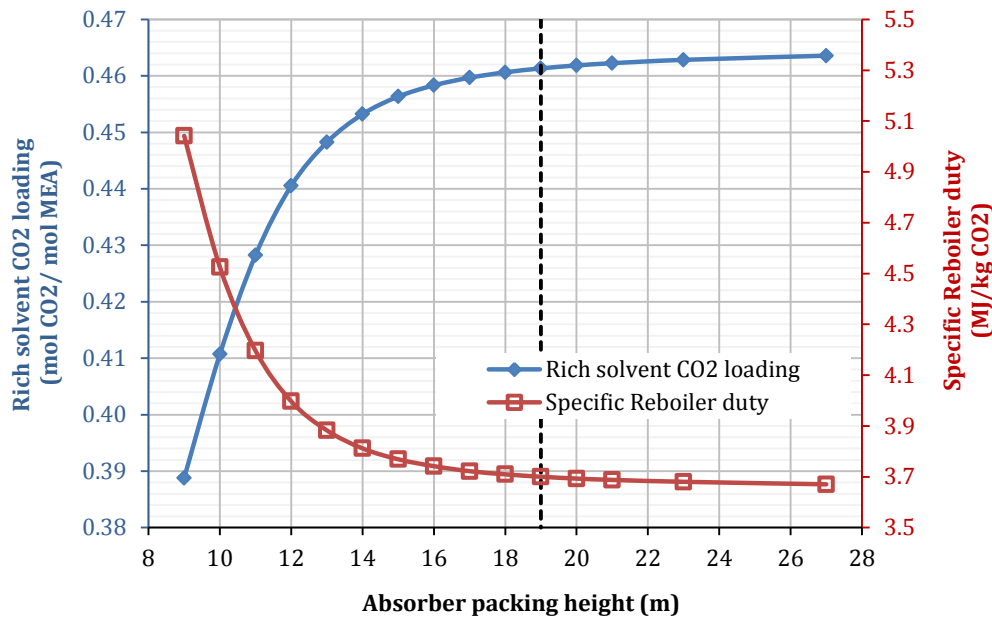


Figure 3.16.- Sensitivity of the rich solvent CO₂ loading and the specific reboiler duty to the absorber packing height for the reference case: air-based combustion CCGT with PCC.

3.3.4. Reboiler duty optimisation

The thermal energy supplied in the reboiler by condensing steam is used in the stripper column to provide: (1) the sensible heat required to heat up the solvent to the reboiler temperature, (2) the heat of desorption of CO₂ required to reverse the chemical reactions between the amine and the CO₂ and release CO₂ into the vapour phase, (3) the latent heat for vaporization of water to produce the stripping steam. The steam is condensed in the overhead condenser at 40 °C. The condensed water returns to the stripper as reflux and the CO₂ rich gas is sent to the compression train. The relative contribution of the three energy sinks to the reboiler heat duty is illustrated in Figure 3.17.

The recovery of CO₂ from the loaded solvent coming from the absorber is an energy intensive process requiring substantial quantities of low/intermediate pressure steam extraction from the power plant steam cycle. The quality/grade of the steam is determined by the required temperature for solvent regeneration.

Aqueous solvents with a relatively high heat of desorption are desired to be regenerated at the highest possible temperature. The ratio of CO₂ and water vapour partial pressures in the

gas phase at equilibrium, $(P_{CO_2}^*/P_{H_2O}^*)$ increases with temperature according to Van't Hoff expression (Freguia and Rochelle 2003; Oexmann and Kather 2009), as Equation [3.75].

$$\frac{d\ln P_{CO_2}^*}{dT} = \left(-\frac{\Delta H_{CO_2}}{RT^2} \right) \quad [3.75]$$

The reboiler duty thus decreases with increased stripper pressure as less amount of stripping steam is generated. The extraction of a higher quality steam, at a higher temperature and a higher pressure, results however in a larger electricity output penalty in the steam cycle, although, an increase in the stripper pressure results in a smaller CO₂ compression work. In thermally integrated power plant, the operating pressure of steam extraction should be a trade-off between the compressor work and the penalty in steam turbine power output.

For conventional MEA solvent, the maximum allowable regeneration temperature is around 120 °C to prevent from thermal degradation (polymerisation) (Rochelle 2012). The temperature of the condensing steam in the reboiler exceeds the solvent temperature by the pinch temperature assumed in the reboiler design. The larger the pinch temperature the lower the heat exchanger surface area but a higher steam flow rate is then required. A pinch temperature of 13 °C is assumed here (Sanchez Fernandez et al. 2014). By condensing saturated steam over the metal tubes/plates in the reboiler, latent heat of condensation is transferred more efficiently than the specific heat from the superheated steam. Therefore, saturated steam at 133 °C and 3 bar needs to be supplied from the power plant steam cycle. The most accessible point for steam extraction in a CCGT power cycle is the IP/LP crossover. The thermal integration with the power plant is explained in Section 3.2.5.

For each configuration with a given CO₂ concentration and flow rate, the minimum specific reboiler duty, in MJ/kg CO₂, is evaluated by carrying out a sensitivity analysis of the lean solvent flow rate entering the absorber. The conditions in the stripper are set to achieve the lean solvent CO₂ loading resulting in the required CO₂ capture efficiency in the absorber to achieve an overall CO₂ capture level of 90%. A fixed CO₂ capture level is considered for the purpose of comparison of the different configurations. The overall CO₂ capture level takes into account the amount of carbon dioxide exiting the boundaries of the plant. This procedure is qualitatively illustrated in Figure 3.17(a). The control strategy to vary the lean solvent CO₂ loading can be designed by varying either the temperature or the pressure in the stripper column. A constant temperature of the saturated steam supplied to the reboiler of 120 °C is assumed here and the total pressure in the stripper column is modified, i.e. with a back pressure valve. The saturated steam flow is evaluated to supply the reboiler duty necessary to achieve the lean solvent CO₂ loading.

A smaller total pressure results in a smaller CO₂ partial pressure, as the water vapour partial pressure is almost constant at a given temperature. This fact displaces the equilibrium towards a lower CO₂ loading of the lean solvent, according to the vapour-liquid equilibrium curves. The larger solvent capacity results in a smaller solvent flow rate to capture 90% of the amount of CO₂ generated in the combustion. However, an increase in the total pressure results in a higher CO₂ loading of the lean solvent and, thus, a larger solvent flow rate is necessary.

The effect on the reboiler duty is that the contribution of the sensible heat increases directly proportional to the solvent flow rate and, thus, becomes more significant at a higher lean solvent CO₂ loading. Meanwhile, the contribution of the latent heat for steam generation is more relevant at a lower solvent flow rate as more steam needs to be generated to strip off the CO₂ and achieve low lean solvent CO₂ loadings. This is qualitatively illustrated in Figure 3.17(a). There is therefore an optimal value of the lean solvent CO₂ loading that results in a minimum specific reboiler duty.

Figure 3.18 shows the optimisation procedure to evaluate the optimum CO₂ loading of the lean solvent and the solvent flow rate that minimises the reboiler duty for the reference case with an air-based combustion CCGT with PCC.

In practice, the optimisation of the reboiler duty should be conducted to maximise the electricity output and, thus, should consider the variation in the CO₂ compression work when varying the pressure in the stripper. Yet, the range of pressures considered to minimise the reboiler duty marginally changed.

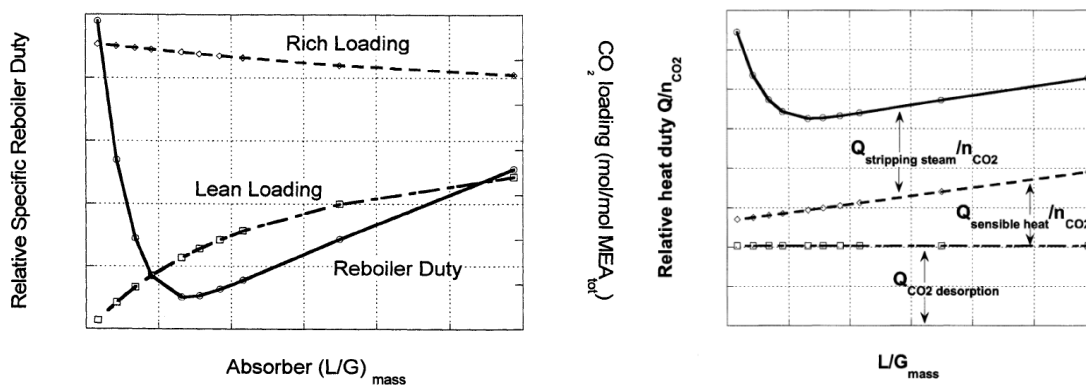


Figure 3.17.- (a) Illustrative example of reboiler duty minimisation as a function of the absorber liquid/gas flow rate ratio and (b) contributions to the specific reboiler heat duty (Freguia and Rochelle 2003)

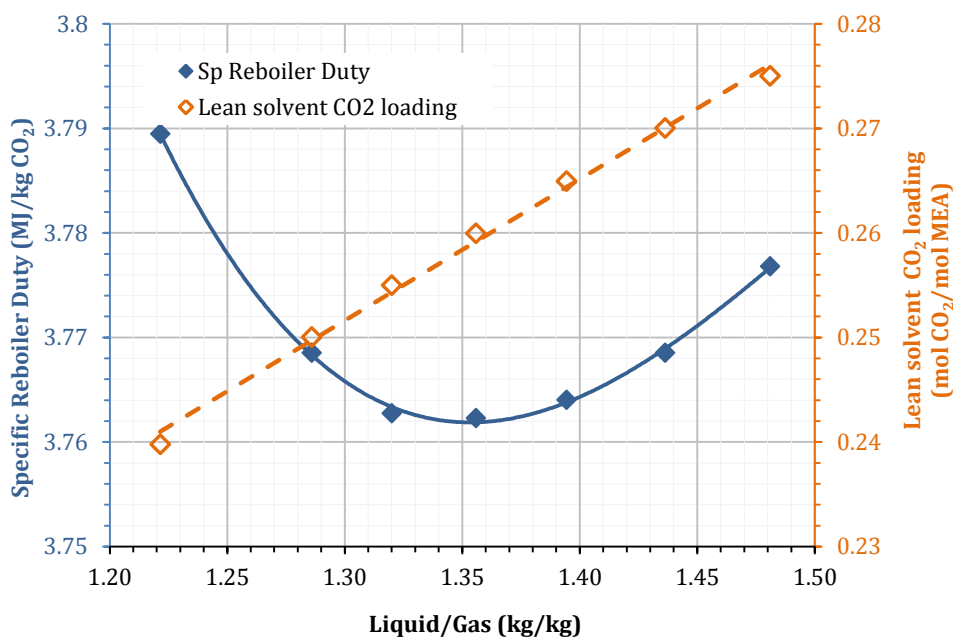


Figure 3.18.- Sensitivity of the specific reboiler duty to the liquid/gas flow rates ratio and the corresponding lean solvent CO₂ loading for the reference case: air-based combustion CCGT with PCC.

3.3.5. CO₂ compression

The electric power duty of the CO₂ compressor contributed to the efficiency penalty of the integrated overall process. The CO₂-rich gas stream leaves the condenser of the stripper column at 40 °C and 2 bar, with a CO₂ purity of 95 % vol and needs to be conditioned prior to transport and storage. The CO₂-rich stream is compressed up to around the critical pressure (73.8 bar) in the compression train, which consists of three stages with intercooling and water separation between stages. Liquid phase CO₂ at 73 bar and 28 °C is pumped up to 110 bar for transport and storage in supercritical/dense phase. The assumptions and operational conditions are defined as in the EBTF common framework document (EBTF 2011) with a fixed isentropic efficiency of 85% and mechanical efficiency of 95%. The CO₂ mass flow rate slightly varies from one configuration to the other due to small variations in the fuel consumption.

- Compression stages discharge pressure: 4.3/18.6/73 bar.
- Gas outlet intercooling temperature: 28 °C.
- CO₂ purity for transport and storage: 99.8 % vol.

The process flow diagram of the compressor train is illustrated in Figure 3.19.

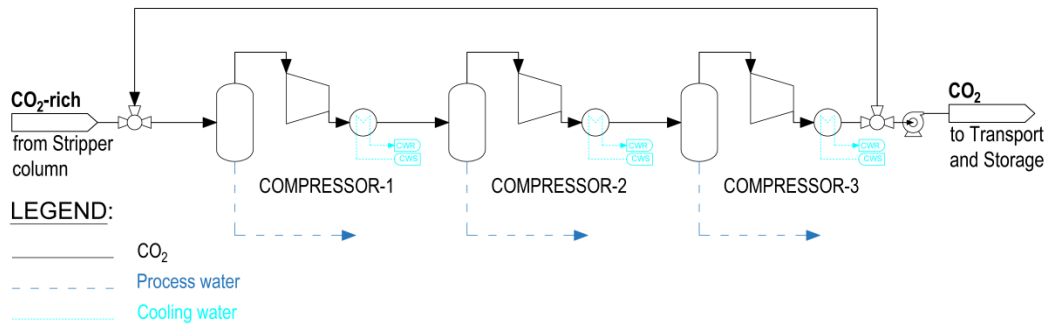


Figure 3.19.- Process flow diagram of the CO₂ compression train.

3.3.6. *Technical and operation parameters of the CO₂ capture and compression systems for the reference plant*

In the reference case consisting of an air-based combustion CCGT plant with PCC, one capture system is considered per GT-HRSG train of the combined cycle power plant with 2-in-1 configuration. A flue gas flow rate of approximately 660 kg/s with 4.2 vol% CO₂ is treated in each capture system, consisting of two absorber columns each.

The dimensions of the absorber are estimated following the procedure described in Section 3.3.3, as illustrated in Figure 3.16. The solvent flow rate and the lean solvent CO₂ loading are optimised for each absorber packing height following the procedure described in Section 3.3.4, as illustrated in Figure 3.18. The minimum reboiler duty of 3.746 MJ/kg CO₂ is achieved with a packing height of the absorber section of 19 m, a CO₂ loading of 0.26 mol_{CO₂}/mol_{MEA} and a ratio of solvent to gas mass flow rate of 1.36.

The capture process operation and technical data of the CO₂ capture process and the CO₂ compression are presented in Table 3.5 for the reference case, consisting of an air-based combustion CCGT plant, as described in Section 3.2, with PCC. Technical parameters and assumptions for the modelling of the CO₂ capture and compression train are included in Appendix A.

Table 3.5.- Technical and operational parameters of the CO₂ capture plant for the reference case: Air based combustion CCGT with PCC per GT-HRSG train

CASE	Air-based combustion (reference case)	
Overall CO ₂ capture level	%	90
Absorber		
<i>Flue gas BOTTOM</i>		
Mass flow rate	kg/s	658
CO ₂ conc.	%vol	4.21
<i>Flue gas TOP</i>		
CO ₂ conc.	%vol	0.43
Absorber efficiency	%	90
Rich solvent loading	mol _{CO₂} /mol _{MEA}	0.26
Lean solvent loading	mol _{CO₂} /mol _{MEA}	0.458
Lean solvent molar flow rate	mol/s	886
<i>Absorber dimensions</i>		
No. Absorbers	--	2
Diameter	m	12
Packing height	m	19
Total packing volume per GT+HRSG train	m ³	4190
Stripper		
Stripper pressure	bar	1.84
Steam specific consumption	kg/kg CO ₂	1.71
Specific reboiler duty	MJ/kg CO ₂	3.746
Reboiler pressure	bar	2.95
Reboiler temperature	°C	133
CO ₂ to pipeline	kg/s	76.5
CO₂ compression train		
CO ₂ final pressure	bar	110
Specific compression work	kJ/kg CO ₂	334

3.4. Rotary gas/gas heat exchangers for water and heat management

The use of rotary regenerative gas/gas heat exchangers is proposed in heat integration options to reduce or eliminate both process and cooling water requirements of the DCC upstream of the CO₂ absorber, and to ensure that the CO₂-depleted gas leaving the absorber reach an appropriate temperature at the stack.

Hybrid and dry air-cooling systems consisting of different configurations of rotary regenerative gas/gas heat exchangers are examined. The technology and the methodology are described in this section. A detailed description of the proposed configurations and results are included in Chapter 6.

Rotary gas/gas heat exchangers rely on a technology used in coal fired power plants to pre-heat the primary and the secondary combustion air streams using the flue gas streams exiting the boiler. The same technology is also used to recover heat from the inlet stream of the flue gas desulphurization (FGD) systems to increase the temperature of the outlet stream and its buoyancy at the inlet of the stack (Kitto and Stultz 1992). The concept of regenerative heat transfer can easily adapted to CCGT with CO₂ capture applications.

3.4.1. Rotary gas/gas heat exchangers technology

In rotary regenerative heaters, heat is indirectly transferred by convention as a heat storage medium is periodically exposed to hot and cold gas streams flowing in opposite directions (counter current flow). Continuous cycling exposure is accomplished by a rotary mechanism and steel elements are used as the heat storage medium. Regenerative heating surface elements are a compact arrangement of pair of specially formed metal plates, providing high surface area per unit volume. Each element pair consists of a combination of flat, notched, corrugated, herringbone or undulate plate profiles which are packed into self-contained baskets installed into the rotor in two or more layers. The main components in a rotary heat exchanger are illustrated in Figure 3.20 (Kitto and Stultz 1992). A bisector, trisector or quadsector configuration can be selected according to the number of streams involved in the heat transfer process and, the open cross section is divided proportionally to their flow rate, so that the gas velocity at either side of the sector plate is similar and does not result in a high pressure drop.

Due to the rotation, leakage occurs between the gas streams. Direct leakage (also called gap leakage) occurs through the radial, axial and other seal between rotation and stationary parts, due to pressure differential between the gas streams on either side of the sector plate. Multiple axial and radial seals under the sector plate are used to lower direct leakage flow.

Entrained leakage (also called carryover leakage) is the gas contained in a rotor sector as it is carried into the other stream by rotor rotation. This leakage is directly proportional to the void volume of the rotor and the rotor speed. Regenerative rotary heat exchangers are therefore designed to meet thermal performance requirements, while maintaining the leakage levels and pressure drop as low as possible.

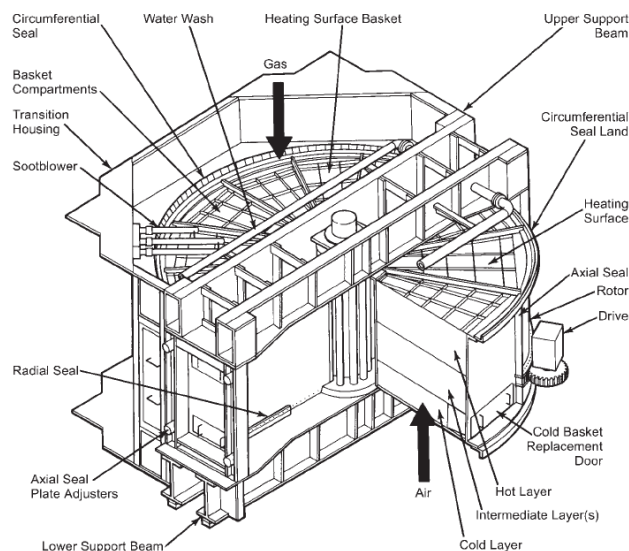


Figure 3.20.- Example of a typical rotary regenerative heat exchanger used in coal-fired power plants (Kitto and Stultz 1992)

3.4.2. Methodology for the selection, sizing and thermal performance analysis of rotary gas/gas heat exchangers

The sizing of the rotary heat exchangers and the thermal performance analysis uses a methodology specifically developed for this novel application and is based on proprietary software developed by Howden Group, a manufacturer of rotary heat exchangers. The dimensions and operational parameters are selected to achieve a satisfactory outlet temperature of the gas streams at the cold and hot ends of the device.

Energy balance and heat transfer equations are solved to obtain the gas and metal temperature profiles at steady state. The overall heat transfer coefficient is evaluated from correlations that include parameters based on Howden's experience and heating surface area is defined by selecting the diameter of the rotor and length of the metal elements. The diameter and the length of the elements are varied in the analysis, with material specifications, metal thickness and rotor speed identical for all configurations and selected according to practical experience. The diameter is first sized to achieve a typical non-erosive gas velocity, below 15 m/s, and the element depth is then sized. Longer elements result in a larger pressure drop while larger diameters result in a lower gas velocity and a lower

pressure drop, although this needs to be balanced against the higher direct and entrained leakage levels. Multiple axial and radial seals are used to minimise direct leakage flow rate. An appropriate design is therefore the result of a trade-off to achieve the required outlet temperature with minimum pressure drop, acceptable leakage levels and heat exchanger size.

Due to the smaller temperature differential at the cold end in this particular application, compared to air preheaters in coal-fired power plants, once a certain heat exchanger size is reached, a large increase in the heating surface area becomes necessary to obtain a marginal decrease/increase of the outlet temperature of the hot/cold streams respectively.

If a temperature of the flue gas stream lower than the dew point at the cold end of the rotary heat exchangers is required, additional cooling capacity will be necessary to remove the latent heat of water condensation. Water condensation will occur on the heating metal elements in the high temperature flue gas section as it is cooled down. With the low rotational speed of the wheel, a fraction of the water drops by gravity, ($\dot{m}_{water\ drained}$), with a carefully selected direction of the gas. The remaining fraction is entrained to either the CO₂-depleted flue gas or the air section due to the rotation of the baskets containing the elements, where it would partially evaporate in the CO₂-depleted or air stream. This is illustrated in Figure 3.21.

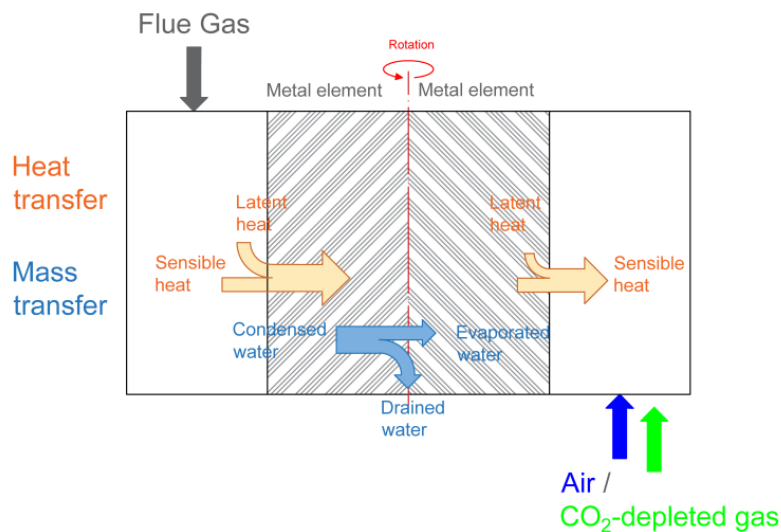


Figure 3.21.- Heat and mass transfer of water for rotary heat exchangers operated below the flue gas dew point (Herraiz et al. 2015).

The overall energy balance for a rotary heat exchanger with a bisector arrangement, where heat is transferred from the flue gas into either the CO₂-depleted gas (gas/gas rotary heat exchanger) or the air streams (air/gas rotary heat exchanger) is given by Equations [3.76], [3.77] and [3.78] and Equations [3.79] and [3.80], respectively. The overall energy balance for a rotary heat exchanger with a trisector arrangement, where the heat is transferred from the flue gas into the CO₂-depleted gas and the air stream in a single device, is given by Equations [3.83] and [3.84]. The phenomena of water condensation is considered in Equations [3.81] and [3.82] for the air/gas heat exchanger and in Equations [3.85] and [3.86] for the air/air/gas heat exchanger. The proposed configurations are described in more detail in Chapter 6.

Gas-gas heat exchanger

$$\dot{Q}_{EFG\ side} = \dot{Q}_{CO_2\text{-depleted}\ gas\ side} \quad [3.76]$$

If $T_{EFG,out} > T_{dew\ point}$ (no water condensation), then:

$$\begin{aligned} \dot{m}_{EFG,in} \cdot h_{EFG,in} - \dot{m}_{EFG,out} \cdot h_{EFG,out} &= \dot{m}_{CO_2\text{-depleted},in} \cdot h_{CO_2\text{-depleted},in} \\ &- \dot{m}_{CO_2\text{-depleted},out} \cdot h_{CO_2\text{-depleted},out} \end{aligned} \quad [3.77]$$

$$\dot{Q} = \dot{m} \cdot A \cdot U \cdot LMTD \quad [3.78]$$

Air-gas heat exchanger

$$\dot{Q}_{EFG\ side} = \dot{Q}_{air\ side} \quad [3.79]$$

If $T_{EFG,out} > T_{dew\ point}$ (no water condensation), then:

$$\dot{m}_{EFG,in} \cdot h_{EFG,in} - \dot{m}_{EFG,out} \cdot h_{EFG,out} = \dot{m}_{air,in} \cdot h_{air,in} - \dot{m}_{air,out} \cdot h_{air,out} \quad [3.80]$$

If $T_{EFG,out} < T_{dew\ point}$ (water condensation), then:

$$\begin{aligned} \dot{m}_{EFG,in} \cdot h_{EFG,in} - \dot{m}_{EFG,out} \cdot h_{EFG,out} + \dot{m}_{EFG,dry}(w_{in} - w_{out}) \cdot h_{latent} \\ = \dot{m}_{air,in} \cdot h_{air,in} - \dot{m}_{air,out} \cdot h_{air,out} - \dot{m}_{air,dry}(w_{in} - w_{out}) \cdot h_{latent} \end{aligned} \quad [3.81]$$

$$\dot{m}_{EFG,dry}(w_{in} - w_{out}) - \dot{m}_{water\ drained} = \dot{m}_{air,dry}(w_{in} - w_{out}) \quad [3.82]$$

Air-gas-gas heat exchanger (trisector)

$$\dot{Q}_{EFG\ side} = \dot{Q}_{CO_2-depleted\ side} + \dot{Q}_{air\ side} \quad [3.83]$$

If $T_{EFG,out} > T_{dew\ point}$ (no water condensation), then:

$$\begin{aligned} \dot{m}_{EFG,in} \cdot h_{EFG,in} - \dot{m}_{EFG,out} \cdot h_{EFG,out} \\ = (\dot{m}_{air,in} \cdot h_{air,in} - \dot{m}_{air,out} \cdot h_{air,out}) \\ + (\dot{m}_{CO_2-depleted,in} \cdot h_{CO_2-depleted,in} - \dot{m}_{CO_2-depleted,out} \\ \cdot h_{CO_2-depleted,out}) \end{aligned} \quad [3.84]$$

If $T_{EFG,out} < T_{dew\ point}$ (water condensation), then:

$$\begin{aligned} \dot{m}_{EFG,in} \cdot h_{EFG,in} - \dot{m}_{EFG,out} \cdot h_{EFG,out} + \dot{m}_{EFG,dry}(w_{in} - w_{out}) \cdot h_{latent} \\ = (\dot{m}_{air,in} \cdot h_{air,in} - \dot{m}_{air,out} \cdot h_{air,out} \\ - \dot{m}_{air,dry}(w_{in} - w_{out}) \cdot h_{latent}) \\ + (\dot{m}_{CO_2-depleted,in} \cdot h_{CO_2-depleted,in} - \dot{m}_{CO_2-depleted,out} \\ \cdot h_{CO_2-depleted,out} - \dot{m}_{CO_2-depleted,dry}(w_{in} - w_{out}) \cdot h_{latent}) \end{aligned} \quad [3.85]$$

$$\begin{aligned} \dot{m}_{EFG,dry}(w_{in} - w_{out}) - \dot{m}_{water\ drained} \\ = \dot{m}_{air,dry}(w_{in} - w_{out}) + \dot{m}_{CO_2-depleted,dry}(w_{in} - w_{out}) \end{aligned} \quad [3.86]$$

The pressure drop through the heater is a combination of duct losses at the inlet of the rotor, the expansion losses at the outlet of the rotor and rotor losses and is proportional to the square of the fluid velocity (V_g) and to the fluid density (ρ_g), according to Equation [3.87] and [3.88]

$$\Delta P = K \cdot \frac{V_g^2}{2} \cdot \rho_g \quad [3.87]$$

$$\Delta P = K \cdot \frac{(\dot{m}_g/A_n)^2}{2 \cdot \rho_g} \quad [3.88]$$

A fundamental expression for direct leakage flow rate, $\dot{m}_{leakage}$, is also provided in Equation [3.89] as a function of the flow area (A), pressure differential across the gap (ΔP_{gap}) and density of the gas (ρ_g). Direct and entrained leakage flow rates are estimated as function of the pressure difference at both sides of the sector plate, the void fraction, the dimensions and geometry of the heat exchanger, and perimeter of sealing and gaps.

$$\dot{m}_{leakage} = K' \cdot A \cdot (2g_c \cdot \Delta P_{gap} \cdot \rho_g)^{1/2} \quad [3.89]$$

The methodology used in this work to evaluate leakage relies on previous experience in the application of regenerative rotary heat exchangers in pulverised coal plants, operating at temperature ranging from 100 to 300 °C. Thermal expansion and contraction of the perimeter of sealing and gaps in the range of operating temperatures 40 – 100 °C can be expected to have a smaller effect on leakages. Leakage level around 0.55% to 1% can be reasonably expected, although it would be possible to engineer purge and scavenge systems to minimise leakage flow rates even further. The sensitivity analysis in Chapter 6 shows that these conservative estimates of leakage rates could be tolerated and are likely to be deemed acceptable since they would only have a limited impact on the operation of the post-combustion capture plant.

3.5. Rotary adsorber for selective CO₂ transfer

The technology proposed for selective CO₂ transfer from flue gas into combustion air is physical adsorption in a rotary system with structured adsorbents. The cycling adsorption/desorption process is driven by the difference in CO₂ partial pressure between the two streams. This section describes the mathematical model developed to conduct a conceptual design. The objective is to investigate the performance and assess the technical feasibility of this technology for the application of S-EGR. The conceptual design assessment consists of two steps:

- A bottom-up approach considers the best class commercially available adsorbent with the objective of evaluating the amount of solid required to achieve certain CO₂ transfer efficiency, and sizing the rotary adsorber for selective CO₂ transfer.
- A top-down approach starts with the size of a large rotary system to assess the material performance and to provide guidelines on the adsorption behaviour for adsorbent material development.

3.5.1. Problem description

The adsorption/desorption cycle occurs when the adsorbent rotates and is periodically exposed to the flue gas and the ambient air streams flowing in opposite directions, i.e. counter current flow. CO₂ is adsorbed on the solid surface as the rotary adsorbent enters into contact with flue gas, in the adsorption section, and it is desorbed out of the solid as the adsorbent enters into contact with fresh ambient air, in the regeneration section. The contacting mode of the rotor adsorber is a cross-flow moving bed. A schematic diagram of the rotor adsorber is illustrated in Figure 3.22.

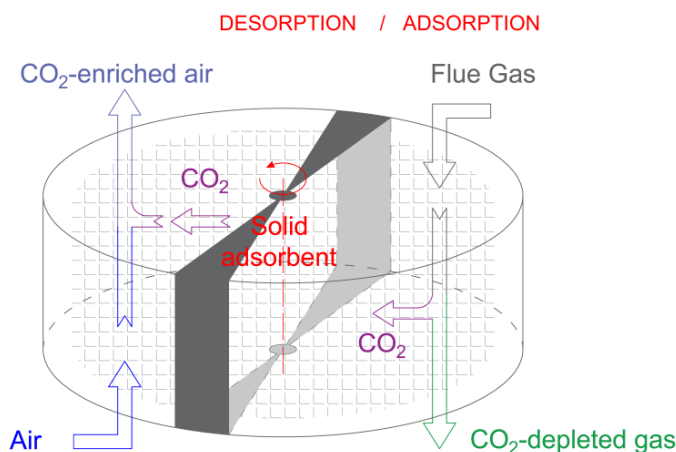


Figure 3.22.- Schematic diagram of the rotary adsorber for selective CO₂ transfer.

Prior to entering the device, the flue gas is cooled to an adequate temperature of 30 °C. A low temperature favours the thermodynamics of the adsorption process, reduces the water content and minimises the heat transferred into the air, which prevents derating the gas turbine with a high temperature CO₂-enriched air entering the compressor. A booster fan and an air fan are required to overcome the pressure drop through the device.

3.5.2. Performance modelling for a conceptual design

Adsorption in rotary wheel configurations has been previously studied for a range of applications, such as dehumidification wheels (Ge et al. 2008). For the purpose of the conceptual design assessment, an equilibrium model of the adsorption/desorption processes is developed. Yet rigorous models including gas side and solid side resistance to mass and heat transfer have been developed in literature. The gas side resistance is due to convective heat and mass transfer between the gas/air and the solid, while the solid side resistance is due to heat conduction and mass diffusion within the solid.

The domain is discretized into $S \times L$ equilibrium stages, as represented in Figure 3.23(a), where S is the number of stages in angular direction and L is the number of stages in longitudinal direction. The contacting mode of the gas and the rotor adsorbent is a cross-flow, as illustrated in Figure 3.23(b). The system is simplified to a two dimensional mathematical model, where the stream variables and properties of flue gas, air and solid are assumed constant along the radial direction. The minimum number of stages is selected so that a further increase results in a marginal increase of the CO₂ transfer efficiency for a given amount of solid.

The model assumes that thermal and mass transfer equilibrium is achieved in each stage. The CO₂ partial pressure ($P_{CO_2}^*$) in the flue gas and the adsorbed amount of CO₂ ($q_{CO_2}^*$) are therefore related by the adsorption equilibrium isotherm at the corresponding stage temperature, qualitatively represented by the black curve in Figure 3.23(d). The operation lines connect the CO₂ partial pressure in gas phase and the adsorbed amount of CO₂ in solid phase, entering and leaving each equilibrium stage, red and orange lines in Figure 3.23(d). For an illustrative purpose, the operation lines can be represented as parallel lines, as the slope is defined by the ratio of flue gas to solid flow rate and the ratio is similar for each stage. This is qualitatively represented in Figure 3.23(d) for the four stages illustrated in Figure 3.23(c). Green and grey dashed lines connect two consecutive equilibrium stages for gas and solid phases respectively.

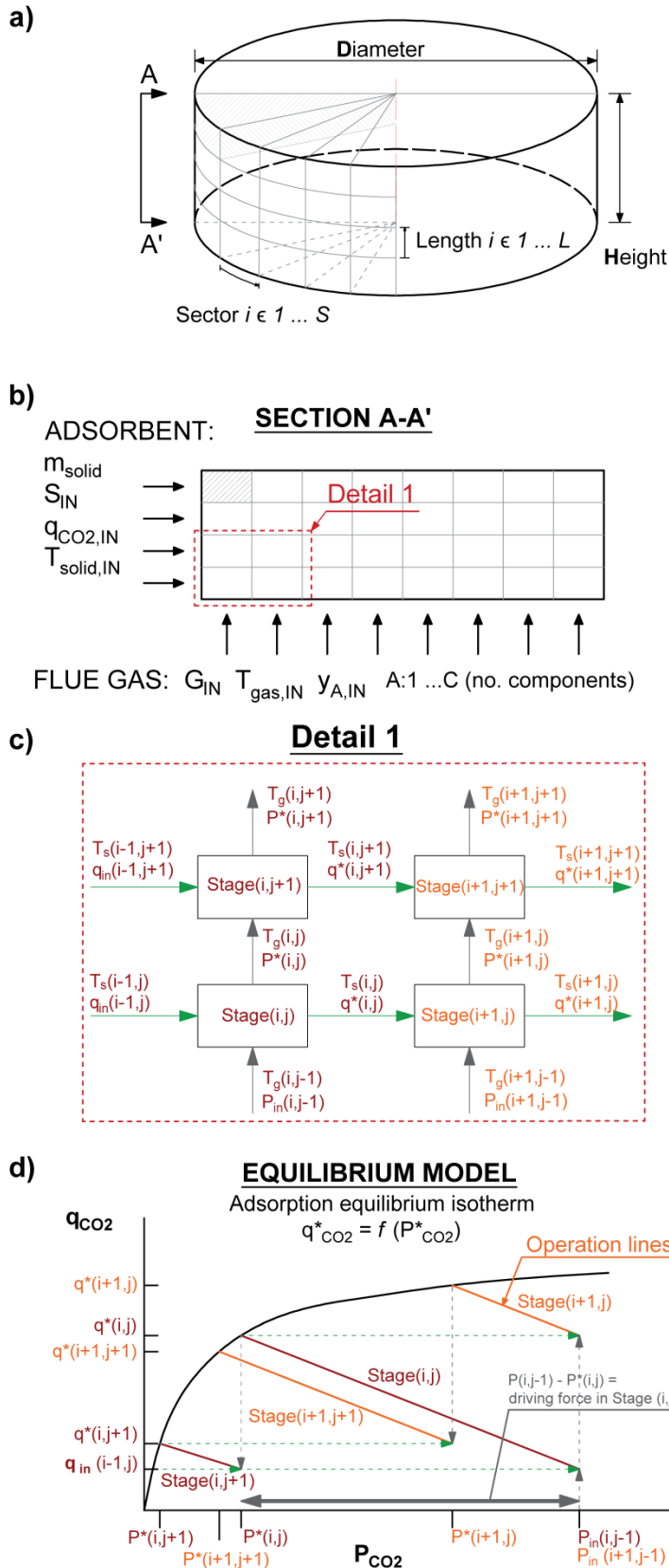


Figure 3.23.- Performance model of the rotary adsorber (a) division of the equilibrium model into cells, (b) cross-flow arrangement, (c) stage equilibrium, (d) operation and equilibrium curves.

3.5.2.1 *Mass and energy transfer*

The mathematical model consists of a system of partial differential equations describing mass and heat transfer in the system, represented in Equation [3.90] and Equation [3.91], respectively. A numerical solution discretises the system into equilibrium stages, as indicated in Equation [3.92], where an incremental step in the axial direction (x) and the rotational direction (τ) are defined in Equations [3.93] and [3.94].

The mass balance for each component k adsorbed/desorbed on/from the solid surface for each stage (i,j) is solved according to the system of Equations from [3.98] and [3.99], where \dot{G} and \dot{S} are the gas/air molar flow rate and the supplying rate of the adsorbent respectively, defined by Equations [3.95] and [3.96], y_k is the molar fraction of the component k in the gas/air, q_k is the adsorbed amount of component k on the solid. The supplying rate of the adsorbent is controlled by the rotation speed of the rotor (N), according to Equation [3.97], where m_{solid} is the total mass of solid and $t_{1/2\text{cycle}}$ is half-time of the adsorption/desorption cycle, given by Equation [3.97].

The energy balance in Equation [3.100] considers the heat generated/consumed in the adsorption/desorption ($\Delta H_{\text{ads } k}$) of the component k and sensible heat transferred between the gas/air and the solid, where Cp_s is the specific heat capacity of the solid material. Mass and energy balances have to be simultaneously considered in developing the mathematical model, as heat is released when CO_2 is adsorbed, decreasing the adsorber capacity.

$$\frac{\partial \dot{n}_k}{\partial x} = m_s \cdot \frac{1}{H} \cdot \frac{\partial q_k}{\partial \tau} = \dot{n}_{k \text{ adsorbed}} \quad [3.90]$$

$$\dot{n}_G \cdot \frac{\partial h_{\text{gas}}}{\partial x} + \sum_{k=1}^c \Delta H_{\text{ads } k} \cdot \frac{\partial \dot{n}_k}{\partial x} = m_s \cdot \frac{Cp_s}{H} \cdot \frac{\partial T_s}{\partial \tau} \quad [3.91]$$

$$\frac{\dot{n}_{G(i,j-1)} \cdot y_{k(i,j-1)} - \dot{n}_{G(i,j)} \cdot y_{k(i,j)}^*}{\Delta x} = m_s \cdot \frac{1}{H} \cdot \frac{q_{k(i,j)}^* - q_{k(i-1,j)}}{\Delta \tau} \quad [3.92]$$

$$\Delta x = \frac{H}{L} \quad [3.93]$$

$$\Delta \tau = \frac{t_{1/2\text{cycle}}}{S} \quad [3.94]$$

$$\dot{G} = \frac{\dot{n}_G}{S} \quad [3.95]$$

$$\dot{S} = m_{\text{solid}}/t_{1/2\text{cycle}} \cdot 1/L \quad [3.96]$$

$$t_{1/2\text{cycle}} = 60/N \cdot 1/2 \quad [3.97]$$

$$\dot{G}_{(i,j-1)} \cdot y_{k(i,j-1)} - \dot{G}_{(i,j)} \cdot y_{k(i,j)}^* = \dot{n}_{k \text{ adsorbed}(i,j)} \quad [3.98]$$

$$\dot{S} \cdot (q_{k(i,j)}^* - q_{k(i-1,j)}) = \dot{n}_{k \text{ adsorbed}(i,j)} \quad [3.99]$$

$$\begin{aligned} \dot{G}_{(i,j-1)} \cdot h_{\text{gas}}(T_{(i,j-1)}) - \dot{G}_{(i,j)} \cdot h_{\text{gas}}(T_{(i,j)}) + \sum_{k=1}^C \Delta H_{\text{ads } k} \cdot n_{k \text{ adsorbed}(i,j)} \\ = \dot{S} \cdot C p_s \cdot (T_{(i,j)} - T_{(i-1,j)}) \end{aligned} \quad [3.100]$$

for $k = 1 \dots C$ (no. components);

$i = 1 \dots S$ (no. sectors); $j = 1 \dots L$ (no. cells in axial direction)

3.5.2.2 Equilibrium conditions

Thermal and mass transfer equilibrium is assumed in each stage. The gas/air and the solid leave the stage (i,j) at the same temperature as indicated in Equation [3.101], and the partial pressure of the adsorbate (P_k^*), i.e. component k in the gas phase, and the adsorbed amount of k in the solid (q_k^*) are related by the adsorption equilibrium isotherm for the pair “adsorbent-adsorbate”, represented generically in Equation [3.102].

By introducing the concept of stage efficiency (η_{stage}), defined in Equation [3.103], limitations to mass transfer due to diffusional resistance can be taken into account. A stage efficiency of 100% is considered in the equilibrium model in this work.

$$T_{\text{gas}(i,j)} = T_{\text{solid}(i,j)} \quad [3.101]$$

$$q_{k(i,j)}^* = f(P_{k(i,j)}^*) \quad [3.102]$$

$$\eta_{\text{stage}(i,j)} = \frac{P_{k(i-1,j)} - P_{k(i,j)}}{P_{k(i-1,j)} - P_{k(i,j)}^*} \quad [3.103]$$

for $k = 1 \dots C$ (no. components);

$i = 1 \dots S$ (no. sectors); $j = 1 \dots L$ (no. cells in axial direction)

3.5.2.3 Boundary conditions

As inlet conditions, mass flow rate, composition, temperature and pressure are defined for the flue gas at the top of the wheel ($j = L$), and for the air at the bottom of the wheel ($j = 0$) to account for a counter-current flow arrangement, as indicated in Equations from [3.104] to [3.106]. The adsorption/desorption cycle requires to define the amount of CO₂ adsorbed and the solid temperature at the boundary between the adsorption and the desorption sections, as indicated in Equations from [3.107] to [3.110].

$$\begin{array}{cc} \text{Gas (desorption)} & \text{Air (adsorption)} \\ \dot{G}_{(i,L)} = \dot{G}_{\text{IN}}/S & \dot{G}_{(i,0)} = \dot{A}_{\text{IN}}/S \end{array} \quad [3.104]$$

$$y_{k(i,L)} = y_{k \text{ flue gas, IN}} \quad y_{k(i,0)} = y_{k \text{ air, IN}} \quad [3.105]$$

$$T_{\text{gas, (i,L)}} = T_{\text{flue gas, IN}} \quad T_{\text{gas, (i,0)}} = T_{\text{air, IN}} \quad [3.106]$$

for $i = 1 \dots S$ (no. sectors); $k = 1 \dots C$ (no. components)

$$[q_{k(0,j)}]_{\text{Adsorption}} = [q_{k(S, L-j)}]_{\text{Desorption}} \quad [3.107]$$

$$[T_{\text{solid}(0,j)}]_{\text{Adsorption}} = [T_{\text{solid}(S, L-j)}]_{\text{Desorption}} \quad [3.108]$$

$$[q_{k(0, L-j)}]_{\text{Desorption}} = [q_{k(S,j)}]_{\text{Adsorption}} \quad [3.109]$$

$$[T_{\text{solid}(0, L-j)}]_{\text{Desorption}} = [T_{\text{solid}(S,j)}]_{\text{Adsorption}} \quad [3.110]$$

for $j = 1 \dots L$ (no. cells in axial direction); $k = 1 \dots C$ (no. components)

3.5.2.4 Adsorbent structure and rotary wheel

The equilibrium model evaluates the minimum amount of solid that is required to achieve certain CO₂ transfer efficiency for a given adsorbent materials and the corresponding equilibrium adsorption model. The volume of the solid is then evaluated according to Equation [3.111], where ρ_{solid} is the solid density, ε_p is the particle porosity and ρ_p is the particle density, which considers the internal porosity of the material.

The structured adsorbents are monoliths, honeycomb and other hierarchical structures contained in the rotor, which consists of a large number of parallel channels that provides

high contact efficiencies. This structure is characterised by a high void fraction which typically result of a trade-off between a large surface area and a low pressure drop. They also present the advantages of short diffusion lengths and no obstruction by particulate matter, compared to conventional configurations such as fixed bed. The volume of the rotor adsorbent (V_{rotor}) is evaluated according to Equation [3.112], where $\varepsilon_{\text{bulk}}$ is the bulk void fraction defined as the ratio of the void spaces in the structured absorber to the total volume of the rotor.

The dimensions of the largest rotary heat exchangers, which have been manufactured and commissioned for industrial applications in coal-fired power plants, are considered as reference to estimate the number of wheels that would be required for the application of S-EGR, as indicated in Equations [3.113] and [3.114].

$$V_{\text{solid}} = \frac{m_{\text{solid}}}{\rho_{\text{solid}} (1 - \varepsilon_{\text{p}})} = \frac{m_{\text{solid}}}{\rho_{\text{p}}} \quad [3.111]$$

$$V_{\text{rotor}} = V_{\text{solid}} / (1 - \varepsilon_{\text{bulk}}) \quad [3.112]$$

$$V_{\text{wheel}} = \pi/4 \cdot D_{\text{wheel}}^2 \cdot L_{\text{wheel}} \quad [3.113]$$

$$V_{\text{wheel}} \cdot n_{\text{wheel}} = V_{\text{bed}} \quad [3.114]$$

Strategies to increase CO₂ concentration in Gas Turbines Exhaust Flue Gas

4.1. Introduction

Selective exhaust gas recirculation (S-EGR) is proposed as a strategy to further increase the CO₂ concentration in the exhaust flue gas from the gas turbine beyond the maximum values achieved with exhaust gas recirculation (EGR), and either reduce the flue gas flow rate or the CO₂ capture efficiency in the post-combustion capture (PCC) process.

Strategies to enhance CO₂ capture rate should aim to introduce minimal modifications in the gas turbine engine as current gas turbine technology presents a high efficiency and plays an important role in achieving a high combined cycle net power output. Any major modifications to gas turbine engines requires long lead development time to be implemented, tested and optimised, and development cost may only be justified if they can be amortised via deployment on a representative fraction of the market, that with CCS. It is therefore important to identify the impact on the CCGT power plant with CCS and determine whether existing class of gas turbines can be operated with a fraction of combustion gases being recycled to the inlet of the system.

This chapter investigates two configurations for a CCGT plant with PCC and S-EGR:

- A configuration consisting of diverting a fraction of the exhaust of the HRSG into a device transferring CO₂ into the inlet air stream of the gas turbine compressor. The selective CO₂ transfer unit operates “in parallel” to the post-combustion capture process.
- A configuration consisting of a selective CO₂ transfer unit operated downstream of, and “in series” to, the post-combustion capture process.

The chapter focuses on new-build units and compares the results to the reference case, i.e. a conventional air-based combustion configuration with a CCGT with PCC and to a configuration with a CCGT with “non-selective” EGR and PCC. The configuration with EGR is investigated in Section 4.2. Section 4.3 and Section 4.4 present the results for the configurations with S-EGR in parallel and S-EGR in series, respectively. A summary a comparison of the results is presented in Section 4.5. Each section is structure as follows:

A sensitivity analysis is first performed to investigate the range of CO₂ concentrations possible in the flue gas and to define the minimum requirements in terms of efficiencies of the PCC system and the selective CO₂ transfer system. It leads to the definition of the range of operating conditions where S-EGR present advantages compared to “non-selective” EGR. The performance assessment of a state-of-the-art gas turbine engine, i.e. GE F-class gas turbine, with EGR and S-EGR is then conducted by evaluating the new operating conditions of the compressor and turbine, their respective pressure ratio, temperatures and deviation from the design operation point. The effect of different gas turbine exhaust conditions with EGR and S-EGR on the steam cycle is investigated in a new design of the HRSG in each configuration, and evaluated in terms of steam production and steam turbines power output.

The potential for the enrichment of the gas turbine compressor inlet stream with CO₂ to reduce both capital and operational cost associated to the post-combustion capture system is investigated for chemical absorption technology using a solution of monoethanolamine (MEA) 30 wt% in water, since it is a benchmarking solvent widely used to assess modifications and improvements to the conventional process. A quantitative evaluation is conducted in terms of reduction in the packing volume and in the specific reboiler duty.

The selective CO₂ transfer system is modelled as a “grey-box” in this chapter and it is further investigated in Chapter 5 for a specific technology, i.e. physical adsorption in a rotary wheel. The concept of “grey-box” in this work implies that inlet stream variables and operating parameters with a relatively large effect on the overall process are defined in the model. The flue gas stream and the air stream supplied by the air fan are inlet streams, and the CO₂-enriched air and the CO₂-depleted gas streams are outlet streams in the model of the selective CO₂ transfer system. The key operating parameters with a larger effect on the performance of the CCGT power plant with PCC when S-EGR is implemented are the selective CO₂ transfer efficiency, the selectivity for CO₂ over other components in the flue gas, the leakage level, the pressure drop in the gas and air sides, and the heat transfer flow or temperature rise in the air side. Initial values of these parameters are chosen based on simulation results in Chapter 5. Yet a sensitivity analysis of the gas turbine power output and the combined cycle power output to a variation of the previous parameters is conducted, with the purpose of covering a wide range of operating conditions and, thus, to extend the results and discussion to other possible technologies and defining minimum requirements for the technology selection and design of the system. Any technology relying on the difference on CO₂ partial pressure between the flue gas and the air and using ambient air, at a relatively low temperature and a low pressure, as the sweep stream for CO₂ recycling could potentially be used for S-EGR applications.

4.2. Exhaust Gas Recirculation

A configuration of a CCGT with “non-selective” EGR and PCC is first investigated in order to compare the benefits of S-EGR on a consistent basis.

4.2.1. Description of the configuration

EGR consists of recycling a portion of the exhaust flue gas back to the gas turbine inlet replacing part of the intake air to the compressor. This is possible due to the large amount of excess air used in the gas turbine which cools down components in contact with high temperature combustion gas.

The process flow diagram for a CCGT power plant with EGR is shown in Figure 4.1. The configuration of the CO₂ capture system with amine-based scrubbing technology is described in Chapter 3, Section 3.3.1.

The flue gas leaving the HRSG is cooled down to achieve a beneficial lower temperature at the PCC unit and the compressor inlet. As proposed in Chapter 3, Section 3.3.1, the flue gas passes first through a gas/gas heat exchanger, transferring sensible heat to the CO₂-depleted gas before it is released through the stack, in order to reduce the amount of cooling in the direct contact coolers. The flue gas leaves at around 60 °C and is then divided into two streams, which are further cooled down in each direct contact cooler.

The non-diverted flue gas enters the absorber of the PCC unit at 45 °C saturated in moisture. This temperature is a trade-off between the kinetics and the enhancement of the solvent capacity. The diverted flue gas is cooled down to 30 °C and mixed with ambient air to keep the temperature of the resulting CO₂-enriched air stream as low as possible. The density of the intake stream decreases with increasing temperature and results in a lower mass flow rate swallowed by the compressor for a fixed position of the variable inlet guide vanes (VIGV), which is detrimental to the gas turbine power output (Bolland and Mathieu 1998).

It is important to highlight that adequate injection system of the recycled exhaust flue gas into the intake ambient air stream is required to be designed to ensure a homogeneous mixture and avoid stratification, which could lead to non-homogeneous combustion, while minimising the increase in the pressure drop upstream the compressor.

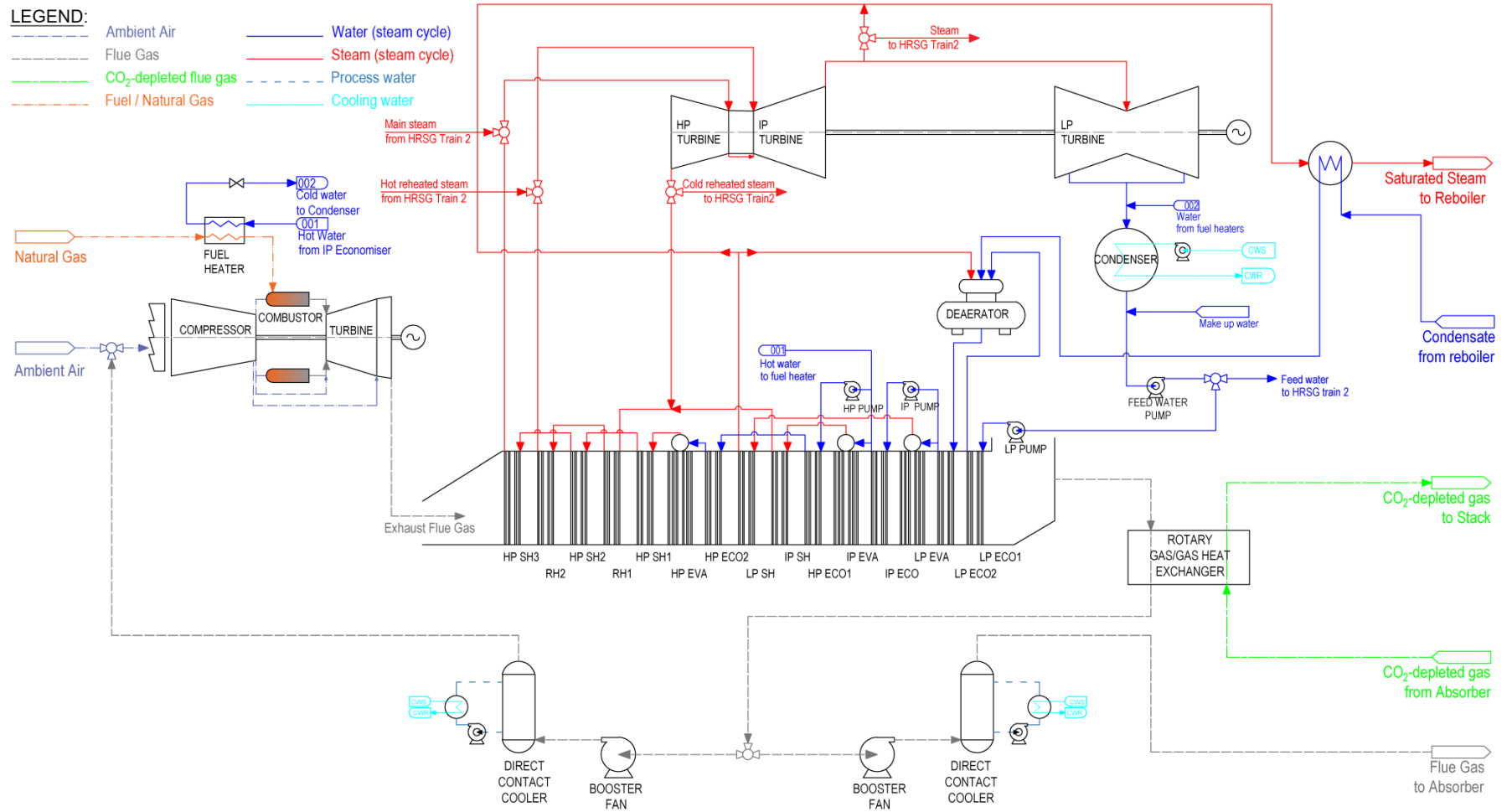


Figure 4.1.- Process flow diagram for a Combined Cycle Gas Turbine plant with Exhaust Gas Recirculation and Post-combustion CO₂ Capture.

4.2.2. Flue gas CO₂ concentration and limitations to the recirculation ratio

For a higher recirculation ratio, the CO₂ concentration in the exhaust flue gas increases. A larger amount of combustion air is replaced by the recycled flue gas and the oxygen is diluted, decreasing its concentration in the combustor. Figure 4.2 shows the CO₂ concentration and flue gas mass flow rate at the inlet of the post-combustion capture unit, e.g. the inlet of the absorber for amine based scrubbing technology, after being cooled to 45°C, and the O₂ concentration at the combustor inlet for a range of recirculation ratios.

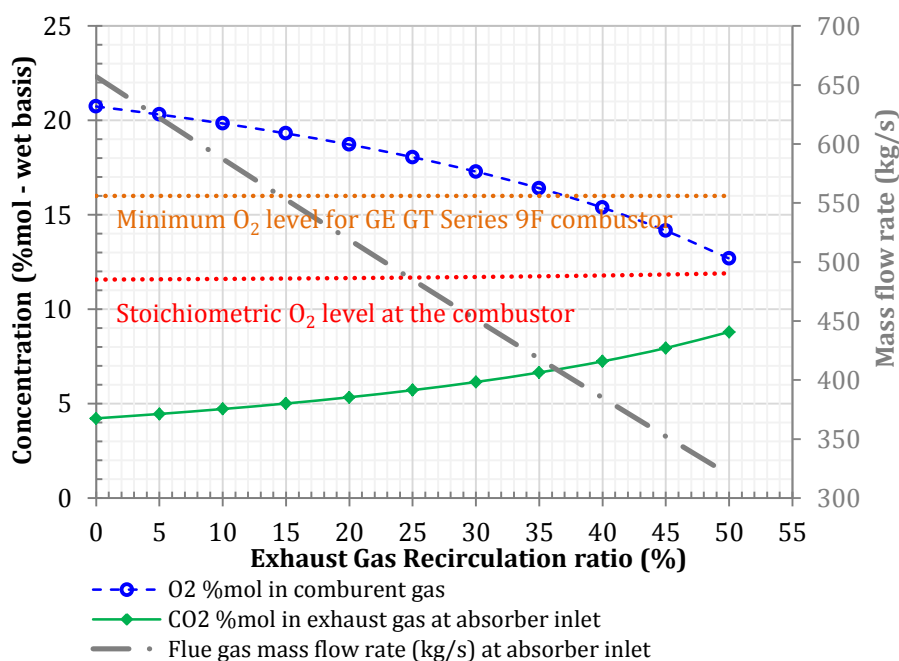


Figure 4.2.- Sensitivity of CO₂ concentration and flue gas mass flow rate at the post-combustion capture unit (absorber) inlet, O₂ concentration at the combustor to the exhaust gas recirculation ratio. Configuration: CCGT with EGR and PCC.

The maximum recirculation ratio and the highest possible CO₂ concentration in the flue gas are limited by the oxygen levels at the combustor. A minimum O₂ concentration of 16-17 vol% is suggested for lean pre-mixed burners used in Dry Low-NO_x (DLN) combustion systems currently employed in General Electric (GE) F-class gas turbine technology (ElKady et al. 2009), in order to ensure flame stability and acceptable levels of CO and unburned hydrocarbon emissions. An oxygen concentration of 16 vol% in the combustor corresponds to approximately 35% recirculation ratio of the GE F-class Frame 9 gas turbine engine considered in this work, operating at a design turbine inlet temperature (TIT) of 1371 °C. The CO₂ concentration achieved in the flue gas is approximately 6.6 % vol (wet basis). As explained in Chapter 2, Section 2.2.1, the EGR ratio that corresponds to a given oxygen concentration in the combustor depends on the TIT, since this is a design parameters that

defines the excess of air, and on the amount of cooling air that is extracted from the compressor last stage and by-passes the combustor. A recirculation ratio of 40% would only be possible with minor modifications of the combustion system (ElKady *et al.* 2009).

For the purpose of a comparison with the configurations with S-EGR, the effect of EGR on the performance of the CCGT power plant is investigated at 35% recirculation ratio and with a commercially available gas turbine engine, i.e. GE F-class Frame 9, identical in all the configurations. The HRSG and the steam cycle are then specifically designed, as new-build unit, for a temperature and a flue gas flow rate at the GT exhaust.

4.2.3. Effects on the Gas Turbine

A gas turbine operating at full load with a fixed position of the variable inlet guide vanes (VIGV) swallows a constant volume of air. The density of the intake air is therefore an important parameter and it determines the mass flow through the turbomachinery.

EGR leads to an increase in the temperature as well as an increase in the CO₂ concentration of the stream entering the compressor, compared to the reference case, i.e. air-based combustion with air at ISO ambient conditions. The higher temperature reduces the gas density, while the larger CO₂ concentration increases the gas density. The effect of the temperature is more significant than the effect of the CO₂ concentration for recirculation ratios within the range from 0% to 50%, when the recycled flue gas is cooled down to 30 °C in the direct contact cooler and, then, is mixed with ambient air at 15 °C. The decrease in density results in a smaller mass flow rate through the turbomachinery.

The properties of the working fluid appear in the fundamental equations describing the turbomachinery performance, as indicated in Chapter 3, and are evaluated at three different locations: compressor inlet, turbine inlet and turbine outlet. Figure 4.3 shows the deviation, from the reference case, i.e. air at ISO ambient conditions, of the molar mass, density and the ratio of specific heats for a range of the CO₂ concentration in the CO₂-enriched air at the compressor inlet. Each point in the graph corresponds to a recirculation ratio within a range from 0% up to 50%. At the other two locations, turbine inlet and turbine outlet, the results are similar. At a higher recirculation ratio, the molar mass increases and the density and ratio of specific heats decrease. The deviation from the design conditions is, however, relatively small for each parameter, e.g. lower than 1.5% for 35% recirculation ratio. Similar deviations were reported by Jonshagen *et al.* (2011) for F-class GE engine, and by Sander *et al.* (2011) for Alstom GT26 engine.

The decrease in the mass flow rate does not significantly affect the pressure ratio in the compressor for a constant turbine swallowing capacity at choke conditions, according to Equation [3.48] shown in Chapter 3, Section 3.2.3.

The dimensionless parameter groups for the mass flow rate, the pressure ratio and the rotation speed, which constitute the basis of compressor and turbine performance maps, as described in Chapter 3 Section 3.2.3, are evaluated for the new working fluid composition and operating conditions. The relative values referred to the design operation point are shown in Figure 4.4. The fact that the relative values are close to one suggests that the increase in the CO₂ content of the working fluid results in a marginal deviation from the compressor and turbine design operation point. It also indicates that the compressor and the turbine isentropic efficiencies are not expected to significantly change from the design values.

The decrease in the ratio of specific heats of the working fluid with the increase in the CO₂ concentration, shown in Figure 4.3, has the effect of decreasing the compressor outlet temperature and increasing the turbine outlet temperature, according to the simplified equation describing the isentropic compression/expansion of an ideal perfect gas. In the compressor, the increase in the CO₂-enriched air inlet temperature counteracts the previous effect, and the overall reduction in the compressor outlet temperature is attenuated so that it is possible to maintain a constant TIT without a significant increase in fuel consumption.

The decrease in the mass flow rate is the critical factor that leads to a reduction of the gas turbine net power output of approximately 5 MW, compared to the reference case, air-based combustion gas turbine at ISO ambient conditions. The gas turbine power output decreases from 286 MW to 282 MW and the open cycle thermal efficiency slightly decreases from 38.2% to 37.7%.

Yet the exhaust flue gas temperature entering the HRSG increases and, despite the lower mass flow rate, shown in Figure 4.5, the overall effect is an increase of the heat available in the bottoming cycle, as discussed in the following section.

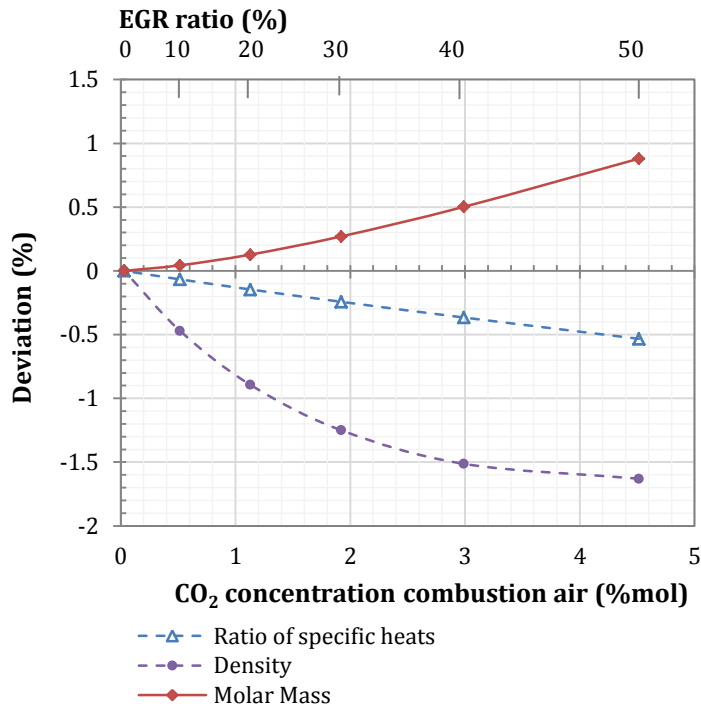


Figure 4.3.- Sensitivity of the deviation of the working fluid properties from the reference configuration with air combustion at ISO conditions to the working fluid CO₂ concentration at the compressor inlet. Configuration: CCGT with PCC and EGR.

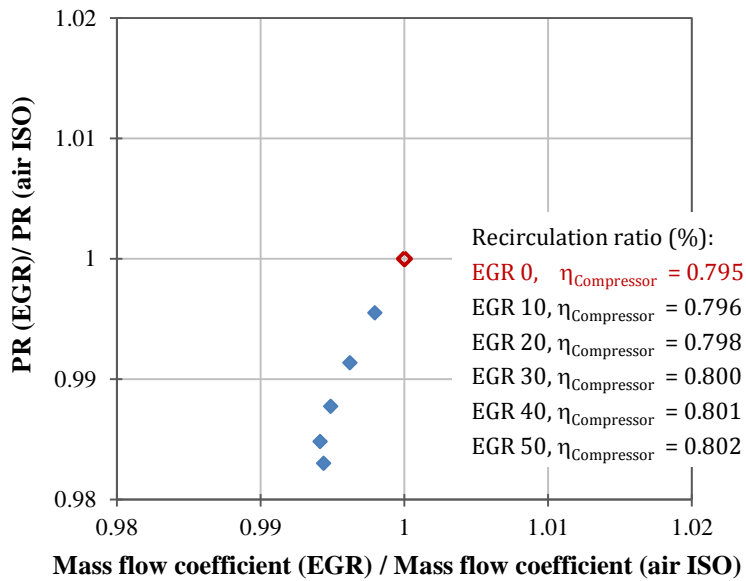


Figure 4.4.- Dimensionless parameter groups constituting the compressor performance curve for a range of EGR ratios from 0% to 50%. Normalised values for the design operating point with air combustion at ISO conditions. The compressor efficiency is indicated at each recirculation ratio. Configuration: CCGT with PCC and EGR.

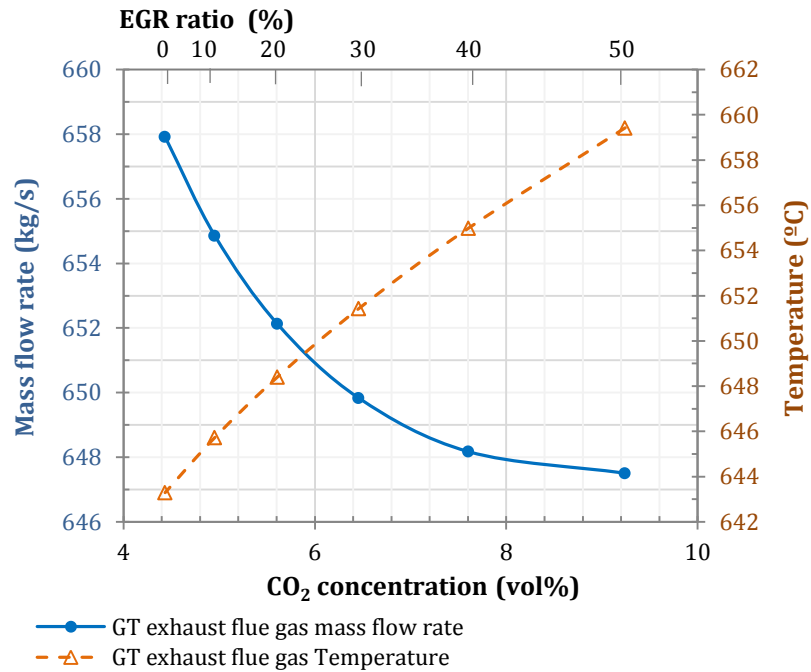


Figure 4.5.- Sensitivity of the gas turbine exhaust gas mass flow rate and temperature to the CO₂ concentration in the flue gas. Configuration: CCGT with PCC and EGR.

4.2.4. Effects on the Steam Cycle

The higher turbine exhaust flue gas temperature increases the heat available in the HRSG despite the lower flue gas mass flow rate. Due to the fact that the maximum inlet temperature in the high pressure and the intermediate pressure steam turbine cylinders is limited to 600 °C (Siemens power generation 2016; General electric thermal power generation 2016), the increase in the amount of heat available results in a larger steam flow rate and, thus, the steam turbine power output increases by approximately 10 MW, in comparison to the reference case without EGR. The steam turbine power output increases from 256 to 266 MWe. The temperature versus heat transfer diagram is shown in Figure 4.6.

Although the approach temperature, i.e. the temperature difference between the flue gas and the steam, in both the superheater and reheater banks increases by 10 °C, for a 35% recirculation ratio, the Rankine efficiency increases by approximately 1.2 %points.

The effect of EGR at 35% recirculation ratio on the CCGT plant net power output and thermal efficiency is further discussed and compared to the configurations with S-EGR in series and in parallel in Section 4.5. Results include the variation in the auxiliary power consumption and power output penalty due to steam extraction for the PCC system.

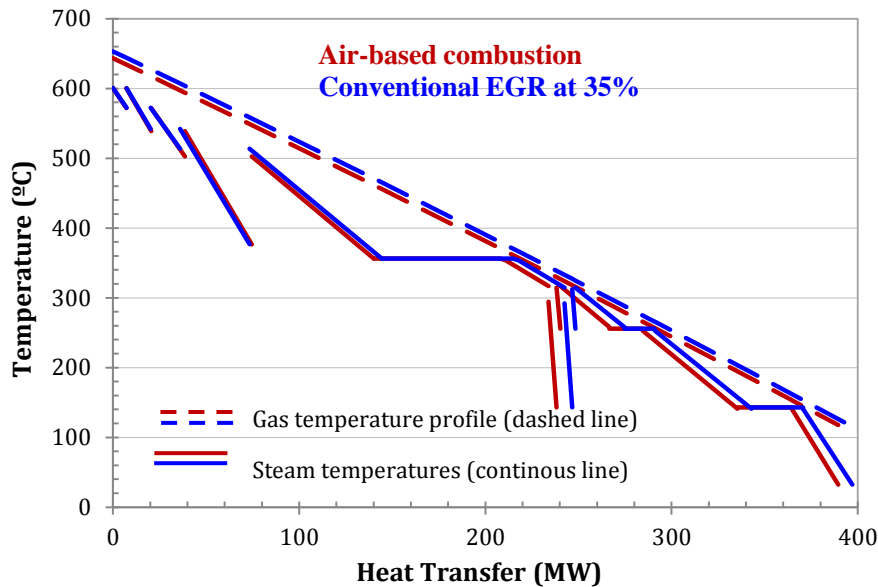


Figure 4.6.- Heat transfer – temperature diagram for EGR configuration at 35% recirculation ratio, compared to air-based combustion configuration.

4.2.5. Effects on the Post combustion capture unit

The effect of exhaust gas recirculation on the post-combustion capture process is examined here for a configuration operating at 35% recirculation ratio and 90% CO₂ capture in the absorber.

The packing volume in the absorber and the lean solvent CO₂ loading that minimises the specific reboiler duty are optimised, for EGR and air-based combustion configurations, following the procedure described in Chapter 3, Section 3.3, and illustrated in Figure 4.7. The packing height is increased until a value at which a further increase results in a marginal gain in the rich solvent CO₂ loading (<0.25% of the previous value). The packing volume selected for the EGR and air-based combustion configurations is indicated by the black dashed line in Figure 4.7, showing a reduction when read from right to left.

A significantly smaller flue gas flow rate, corresponding to 65% of the total gas turbine exhaust gas, enters the bottom of the absorber. The flue gas is saturated in moisture at 45 °C and presents a CO₂ concentration of 6.6 vol%. For a flue gas flow rate of 418 kg/s, one column with an internal diameter of approximately 14 m is therefore required to operate with a flue gas velocity corresponding to 0.8 of the flooding velocity of the packed column with Sulzer Mellapak 250Y structured packing. In comparison, the air-based combustion, with a flue gas flow rate of 658 kg/s, requires two absorbers with an internal diameter of approximately 12 m.

The higher CO₂ concentration of 6.6 vol%, compared to 4.2 vol% in the air-based combustion configuration, leads to a larger driving force for mass transfer and displaces the equilibrium towards a higher solvent CO₂ loading. A smaller packing volume is required and the solvent capacity is moderately increased from 0.198 to 0.207 mol_{CO₂}/ mol_{MEA}. The CO₂ loading of the rich solvent leaving the bottom of the absorber increases to 0.467 mol_{CO₂}/ mol_{MEA}, compared to the air-based combustion configuration loading of 0.458 mol_{CO₂}/ mol_{MEA}. The optimal CO₂ loading of the lean solvent that minimises the reboiler duty is 0.26 mol_{CO₂}/ mol_{MEA} for both configurations. The packing volume is reduced by 40%, from 4190 m³ to 2500 m³. A reduction in the packing volume of the order of the recirculation ratio is also reported by Sipöcz and co-workers (Sipöcz and Tobiesen 2012).

The moderate higher solvent capacity and the smaller solvent flow rate required for a 90% CO₂ capture efficiency in the absorber results in a reduction of the specific reboiler duty of approximately 2.8%, from 3.75 to 3.64 MJ/kg_{CO₂}.

The reduction is smaller compared to the approximately 8% reduction reported in literature for 40% EGR (Li et al. 2011a; Sipöcz and Tobiesen 2012). This is explained due to the higher specific reboiler duty for the reference case, i.e. air-based combustion without EGR, of approximately 4 MJ/kg_{CO₂}, in literature, compared to 3.75 MJ/kg_{CO₂}, in this work, for a flue gas with a similar CO₂ concentration of approximately 4 vol%. This difference may be due to a different criterion in the optimisation of the absorber height and of the lean solvent loading, which has not been specified in the literature, or due to different design parameters, e.g. pinch temperature in the reboiler and in the lean-rich heat exchanger, or operating parameters, e.g. flue gas inlet temperature, with a significant effect on the reboiler energy consumption (Kvamsdal et al. 2011).

Yet the specific reboiler duty for the reference case in this work is a good agreement compared to the base-case test campaign conducted at the Technology Centre Mongstad (TCM DA) in Norway. For the base case test campaign an aqueous 30 wt% monoethanolamine solvent system was used to treat flue gas from a natural gas-fired combined heat and power (CHP) plant with a CO₂ concentration of 3.5 vol%, and the thermal steam consumption was approximately 4.1 MJ/kg_{CO₂} for 90% CO₂ capture rate (Thimsen et al. 2014; Hamborg et al. 2014).

A larger reduction in packing height and, by extension, packing volume can be achieved if the benefits of increased CO₂ concentration are capitalised on lower capital cost instead of reducing the reboiler energy requirements, as indicated by the horizontal red dotted line in Figure 4.7. This can be achieved by adjusting the solvent lean loading accordingly. This

may, however, not be a design from the operability and controllability point of view, as a small decrease in the flue gas CO₂ concentration in an absorber with a packing volume smaller than 2000 m³ would result in an exponential increase of the specific reboiler duty.

This fact explains the large reboiler duty reduction reported in experimental tests, where a pilot plant uses an undersized absorber height and the reboiler duty has not been optimised for the base case with a CO₂ concentration in the flue gas from natural-gas firing without EGR (Akram et al. 2016).

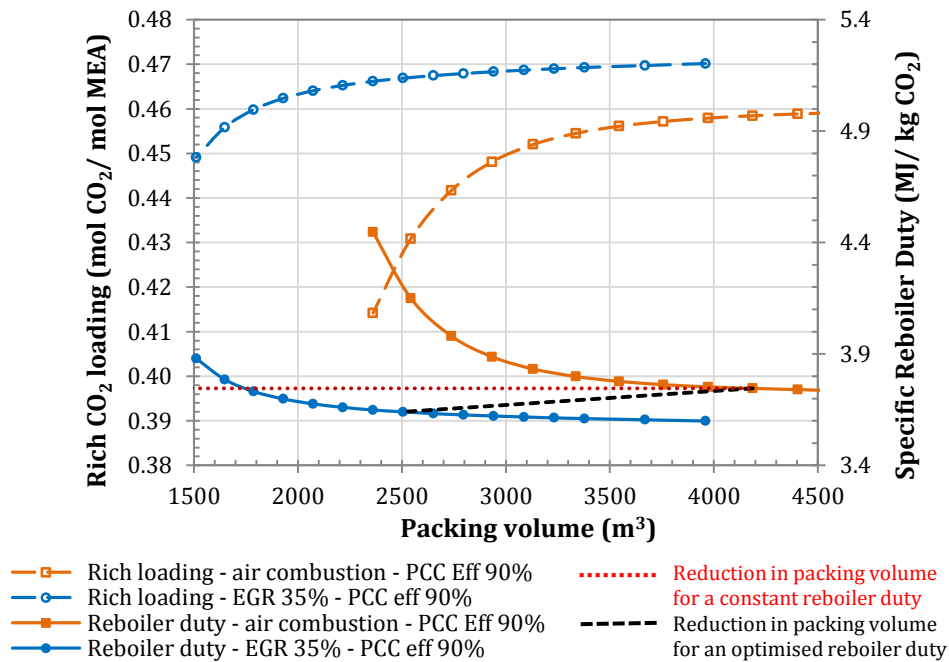


Figure 4.7.- Sensitivity of the rich solvent CO₂ loading and the specific reboiler duty to the packing volume required to achieve 90% CO₂ capture efficiency for the conventional exhaust gas recirculation configuration. The reference case is an air-based combustion configuration.

When investigated the effect of increasing the CO₂ concentration in the flue gas on the thermodynamics of the CO₂ absorption process, it is important to identify the operation line in the vapor-liquid equilibrium (VLE) curves for the CO₂-MEA-H₂O system, shown in Figure 4.8. The small increase in the rich solvent CO₂ loading is explained by the fact that operation point at the bottom of the absorber is already close to the thermodynamic equilibrium. At high CO₂ loadings, a substantial increase in the CO₂ partial pressure is required to significantly increase the CO₂ loading in the solvent.

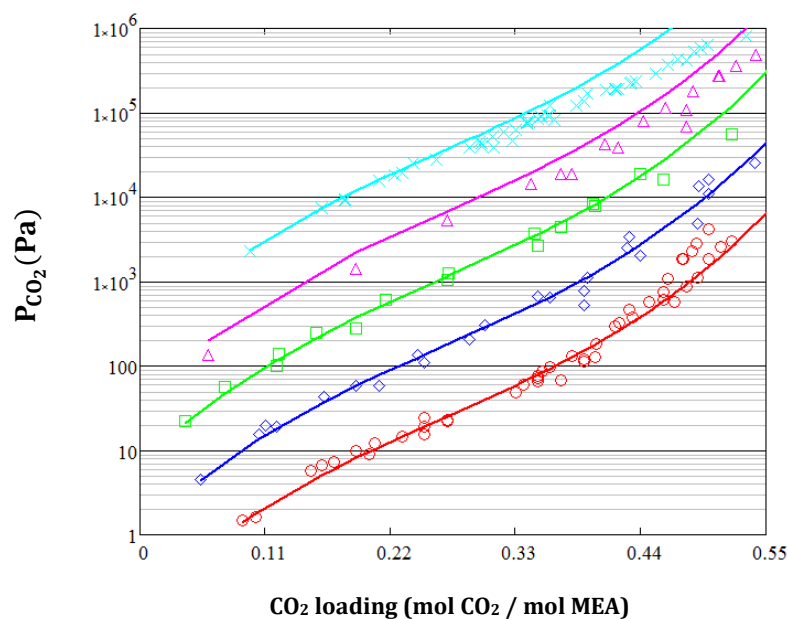


Figure 4.8.- CO₂ partial pressure as function of loading for H₂O-MEA-CO₂ system with a 30 mass% MEA aqueous solution, experimental data at equilibrium for ○, 40°C; ◇, 60°C; □, 80°C; △, 100°C; ×, 120°C (Fang-Yuan et al. 1994; Ma'mun et al. 2005; Hilliard 2008; Dugas 2009; Aronu et al. 2011).

4.2.6. Sensitivity analysis to the recycled flue gas temperature

In a configuration with EGR, the temperature of the recycled flue gas stream has an important effect on the gas turbine net power output and, thus, on the combined cycle gas turbine power output and thermal efficiency. It constitutes an important parameter when comparing with the reference configuration with ambient air at 15 °C.

For a closed-loop cooling system and ambient air at ISO conditions, the lowest possible temperature to which the gas is cooled is approximately 30 °C, as explained in Chapter 3, Section 3.2.4. A higher temperature results in an increase of the compressor inlet temperature and the gas turbine power output decreases proportionally. Figure 4.9 shows a sensitivity analysis of the gas turbine power output, the CCGT net power output and the compressor intake mass flow rate to the recycled flue gas temperature. The CCGT net power output decreases 5 MW per 2 °C increase at the compressor inlet, which corresponds to a 5 °C increase of the recycled flue gas temperature, prior mixing with ambient air at the inlet of the gas turbine compressor.

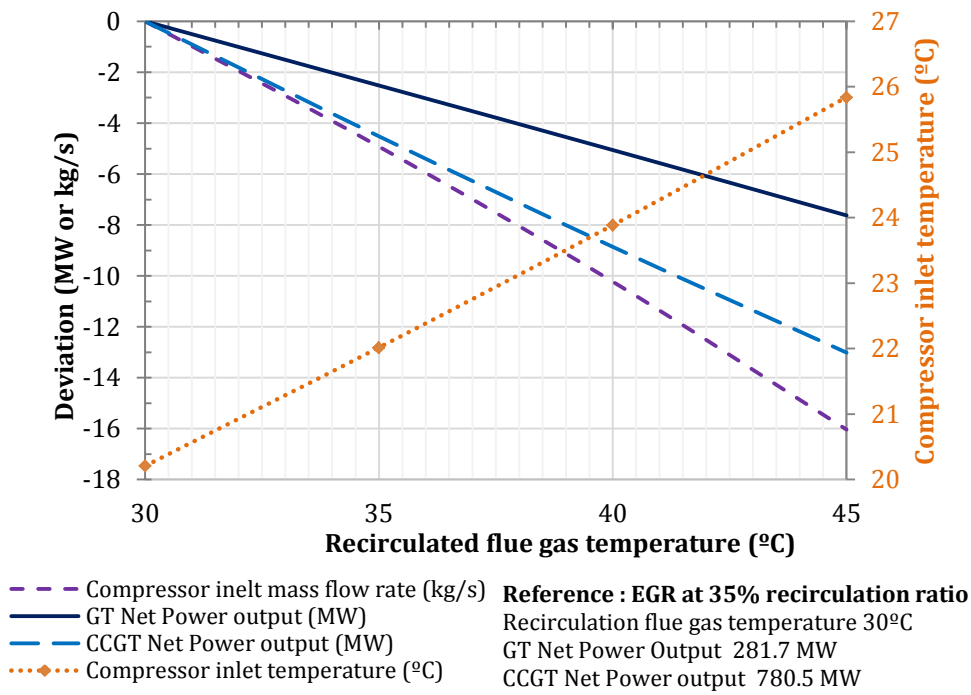


Figure 4.9.- Sensitivity analysis of the GT and CCGT power output, mass flow rate and compressor inlet temperature to the recirculated flue gas temperature. Configuration: exhaust gas recirculation at 35% recirculation ratio.

4.3. Selective Exhaust Gas Recirculation in Parallel

A configuration consisting on a selective CO₂ transfer unit operated “in parallel” to the post-combustion capture process is first proposed to further increase the CO₂ concentration in the flue gas and to reduce the flue gas flow rate treated in the post-combustion capture process, compared to the configuration with “non-selective” EGR.

4.3.1. Description of the configuration

A portion of the exhaust flue gas is diverted and sent to a unit where CO₂ is selectively transferred into the stream of ambient air eventually entering the gas turbine compressor. The selective CO₂ transfer device operates in parallel with the PCC process. The CO₂-enriched air is swallowed by the gas turbine compressor and used as the comburent in the combustion of the natural gas. The non-diverted flue gas stream is treated in the post-combustion capture unit.

The flue gas leaving the HRSG needs to be conditioned to achieve an appropriate pressure and temperature before entering either the capture process or the selective CO₂ transfer process. It is first cooled down in a gas/gas heat exchanger and then divided into two streams. Two booster fans, one in each stream, raise the pressure to overcome the pressure drop through the gas path. The diverted and non-diverted flue gas streams are then cooled down in each direct contact cooler to reach the appropriate temperature at the selective CO₂ transfer unit and at the inlet of the PCC unit, respectively. The two CO₂-depleted gas streams are mixed and reheated in the gas/gas heat exchanger prior to being released through the stack of the power plant. The process flow diagram for a CCGT power plant with S-EGR in parallel with the PCC system is shown in Figure 4.10. The configurations of the CO₂ capture system with amine-based scrubbing technology is described in Chapter 3 Section 3.3.1.

As in the EGR configuration, the flue gas enters the absorber saturated in moisture at 45 °C. A low temperature is also preferable at the inlet of the selective CO₂ transfer device to minimise sensible heat transfer to the inlet stream of the compressor and to enhance the CO₂ transfer capacity. For physical adsorption technology, the solid capacity increases at a lower temperature due to the exothermic nature of the process. The diverted flue gas stream is therefore cooled down to 30 °C.

The amount of CO₂ abated relative to the amount of CO₂ generated in the combustion is referred to as the *overall CO₂ capture level*. For a 90% overall CO₂ capture level, which is assumed for all the configurations, the operation with S-EGR in parallel requires the

following parameters to be defined: selective exhaust gas recirculation ratio, post-combustion CO₂ capture efficiency and selective CO₂ transfer efficiency. The *S-EGR ratio* is defined as the flow rate of the diverted flue gas stream over the total flow rate of the flue gas generated in the gas turbine. *Selective CO₂ transfer efficiency* refers to the amount of CO₂ removed from the diverted flue gas and transferred into the air stream, relative to the total amount of CO₂ at the inlet of the device. *Post-combustion CO₂ capture efficiency* refers to the amount of CO₂ removed from the flue gas and captured for transport and storage relative to the total amount of the CO₂ entering the capture unit.

The integration of S-EGR in parallel in the power cycle presents advantages over EGR for a CO₂ concentration in the flue gas beyond 6.6 vol%, the concentration achieved with EGR at 35% recirculation ratio, and S-EGR ratio beyond 35%. In practice, it would require achieving a CO₂ concentration significantly higher and a flue gas flow rate significantly smaller to justify the addition of selective CO₂ transfer unit. In Section 4.3.2, the range of possible CO₂ concentrations and the minimum requirements in terms of efficiency in both the PCC unit and the selective CO₂ transfer unit are investigated in order to define an operating framework.

4.3.2. Operating framework

The CO₂ concentration in the exhaust flue gas increases for a larger S-EGR ratio; while the oxygen level in the combustor is maintained above the limiting value of 16 vol%, for a wide range of recirculation ratios up to 80% and for a 90% overall CO₂ capture level, as illustrated in Figure 4.11.

A sensitivity analysis of the PCC efficiency to the recirculation ratio for a range of selective CO₂ transfer efficiencies is presented in Figure 4.12, for a 90% overall CO₂ capture level. For a given selective CO₂ transfer efficiency, the PCC efficiency that is required to capture 90% of the CO₂ generated in the combustion increases at a higher recirculation ratio. The absolute amount of CO₂ emitted with the CO₂-depleted gas leaving the selective CO₂ transfer unit increases with increasing the recirculation ratio, since the inlet stream presents a larger CO₂ concentration, and a larger amount of CO₂ needs therefore to be capture in the PCC unit. The S-EGR ratio and the CO₂ concentration in the flue gas are therefore limited by the maximum efficiencies that can be achieved, in practice, with each technology.

Figure 4.11 and Figure 4.12 indicate that a higher selective CO₂ transfer efficiency than 85% in combination with a recirculation ratio above 40% are required to further increase the exhaust flue gas CO₂ concentration beyond 6.6 vol%, which is the maximum concentration that could be achieved with EGR at 35% recirculation ratio for currently available gas turbine technology. This operating framework corresponds to the white region in Figure 4.11 and Figure 4.12. Likewise, at a higher selective CO₂ transfer efficiency of 90%, the PCC efficiency tends asymptotically to 100% for recirculation ratios marginally above 50%. Figure 4.11 shows that the CO₂ concentration increases from 6.6 vol% with 35% EGR to 8.4 vol%, which may not constitute a sufficiently large increase to justify transitioning to S-EGR. These two figures indicate the selective CO₂ transfer efficiency above 90% must be achieved, for the implementation of S-EGR and the associated CO₂ transfer unit to be justified.

In the following sections, the performance of the CCGT power plant with S-EGR is examined, with a state-of-the-art gas turbine technology initially designed for air-based combustion. The temperature rise in the air side, the pressure drop and the CO₂ selectivity are input data in the model, in which the selective CO₂ transfer device is considered as a “grey box”, to evaluate the CO₂-enriched air temperature, pressure and composition.

The performance of the PCC process with MEA based scrubbing technology is investigated and optimised for the case where a CO₂ concentration of 14 vol% is possible, defined by the following operating parameters:

- Selective recirculation ratio of 70%, post-combustion CO₂ capture efficiency of 96% and selective CO₂ transfer efficiency of 97%. This configuration is chosen since the CO₂ concentration is comparable to typical concentration in the flue gas from coal-fired power plants. The potential benefits of higher CO₂ concentration and smaller flue gas flow rate are identified and compared to conventional EGR at 35% recirculation ratio.

The limiting oxygen level in the comburent of 16 vol% is taken as reference for S-EGR configurations, despite being suggested in experimental work performed with combustion conditions of “conventional” EGR (ElKady et al. 2009). The combustion of natural gas with a CO₂-enriched comburent containing 8-9 vol% CO₂ may, however, result in a different minimum oxygen level for flame stability, complete combustion and acceptable CO and UHC emissions. This aspect is currently being investigated within the scope of the EPSRC project “Selective Exhaust Gas Recirculation for Carbon Capture with Gas Turbines: Integration, Intensification, Scale-up and Optimisation” (SELECT 2014).

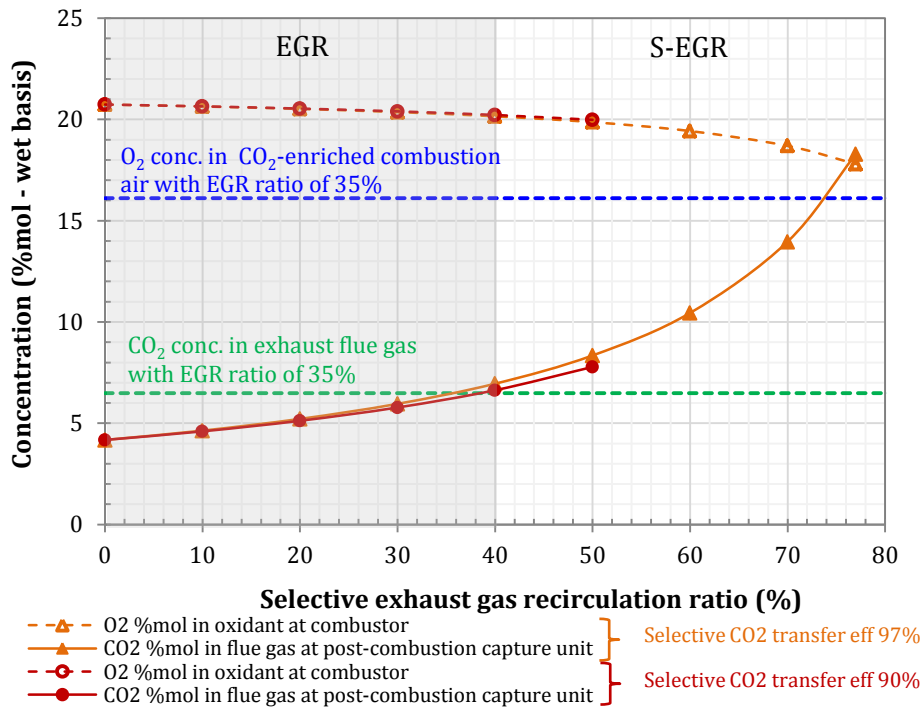


Figure 4.11.- Sensitivity of CO₂ concentration in the exhaust flue gas at the post-combustion capture unit inlet and O₂ concentration in the CO₂-enriched combustion air to the selective exhaust gas recirculation ratio, for a selective CO₂ transfer efficiencies of 90 and 97%. Configuration in parallel with an overall CO₂ capture level of 90%.

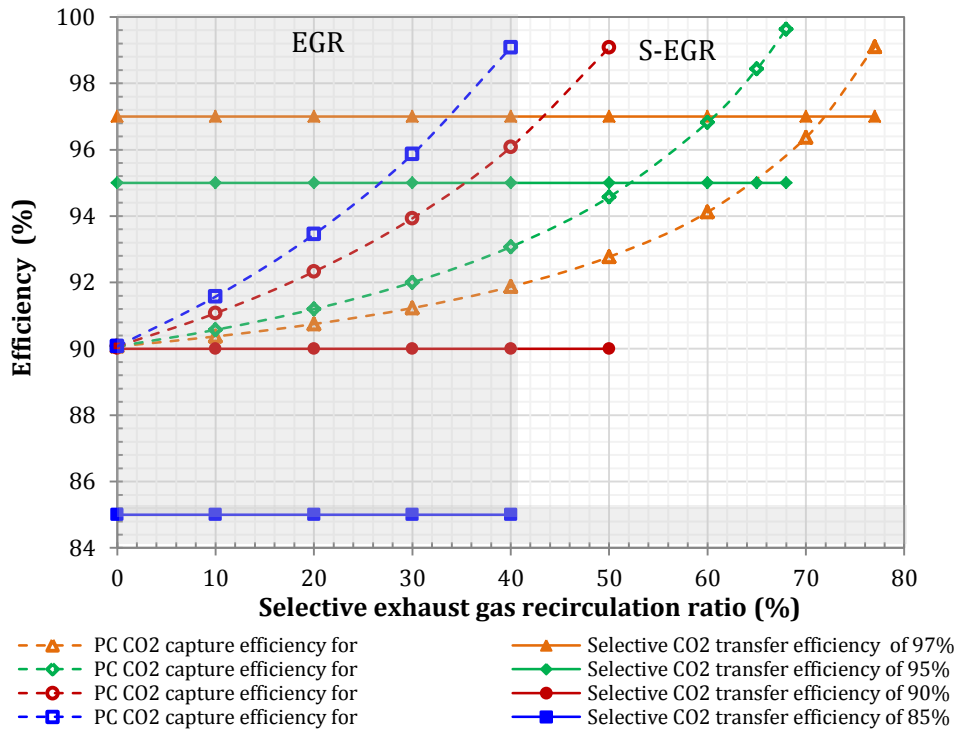


Figure 4.12.- Sensitivity of the post-combustion CO₂ capture efficiency to the selective exhaust gas recirculation ratio for a range of selective CO₂ transfer efficiencies. Configuration in parallel with an overall CO₂ capture level of 90%.

4.3.3. *Effects on the Gas Turbine*

As mentioned in Section 4.2.3, the density of the intake air is an important parameter to determine the mass flow rate swallowed by the compressor, in a gas turbine operating at a fixed position of the VIGV. The inlet temperature, the pressure and the CO₂ concentration have therefore an important role.

The temperature of the air stream rises as it passes through the selective CO₂ transfer device, mainly due to sensible heat transferred from the flue gas, regardless the technology used. For rotary adsorption, the temperature of the CO₂-enriched air stream leaving the device is the result of an energy balance with the following contributions: the enthalpy of CO₂ desorption and the sensible heat transfer, as the solid acts as a heat storage medium. The higher the temperature, the smaller the density of the CO₂-enriched air stream. For a CO₂ concentration in the CO₂-enriched air higher than 5 vol%, which is possible when 55% of the flue gas is diverted towards the selective CO₂ transfer device, the overall effect is, however, an increase of the density due to the higher CO₂ content. The mass flow rate swallowed by the compressor increases.

The working fluid properties which appear in the fundamental equations describing the turbomachinery performance are evaluated at the compressor inlet, turbine inlet and turbine outlet. Figure 4.13 shows the deviation of the molar mass, the density and the ratio of specific heats from the reference case, i.e. air at ISO ambient conditions, for a range of the CO₂ concentration in the CO₂-enriched air at the compressor inlet. Each point in the graph corresponds to S-EGR ratios from 0% to 80%, in increments of 10%. For a larger S-EGR ratio, the molar mass and the density increases and the ratio of specific heats decreases with larger deviations than with EGR at 35%.

The increase in the mass flow rate does not significantly affect the pressure ratio in the compressor for a constant turbine swallowing capacity at choke conditions, according to Equation [3.48] derived in Chapter 3, Section 3.2.3. The compressor operates below the surge margin limit for the range of S-EGR ratios considered.

The dimensionless parameter groups for the mass flow rate, the pressure ratio and the rotational speed constituting the compressor and turbine performance maps described in Chapter 3, Section 3.2.3, are evaluated for the new working fluid composition and operational conditions with S-EGR at different recirculation ratios. The relative values referred to the design operation point are shown in in Figure 4.14. Since the relative values

are close to one, this suggests that a higher CO₂ concentration in the working fluid results in a marginal deviation from the compressor and the turbine design operation points.

The increase in the ratio of specific heats with the increase in the CO₂ concentration, as previously explained for the EGR configuration, results in a decrease in the compressor outlet temperature and in an increase in the turbine outlet temperature. In the compressor, the increase in the CO₂-enriched air inlet temperature counteracts the previous effect, and the reduction of the compressor outlet temperature is attenuated.

The increase in the mass flow rate through the turbomachinery is the important aspect that increases the gas turbine net power output by approximately 3 MW, compared to the reference case. A larger increase could be achieved if the temperature of the CO₂-enriched air swallowed by the compressor was lower.

With S-EGR at 70% recirculation ratio, the exhaust flue gas temperature entering the HRSG increases from 643 °C with air-based combustion, to 669 °C, and the mass flow rate also increases from 658 kg/s to 674 kg/s, as shown in Figure 4.15. The overall effect is an increase of the heat available in the bottoming cycle, as discussed in the following section.

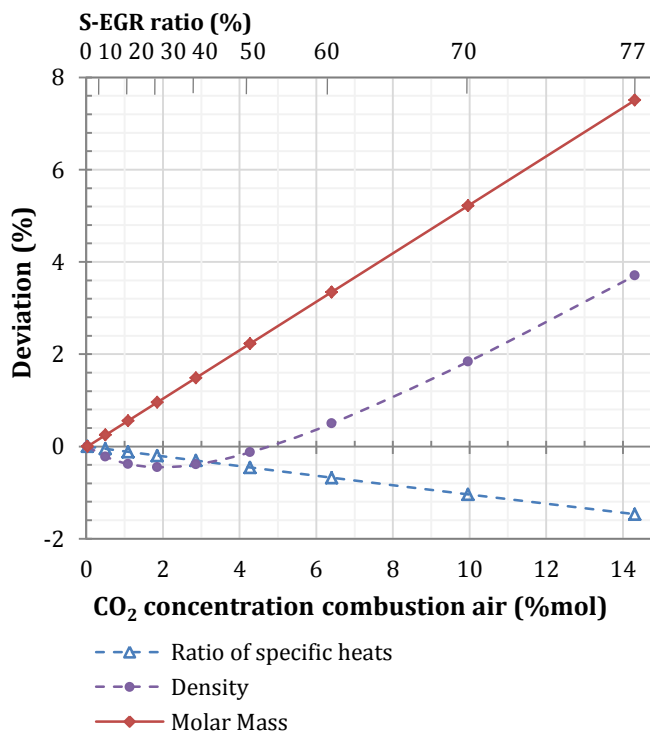


Figure 4.13.- Sensitivity of the deviation of the working fluid properties from the reference configuration with air combustion at ISO conditions as function of the working fluid CO₂ concentration at the compressor inlet. Configuration: CCGT with PCC and S-EGR in parallel.

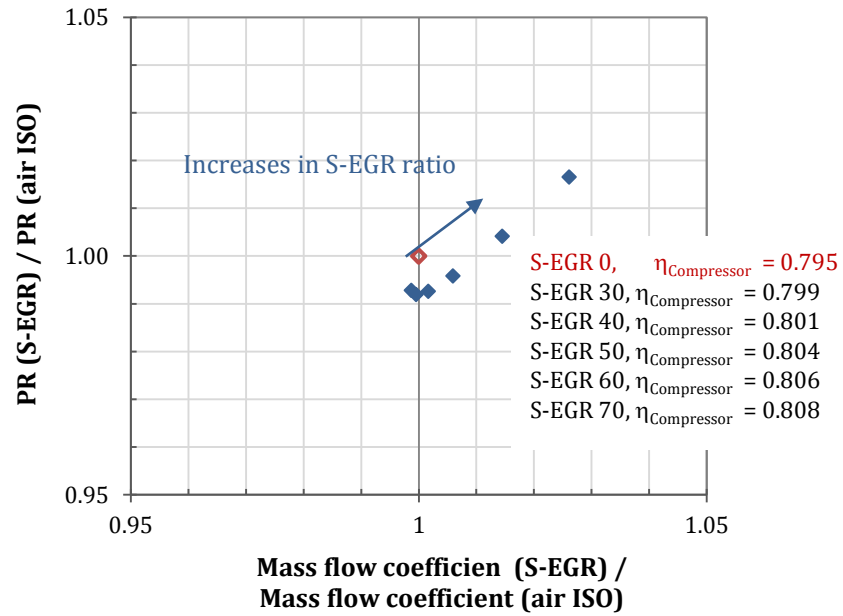


Figure 4.14.- Dimensionless parameter groups constituting the compressor performance curve for a range of S-EGR ratios from 30% to 70%. Normalised values for the design operating point with air combustion at ISO conditions. The compressor efficiency is indicated at each recirculation ratio. Configuration: CCGT with PCC and S-EGR in parallel.

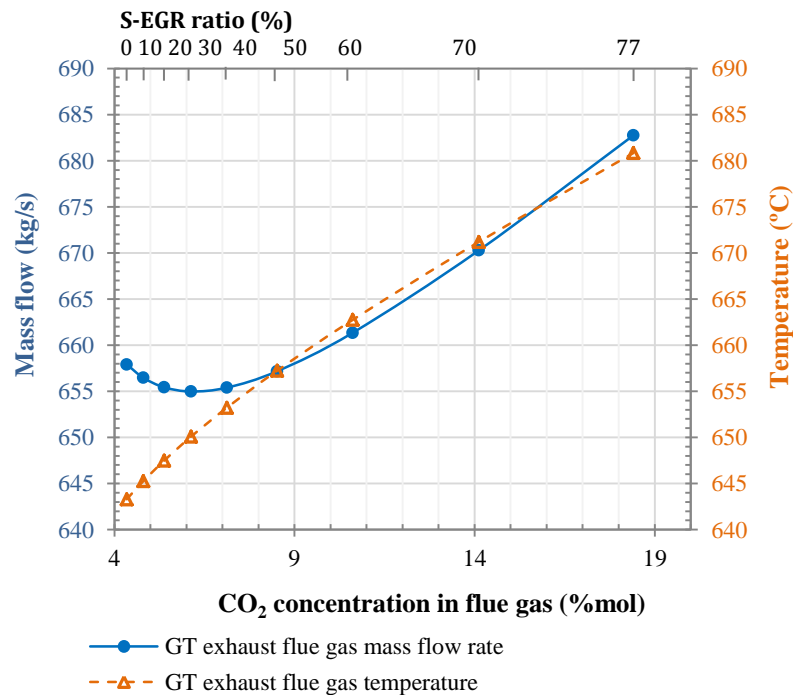


Figure 4.15.- Sensitivity of the gas turbine exhaust gas mass flow rate and temperature to the flue gas CO₂ concentration, for a range of S-EGR ratios from 0 to 80%, increments of 10%. Configuration: CCGT with PCC and S-EGR in parallel.

4.3.4. Effects on the Steam Cycle

The higher exhaust flue gas temperature and mass flow rate results in a larger amount of heat available in the HRSG which generates a larger steam flow rate. The steam turbine net power output is increased by approximately 34 MW, from 256 to 290 MW, compared to the reference case, i.e. air-combustion CCGT with PCC.

The temperature versus heat transfer diagram is shown in Figure 4.16 for the S-EGR in parallel with 70% recirculation ratio and is compared to the 35% EGR and air-combustion.

The temperature of the superheated high-pressure steam and reheated steam entering the high pressure and intermediate pressure steam cyclers is limited to 600 °C (Siemens power generation 2016; General electric thermal power generation 2016) and, thus, the approach temperatures, i.e. the difference between the steam temperature and the gas temperature entering the corresponding heat transfer banks in the HRSG, increases by 28 °C in the configuration with S-EGR at 70% recirculation ratio, compared to the reference case. Despite of this, the Rankine efficiency increases by approximately 3 %points, from 64% to 67% due to the larger amount of heat recovered.

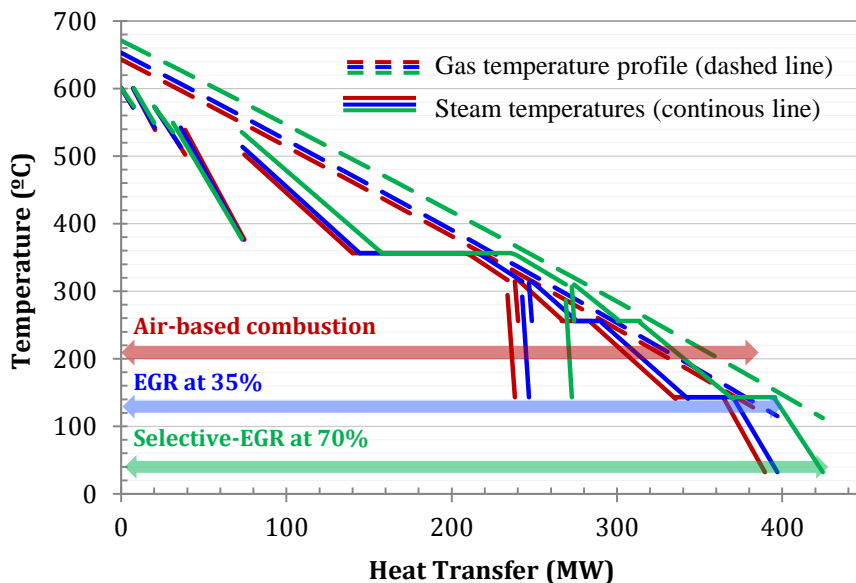


Figure 4.16.- Heat transfer – temperature diagram for S-EGR configuration in parallel at 70% recirculation ratio, 97% selective CO₂ transfer efficiency and 96% post-combustion CO₂ capture efficiency, compared to air-based combustion and EGR at 35% recirculation ratio configurations.

4.3.5. *Effects on the Post-combustion Carbon Capture unit*

The effects of S-EGR in parallel on the PCC process are examined here for a configuration operating at 70% recirculation ratio and 96% CO₂ capture in the absorber. The flue gas flow rate fed to the absorber is approximately 200 kg/s, which corresponds to 30% of the total gas turbine exhaust flue gas flow rate. The CO₂ concentration is 14 vol%, which is considerably higher than in the air-based combustion and in the 35% EGR configurations, with CO₂ concentrations of 4.2 vol% and 6.6 vol% respectively.

The higher CO₂ concentration results in a larger driving force for CO₂ transfer throughout the absorber column and displaces the equilibrium towards higher rich solvent CO₂ loadings, increasing the solvent capacity. The rich solvent CO₂ loading reaches a value of 0.475 mol_{CO₂}/mol_{MEA} compared to 0.458 and 0.466 mol_{CO₂}/mol_{MEA} for the air-based combustion and the 35% EGR configurations, respectively. The lean solvent CO₂ loading that minimises the reboiler duty is 0.25 mol_{CO₂}/ mol_{MEA}, compared to 0.26 mol_{CO₂}/ mol_{MEA} in both air-based combustion and 35% EGR. It results in an increase of the solvent capacity to 0.225 mol_{CO₂}/ mol_{MEA} from 0.207 and 0.198 mol_{CO₂}/ mol_{MEA} for air-based combustion and 35% EGR configurations, respectively. The increase of the CO₂ partial pressure from 4.2 kPa to 14 kPa results in a small increase in the rich solvent CO₂ loading due to the exponential dependency near the stoichiometric loading of 0.5 mol_{CO₂}/ mol_{MEA}, as explained in Section 4.2.5.

The higher CO₂ absorber efficiency of 97% required in S-EGR in parallel at 70% recirculation ratio results in a relatively small CO₂ partial pressure of 0.52 kPa at the top of the absorber column and, thus, a smaller driving force for mass transfer, compared to 35% EGR where the CO₂ partial pressure is 0.67 kPa. This explains the small reduction of the absorber packing volume of around 4%, compared to EGR configuration, from 2500 m³ to 2262 m³. A significant reduction of the absorber packing volume of 45% is, however, found when parallel S-EGR is compared to air-based combustion. The absorber sizing procedure, described in Chapter 3, Section 3.3, is illustrated in Figure 4.17.

The relatively small CO₂ concentration at the top of the column also requires a low CO₂ loading of the lean solvent entering the top of the absorber, which explains the small reduction in the reboiler duty despite the enhanced solvent capacity. The reboiler duty is around 3.56 MJ/kg_{CO₂} comparing to 3.64 and 3.75 MJ/kg_{CO₂} for the air-based and 35% EGR configurations, which corresponds to 2% and 5% reduction respectively.

The black dashed line in Figure 4.17 indicates the packing volume selected for each configuration, following the criterion of minimising both the reboiler duty and the absorber packing volume. The red dotted line results in a largest reduction in the absorber size capitalised on lower capital cost if the same reboiler duty for each configuration is maintained.

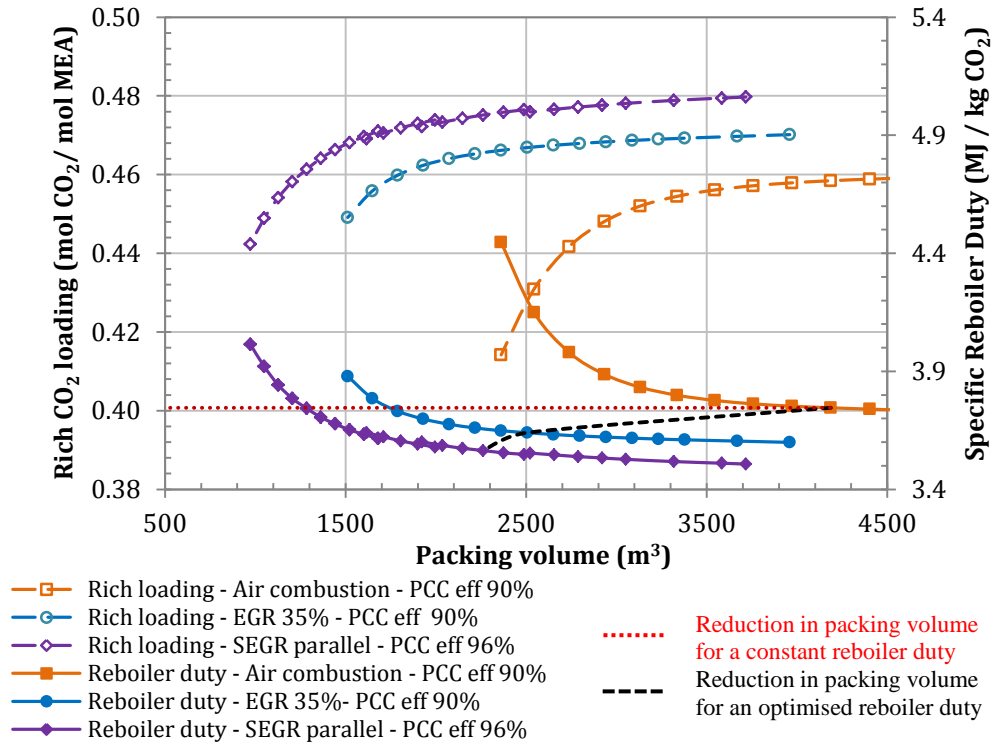


Figure 4.17.- Sensitivity of the rich solvent CO₂ loading and the specific reboiler duty to the packing volume for S-EGR in parallel at 70% recirculation ratio and 96% post-combustion CO₂ capture efficiency. Compared to air-based combustion configuration and EGR at 35% recirculation ratio and 90% post-combustion CO₂ capture efficiency.

4.3.6. Sensitivity analysis

Technology selection and design of the S-EGR system should aim to maximise CO₂ concentration in flue gases, while minimising the gas turbine derating and the impact on the performance of the components of the power plant. It is therefore important to identify design and operating parameters in the CO₂ transfer process with a large effect on the gas turbine and the combined cycle performance with S-EGR. It has to be noted that CO₂ and O₂ concentrations reported in Section 4.3.2 are evaluated assuming that only CO₂ is transferred from flue gas into air and for zero leakage levels.

The pressure drop, the temperature rise in the air side, the selectivity of CO₂ transfer over other components in the flue gas or the leak flow from the air side into the flue gas side are important parameters in the assessment of S-EGR application. The effect of deviations of these parameters from the ideal design conditions on gas turbine power output, combined cycle power output, thermal efficiency and/or composition of the flue gas and the comburent are investigated in this section.

4.3.6.1 Selectivity of CO₂ over other components in the flue gas

Any technology relying on the gradient of CO₂ partial pressure as the driving force for mass transfer could potentially be used for S-EGR. The concentration of oxygen, water vapour and nitrogen are also different in the flue gas and the air streams and, they could be transferred along with the CO₂, either in a competitive or non-competitive mechanism. In order to maintain the capacity for CO₂ transfer in case of competitive mass transfer, a larger surface area for CO₂ transfer would be required. A high CO₂ selectivity over other components in the flue gas is therefore desired.

The nitrogen partial pressure difference between the air and the flue gas is small, e.g. 70 vol% in flue gas and 77 vol% in air, and a low transfer rate is therefore expected. The higher water vapour concentration in the flue gas, 4.5 vol%, compared to air, 1 vol%, may result in water being transferred into the air. The oxygen concentration in the air, 21 vol% is higher than in the flue gas, 9.8 vol%. The concentrations are reported for flue gas saturated in moisture at 30 °C and ambient air at 60% relative humidity.

Figure 4.18 shows a sensitivity analysis of the O₂ concentration in the comburent and the CO₂ concentration in the flue gas, at the inlet of the PCC system, to the amount of oxygen transferred from air into flue gas (x axis), for a range of values of the amount of water vapour transferred from flue gas into air (parameter). The amount of each component transferred is expressed as a percentage of the inlet flow rate of the component. The oxygen concentration in the comburent decreases with increasing either the amount of oxygen transferred from air into flue gas or the amount of water transferred from flue gas into air, since a larger amount of intake air is replaced by the water vapour. The effect of oxygen transfer on the concentrations is larger compared to the effect of water transfer, since the oxygen concentration in air is considerably larger compared to the water vapour concentration in the flue gas stream, approximately 4.5% for a saturated gas at 30 °C.

The CO₂ concentration in the flue gas does not vary if oxygen is transferred, and it increases with increasing the amount of water vapour transferred, since the excess of humidity is condensed in the direct contact cooler upstream the absorber. For instance, a transfer of 10% of the amount of oxygen in the ambient air stream would reduce the oxygen concentration in the CO₂-enriched combustion air by around 1% points.

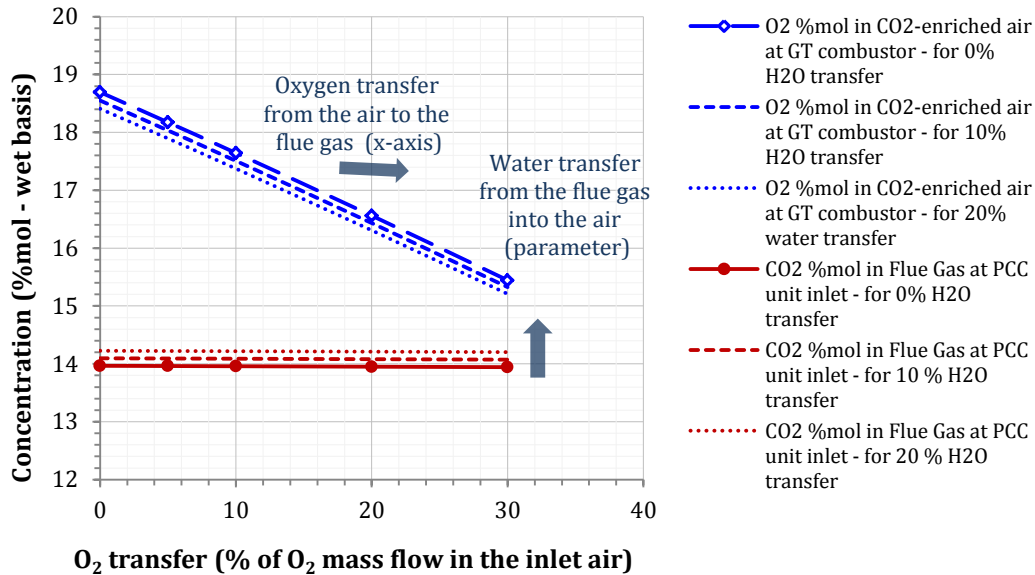


Figure 4.18.- Sensitivity of the flue gas CO₂ concentration and the combustor O₂ concentration to the O₂ transfer level from the air into the flue gas, for a range of water vapour transfer levels from the flue gas into the air. Configuration: S-EGR in parallel with a recirculation ratio of 70%, a selective CO₂ transfer efficiency of 97% and a post-combustion capture efficiency of 96.7%.

4.3.6.2 *Heat transfer*

The compressor inlet temperature is a critical parameter in the assessment of the gas turbine performance with S-EGR strategy and in the evaluation of the power output and the exhaust flue gas mass flow rate and temperature. It is therefore important to understand the mechanisms for heat transfer and the possible heat generation/consumption in the selective CO₂ transfer unit and their effect on the CO₂-enriched air temperature entering the compressor, e.g. sensible heat is transferred into the air stream since the flue gas enters the selective CO₂ transfer device at a higher temperature than the ambient air, heat of adsorption/desorption, latent heat of water condensation/evaporation, etc.

In practice, the technologies proposed for selective CO₂ transfer are likely to benefit from lower flue gas temperature. It is for instance the case of CO₂ adsorption/desorption. In the process flow diagram of Figure 4.10 the flue gas stream is cooled down to the lowest

possible temperature achievable for the cooling technology used, i.e. a direct contact cooler with cooling water supplied by a closed-loop evaporative cooling system.

Figure 4.19 shows the sensitivity of the gas turbine power output and the variation in thermal efficiency to the CO₂-enriched air temperature at the inlet of the compressor. The air temperature increases from 15 °C (ISO ambient conditions) to 17 °C due to the compression in the air fan.

For S-EGR in parallel at 70% recirculation ratio, an increase in temperature of 8 °C is assumed, estimated from the conceptual design assessment of S-EGR in parallel performed in Chapter 5. A smaller increase in temperature through the selective CO₂ transfer device results in a lower CO₂-enriched air temperature and a smaller energy penalty in the gas turbine power output. The strategy of S-EGR would increase the gas turbine power output by approximately 13 MWe, compared to the power output in the reference case of air-based combustion at ISO ambient conditions, if there was not an increase in the air temperature. It is indicated by the green dotted lines in Figure 4.19. This is due to the larger CO₂ concentration in the working fluid as explained in Section 4.3.3.

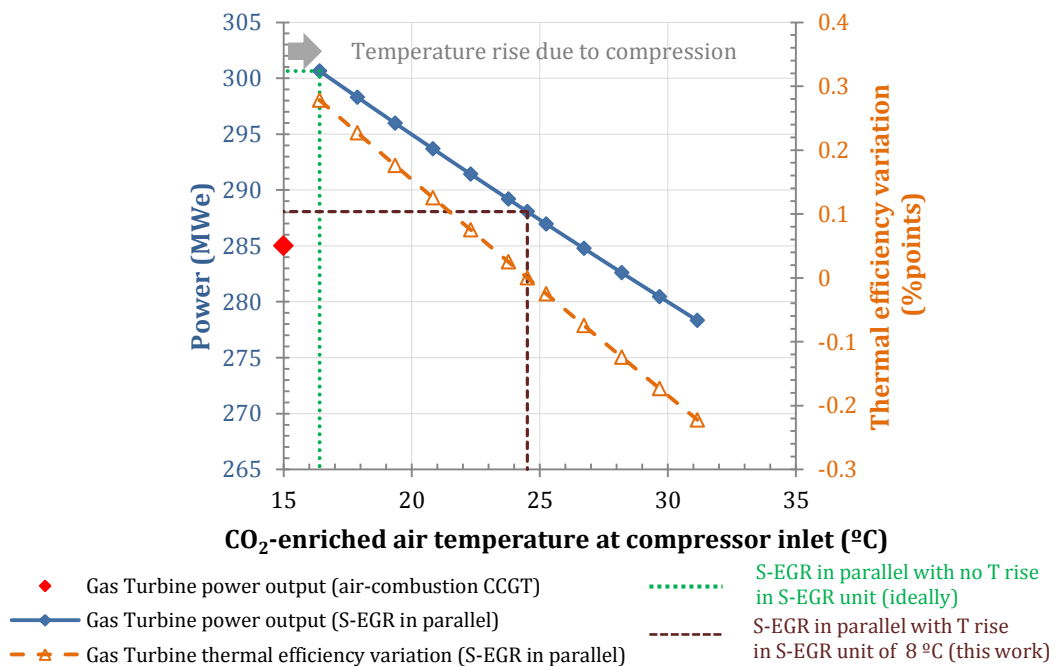


Figure 4.19.- Sensitivity of the gas turbine power output and thermal efficiency to the CO₂-enriched air temperature at the inlet of the compressor. Configuration: parallel S-EGR with a recirculation ratio of 70%, a selective transfer efficiency of 97% and a post-combustion capture efficiency of 96.7%.

4.3.6.3 Pressure drop

In order to overcome the additional pressure drop in the air and the diverted flue gas pathway when the selective CO₂ transfer unit is implemented, an air fan and a booster fan are considered, as shown in Figure 4.10. The air fan is located upstream of the selective CO₂ transfer unit and aims to reduce the penalty in the gas turbine power output.

Figure 4.20 shows sensitivity analysis of the gas turbine power output to the pressure drop on the selective CO₂ transfer unit for a configuration without air fan and with air fan. With an air fan, a reduction in the power output still happens due to temperature rise associated to the air compression in the air fan, which added to the fan power consumption results in a smaller gas turbine power penalty that in the configuration without the air fan, where the gas turbine compressor overcomes the additional pressure drop. An increase in the pressure drop of 1 kPa (10 mbar) results in a power penalty of around 2 MW with an air fan and of 4.5 MW without air fan.

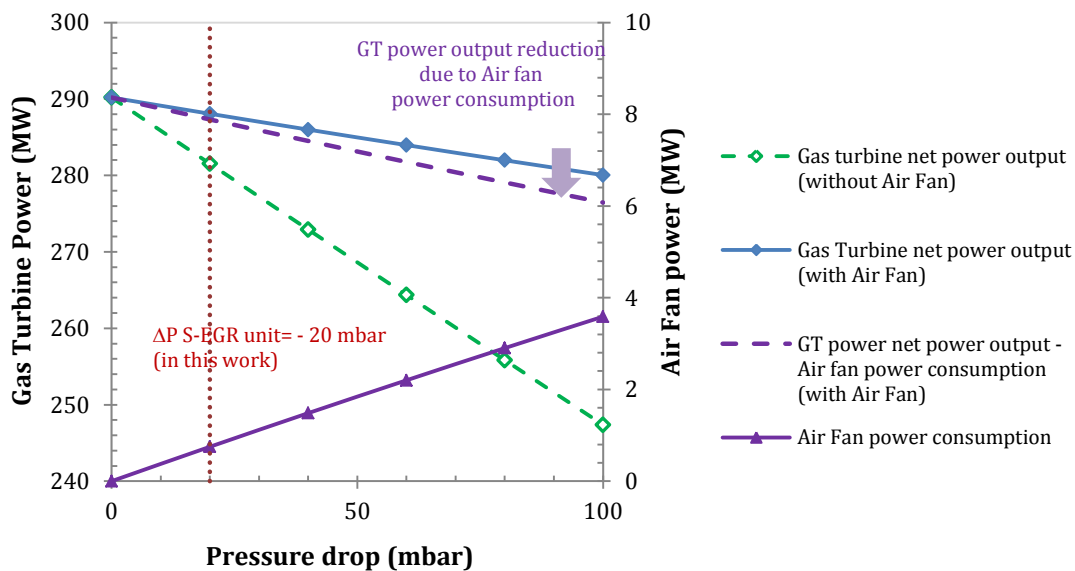


Figure 4.20.- Sensitivity of the gas turbine power output and air fan power consumption to the pressure drop in the air side of the selective CO₂ transfer device for the configuration in parallel with and without an air fan. Configuration: parallel S-EGR with a recirculation ratio of 70%, a selective transfer efficiency of 97% and a post-combustion capture efficiency of 96.7

4.4. Selective Exhaust Gas Recirculation in Series

A configuration consisting of a selective CO₂ transfer unit operated downstream of, and “in series” to, the post combustion capture process is proposed to further increase the CO₂ concentration in the flue gas, compared to a configuration with non-selective” EGR. In this configuration, the CO₂ capture efficiency in the PCC unit to achieve 90% CO₂ overall capture level is smaller than in the configurations with EGR and S-EGR in parallel, despite the fact that the total amount of flue gas needs to be treated in the PCC unit and in the selective CO₂ transfer unit.

4.4.1. Description of the configuration

In the configuration in series, the selective CO₂ transfer device is located downstream of the post-combustion CO₂ capture unit. The exhaust flue gas leaving the HRSG is first treated in the PCC unit where the CO₂ is partially removed. The flue gas still contains a relatively high CO₂ concentration, for certain operating conditions, and is then sent to the selective CO₂ transfer unit where the CO₂ is transferred into the ambient air stream. The CO₂-enriched air is then compressed and used as comburent for natural gas combustion.

As in the previous configurations, the flue gas leaving the HRSG is first cooled down in the gas/gas heat exchanger and then in the direct contact cooler and enters the absorber saturated in moisture at 45 °C. The partially CO₂-depleted gas stream leaving the absorber enters the selective CO₂ transfer unit saturated in moisture at a lower temperature of around 30 °C. In order to reach this temperature, the partially CO₂-depleted gas stream needs to be cooled either in the water wash section at the top of the absorber or in an additional direct contact cooler upstream of the selective CO₂ transfer unit. The difference in the absolute humidity between the flue gas at the inlet of the absorber and at the inlet of the selective CO₂ transfer unit results in a production of water, which may contain dissolved solvent and needs to be treated for ultimate use or disposal.

The CO₂-depleted gas stream leaving the selective CO₂ capture unit is reheated in the gas/gas heat exchanger prior to being released through the stack of the power plant.

The process flow diagram for a CCGT power plant with S-EGR in series with the PCC system is shown in Figure 4.21. The configurations of the CO₂ capture system with amine-based scrubbing technology is described in Chapter 3, Section 3.3.1.

For a 90% overall CO₂ capture level, the operation with S-EGR in series requires the following parameters to be specified: the post-combustion CO₂ capture efficiency and the selective CO₂ transfer efficiency, which are defined in Section 4.3.1.

The integration of S-EGR in series with the power cycle presents advantages over EGR for a CO₂ concentration in the flue gas above 6.6 vol% and a post-combustion CO₂ capture efficiency in the absorber considerably below 90%, since this configuration does not offer the advantage of a flue gas flow rate reduction. In Section 4.4.2, the range of possible CO₂ concentrations and the minimum requirements in terms of efficiency in both the PCC unit and the selective CO₂ transfer unit are investigated in order to define an operating framework.

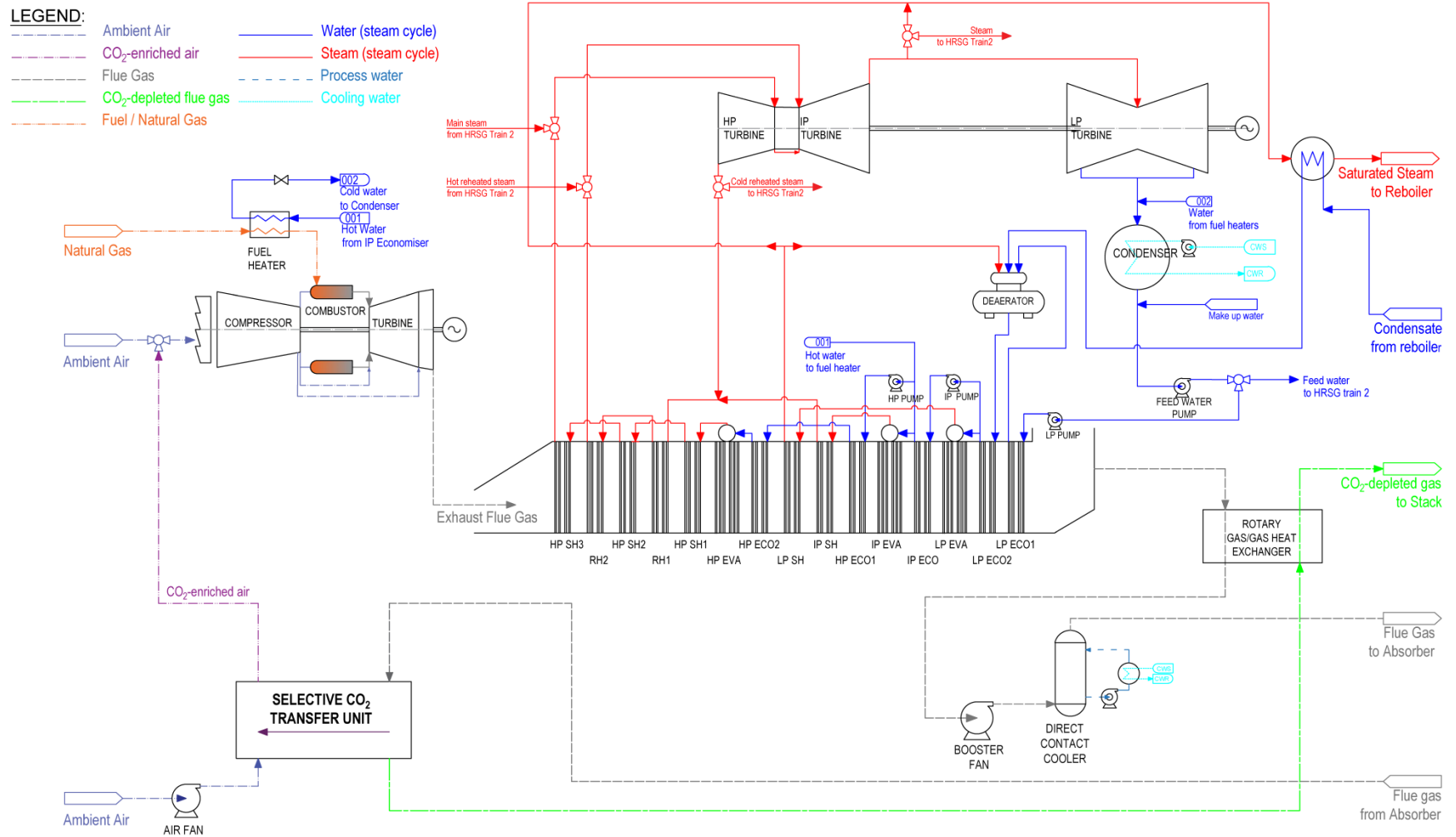


Figure 4.21.- Process flow diagram for a Combined Cycle Gas Turbine power plant with Selective Exhaust Gas Recirculation in series to the Post-combustion CO₂ Capture process.

4.4.2. Operating framework

The CO₂ concentration in the flue gas increases at a higher selective CO₂ transfer efficiency, while the oxygen level in the combustor remains above the limiting value of 16 vol% for a wide range of selective CO₂ transfer efficiencies, as illustrated in Figure 4.22. The CO₂ concentration at the inlet of the selective CO₂ transfer unit is lower than at the inlet of the PCC unit since the CO₂ is partially removed in the later unit.

A sensitivity analysis of the PCC efficiency to achieve a 90% overall CO₂ capture level as a function of the selective CO₂ transfer efficiency is shown in Figure 4.23. The higher the amount of CO₂ transferred into the combustion air, the lower the PCC efficiency.

Figure 4.22 and Figure 4.23 indicate that a higher selective CO₂ transfer efficiency than 85% is required to further increase the exhaust flue gas CO₂ concentration above 6.6 vol%, the maximum concentration with EGR at 35% recirculation ratio. The corresponding PCC efficiency is then lower than 58%. Although the total flue gas flow rate is treated in the PCC unit, unlike in the configuration with S-EGR in parallel, the lower PCC efficiency may potentially constitute an advantage compared to EGR and S-EGR in parallel configurations, where a 90% PCC efficiency or higher is required. This operating frame work corresponds to the white region in Figure 4.22 and Figure 4.23.

In the following sections, the performance of the CCGT power plant with S-EGR is investigated, with a state-of-the-art gas turbine technology originally designed for air-based combustion. As in the parallel S-EGR configuration, the temperature rise in the air side, the pressure drop and the selective CO₂ transfer efficiency are input parameters in the model, in which the CO₂ transfer device is considered as a “grey box”, to evaluate the CO₂-enriched air temperature, pressure and composition.

The performance of the PCC system based on chemical absorption with an aqueous solution of MEA is investigated and optimised for three configurations defined by the following operating parameters:

- S-EGR in series (series 85/58) operating with 85% selective CO₂ transfer efficiency and 58% PCC efficiency, since the CO₂ concentration in the flue gas is approximately 6 vol%, similar to the concentration achieved with EGR at 35% recirculation ratio.
- S-EGR in series (series 90/48) operating with 90% selective CO₂ transfer efficiency and 48% PCC efficiency. The flue gas CO₂ concentration is approximately 8 vol%.
- S-EGR in series (series 95/31) operating with 95% selective CO₂ transfer efficiency and 31% PCC efficiency, since the CO₂ concentration in the flue gas is approximately 13 vol%, similar to the concentration achieved with S-EGR in parallel at 70% recirculation ratio.

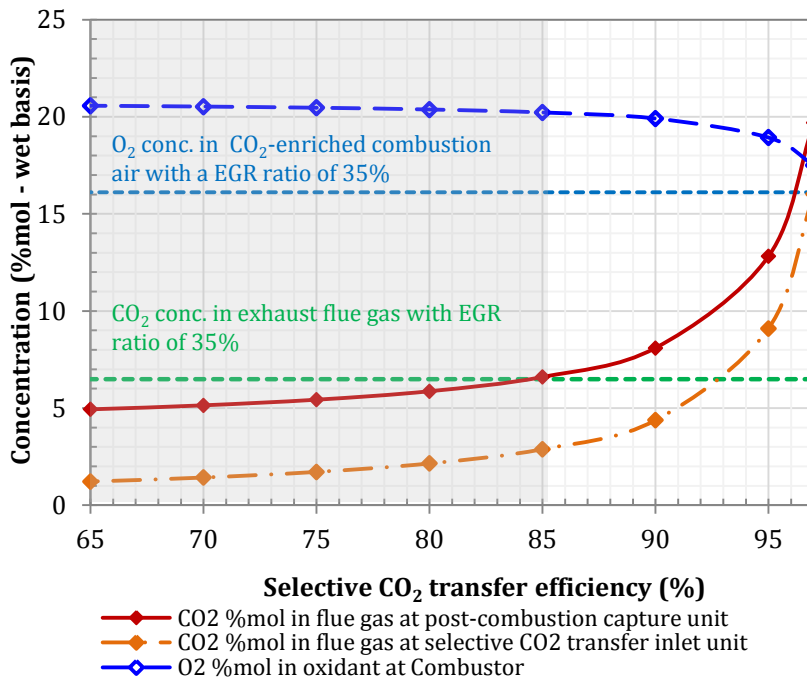


Figure 4.22.- Sensitivity of CO₂ concentration in the exhaust flue gas, at the inlet of the post-combustion capture unit and the selective CO₂ transfer unit, and O₂ concentration in the CO₂-enriched combustion air to the selective CO₂ transfer efficiency. Configuration S-EGR in series with an overall CO₂ capture level of 90%.

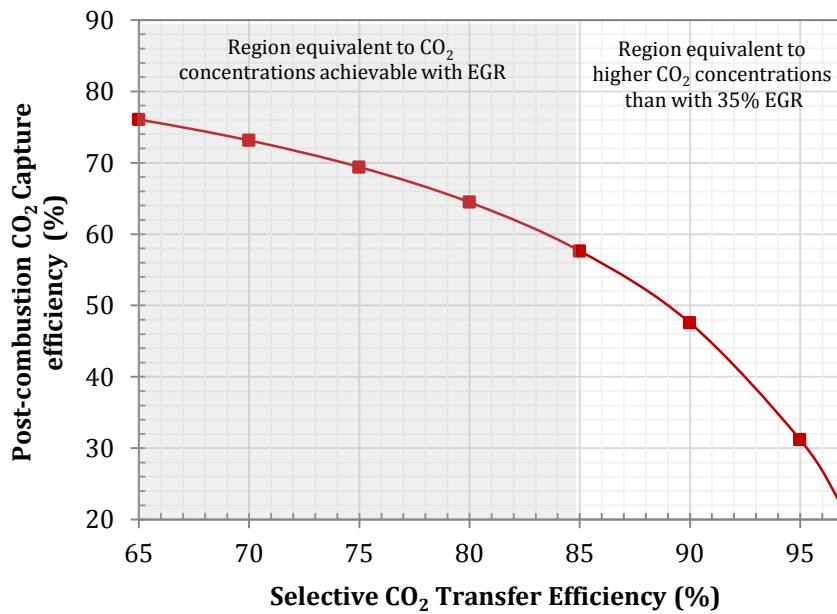


Figure 4.23.- Sensitivity of the post-combustion CO₂ capture efficiency to the selective CO₂ transfer efficiency. Configuration S-EGR in series with an overall CO₂ capture level of 90%.

4.4.3. *Effects on the Gas Turbine*

The addition to the CCGT power plant of S-EGR in series or in parallel with the PCC system has similar effects on the gas turbine performance at similar CO₂ concentration in the working fluid, pressure and temperature at the compressor inlet. The ratio of air mass flow rate to flue gas flow rate in the selective CO₂ transfer unit is smaller in S-EGR in series, compared to S-EGR in parallel, and, thus, larger amount of sensible heat is transferred into the air stream, which results in a slightly higher CO₂-enriched air temperature at the compressor inlet. It constitutes a higher gas turbine power output penalty with S-EGR in series, compared to S-EGR in parallel, for the same CO₂ concentration the working fluid.

For the configuration with 95% selective CO₂ transfer efficiency and 32% PCC efficiency, the CO₂-enriched air enters the compressor at 28 °C and the gas turbine power output decreases in approximately 4 MW, compared to air-combustion configuration.

Figure 4.24 shows the deviation, from the reference case with air at ISO ambient conditions, of the molar mass, the density and the ratio of specific heat capacities at the compressor inlet, for the CO₂ concentrations in the intake CO₂-enriched air that correspond to the three configurations investigated, as described in Section 4.4.2. Due to the greater inlet temperature, the density decreases compared to both the reference case and the corresponding S-EGR configuration in parallel with the same CO₂ concentration.

The dimensionless parameter groups for the mass flow rate, the pressure ratio and the rotational speed are evaluated for the working fluid composition and operational conditions with S-EGR. The relative values referred to the design operation point are represented in Figure 4.25. Since the relative values are close to one, this suggests that a higher CO₂ concentration in the working fluid results in a marginal deviation from the compressor and the turbine design operation points.

The increase in the ratio of specific heat capacities with the increase in CO₂ concentration, a similar effect to that previously explained for the EGR configuration, results in a decrease in the compressor outlet temperature and an increase in the turbine outlet temperature. In the compressor, the increase in the CO₂-enriched air inlet temperature counteracts the previous effect, and the reduction in the compressor outlet temperature is attenuated.

The temperature of the flue gas entering the HRSG is higher in S-EGR in series, compared to air-based combustion, for selective CO₂ transfer efficiencies higher than 90%, as shown in Figure 4.26. An increase in the heat available in the bottoming cycle is therefore only observed when the transfer efficiency of the selective CO₂ transfer unit is higher than 90%.

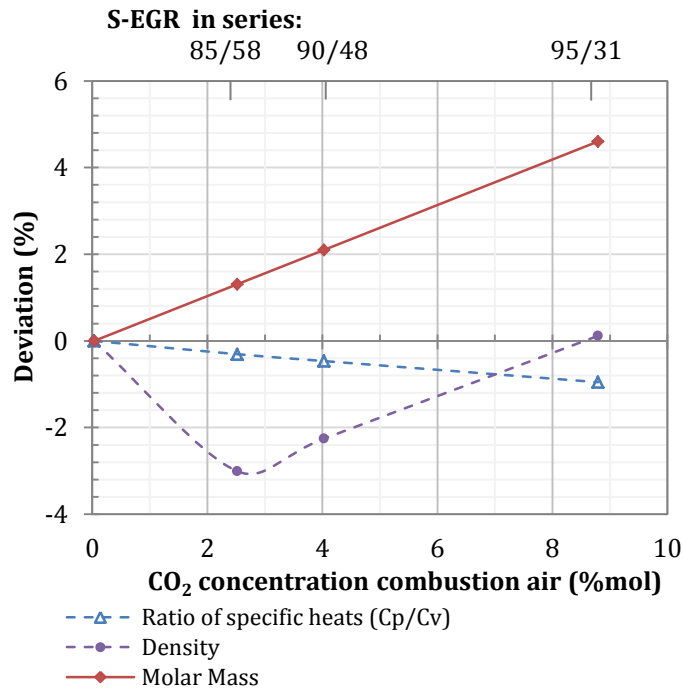


Figure 4.24.- Sensitivity of the deviation of the working fluid properties from the reference configuration with air combustion at ISO conditions, to the working fluid CO₂ concentration at the compressor inlet. Configuration: CCGT with PCC and S-EGR in series, for 85%, 90% and 95% selective CO₂ transfer efficiency.

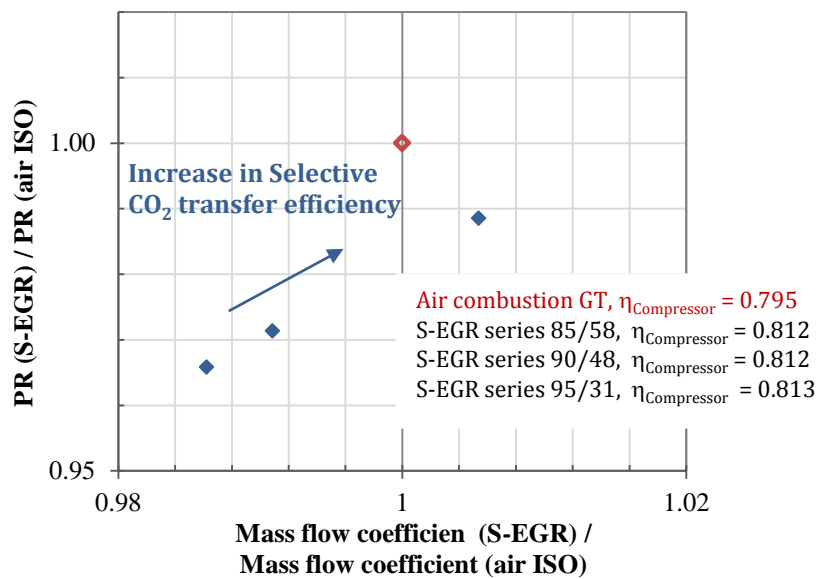


Figure 4.25.- Dimensionless parameter groups constituting the compressor performance curve for the configurations of S-EGR in series with 85%, 90% and 95% selective CO₂ transfer efficiency. Normalised values for the design operating point with air combustion at ISO conditions. Configuration: CCGT with PCC and S-EGR in series .

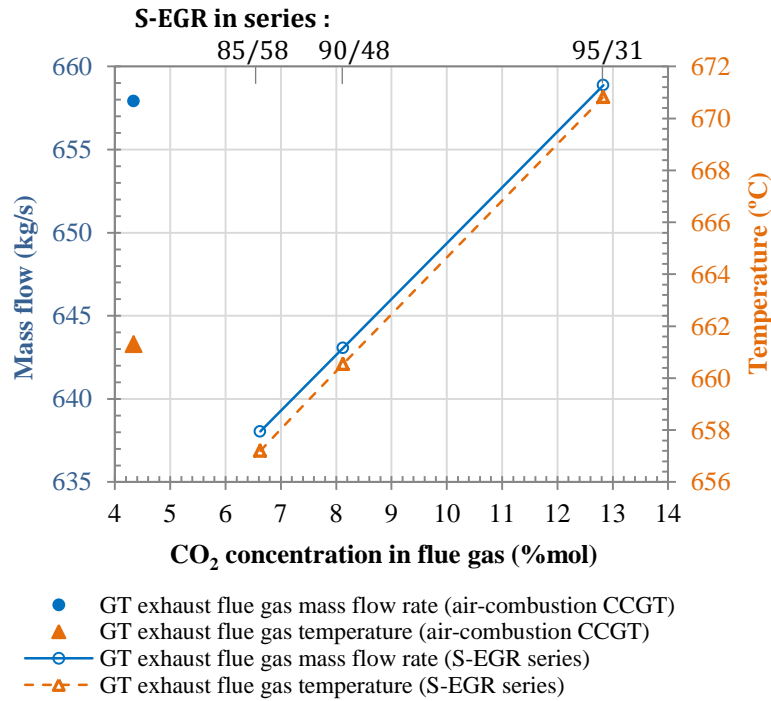


Figure 4.26.- Sensitivity of the gas turbine exhaust gas mass flow rate and temperature to the CO₂ concentration in the flue gas. Configuration: CCGT with PCC and S-EGR in series, for 85%, 90% and 95% selective CO₂ transfer efficiency.

4.4.4. Effects on the Steam Cycle

Similarly to the configuration with S-EGR in parallel, the relatively higher exhaust flue gas temperature and mass flow rate leads to a larger amount of heat available in the HRSG which is employed to increase the high pressure steam flow rate. The steam turbine net power output increases from 256 MW to 286 MW, compared to the reference case, air-based combustion CCGT with PCC.

The temperature vs. heat transfer diagram is shown in Figure 4.27 for the configuration with S-EGR in series operating at 95% selective CO₂ transfer efficiency, and, is compared to the diagrams corresponding to EGR at 35% recirculation ratio and to air-based combustion.

The temperature of the high-pressure superheated steam and reheated steam entering the HP and IP steam turbines is limited to 600 °C, and thus the approach temperatures in the corresponding heat transfer banks in the HRSG increase by 19 °C and 32 °C, respectively, in S-EGR in series compared to the reference case. Despite this, the Rankine efficiency increases by approximately 3 %points, from 64% to 67%.

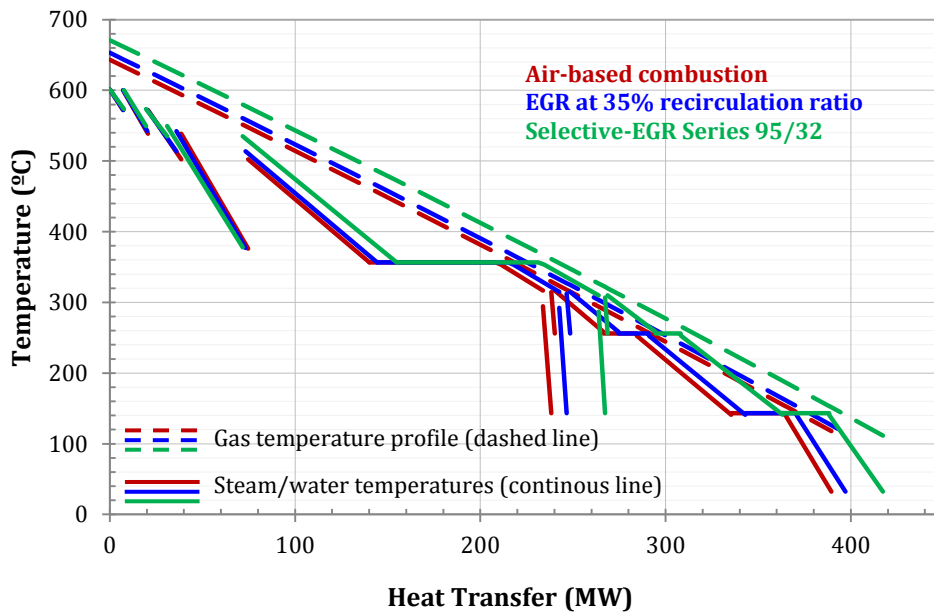


Figure 4.27.- Heat transfer – temperature diagram for S-EGR in series configuration, with 95% selective CO₂ transfer efficiency and 32% post-combustion CO₂ capture efficiency, compared to air-based combustion and EGR at 35% recirculation ratio diagrams.

4.4.5. Effects on the Post-combustion Carbon Capture unit

With a selective CO₂ transfer efficiency of 85%, a CO₂ concentration in the flue gas of 6.6 vol% is achieved, similar to EGR at 35% recirculation ratio. A CO₂ capture efficiency in the absorber of 58% is required to achieve a 90% overall CO₂ capture level.

Since the total amount of flue gas is treated in the post-combustion capture unit, two absorber columns with an internal diameter of approximately 12 m each are required in S-EGR in series and in the reference case, air-based combustion. The higher CO₂ concentration and the smaller CO₂ capture efficiency, however, results in a larger driving force throughout the absorber column and the packing height significantly decreases with S-EGR in series. For S-EGR in series with a selective CO₂ transfer efficiency of 85%, the packing volume is reduced by approximately 40%, from 4190 m³ to 2480 m³, compared to air-based combustion, as indicated by the black dotted line in Figure 4.28.

The smaller absorber efficiency of 58% in S-EGR in series, compared to 90% in EGR at 35% recirculation ratio, leads to a higher driving force specifically at the top of the absorber. Two absorbers of smaller height are therefore required with S-EGR in series and only one higher absorber with 35% EGR. It results in a similar packing volume, 2506 m³ in 35% EGR and 2480 m³ in S-EGR in series, for the same CO₂ concentration at the absorber inlet.

The rich solvent CO_2 loading increases from 0.458 to 0.469 $\text{mol}_{\text{CO}_2}/\text{mol}_{\text{MEA}}$, compared to air-based combustion, and it is similar to 35% EGR. The lean solvent CO_2 loading that minimises the reboiler duty in S-EGR in series is 0.28 $\text{mol}_{\text{CO}_2}/\text{mol}_{\text{MEA}}$, and it is higher than in air-based combustion and 35% EGR. It results in a small reduction of the solvent working capacity, from 0.198 and 0.207 to 0.189 $\text{mol}_{\text{CO}_2}/\text{mol}_{\text{MEA}}$, with S-EGR in series. Although a larger solvent flow rate is required, the higher CO_2 loading of the lean solvent leads to a decrease of the specific reboiler duty from 3.75 $\text{MJ}/\text{kg}_{\text{CO}_2}$, with air-based combustion, to 3.62 $\text{MJ}/\text{kg}_{\text{CO}_2}$, with S-EGR in series, similar to 3.64 $\text{MJ}/\text{kg}_{\text{CO}_2}$, with 35% EGR.

The flue gas CO_2 concentration can be further increased by operating at a higher selective CO_2 transfer efficiency. With a 95% selective CO_2 transfer efficiency and 32% CO_2 capture efficiency, a CO_2 concentration of approximately 13 vol% is achieved, similar to the configuration with S-EGR in parallel at 70% recirculation ratio investigated in Section 4.3.5.

The higher CO_2 concentration and the smaller CO_2 capture efficiency, compared to air-based combustion, results in a larger driving force throughout the absorber column. Two absorber columns with a similar diameter are required in both configurations. The packing height, however, significantly decreases with S-EGR in series. This results in reduction of the packing volume of approximately 64%, from 4190 to 1530 m^3 .

The smaller CO_2 capture efficiency of 32% for this configuration, compared to S-EGR in parallel at 70% recirculation ratio and 96% CO_2 capture efficiency, leads to a considerably higher driving force at the top of the absorber. Despite the fact that two absorbers are required with S-EGR in series and only one with S-EGR in parallel, a reduction of the packing volume of approximately 33% is obtained, from 2262 to 1530 m^3 .

The rich solvent CO_2 loading increases from 0.458 to 0.479 $\text{mol}_{\text{CO}_2}/\text{mol}_{\text{MEA}}$, compared to the air-based combustion. It is, however, similar to S-EGR in parallel, as the CO_2 concentration of the flue gas entering the absorber is also similar. The lean solvent CO_2 loading that minimises the reboiler duty is, however, higher, i.e. 0.28 $\text{mol}_{\text{CO}_2}/\text{mol}_{\text{MEA}}$, compared to 0.26 $\text{mol}_{\text{CO}_2}/\text{mol}_{\text{MEA}}$ in air-based combustion and 0.25 $\text{mol}_{\text{CO}_2}/\text{mol}_{\text{MEA}}$ in S-EGR in parallel. It results in a similar solvent capacity compared to air-based combustion and in a reduction of the solvent capacity compared to S-EGR in parallel, from 0.225 to 0.199 $\text{mol}_{\text{CO}_2}/\text{mol}_{\text{MEA}}$.

Despite the larger solvent flow rate and, thus, the higher contribution of the specific heat to the reboiler duty, the higher lean solvent CO_2 loading results in a reduction of the specific reboiler duty of approximately 6.6 % and 1.9% compared to air-based combustion and S-EGR in parallel respectively, from 3.64 and 3.56 $\text{MJ}/\text{kg}_{\text{CO}_2}$, respectively, to 3.50 $\text{MJ}/\text{kg}_{\text{CO}_2}$.

The procedure followed to size the absorber is described in Chapter 3, Section 3.3, and is illustrated in Figure 4.28 for the configurations of S-EGR in series operating at 32%, 48% and 58% post-combustion CO₂ capture efficiency. The reduction in the packing volume, compared to air-based combustion and EGR at 35% is indicated in Figure 4.28 by the black dotted line, following the criterion of minimising both the reboiler duty and the absorber packing volume, and by the red dotted line, if the design is capitalised on lower capital cost.

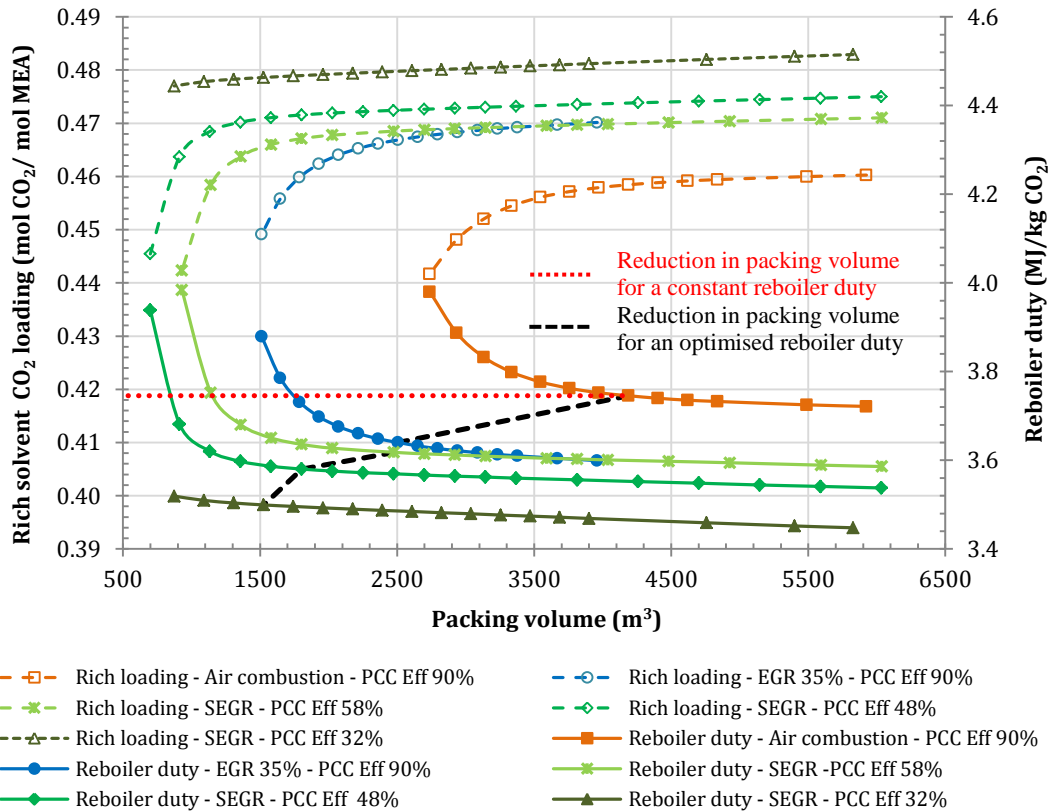


Figure 4.28.- Sensitivity of the rich solvent CO₂ loading and the specific reboiler duty to the packing volume for S-EGR in series for the configurations operating at 32%, 48% and 58% CO₂ capture efficiency. Compared to air-based combustion configuration and EGR at 35% recirculation ratio for 90% CO₂ capture efficiency.

4.4.6. Sensitivity analysis

As explained in Section 4.3.6, the pressure drop, the temperature rise, the selectivity of CO₂ transfer over other components in the flue gas and air leaks into the flue gas are important parameters in the CO₂ transfer device, which needs to be considered in the assessment of the impact of S-EGR on the gas turbine performance. The effects of a deviation of these parameters from the design conditions on the gas turbine power output, the thermal efficiency and/or the composition of the flue gas and the comburent streams are investigated in this section.

4.4.6.1. Selectivity of CO₂ over other components in the flue gas

The technologies proposed for selective CO₂ transfer rely on the gradient of CO₂ partial pressure between the flue gas and the air streams. The concentration of oxygen, water vapour and nitrogen are also different in the flue gas and the air streams and, they could be transferred along with the CO₂.

For instance, in the S-EGR in series configuration operating at 95% selective CO₂ transfer efficiency and 32% PCC efficiency, the nitrogen partial pressure difference between the air and the flue gas is small, e.g. 74 vol% in flue gas and 77 vol% in air, and a low transfer rate is expected. The water vapour concentration in the flue gas is higher than in the air, e.g. 4.5 vol% and 1% respectively, and water could be transferred into the air steam replacing part of excess air. The higher oxygen concentration in the air, 21 vol%, than in the flue gas, 11 vol% could result in oxygen transferred and reduce the oxygen available for combustion. The concentrations are reported for flue gas saturated in moisture at 30 °C and ambient air at 60% relative humidity.

A sensitivity analysis of the O₂ concentration in the comburent and the CO₂ concentration in the flue gas entering the PCC unit to the amount of oxygen transferred (x axis) for a range of water vapour transfer levels (parameter) is shown in Figure 4.29. The amount transferred for each component is expressed as a percentage of the inlet flow rate for each component. The effect of oxygen transfer on the concentrations is larger compared to the effect of water transfer, since the oxygen concentration in air is considerably larger compared to the water vapour concentration in the flue gas stream, approximately 4.5% for a saturated gas at 30 °C.

Similarly to the S-EGR in parallel, the oxygen concentration in the CO₂-enriched air used as the comburent decreases with increasing the amount of oxygen transfer from air into flue gas or the amount of water transfer from flue gas into air. The CO₂ concentration in the flue gas remains almost constant when oxygen is transferred and increases when water is transferred into the air stream, since a larger amount of excess air is replaced and the excess of humidity condenses in the direct contact cooler upstream of the absorber.

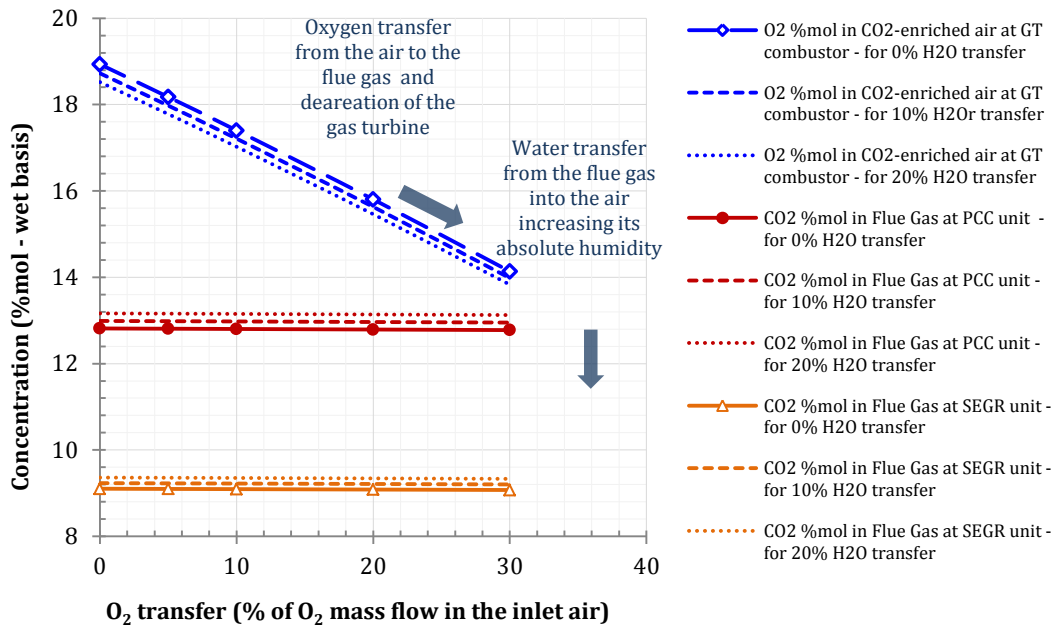


Figure 4.29.- Sensitivity of CO₂ concentration in flue gas at PCC unit inlet and the O₂ concentration in the comburent to the O₂ transfer level from the air into the flue gas, for a range of water vapour transfer levels from the flue gas into the air. Configuration: S-EGR in series operating at 95% selective CO₂ transfer efficiency and 32% post-combustion capture efficiency.

4.4.6.2. *Heat transfer*

As explained in Section 4.3.6, the compressor inlet temperature is a critical parameter in the assessment of the gas turbine performance with S-EGR and in the evaluation of the power output, the exhaust flue gas mass flow rate and temperature.

In S-EGR in series the partially CO₂-depleted flue gas is cooled in the water wash section at the top of the absorber and enters the selective CO₂ transfer device at 30 °C.

The sensitivity of the gas turbine power output and the thermal efficiency variation as function of the CO₂-enriched air temperature at the inlet of the compressor is illustrated in Figure 4.30, for S-EGR in series configuration operating with 95% CO₂ transfer efficiency. The air temperature increases from 15 °C (ISO ambient conditions) to 17 °C due to the compression in the air fan. An increase in temperature of 11 °C is assumed, estimated from the conceptual design assessment performed in Chapter 5. A smaller increase in temperature

through the selective CO₂ transfer device results in a lower CO₂-enriched air temperature and a smaller energy penalty in the gas turbine power output. The strategy of S-EGR in series would result in an increase of the gas turbine power output by approximately 13 MWe, compared to the power output in air-based combustion at ISO conditions, with no rise in temperature in the air side. It is indicated by the green dotted lines in Figure 4.30. This is due to the larger CO₂ concentration in the working fluid as explained in Section 4.4.3.

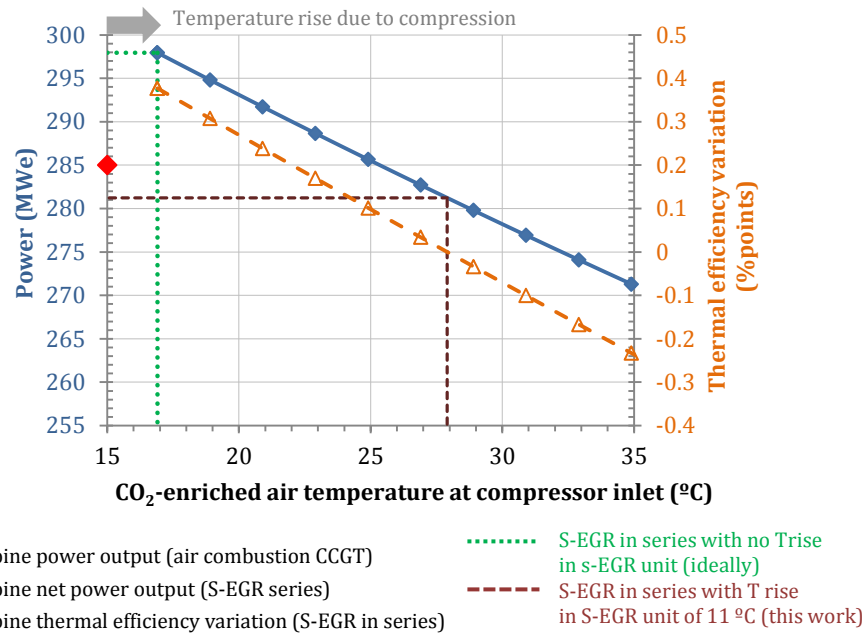


Figure 4.30.- Sensitivity of the gas turbine power output and thermal efficiency to the CO₂-enriched air temperature at the inlet of the compressor. Configuration: S-EGR in series with a selective transfer efficiency of 95%, post-combustion capture efficiency of 32%.

4.4.6.3. *Pressure drop*

An air fan is located upstream of the selective CO₂ transfer unit to overcome the pressure drop in the air pathway, which otherwise would have to be overcome by the compressor. The booster fan is sized to overcome the pressure drop through the gas pathway, i.e. the gas/gas heat exchanger, the direct contact cooler, the absorber and the selective CO₂ transfer unit.

Figure 4.31 shows the sensitivity analysis of the gas turbine power output to the pressure drop through the selective CO₂ transfer unit for a configuration without air fan and with air fan. With an air fan, a reduction in the power output still happens due to temperature rise in the air fan, which added to the fan power consumption results in a smaller gas turbine power penalty that in the configuration without the air fan, where the gas turbine compressor overcomes the additional pressure drop. An increase in the pressure drop of 1 kPa results in a power penalty of around 2 MW with an air fan and of 4.5 MW without air fan.

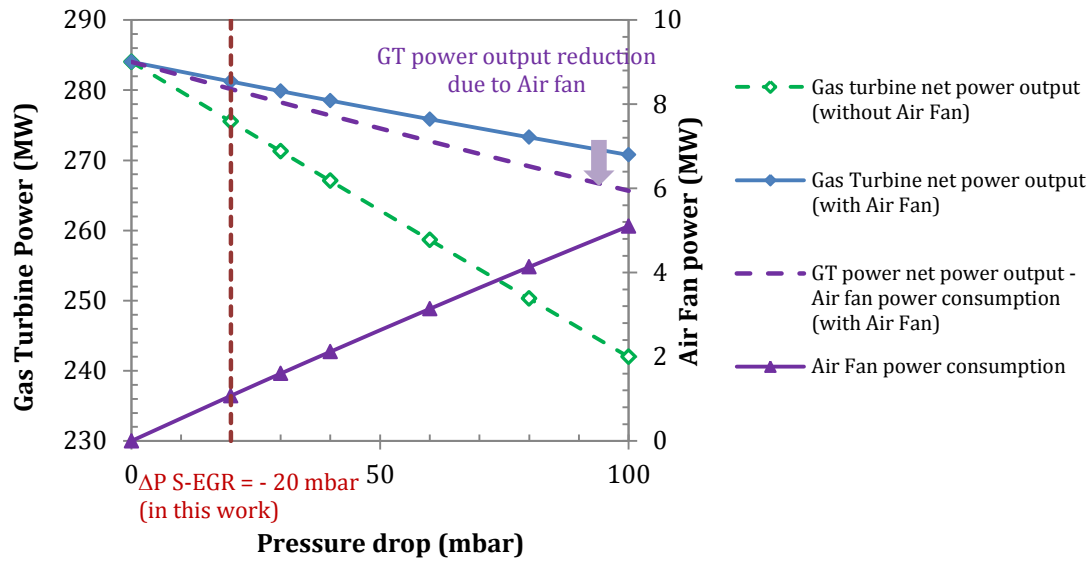


Figure 4.31.- Sensitivity of the gas turbine power output and air fan power consumption to the pressure drop in the air side of the selective CO₂ transfer device for the configuration in parallel with and without an air fan. Configuration in series with selective transfer efficiency of 95% and post-combustion capture efficiency of 32%.

4.5. Comparison and discussion of the results

Results obtained from the assessment of the performance a CCGT power plant with carbon capture system using MEA aqueous solutions with either S-EGR in parallel or S-EGR in series are further discussed in this section for the following configurations, named in this section by two numbers, the first indicates the selective CO₂ transfer efficiency and the second indicates the post-combustion CO₂ capture efficiency:

- S-EGR in parallel (parallel 97/96) operating at 70% recirculation ratio, 96% PCC efficiency and 97% selective CO₂ transfer efficiency, since the CO₂ concentration in the flue gas is comparable to the CO₂ concentration in coal-fired power plants for a feasible efficiencies in the capture and the CO₂ transfer systems.
- S-EGR in series (series 85/58) operating with 85% selective CO₂ transfer efficiency and 58% PCC efficiency, since the CO₂ concentration in the flue gas is approximately 6 vol%, similar to the concentration achieve with EGR at 35% recirculation ratio.
- S-EGR in series (series 90/48) operating with 90% selective CO₂ transfer efficiency and 48% PCC efficiency. The flue gas CO₂ concentration is approximately 8 vol%.
- S-EGR in series (series 95/31) operating with 95% selective CO₂ transfer efficiency and 31% PCC efficiency, since the CO₂ concentration in the flue gas is approximately 13 vol%, similar to the concentration achieved with S-EGR in parallel at 70% recirculation ratio.

Results have been compared to the reference configuration, i.e. an air-based CCGT with PCC, and a configuration of a CCGT with PCC at 35% EGR ratio. Table 4.1 summarises the operating conditions and CO₂ concentration achievable in the flue gas.

Table 4.1.- Operating parameters and concentrations of the investigated configurations

Configuration/ Case		Air-based combustion (reference case)	EGR	S-EGR Parallel 97/96	S-EGR Series 95/31	S-EGR Series 90/48	S-EGR Series 85/58
Recirculation ratio	%		35	70	N/A	N/A	N/A
Overall CO ₂ capture level	%	90	90	90	90	90	90
PCC efficiency	%	90	90	96	31	48	58
Selective CO ₂ transfer efficiency	%	N/A	N/A	97	95	90	85
O ₂ conc. in combustion air	%mol	20.74	16.40	18.68	18.92	19.91	20.22
CO ₂ conc. in comburent	%mol	0.03	2.41	9.96	8.79	4.03	2.52
CO ₂ conc. in flue gas	%mol	4.34	6.56	14.12	12.91	8.15	6.65

4.5.1. Overall effect on the post-combustion CO₂ capture system

In Section 4.3.2 and Section 4.4.2, it has been shown that S-EGR significantly increases the CO₂ concentration in the exhaust flue gas of a CCGT power plant to approximately 14 vol%, compared to 6.6 vol% with “non-selective” EGR at 35% recirculation ratio. A high CO₂ concentration in the gas phase enhances the CO₂ absorption rate due to an increase in the driving force for mass transfer and the displacement of the thermodynamic equilibrium towards high CO₂ loadings in the solvent. A higher CO₂ absorption rate results in a reduction of the absorber packing volume and in a higher solvent capacity, which also results in smaller energy requirements for solvent regeneration.

The configuration with S-EGR in parallel to the PCC process also reduces the flow rate of the flue gas stream treated in the absorber, compared to 35% EGR. A higher PCC efficiency is, however, required to achieve a 90% overall CO₂ capture level with increasing the fraction of the flue gas diverted to the CO₂ transfer unit. It results in a relatively small driving force towards the top of the absorber column and a smaller CO₂ loading in the lean solvent is required. The diameter of the absorber column is significantly smaller, yet a larger packing height for absorption is necessary, compared to air-based combustion and 35% EGR.

The configuration with S-EGR in series to the PCC process requires a lower PCC efficiency than 90% to achieve a 90% overall CO₂ capture level, which results in a higher driving force throughout the whole absorber column and higher CO₂ loading at the top of the absorber is possible. The total amount of the flue gas is, however, treated and two absorber columns of similar internal diameter than in air-based combustion, yet the packing height is smaller than in both air-based combustion and 35% EGR configurations.

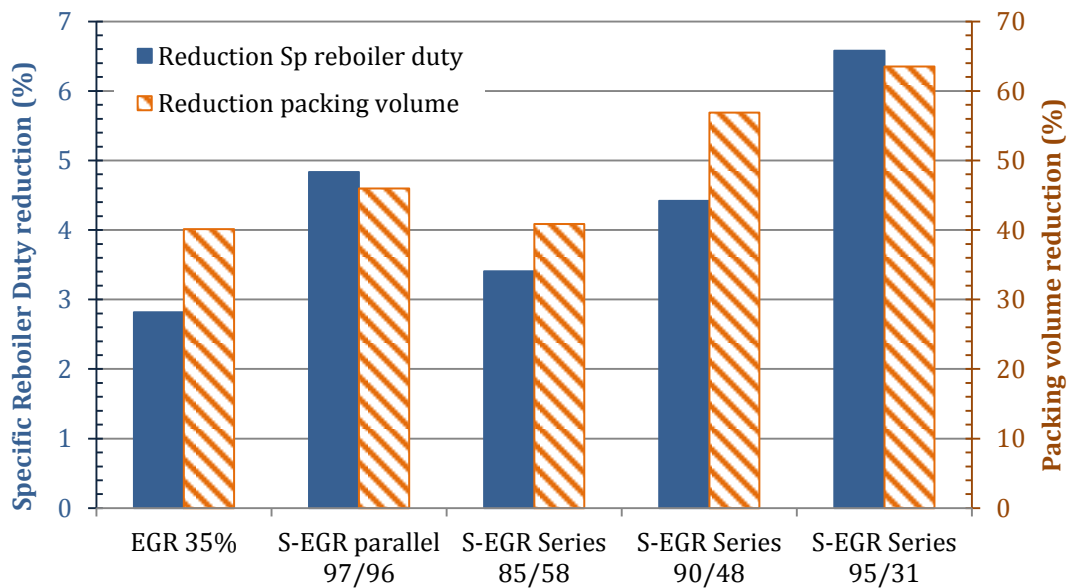
Table 4.2 includes the design and operating parameters of the CO₂ capture system for chemical absorption with a 30 wt% aqueous MEA solution. A comparison of the results in terms of reduction in packing volume and in specific reboiler duty is illustrated in Figure 4.32 for the investigated configurations, considering as the reference case an air-based combustion CCGT plant with PCC.

The configuration of S-EGR in parallel operating at 70% recirculation ratio and 96% PCC efficiency leads to a reduction of 46% in packing volume and 5% in specific reboiler duty, compared to air-based combustion, and of 10% in packing volume and 2% in specific reboiler duty, compared to EGR at 35% recirculation ratio.

The configuration of S-EGR in series operating at 32% PCC efficiency results in a reduction of 64% in packing volume and 6.6% in specific reboiler duty, compared to air-based

configuration, and of 33% in packing volume and 2% in specific reboiler duty, compared to S-EGR in parallel at 70% recirculation ratio for a similar CO₂ concentration in the flue gas of approximately 13-14 vol%.

The solvent flow rate is similar in all the configurations since the operation with EGR or S-EGR does not change significantly the heat input to the gas turbine. For 90% overall CO₂ capture level, the CO₂ flow rate captured for transport and storage/utilization is therefore similar. It also explains the small reduction in the reboiler duty, since the contribution of the specific heat to raise the temperature of the solvent is important.



S-EGR parallel 97/96: Recirculation ratio 70%, post-combustion capture efficiency 96.7%, selective CO₂ transfer eff. 97%.
 S-EGR series 85/58: post-combustion capture efficiency 58%, and selective CO₂ transfer efficiency 85%.
 S-EGR series 90/48: post-combustion capture efficiency 48%, and selective CO₂ transfer efficiency 90%.
 S-EGR series 95/31: post-combustion capture efficiency 31%, and selective CO₂ transfer efficiency 95%.

Figure 4.32.- Specific reboiler duty and packing volume reduction for a CCGT plant with Post-combustion Carbon Capture for the configurations: 30% exhaust gas recirculation, selective exhaust gas recirculation in parallel and in series, compared to the reference case: air-based combustion CCGT with PCC.

Table 4.2.- Technical parameters and operational variables of the CO₂ capture process with chemical absorption using 30 wt% MEA aqueous solution

Configuration/ Case		Air-based combustion (reference case)	EGR	S-EGR Parallel 97/96	S-EGR Series 95/31	S-EGR Series 90/48	S-EGR Series 85/58
Operation conditions							
Recirculation ratio	%		35	70	N/A	N/A	N/A
Overall CO ₂ capture level	%	90	90	90	90	90	90
PCC efficiency	%	90	90	96	31	48	58
Selective CO ₂ transfer efficiency	%	N/A	N/A	97	95	90	85
Absorber (per GT-HRSG-PCC train)							
<i>Flue gas BOTTOM</i>							
Mass flow rate	kg/s	658	418	200	659	642	637
CO ₂ conc.	vol%	4.21	6.65	14.00	12.89	8.15	6.64
Temperature	°C	45	45	45	45	45	45
<i>Flue gas TOP</i>							
Mass flow rate	kg/s	622	382	161	599	585	581
CO ₂ conc.	vol%	0.43	0.70	0.59	8.8	4.67	3.08
Temperature	°C	54	58.4	66	55	55	55
Absorber efficiency	%	90	90	96	31	48	58
Lean solvent loading	mol _{CO₂} / mol _{MEA}	0.26	0.26	0.25	0.28	0.28	0.28
Rich solvent loading	mol _{CO₂} / mol _{MEA}	0.458	0.466	0.479	0.472	0.469	0.467
Solvent capacity	mol _{CO₂} / mol _{MEA}	0.198	0.207	0.225	0.189	0.192	0.199
Lean solvent molar flow rate	mol/s	886	851	808	942	947	969
Liquid / Gas ratio	kg/kg	1.35	2.05	3.99	1.38	1.42	1.44
<i>Environmental</i>							
Emissions MEA	mg/Nm ³	<1.53	<1.53	<2.22	<0.14	<0.14	<0.14
<i>Structural parameters</i>							
No. Absorbers	--	2	1	1	2	2	2
Packing diameter	m	12	14	12	12	12	12
Packing height	m	19	17	20	11	8	7
Packing volume Total	m³	4187	2506	2262	1526	1804	2476
Stripper							
Stripper pressure	bar	1.84	1.84	1.82	1.92	1.89	1.89
Rich solvent temperature	°C	120	120	120	120	120	120
Steam specific consumption	kg/ kg _{CO₂}	1.71	1.66	1.62	1.59	1.62	1.65
Specific Reboiler Duty	MJ/ kg_{CO₂}	3.75	3.64	3.56	3.50	3.58	3.62
Reboiler pressure	bar	2.95	2.95	2.95	2.95	2.95	2.95
Reboiler temperature	°C	133	133	133	133	133	133
CO ₂ to pipeline	kg/s	76.5	76.89	80.12	78.3	75.53	74.64

The largest reduction in absorber packing volume is observed for S-EGR in series operating at a high efficiency in the CO₂ transfer system and at a low efficiency in the PCC system. The reduction is even higher than for the configuration with S-EGR in parallel which results in a similar CO₂ concentration in the flue gas entering the PCC process. It has to be noted that the design and the operating conditions to achieve a high CO₂ transfer efficiency for the selective CO₂ transfer system is significantly more challenging for S-EGR in series than for S-EGR in parallel, as the CO₂ concentration in the inlet flue gas stream is smaller in the former configuration, since the CO₂ is partially removed from the flue gas in the PCC plant upstream of the selective CO₂ transfer system.

The operation and cost benefit of S-EGR on the PCC system has to be balanced against the additional unit operation for selective CO₂ transfer. A conceptual design assessment of the selective CO₂ transfer process is conducted in Chapter 5 in order to provide preliminary dimensions of the device. A detailed economic analysis is however necessary to fully assess the advantage of S-EGR over “non-selective” EGR.

Moreover, in the configuration with S-EGR in parallel, operating at a high recirculation ratio and a high PCC efficiency, the temperature of the CO₂-depleted gas leaving the packing section for absorption is relatively high due to the significantly higher ratio of the solvent flow rate over the gas flow rate (L/G), compared to air-based combustion, 35% EGR and S-EGR in series. The temperature profiles of the liquid and the gas in the absorber column are illustrated in Figure 4.33, for the investigated configurations. The temperature increases due to the heat of adsorption reaching a maximum, i.e. temperature bulge, close to the top of the absorption section. The temperature then decreases due to the cooling effect of the lean solvent and the water vaporization. The amount of evaporated water is smaller at higher L/G ratios and so the cooling effect (Kvamsdal et al. 2011). The CO₂-depleted gas leaves the absorption section at approximately 65 °C with S-EGR in parallel and at approximately 55-60 °C in other configurations. A higher water wash section is therefore required in S-EGR in parallel to cool the CO₂-depleted gas to 45 °C and reduce MEA emissions to a similar level.

The packing of the water wash section has not been included in the total packing volume reported in Table 4.2, since less expensive random packing can be used. The same effect of the L/G ratio on the temperature profiles is also found in the experimental data from the a test campaign of the CO₂ capture pilot plant located at Esbjerg power station, as part of the “CO₂ Enhanced Separation and Recovery” (CESAR) project, performed to optimise the flow rate of the lean solution to the absorber with respect to a minimal reboiler duty (Abu Zahra 2009; Oexmann 2011).

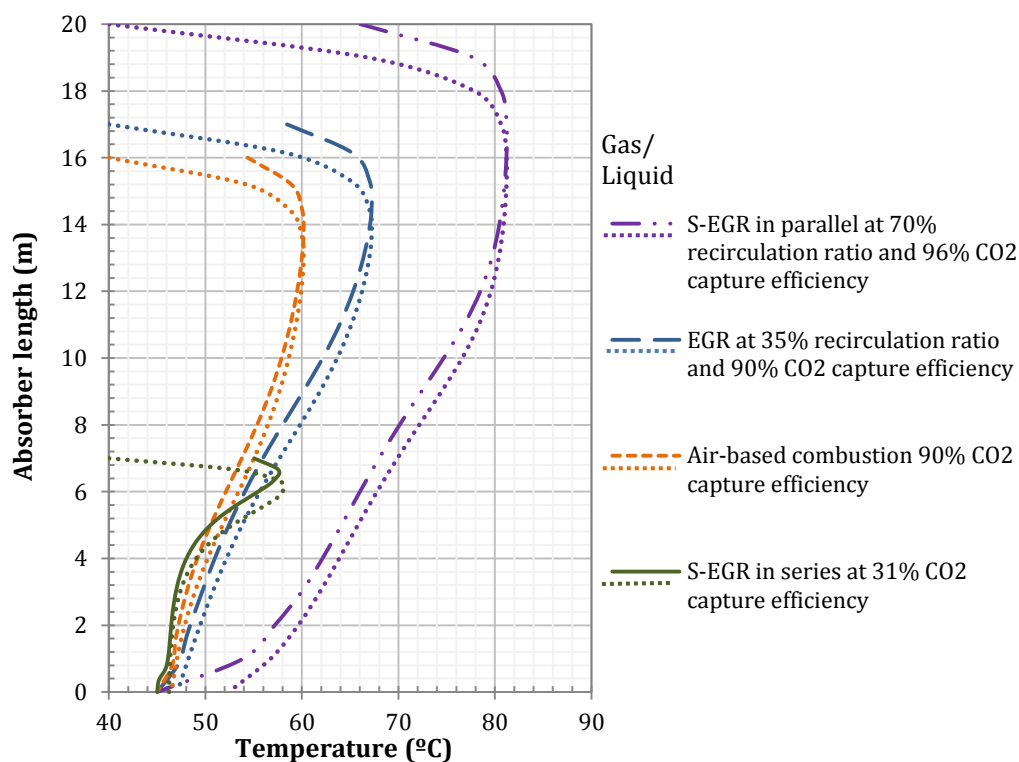


Figure 4.33.- Temperature profile of the gas phase (continuous and dashed lines) and the liquid phase (dotted lines) in the absorber for the configurations with: air-based combustion with 90% CO₂ absorption efficiency, 35% EGR with 90% CO₂ absorption efficiency, S-EGR in parallel at 70% recirculation ratio and 96% CO₂ absorption efficiency, and for S-EGR in at 32%, 48% and 58% CO₂ absorption efficiencies.

The effect of increasing CO₂ partial pressure of the flue gas on the CO₂ absorption process depends on the thermodynamics and the kinetics of the process and, thus, on the solvent. For a 30 wt% MEA aqueous solution, the vapour-equilibrium curves of the system shows a small effect of increasing CO₂ partial pressure on the CO₂ loading at high solvent loadings close to the stoichiometric limit of 0.5 mol_{CO₂}/mol_{MEA}. On the other hand, higher CO₂ partial pressures can lead to faster absorption rates, higher enhancement factors and high mass transfer coefficients in the liquid phase. A small increase in the rich solvent CO₂ loading is observed in the final results when the CO₂ partial pressure increases from 4 kPa to 14 kPa indicating that an increase in the driving force has a marginal effect on the CO₂ absorption rate and that the vapour-liquid equilibrium is limiting the enhancement effect. Other solvents may therefore benefit more of the increase in the flue gas CO₂ partial pressure achieved with S-EGR. For this particular case, solvents with slower CO₂ adsorption/desorption rates, higher CO₂ adsorption capacity and smaller enthalpy of adsorption, such as tertiary amines, e.g. methyldiethanolamine (MDEA), or hindered amines, e.g. 2-amino-2-methyl-1-propanol (AMP) (Ma'mun et al. 2005) might benefit more of the increased CO₂ partial pressure achieved with S-EGR.

4.5.2. Overall effect on the CCGT power plant

Strategies to enhance CO₂ capture rate should aim to introduce minimal modifications in the gas turbine engine, as current gas turbine technology presents a high efficiency and plays an important role in achieving a high combined cycle net power output.

The performance of a state-of-the-art gas turbine engine, when EGR and S-EGR are implemented, is investigated for a GE Class F Frame 9 engine. The exhaust flue gas composition and flow rate, and thus achievable CO₂ concentrations, are specific to the gas turbine engine, since the design TIT defines the excess of air. Yet results from the performance assessment are valid for any gas turbine engine, since it is based on a dimensionless analysis.

The physical properties of the working fluid which appear in the equations used for the performance modelling of the turbomachinery, i.e. density, ratio of specific heats and molar weight, are evaluate at three locations along the gas turbine, i.e. compressor inlet, turbine inlet and turbine outlet. Results are shown in Table 4.3 for each configuration. The overall effect of an increase in the density of a CO₂-enriched air, compared to ambient air at ISO conditions, at relatively high CO₂ concentrations achieved, for instance, with S-EGR in parallel 97/96 and S-EGR in series 95/31, contributes to an increase in the gas turbine power output.

A small deviation in the compressor and turbine operating point from design conditions is also found for the gas turbine operating with EGR or S-EGR. Table 4.4 provides values of the temperature and pressure at the compressor and the turbine inlet, the relative values of the dimensionless parameter groups to the design values that constitute the compressor and the turbine performance maps, the exhaust flue gas temperature, mass flow rate and composition.

The exhaust flue gas temperature increases for all the configurations and the exhaust mass flow rate increases for S-EGR in parallel 97/96 and S-EGR in series 95/31, as shown in Table 4.5. It results in an increase of the heat available in the bottoming cycle, which leads to an increase in the steam turbines power output.

Despite the increase in the net power output of the combined cycle, the thermal efficiency marginally increases by less than 1%. It is due to the increase in the heat input to maintain the TIT at the design value, as result of the change in the thermodynamic properties of the mix of the natural gas and the CO₂-enriched comburent.

The gas turbine power output, the steam turbines power output, the combined cycle power output and thermal efficiency, as well as the auxiliary power consumption and power output penalty for solvent regeneration is presented in Table 4.6. The variation of the previous parameters compared to the reference configuration, i.e. an air-based combustion CCGT plant with PCC is illustrated in Figure 4.32.

The sensitivity analysis performed in Section 4.3.6 and Section 4.4.6, for the configurations with S-EGR in parallel at 70% recirculation ratio and with S-EGR in series operating at 31% PCC efficiency and 95% selective CO₂ transfer efficiency, showed that design and operating parameters of the selective CO₂ transfer system have a significant effect on the overall performance of a CCGT power plant with PCC and S-EGR. The effect of the pressure drop, the temperature rise in the air stream, the selectivity of CO₂ over other components in the flue gas and the air leak flow into the flue gas, on the gas turbine power output and on the composition of the flue gas and the comburent are quantified.

An increase of 10 °C in the air stream temperature results in a decrease of the gas turbine power output of approximately 13 MW for both S-EGR in parallel and S-EGR in series. Yet an increase of the gas turbine power output of approximately 13 MW, compared to the air-based combustion configuration, could be achieved if the temperature of the air remains at 15 °C when it gets enriched in CO₂. It is due to the high density of a CO₂-enriched air compared to ambient air. A pressure drop of 20 mbar results in an overall penalty in the gas turbine power output of approximately 3 Mw, due to the air fan power consumption and the temperature rise due to compression. Any possible leakage should be minimised and a high selectivity of CO₂ is required so that other components, mainly oxygen, is not transferred into the flue gas, maintaining high oxygen levels in the comburent.

Results from the sensitivity analysis also establish the basis and the performance requirements for the selection of technologies that could potentially be used for S-EGR application. It is required a low pressure drop, a small sensible heat transfer rate and the possibility for dissipation of generated heat in the process, a high selectivity to CO₂ over oxygen, nitrogen and water vapour and a low leakage level. An additional consideration is that the flue gas contains water vapour, e.g. 4.6 vol% in a flue gas saturated in moisture at 30 °C. The technology selected for CO₂ transfer should therefore be insensitive to the presence of moisture, without reducing the capacity for CO₂ transfer. Based on this, a conceptual design of the selective CO₂ transfer system is conducted in Chapter 5 for the technology of physical adsorption in a rotary wheel configuration with structured adsorbents.

Table 4.3.- Working fluid properties at compressor inlet, turbine inlet and turbine outlet for the investigated configurations

Configuration/ Case		Air-based combustion (reference case)	EGR	S-EGR Parallel 97/96	S-EGR Series 95/31	S-EGR Series 90/48	S-EGR Series 85/58
O ₂ conc. in combustion air	%mol	20.74	16.40	18.68	18.92	19.91	20.22
CO ₂ conc. in comburent	%mol	0.03	2.41	9.96	8.79	4.03	2.52
CO ₂ conc. in flue gas	%mol	4.34	6.56	14.12	12.91	8.15	6.65
<i>At compressor inlet</i>							
Specific heats ratio (Cp/Cv)	--	1.402	1.398	1.387	1.388	1.395	1.397
Density	kg/m ³	1.208	1.192	1.230	1.210	1.181	1.172
Molar mass	g/mol	28.85	28.96	30.36	30.18	29.46	29.23
<i>At turbine inlet</i>							
Specific heats ratio (Cp/Cv)	--	1.281	1.276	1.263	1.265	1.274	1.277
Density	kg/m ³	3.576	3.532	3.768	3.689	3.544	3.498
Molar mass	g/mol	28.37	28.47	29.78	29.613	28.94	28.72
<i>At turbine outlet</i>							
Specific heats ratio (Cp/Cv)	--	1.324	1.317	1.298	1.301	1.313	1.317
Density	kg/m ³	0.385	0.382	0.391	8.424	8.891	8.536
Molar mass	g/mol	28.37	28.47	29.78	29.61	28.94	28.73

Table 4.4.- Dimensionless parameter groups constituting the compressor and turbine performance curves for the investigated configurations.

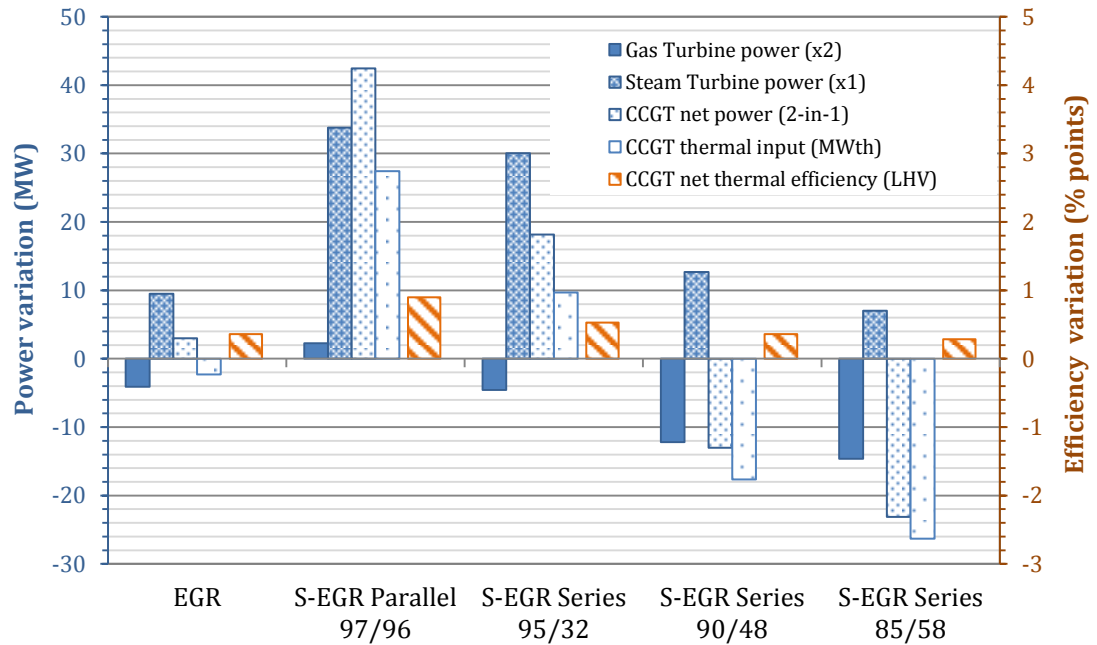
Configuration/ Case		Air-based combustion (reference case)	EGR	S-EGR Parallel 97/96	S-EGR Series 95/31	S-EGR Series 90/48	S-EGR Series 85/58
Compressor							
Inlet temperature	°C	15.00	20.21	24.51	28	28	28
Inlet pressure	bar	1.003	1.003	1.003	1.003	1.003	1.003
Mass flow coefficient Equation [3.63]	--	1.000	0.995	1.015	1.005	0.991	0.986
Pressure ratio Equation [3.64]	--	1.000	0.989	1.004	0.989	0.971	0.966
Rotational speed Equation [3.65]	--	1.000	0.995	1.015	1.005	0.991	0.986
Turbine							
Turbine inlet temperature	°C	1371	1371	1371	1371	1371	1371
Inlet pressure	bar	17.23	17.01	17.30	17.03	16.74	16.64
Constant capacity Equation [3.44]	mol K ^{1/2} bar ⁻¹ s ⁻¹	423	423	423	423	423	423
Mass flow coefficient Equation [[3.63]	--	1	1	1	1	1	1
Pressure ratio Equation [3.64]	--	1	0.989	1.004	0.989	0.972	0.966
Rotational speed Equation [3.65]	--	1	1.008	1.032	1.028	1.013	1.008

Table 4.5.- Exhaust flue gas stream variables

Configuration/ Case		Air-based combustion (reference case)	EGR	S-EGR Parallel 97/96	S-EGR Series 95/31	S-EGR Series 90/48	S-EGR Series 85/58
Gas Turbine exhaust flue gas							
Temperature	°C	643	649	671	671	661	657
Pressure (set point)	bar	1.04	1.04	1.04	1.04	1.04	1.04
Mass flow	kg/s	658	643	670	659	643	638
<i>Composition:</i>							
CO ₂	% mol	4.34	6.56	14.12	12.83	8.13	6.63
H ₂ O	% mol	9.06	9.91	9.51	9.17	8.93	8.85
N ₂	% mol	74.11	75.05	66.56	67.55	71.19	72.34
O ₂	% mol	11.59	7.59	9.01	9.64	10.90	11.31
Ar	% mol	0.89	0.90	0.80	0.81	0.85	0.87

Table 4.6.- Power and thermal efficiencies for a CCGT power plant with PCC and strategies to increase exhaust gas CO₂ concentration.

		Air-based combustion (reference case)	EGR	S-EGR Parallel 97/96	S-EGR Series 95/32	S-EGR Series 90/48	S-EGR Series 85/58
Gas turbine net power x 2	MWe	286	282	288	281	274	271
Gas turbines net power	MWe	572	563	576	562	547	542
GT thermal efficiency	%	38.18	37.75	37.13	37.09	37.44	37.54
Steam turbine Power x 1	MWe	256	266	290	286	269	263
Gross power	MWe	827.6	828.9	866.0	848.5	815.9	805.3
Gross thermal efficiency	%	55.50	55.55	55.80	55.96	55.82	55.76
Air fan x 2	MWe	N/A	N/A	0.75	1.07	1.13	1.15
Booster fan x 2	MWe	7.31	4.67	2.06	7.01	7.01	7.00
Booster fan for exhaust gas recycling x 2	MWe	N/A	1.28	0.99	N/A	N/A	N/A
Pumps in Steam cycle x 1	MWe	7.46	7.77	8.54	8.43	7.88	7.71
Pumps in PCC x 2	MWe	0.75	0.70	0.69	0.78	0.79	0.79
DCC pumps x 2	MWe	0.37	0.85	0.88	0.43	0.38	0.37
Compression work x 2	MWe	12.91	12.83	13.38	12.96	12.50	12.35
Net power output	MWe	777.4	780.5	819.9	795.6	764.5	754.3
Net thermal efficiency	%	51.94	52.30	52.84	52.47	52.30	52.23
Heat input	MWth	748	746	776	758	731	722
Fuel LHV	kJ/kg	46938	46938	46938	46938	46938	46938
Fuel input	kg/s	15.95	15.90	16.53	16.15	15.57	15.39



S-EGR parallel: Recirculation ratio 70%, post-combustion capture efficiency 96%, selective CO₂ transfer eff. 97%.
 S-EGR series 95/32: post-combustion capture efficiency 58%, and selective CO₂ transfer efficiency 85%.
 S-EGR series 90/48: post-combustion capture efficiency 48%, and selective CO₂ transfer efficiency 90%.
 S-EGR series 85/58: post-combustion capture efficiency 31%, and selective CO₂ transfer efficiency 95%.

Figure 4.34.- CCGT net power output and net thermal efficiency variation with post-combustion carbon capture (PCC) and the operational strategies of conventional EGR, selective EGR in parallel and in series, compared to the reference case: air-based combustion CCGT with PCC.

Rotary Adsorption for Selective Exhaust Gas Recirculation

5.1. Introduction

The implications of adding Selective Exhaust Gas Recirculation (S-EGR) to combined cycle gas turbine (CCGT) power plants with post-combustion carbon capture (PCC), using chemical absorption technology with monoethanolamine aqueous solutions, are investigated in Chapter 4.

The systems for selective CO₂ transfer is modelled as a “grey-box” in process flow simulations conducted in Chapter 4 and is further investigated through a conceptual design in this chapter. The concept of “grey-box” in this work implies that inlet stream variables and operating parameters with a relatively large effect on the overall process are defined in the model. A flue gas stream from the cooling device and an air stream supplied by an air fan enter into the system where the CO₂ is selectively transferred. A CO₂-enriched air and a CO₂-depleted gas streams leave the system towards the gas turbine compressor and the gas/gas rotary heat exchangers, respectively, as illustrated in the process flow diagrams in Chapter 4. The selective CO₂ transfer efficiency, the pressure drop and the heat transfer flow rate, which results in a temperature rise in the air stream, are input parameters in the operation unit. The values of these parameters in Chapter 4 are based on results from simulations performed in the present chapter. Sensitivity analysis conducted in Chapter 4 take account of different operating conditions, so that results and discussion sections are valid for a range of CO₂ transfer technologies.

The operation and cost benefit of S-EGR on the PCC system need to be compared to the cost and operation of introducing an additional system for selective CO₂ transfer. S-EGR is further investigated in this chapter by performing a conceptual design assessment of technologies for the CO₂ transfer process.

The technology proposed for selective CO₂ transfer is physical adsorption in a rotary wheel configuration, as an alternative to selective CO₂ membrane systems investigated in literature (Merkel et al. 2013; Voleno et al. 2014; Swisher and Bhowan 2014; Zhang et al. 2016). The relatively weak interaction between the CO₂ and the adsorbent surface involved in physisorption allows regenerate the adsorbent with ambient air at near ambient temperature

and pressure and thus a selective CO₂ transfer from a flue gas stream into an air stream, relying on the CO₂ partial pressure difference. Moreover, structured adsorbents in a rotary wheel offer a relatively simple configuration to perform consecutive adsorption/desorption cycles with fast heat transfer rates and a favourable temperature distribution, since the solid material is simultaneously regenerated and cooled down in contact with air. Structure adsorbents result in low pressure drop, compared to conventional adsorption systems, e.g. packed columns, (Boulet and Khiavi 2015) and membrane systems. A low pressure drop is critical for S-EGR applications as Section 4.3.6 and Section 4.4.6, where 2 kPa pressure drop through the CO₂ transfer system results in a derating of 9 MW, corresponding to 3% of the gas turbine net power output.

Industrial applications of rotary adsorption are presented in Chapter 2, Section 2.5. Rotary adsorption is currently investigated at pilot plant scale for CO₂ capture (Inventys 2016) and rotary wheel equipment have been dimensioned, implemented and operated at large-scale industrial applications in heat exchange applications for large volume of flue gas typically generated in thermal power plans (Howden Group 2016).

The conceptual design of the selective CO₂ transfer system is based on mass transfer and thermal equilibrium performance. At the stage of concept development, an equilibrium model allows to understand the process, to investigate the solid properties and to establish the basis for a detailed design, out of the scope of this thesis. A detailed design requires mass transfer effects and kinetics to be considered, in order to optimise the height of the wheel, the flue gas residence time and the rotation speed. The conceptual design consists of two stages:

- A bottom-up approach is followed in the first step, in which best class commercially available adsorbents are considered to estimate the adsorbent mass requirements to size the rotary adsorber. The objective is to assess the technical/practical feasibility of applying rotary adsorption technology for S-EGR and identify the key parameters for the optimisation study in the second step. This is performed by evaluating the amount of solid material, the dimensions of the rotor adsorbent and the number of rotary wheels that would be necessary to achieve the CO₂ transfer efficiency indicated in the S-EGR configurations investigated in Chapter 4. In Section 5.2, the process and the parameters used in the conceptual design are described. Results from the first part of the conceptual design assessment are presented in Section 5.3. In order to fully understand the adsorption/desorption process in the rotary wheel, the profiles of the temperature, the adsorbate in the gas phase and the amount adsorbed in the solid are described in Section 5.4.

-
- The second step of the conceptual design assessment follows a top-down approach, starting with the size of a large rotary system to assess the material performance. An optimisation study is conducted with the objective of minimising the dimensions of the selective CO₂ transfer device. Materials properties and process parameters with a large effect on the inventory of solid material are:
 - the parameters of the isotherms modelling the adsorption equilibrium of each component in the flue gas mixture on the solid surface, and
 - the temperatures of the flue gas and the air entering the system.

A parametric analysis quantitatively provides the range of physical properties, namely adsorption saturation capacity, equilibrium constant and enthalpy of adsorption for the adsorbed components, resulting in minimum adsorbent mass requirements and practical rotary wheel dimensions.

The criterion of practicality for the dimensions of the rotary wheel system is based on an analogy with the rotary wheel applications for gas/gas heat exchangers. The dimensions of the largest heat exchangers manufactured, implemented and commissioned in the power generation sector are taken as the maximum practical size. The purpose of this second step is to provide guidelines for new materials development to match the criterion of practicality of rotary wheel systems.

5.2. Description of adsorption process and parameters used in conceptual design assessment

Carbon dioxide is selectively transferred from the flue gas into the combustion air as result of adsorption/desorption cycles. The adsorption/desorption process is performed with a rotary adsorbent periodically exposed to the flue gas and the ambient air streams, flowing in opposite directions, i.e. counter current flow. The contacting model between the gas/air and the solid is cross-flow. A schematic diagram of the rotor adsorber is illustrated in Chapter 3, Figure 3.17 and is reproduced in Figure 5.1 for convenience.

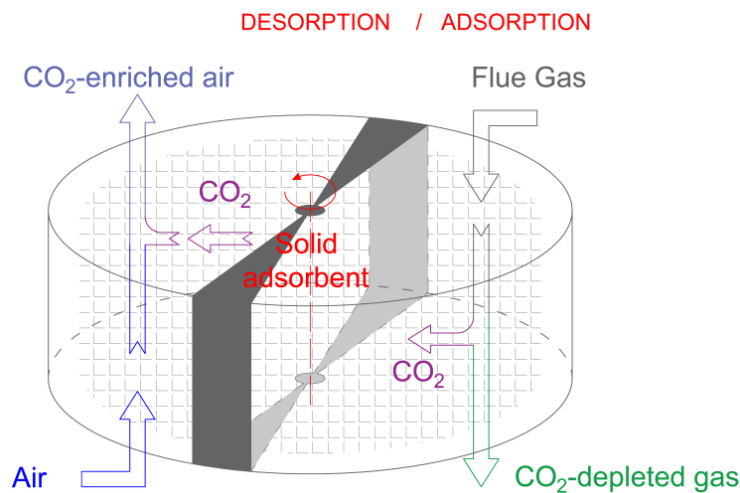

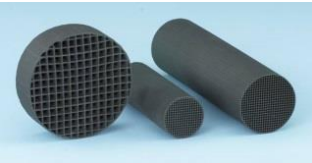
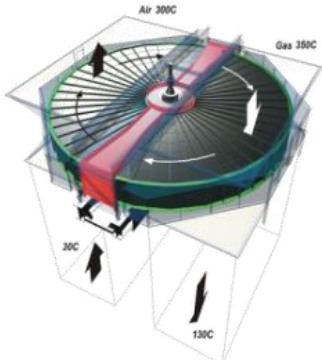


Figure 5.1.- Schematic diagram of the rotary adsorber for selective CO₂ transfer.

The conceptual design is based on the mass transfer and thermal equilibrium of the adsorption and the desorption processes. The mathematical model developed for this purpose is described in Chapter 3, Section 3.5. At the stage of concept development, the equilibrium model is used to understand the process and to investigate the effect of the equilibrium properties of the adsorbent material. It allows to evaluate the minimum solid material inventory for existing adsorbent materials and to provide guidelines for materials development. Limitations of the model are described in Section 5.5.

The first step of the conceptual design assessment is performed for commercially available adsorbents. Relevant properties to assess adsorbents are adsorption equilibrium isotherms for adsorbed components in the flue gas, i.e. carbon dioxide, nitrogen and oxygen, thermal, e.g. specific heat, and physical properties, e.g. density and porosity. This is further extended in Section 5.2.1. The arrangement of the adsorption in the rotary device requires knowledge of geometry parameters described in Section 5.2.2 and Section 5.2.3. The main parameters in the equilibrium model are summarized in Table 5.1

Table 5.1.- Material properties and structural parameters for rotary adsorption process modelling

<i>Adsorbent material</i>	<i>Adsorbent structure</i>	<i>Rotary wheel</i>
Extended Langmuir isotherm: <ul style="list-style-type: none"> • Saturation capacity, q_s • Heat of adsorption, $(-\Delta H_{ads})$ • Equilibrium constant, K_{eq} Solid density, ρ_s Particle density, ρ_p Particle porosity, ε_p Specific heat, C_p	Bulk density of adsorbent rotor, ρ_{bulk} Void fraction of adsorbent rotor, ε_{bulk} Open surface area	Angular/rotation speed (typ. 0.5 – 1.5 rpm) Dimensional parameters: <ul style="list-style-type: none"> • Diameter, D 24 m⁽¹⁾ • Length, L 2 m⁽¹⁾
		
Note 1: Dimensions of the largest rotary heat exchanger manufactured, implemented and operated by Howden (Hogg 2015)		

5.2.1. Adsorbent material

The selection of adsorbent materials for selective CO₂ transfer application is based on both, general criteria which apply to any CO₂ adsorption process from diluted sources and specific criteria for S-EGR application. An important aspect in this application is the regeneration of the solid with ambient air at near-ambient temperature and pressure, unlike in post-combustion CO₂ capture applications where a temperature or a pressure swing is used to regenerate the adsorbent capacity. The ideal adsorbent materials should therefore present: a large capacity for CO₂ adsorption for a CO₂ partial pressure ranging from 0.04 to 0.2 bar, a high selectivity of CO₂ over nitrogen and oxygen but moderate affinity for CO₂ allowing CO₂ desorption into air, low sensitivity to moisture for water concentrations up to 10 vol%, and large availability at relatively low cost.

Among all the solid materials proposed for CO₂ capture in the literature, activated carbon and Zeolite X13 are selected in the bottom-up approach of the conceptual design assessment. Both are commercially available, widely studied in the literature and represent, in this context, benchmark adsorption materials for this application.

Activated carbon is an inexpensive material widely available. Despite its relatively low CO₂ adsorption capacity, activated carbon has a hydrophobic character and its capacity for CO₂ adsorption is not affected by the presence of moisture.

Zeolite X13 is a well-known porous material with a high CO₂ adsorption capacity, compared to activated carbon. One of the main disadvantages for gas combustion applications is that adsorption capacity is greatly reduced in the presence of moisture, and that dehydration is required to reduce the water content down to 0.1 vol%, as discussed previously in Chapter 2.

For the purpose of the adsorption/desorption process modelling, the equilibrium adsorption isotherms for CO₂, N₂ and O₂ in the flue gas on each adsorbent as well as the thermal and physical properties of the solid material are used. A large amount of experimental work is available in literature providing adsorption equilibrium data for each component on activated carbon and Zeolite X13, fitted to different adsorption models (Xiao et al. 2008; Dantas et al. 2011; Dantas et al. 2011a; Delgado et al. 2011; Xu et al. 2013). The dual-site Langmuir model is proposed for Zeolite X13 by Xiao and co-workers (Xiao et al. 2008) and the Toth model is proposed for Activated Carbon by Dantas and co-workers (Dantas et al. 2011).

The rotary adsorber model developed in this work uses the single-site Langmuir isotherm extended to a multicomponent gas mixture. The Langmuir model is based on the following assumptions: (1) adsorption takes place at specific localised sites on the solid surface and the saturation coverage corresponds to complete occupancy of the sites. This implies that the maximum adsorption capacity correspond to a monolayer. (2) The differential energy of adsorption is independent of surface coverage. This implies that the surface containing the active sites for adsorption is homogeneous and there is the same probability of adsorption on all sites. The probability of adsorption on an empty site is independent on whether or not an adjacent site is occupied, as there is not interaction between adsorbent molecules on adjacent sites (Ruthven 1984). Despite its idealistic simplicity, the Extended Langmuir model remains as a useful model in the study and design of novel adsorption systems. The reduced number of parameters accelerates the convergence and simplifies the parametric analysis conducted in Section 5.5.

The Extended Langmuir (EL) model to CO₂, N₂ and O₂ adsorption is mathematically expressed in Equation [5.1], where q_i^* is the adsorbed amount of component i at a partial pressure P_i^* in the gas mixture, q_s the maximum adsorbed concentration or the adsorbed saturation capacity and K_L is the equilibrium constant, related to the enthalpy change of the process and the affinity of gas molecules to the adsorption sites. The dependence of K_L on the temperature is described according to the Van't Hoff equation, as shown in Equation

[5.2], where $(-\Delta H_{ads})$ is the enthalpy of adsorption and K_{L0} the pre-exponential factor. For the thermodynamic consistence of Equation [5.1], the adsorbed saturation capacity q_s must be the same for all the components: CO_2 , N_2 and O_2 (Bai and Yang 2001).

The parameters of the Extended Langmuir model for Zeolite X13 and activated carbon are calculated in this work for a range of partial pressures including values expected in this application, i.e. 0.1 – 100 kPa. The adsorbed amount of each component predicted by the Extended Langmuir (EL) model in this work and the equilibrium data in literature reported by Xiao et al. (2008) and Dantas et al. (2011) are in a good agreement. The deviation is based on the average percentage deviation (ARD%), defined in Equation [5.3], where N_t is the number of data points (Bai and Yang 2001).

$$q_i^* = \frac{q_s \cdot K_{L,i} \cdot P_i^*}{1 + \sum_{j=1}^C K_{L,j} \cdot P_j^*} \quad i, j = CO_2, N_2, O_2 \quad [5.1]$$

$$K_{L,i} = K_{L0,i} \exp\left(\frac{-\Delta H_{ads,i}}{RT}\right) \quad i = CO_2, N_2 \quad [5.2]$$

$$ARD\% = \frac{1}{N_t} \sum_{i=1}^{N_t} \frac{|q_{i,EL} - q_{i,literature}|}{q_{i,literature}} 100 \quad [5.3]$$

For each solid, the properties and the parameters of the extended Langmuir isotherm are presented in Table 5.2. Zeolite X13 presents a higher CO_2 adsorption saturation capacity and a higher equilibrium constant for CO_2 compared to activated carbon, and also higher compared to the equilibrium constant for N_2 and O_2 . This indicate that Zeolite X13 present more affinity and selectivity for CO_2 than activated carbon.

Table 5.2.- Properties of the solids and Extended Langmuir equation parameters

Solid	Fitted to exp. data from:	Activated Carbon		Zeolite X13		
		Dantas et al. 2011		Xiao et al. 2008		
Solid density	kg m ⁻³	2147		1950		
Particle density	kg m ⁻³	1138		1229		
Particle porosity	m ³ m ⁻³	0.47		0.37		
Specific heat	J kg ⁻¹ K ⁻¹	1050		920		
<i>Extended Langmuir model parameters</i> ^[1]						
		CO₂	N₂	CO₂	N₂	O₂
Saturation capacity, q_s	mol kg ⁻¹	3.084	3.084	4.07	4.07	4.07
Pre-exponential factor, $K_{LD} * 10^{-6}$	1/kPa	2.261	2.508	0.1723	1.105	6.270
Heat of adsorption, $(-\Delta H_{ADS})$	kJ/mol	21.981	15.742	33.387	14.604	1.312
Equilibrium constant, K_L at 25 °C	1/kPa	5.42E-02	3.44E-03	7.74E-01	8.98E-04	1.14E-05
Pressure range	kPa	0.1 - 20	0.1 - 80	0.1 - 20	0.1 - 80	0.1 - 20
RSQ ^[2]	--	0.99	0.98	0.99	0.99	0.99
ARD% ^[3]	%	0.43	1.49	2.59	0.90	0.74

[1] Extended Langmuir model to multicomponent adsorption recalculated for thermodynamic consistency
[2] RSQ: r-squared value or the coefficient of determination or coefficient of multiple determination for multiple regression
[3] ARD%: Averaged relative deviation

5.2.2. Adsorbent structure

For rotary adsorption wheels, the adsorbent is arranged into a monolithic honeycomb structure contained in the rotor, similarly to the pairs of specially formed plates that constitute the heating elements in rotary gas/gas heat exchanger technology described in Chapter 2, Section 2.6. Structured adsorbents results in low pressure drop and small booster fan power consumption, which is important for S-EGR applications.

Monolithic structures consist of parallel channels separated by thin walls, characterised by a high void fraction to provide a large surface contact area and low pressure drop. The void fraction is an important parameter to evaluate the volume of the monolithic rotor adsorbent, as described in Chapter 3, Section 3.5. The bulk void fraction depends on geometric parameters, e.g. diameter of the channels and wall thickness, and its optimal value generally results from a trade-off to maximise surface contact area and minimise pressure drop, while providing high resistance to erosion and avoiding obstruction by particular matter. Since the later aspects are not significant for flue gas from natural gas-firing, a value of 0.78 is considered for bulk void fraction based on rotary adsorption application for air dehumidification (Yamauchi et al. 2007).

5.2.3. Rotary wheel

The number of rotary devices required to contain the adsorbent inventory is calculated considering the dimensions of the largest regenerative rotary gas/gas heat exchangers manufactured, implemented and commissioned in thermal power generation. The dimensions of the rotor containing the heating elements are approximately 24 m diameter and 2 m length, with an effective cross section factor of 0.89 (Hogg 2015). The largest weight of the rotating baskets containing heating metal elements is approximately 1000 kg. Due to the considerably smaller density of the adsorbent material, e.g. typically around 1200 kg/m^3 , compared to steel, e.g. typically around 8000 kg/m^3 , larger dimensions for the rotor might be possible and a structural analysis would have to be conducted.

In detailed design, the length and the diameter should be optimised to provide enough residence time for the flue gas for the smaller possible pressure drop. For this purpose mass transfer limitation and diffusion in the porous structure need to be considered.

5.3. Conceptual design assessment

The conceptual design assessment is conducted for the three configurations of the CCGT power plant with PCC and S-EGR considered in Chapter 4, where the effects of selectively recycling CO_2 on both the power plant and the PCC system were investigated. The operating conditions in terms of efficiencies for each configuration are described below:

- Parallel S-EGR (97/96) at 70% recirculation ratio, with 97% selective CO_2 transfer efficiency and 96% post-combustion CO_2 capture efficiency.
- Series S-EGR (95/31) with 95% selective CO_2 transfer efficiency and 31% post-combustion CO_2 capture efficiency.
- Series S-EGR (90/46) with 90% selective CO_2 transfer efficiency and 46% post-combustion CO_2 capture efficiency.

The CO_2 concentration, mass flow rate and temperature of the flue gas and the air streams are important operation parameters to be defined. The boundaries of the system are described in Section 5.3.1.

In the bottom-up approach followed in the first step of the conceptual design, the adsorbents described in Section 5.2.1 are considered for the purpose of sizing the rotary wheel for selective CO_2 transfer for the three configurations, and results are discussed in Section 5.3.2.

5.3.1. Boundaries within the CCGT power plant and the PCC system integrated model

The air is supplied to the selective CO₂ transfer device by an air fan to overcome the pressure drop along the air pathway upstream of the gas turbine. The rise in pressure implies an increase in the air temperature above the ambient conditions, i.e. 15 °C ISO. An important consideration is that the air mass flow rate is limited by the maximum amount of air swallowed by the compressor for a fixed geometry, as explained in Chapter 4.

The flue gas is cooled down to 30 °C, the lowest temperature achievable with the cooling system proposed for the main power plant. A low flue gas temperature enhances the adsorbent equilibrium capacity and reduces the amount of heat transferred into the air stream. It results in a lower temperature of the CO₂-enriched air entering the compressor, preventing derating the gas turbine, as explained in Chapter 4. The CO₂ concentration and the water vapour content in the flue gas vary with the temperature at the outlet of the cooling system as explained below.

5.3.1.1. S-EGR in parallel

In the parallel configuration, the fraction of the flue gas that is diverted immediately after the gas/gas rotary heat exchanger is further cooled down in a direct contact cooler. Figure 5.2 shows the sensitivity to the cooling temperature of the CO₂ concentration, the water vapour content and the mass flow rate of the flue gas stream entering the selective CO₂ transfer device. For a cooling temperature below the dew point, approximately 45 °C for the water content at the HRSG outlet, the excess of humidity in the flue gas condenses and the condensed water is drained out of the system. At a lower temperature the adsorption process is thermodynamically favoured. The CO₂ concentration slightly increases as result of water condensation, marginally increasing the driving force for mass transfer.

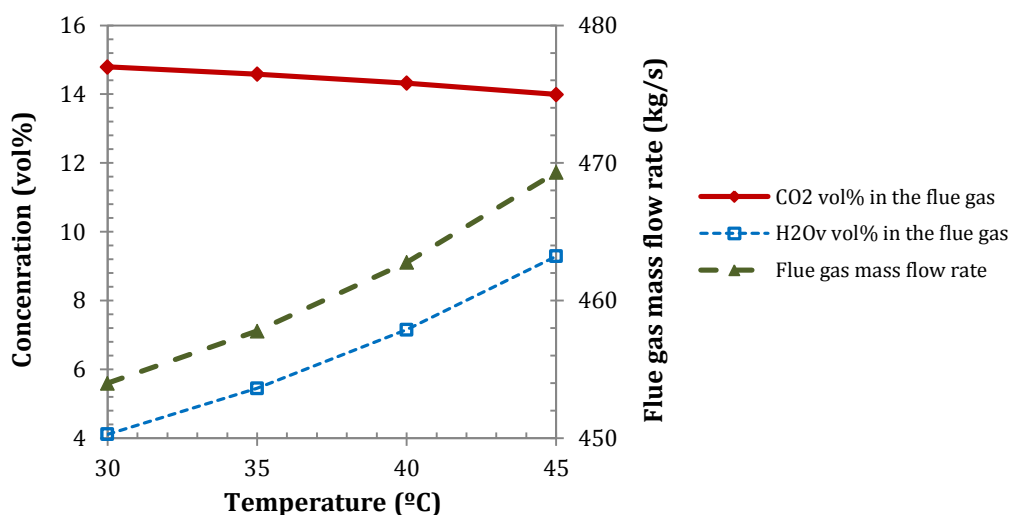


Figure 5.2.- Sensitivity to temperature of CO₂ and water vapour concentrations and mass flow rate of the flue gas stream prior to CO₂ transfer. Configuration S-EGR in parallel at 70% recirculation ratio, 97% selective CO₂ transfer efficiency and 96% post-combustion CO₂ capture efficiency.

5.3.1.2. *S-EGR in series*

In the series configuration, the partially CO₂-depleted flue gas stream leaving the absorber is cooled, either in the water wash section at the top of the absorber column or in a dedicated direct contact cooler, to a lower temperature than the temperature of the saturated flue gas entering the absorber, set at 45 °C. The condensed water is drained out of the system. Figure 5.3 shows the sensitivity to the cooling temperature of the CO₂ concentration, the water content and the mass flow rate of the flue gas stream entering the selective CO₂ transfer device for the two configurations corresponding to 90% and 95% selective CO₂ transfer efficiencies. As the CO₂ is partially removed in the PCC unit, the CO₂ concentration is smaller than in the configuration in parallel, and it decreases with decreasing selective CO₂ transfer efficiency, since the absorber operates at high post-combustion CO₂ capture efficiency to maintain 90% overall CO₂ capture ratio, as discussed in Chapter 4.

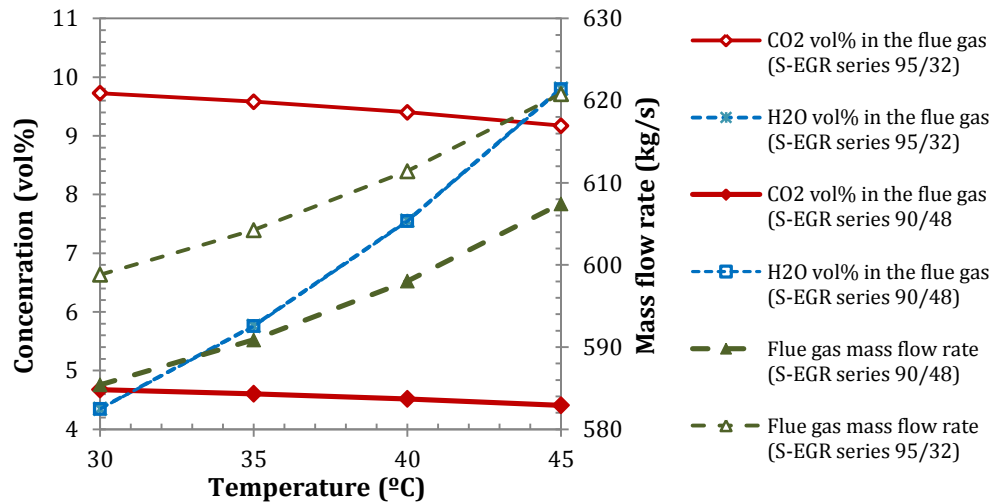


Figure 5.3.- Sensitivity to temperature of CO₂ and water vapour concentrations and mass flow rate of the inlet flue gas stream prior to CO₂ transfer. Configuration S-EGR in parallel at 70% recirculation ratio, 97% selective CO₂ transfer efficiency and 96% post-combustion CO₂ capture efficiency.

In both configurations, by cooling the flue gas to 30 °C in the direct contact cooler, the water content is significantly reduced from 9-10 vol% to 4.5 vol%, allowing the use of adsorbents with certain hydrophobic character. With zeolites and other polar solvent, the water content needs to be further reduce below 0.1 vol%. This is possible at the expense of introducing an additional systems for flue gas dehydration (Hasan et al. 2012).

5.3.2. Estimations of adsorption design parameters

The parameters evaluated to assess the technical and practical feasibility are as follows: the minimum amount of adsorbent necessary to achieve the required CO₂ transfer efficiency specified for each configuration; the volume of the rotor for a bulk void fraction of 0.78; and the number of rotary wheel devices, considering as reference the dimensions of the largest size rotary gas/gas heat exchanger manufactured and implemented, i.e. 24 m diameter and 2 m length. A preliminary sizing of the S-EGR wheel is presented in Table 5.3

The amount of solid material increases by around 100% with activated carbon compared to Zeolite X13, for the parallel S-EGR (97/96) and the series S-EGR (95/31) configurations where the flue gas CO₂ concentration is approximately 14.8 vol% and 9.7 vol% respectively. At a lower flue gas CO₂ concentration of approximately 5.7 vol% in the S-EGR in series (90/46), the increase in the amount of solid material is around 200% higher with activated carbon compared to Zeolite X13. This indicates the large effect of the equilibrium adsorption isotherm in the equilibrium model.

Comparing the two configurations with S-EGR in series, a significantly larger amount of solid is required to achieve 95% CO₂ transfer efficiency in the former configuration than to achieve 90% CO₂ transfer efficiency, despite the higher flue gas CO₂ concentration in the series S-EGR (95/31) configuration of around 9.7 vol%, compared to 5.7 vol% in the series S-EGR (90/46) configuration. This indicates that, at higher CO₂ transfer efficiencies, a significant increase in the amount of solid material is required to gain a marginal increase in the efficiency.

One rotary device would be necessary for the parallel S-EGR (97/96) and the series S-EGR (90/48) configurations using Zeolite X13. Larger dimensions of the rotary wheel might however be possible with appropriate structural analysis, since the adsorbent rotor weight is much smaller than the weight of the rotating baskets containing the steel elements in gas/gas heater applications.

The equilibrium isotherms describing the CO₂ adsorption on the adsorbent is the key aspect to evaluate the amount of solid material. Prior to the investigation of the mass transfer resistance and the diffusion it appears necessary to develop new materials with increased capacity in order to significantly reduce the amount of solid required.

The rotary adsorbent process designed for the parallel S-EGR (97/96) with activated carbon is considered as the base case to perform an optimisation study. A parametric analysis is performed in Section 5.4 with the objective of quantitatively identify the optimal range of values for the parameters of the Langmuir adsorption model: adsorbed saturation capacity, pre-exponential factor of the equilibrium constant and enthalpy of adsorption, to minimise the inventory of solid.

The ratio of air to gas mass flow rate is also an important parameter. For a given amount of CO₂ to be desorbed, the CO₂ gets more diluted for a higher air mass flow rate, increasing the driving force for mass transfer for solvent regeneration. It has to be noted that the largest air mass flow rate that can be used is limited by the maximum amount of air swallowed by the gas turbine for a fully opened position of the inlet guide vanes in the compressor. The air to gas mass ratio is greater in the parallel configuration, where a fraction of the flue gas passes through the selective CO₂ transfer device, than in the series configuration.

Table 5.3.- Adsorbent requirements and preliminary dimensions of the rotary adsorber

<i>Configuration</i>		S-EGR Parallel 97/96		S-EGR Series 95/31		S-EGR Series 90/48	
Recirculation ratio	%	70		N/A		N/A	
Selective CO ₂ transfer efficiency	%	97		95		90	
PCC efficiency	%	96		31		48	
CO ₂ conc. in flue gas	vol%	14.79		9.73		4.67	
Air/Gas mass flow ratio	--	1.12		0.91		1.00	
<i>Solid</i>		Zeolite X13	Activated Carbon	Zeolite X13	Activated Carbon	Zeolite X13	Activated Carbon
Mass x 1000	kg	191	326	507	959	140	388
Volume	m ³	156	287	413	843	114	341
<i>Rotary adsorber</i>							
Bulk void fraction	m ³ / m ³	0.78	0.78	0.78	0.78	0.78	0.78
Bulk density	kg/ m ³	270	250	270	250	270	250
Rotor volume	m ³	708	1303	1877	3831	517	1549
<i>Rotary wheel</i>							
Diameter	m	24	24	24	24	24	24
Length	m	2	2	2	2	2	2
Total rotor area	m ²	452	452	452	452	452	452
Active rotor area	m ²	403	403	403	403	403	403
Wheel volume	m ³	806	806	806	806	806	806
No. of rotary wheels (theoretically)		0.88	1.62	2.33	4.75	0.64	1.92
No. of devices		1	2	3	5	1	2

5.4. Performance and operating profiles

In order to gain a better understanding of the adsorption/desorption process in a rotary adsorbent configuration, the following profiles are represented:

- The CO₂ partial pressure and the temperature profiles in the flue gas and the air as a function of the height/length of the rotor are represented at different longitudinal sections (vertical slides), as illustrated in Figure 5.5 and Figure 5.6.
- The CO₂ adsorbed and the temperature profiles in the adsorbent as a function of the residence time are represented at different cross sections (horizontal slides), as illustrated in Figure 5.7 and
- Figure 5.8. The total residence time of the solid is considered here as the period of an adsorption/desorption cycle and is inversely proportional to the rotation speed.

The profiles are obtained for the operational conditions corresponding to the configuration of S-EGR in parallel using activated carbon (Dantas et al. 2011). The profiles present the same tendency for the configuration of S-EGR in series and for Zeolite X13.

Figure 5.4(a) illustrates the longitudinal sections or vertical slides representing the profiles of the flue gas and the air. Figure 5.4(b) illustrates the cross sections or horizontal slides representing the profiles of a volume of adsorbent contained in the rotor of the wheel. The flue gas/air composition, pressure and temperature, as well as the adsorbent loading, properties and temperature are assumed to be constant along the radial direction.

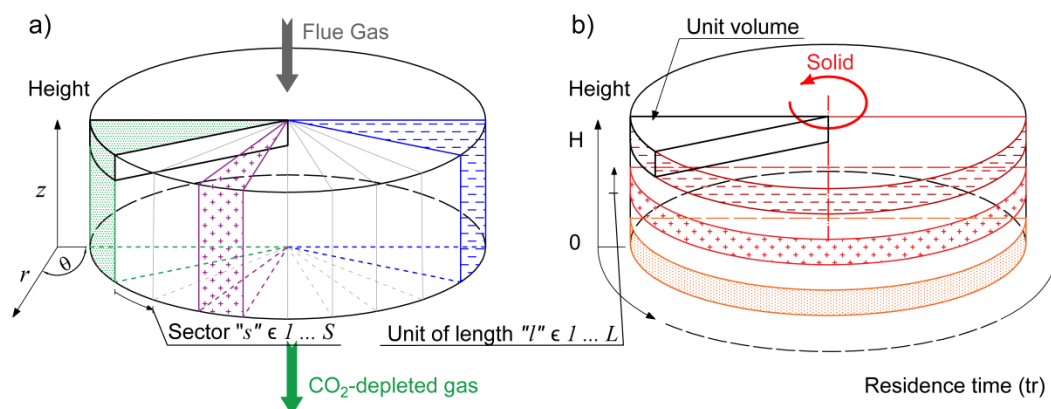


Figure 5.4.- (a) Longitudinal sections (vertical slices) representing the flue gas and air profiles and (b) horizontal slices representing the profiles of the adsorbent contained in the rotor.

5.4.1. Flue gas and air: CO₂ concentration and temperature profiles

The CO₂ adsorption rate is proportional to the difference between the CO₂ partial pressure in the gas phase, either in the flue gas (adsorption side) or in the air (desorption side), and the CO₂ partial pressure in equilibrium with the CO₂ adsorbed on the adsorbent. The highest values of the CO₂ adsorption rate correspond to the largest CO₂ partial pressure gradient in the profiles illustrated in Figure 5.5.

The CO₂ partial pressure rapidly decreases when the flue gas enters into contact with the fresh solid coming from the regeneration side, as it is shown in the profiles along the first longitudinal section (green line) in Figure 5.5(a). The closest unit volume of adsorbent to the flue gas inlet, i.e. top end of the rotor, gets rapidly saturated and the saturation front moves horizontally as the adsorber rotates. The maximum CO₂ partial pressure gradient in the gas moves then towards the flue gas outlet, i.e. the bottom end of the rotor, as shown in the CO₂ partial pressure profile along the last longitudinal section (blue line) in Figure 5.5(a). The partial pressure gradient corresponds to the ratio of the marginal change of partial pressure of

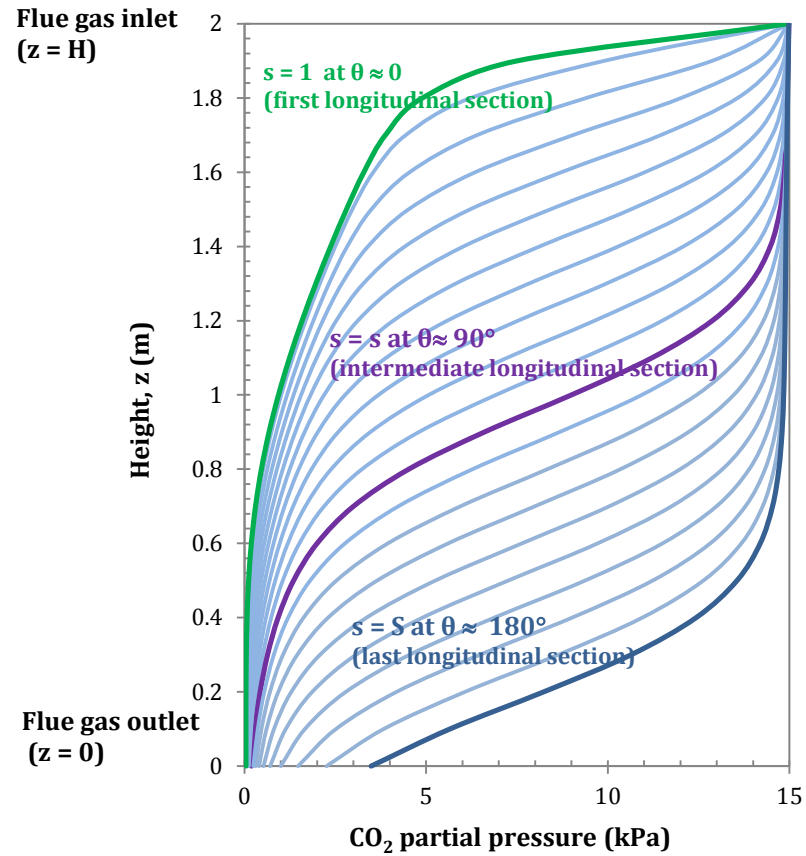
CO₂ for a given change of adsorbent height (Δz) as indicated in Equation [5.4]. In Figure 5.5(a), this corresponds – counter intuitively - to nearly horizontal sections of the lines. For example, there is a steep partial pressure gradient when the flue gas enters at the top of the rotor and the partial pressure is reduced from 15 kPa to nearly 0.5 kPa from a height of 2 m to 1.8 m, as the flue gas flows from top to bottom.

Similarly, the CO₂ partial pressure in the air increases rapidly when the air enters into contact with solid containing a large amount of CO₂ adsorbed (first longitudinal section, green line). The CO₂ partial pressure gradient becomes less steep and gradually occurs closer to the air outlet as the adsorbent rotates (last longitudinal section, blue line), as shown in Figure 5.5(b).

$$\frac{\partial P_{CO_2}}{\partial z} = \frac{P_{CO_2,z+1} - P_{CO_2,z}}{\Delta z} \quad z = 0 \dots H \quad [5.4]$$

The flue gas temperature profile shows a temperature drop when the flue gas enters into contact with the regenerated adsorbent, as it is cooled down by the ambient air in the regeneration section. A temperature bulge occurs at the locations where the CO₂ adsorption rate reach maximum, as shown in Figure 5.6(a). The air enters at a temperature slightly higher than 15 °C (ISO), due to the temperature rise in the air fan, and the temperature increases as result of the sensible heat transfer from the solid into the air and the endothermic effect of CO₂ desorption. The solid acts as heat storage medium transferring heat from the flue gas into the air stream. The temperature profiles for the flue gas and the air are shown in Figure 5.6(b). The implications of the higher temperature of the CO₂ enriched air, compared to ambient temperature, entering the gas turbine on the power plant performance are discussed in Chapter 4.

(a) ADSORPTION



(b) DESORPTION

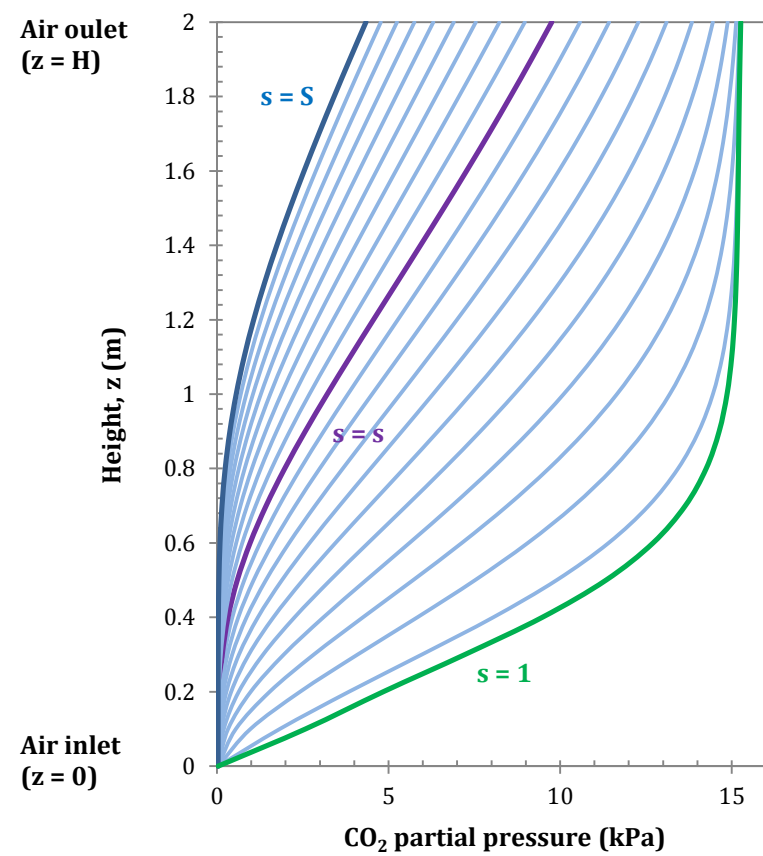
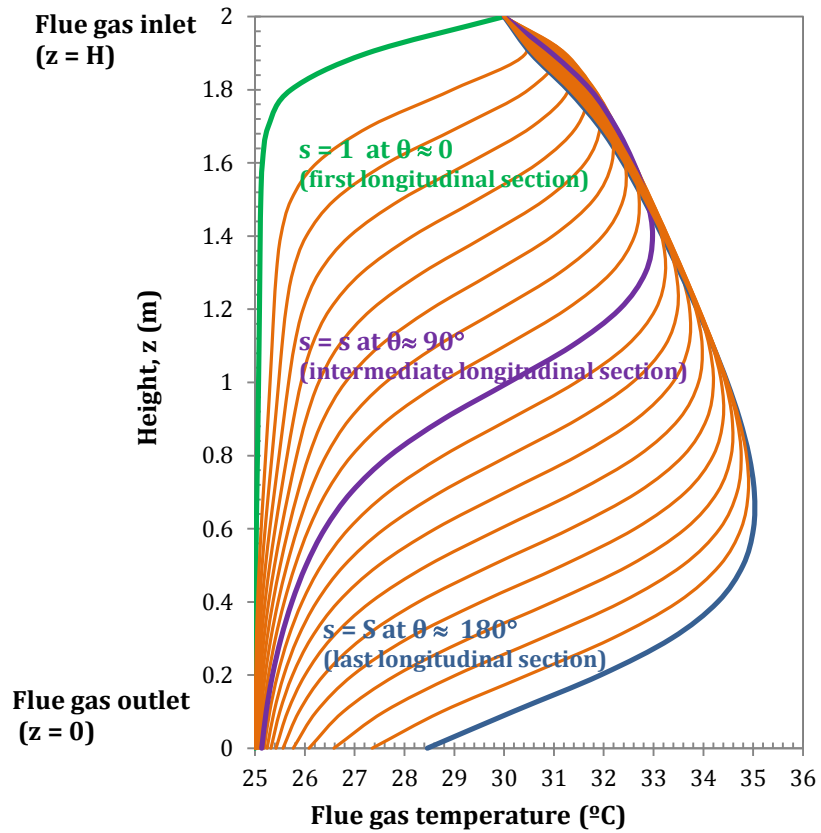


Figure 5.5.- CO_2 partial pressure profiles of (a) the flue gas (adsorption) and (b) the air (desorption) in longitudinal direction for each vertical slide. Configuration: S-EGR in parallel at 70% recirculation ratio. Adsorbent: Activated Carbon

(a) ADSORPTION



(b) DESORPTION

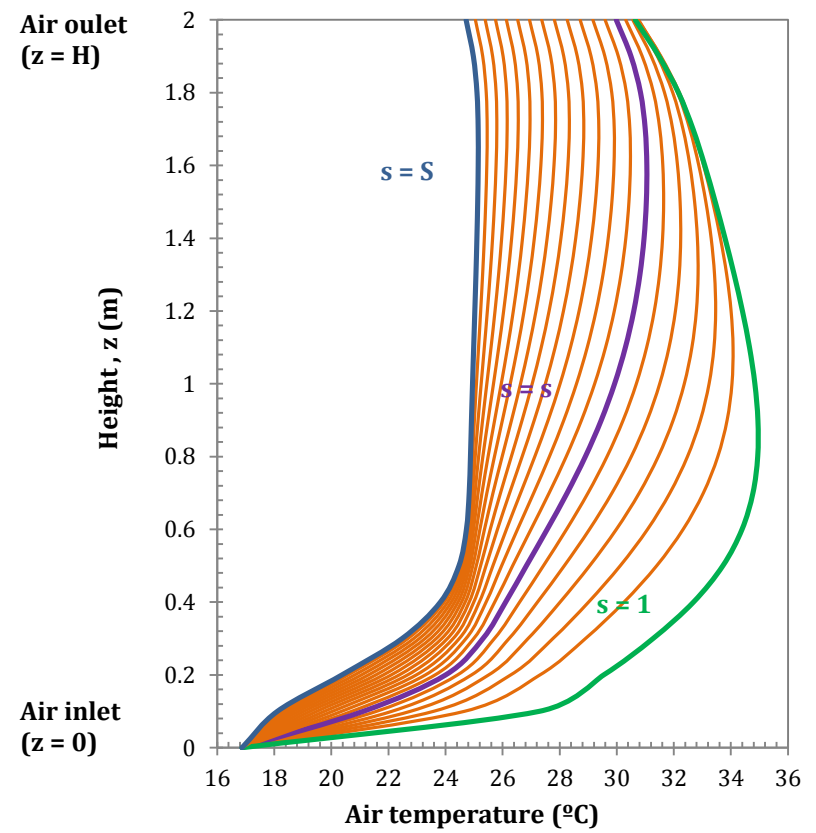


Figure 5.6.- Temperature profiles of (a) the flue gas (adsorption) and (b) the air (desorption) in longitudinal direction for each vertical slide. Configuration: S-EGR in parallel at 70% recirculation ratio. Adsorbent: Activated Carbon

5.4.2. Adsorbent: CO₂ adsorbed and temperature profiles

The amount of CO₂ adsorbed by the solid increases as the solid inventory contained in a given unit of volume rotates around the vertical axis, as illustrated in Figure 5.1 and enters into contact with flue gas with an increasingly high CO₂ partial pressure. The closed unit volume of solid to the flue gas inlet (top cross section, $l=L$) are fully loaded due to the larger driving force for CO₂ mass transfer, while the adsorbent located in the unit volumes closer to the flue gas outlet (bottom cross section, $l=1$) are partially loaded at the end of the adsorption period, i.e. a half rotation of 30 s for 1 rpm rotation speed, due to the high CO₂ transfer efficiency of 97% required in the parallel S-EGR configuration. This is illustrated in Figure 5.7(a).

The adsorbent enters then the regeneration section and the CO₂ desorbs into the air. The CO₂ desorbs rapidly from the adsorber sites closer to the air inlet (bottom cross section, $l=1$), this is where the driving force is the highest. As the air gets enriched in CO₂, the driving force and the rate of desorption decrease. Figure 5.7(b) shows that the adsorbent is not fully regenerated at end of the cycle, e.g. 60 s for 1 rpm rotational speed, and enters again the adsorption section partially loaded. The solid working cycle capacity is defined as difference between the amount of CO₂ adsorbed on the solid at the beginning ($t = 0$) and at the end ($t = t_{1/2}$) of the adsorption process, according to Equation [5.5], where $t_{1/2}$ is half of the time of the adsorption/desorption cycle and L is the number of equilibrium stages in the longitudinal direction. The working cycle capacity is illustrated in Figure 5.9 along the longitudinal direction.

$$\text{Working cycle capacity} = \sum_{l=1}^L q_{CO_2, t=0} - \sum_{l=1}^L q_{CO_2, t=t_{1/2}}; \text{ for } l = 1 \dots L \quad [5.5]$$

The solid temperature profiles during the adsorption-desorption cycle are illustrated in

Figure 5.8. In the adsorption section, the adsorbent temperature increases due to the heat of adsorption released as the CO₂ is adsorbed and the sensible heat transferred from the flue gas at a higher temperature. The highest temperatures are reached in the solid locations with higher rates of CO₂ adsorption. In the regeneration section, the solid temperature decreases due to the endothermic effect of CO₂ desorption and sensible heat transferred from the solid to the air. This constitutes an advantage compared to fixed beds, where a rapid increase in temperature of the adsorption front occurs and the adsorption capacity decreases.

The duration of the adsorption/desorption cycle obviously depends on the rotation speed. A rotation speed of 1 rpm is assumed based on typical values for rotary gas/gas heat exchangers of similar sizes comprised within a range of 0.6 to 1 rpm (Howden 2008). Interestingly, the optimum rotation speed depends on both capacity and kinetics. It defines the rate of solid supplied and is equivalent to the solvent flow rate in an amine process. One could define an equivalent metric to the L/G ratio of an absorber.

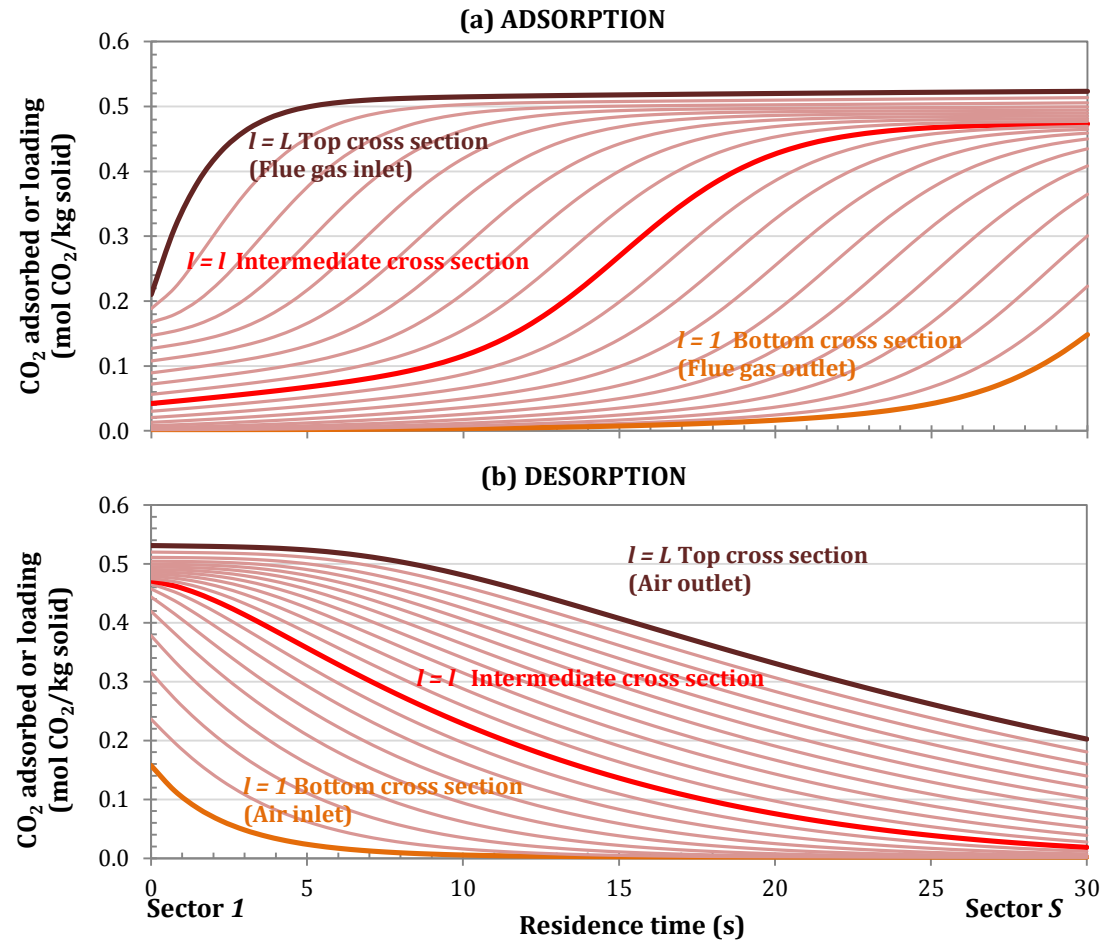


Figure 5.7.- CO₂ adsorbed profile for adsorption (a) and desorption (b) for several cross sections (horizontal slides). Rotation speed of 1 rpm. Configuration: parallel S-EGR at 70% recirculation ratio. Adsorbent: Activated Carbon

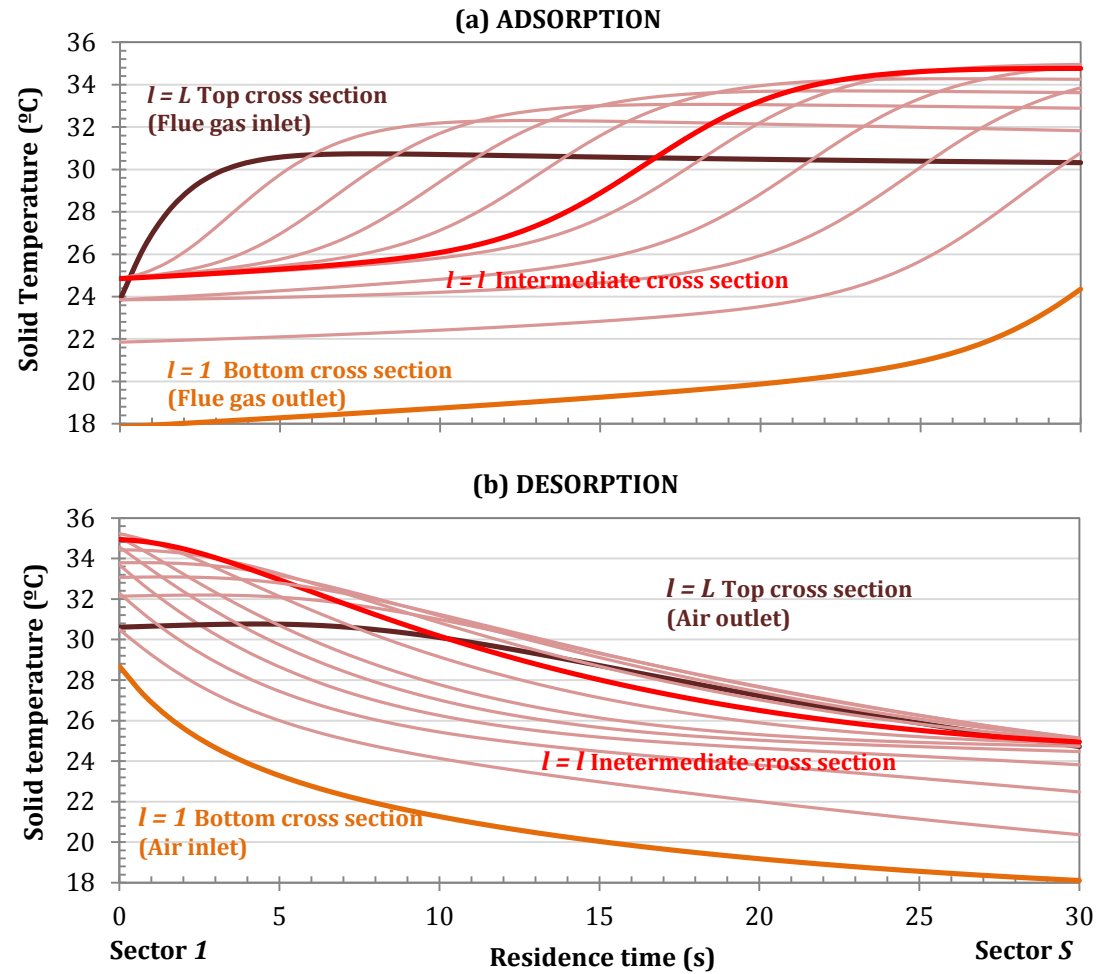


Figure 5.8.- Solid temperature profile in adsorption (a) and desorption (b) for several cross sections (horizontal slides). Rotation speed of 1 rpm. Configuration: parallel S-EGR at 70% recirculation ratio. Adsorbent: Activated Carbon

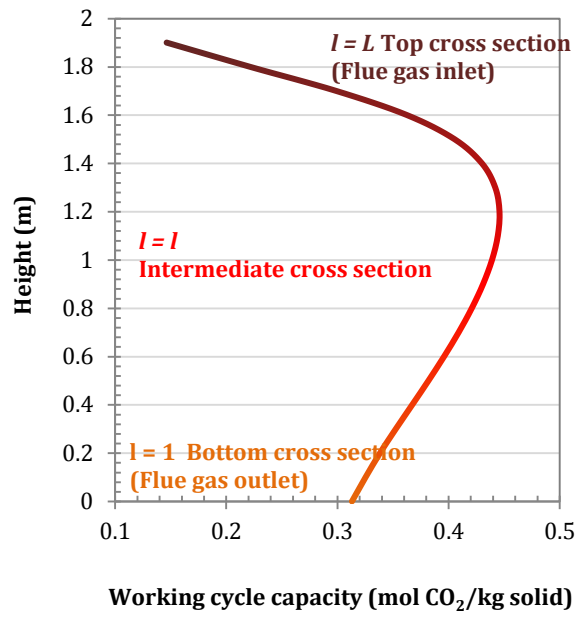


Figure 5.9.- Working cycle capacity of the adsorbent along the longitudinal direction. Configuration: parallel S-EGR at 70% recirculation ratio. Adsorbent: Activated Carbon

5.5. Feasibility and discussion

An optimisation study of the reference case, i.e. S-EGR system with activated carbon for the S-EGR in parallel configuration, operating at 70% recirculation ratio, 97% selective CO₂ transfer efficiency and 96% PCC efficiency, presented in the previous sections is conducted in this section.

The optimisation has the objective of minimising the dimensions of the selective CO₂ transfer device, so that the operational and cost benefits of adding S-EGR to the CCGT power plant with PCC outweigh the additional cost of introducing new equipment in the plant. The first step in reducing the overall dimensions of the rotary wheel is minimising the amount of solid material in the rotary adsorption process, which strongly depends on the adsorption equilibrium model and the flue gas and the air inlet temperatures.

The parametric analysis performed in Section 5.5.1 presents the objective of quantitatively identifying the optimal range of values for the parameters of the Langmuir adsorption model: adsorbent saturation capacity, pre-exponential factor of the equilibrium constant and enthalpy of adsorption, for minimum solid inventory. It is assumed that the adsorbed saturation capacity (physical property) and the adsorption equilibrium (thermodynamic property) vary independently since the homogeneity of the surface and the probability of adsorption of the adsorbent molecules on the solid surface is independent of the surface coverage.

For a given adsorbent material, the adsorption equilibrium depends on the temperature. It is more pronounced for class of adsorbents with high enthalpy of adsorption. A sensitivity analysis of the amount of solid required for the flue gas and the air temperatures is performed in Section 5.5.2, for a reference configuration with S-EGR in parallel and with activated carbon as the adsorbent of the rotary adsorption wheel used for CO₂ transfer. The objective is to investigate the effect of a higher temperature of the flue gas leaving the cooling system and the possible trade-offs between carrying out the adsorbent regeneration at a higher temperature and feeding a hotter stream to the inlet of the gas turbine compressor.

5.5.1. Sensitivity analysis to the solid properties

5.5.1.1 Saturation capacity

An increase in the adsorbed saturation capacity results in a smaller amount of solid to achieve a 97% CO₂ transfer efficiency in the configuration of S-EGR in parallel, as shown in Figure 5.10. The asymptotic behaviour beyond 10 mol/kg indicates that a further increase of 1 mol/kg in saturation capacity results in a reduction of less than 5% in the adsorbent mass requirements. In physical adsorption described by the Langmuir model, an increase in the adsorbent saturation capacity is related to a larger number of active sites on the adsorbent surface. Adsorbed saturation capacities of zeolites are typically in the range of 3 and 5 mol/kg. Larger values closer to 10 mol/kg are presented for some Metal-organic-frameworks (Mangano et al. 2013; Abanades et al. 2015).

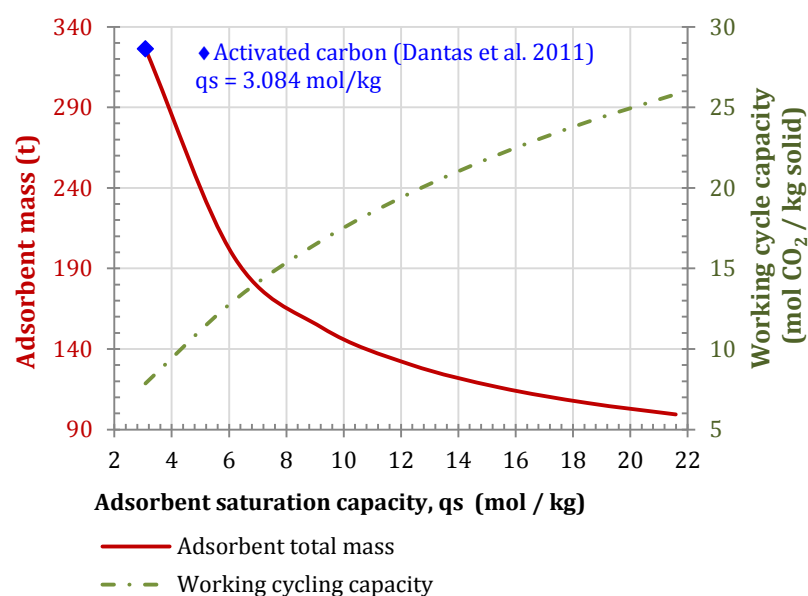


Figure 5.10.- Sensitivity of adsorbent mass and working cycle capacity to the adsorbed saturation capacity. Configuration parallel S-EGR at 70% recirculation ratio, 97% selective CO₂ transfer efficiency and 96% post-combustion CO₂ capture efficiency.

5.5.1.2 Equilibrium constant and enthalpy of adsorption

The parametric analysis of the adsorbent total mass to the pre-exponential factor of the equilibrium constant and the enthalpy of adsorption for CO₂ is illustrated in Figure 5.11, for three adsorbed saturation capacities of 3, 6.2 and 13.3 mol_{CO₂}/kg_{solid}. Both are varied within the typical range of activated carbon materials and zeolites. Results indicate that, for a given saturation capacity, there is a unique combination of enthalpy of adsorption and pre-exponential factor of the equilibrium constant which result in an optimum value. The equilibrium constant is an indicative parameter of the affinity of the adsorbent for the

adsorbate. A large value, due to either a large pre-exponential factor or large enthalpy of adsorption, as shown in Equation [5.2], indicates a strong affinity of the adsorbent for CO₂ molecules. This favours CO₂ adsorption but is detrimental for CO₂ desorption, resulting in a reduction of the working cycling capacity and an increase in the amount of solid required to achieve certain CO₂ transfer efficiency. This is illustrated in the top-right corner of the surface/contours plot in Figure 5.12. On the other side, a small equilibrium constant is detrimental for CO₂ adsorption, as illustrated in the bottom-left corner of surface/contours plot in Figure 5.12.

According to results in Section 5.3.2, adsorbent with physical properties results in a total solid mass below approximately 200 kg would necessitate one rotary device. This corresponds to blue, red and green region in Figure 5.12. For instance, for a saturation adsorbed capacity of 3 mol/kg, an enthalpy of adsorption in the range of 24 and 28 kJ/mol_{CO2} and pre-exponential factors values from $2 \cdot 10^{-6}$ to $9 \cdot 10^{-6}$ kPa⁻¹, results in a solid material inventory below 200 kg. At higher adsorbed saturation capacity, the parametric space consisting of the enthalpy of adsorption and the pre-exponential factor widens, e.g. for a saturation adsorbed capacity of 6 mol/kg, an enthalpy of adsorption in the range of 24 and 30 kJ/mol_{CO2} and pre-exponential factors from $7 \cdot 10^{-7}$ to $9 \cdot 10^{-6}$ kPa⁻¹, results in a solid material inventory below 200 kg. Heat of adsorption of activated carbon are between 17 and 22 kJ/mol and of zeolites and metal-organic-frameworks are in the range of 30 and 45 kJ/mol (Mangano et al. 2013; Abanades et al. 2015).

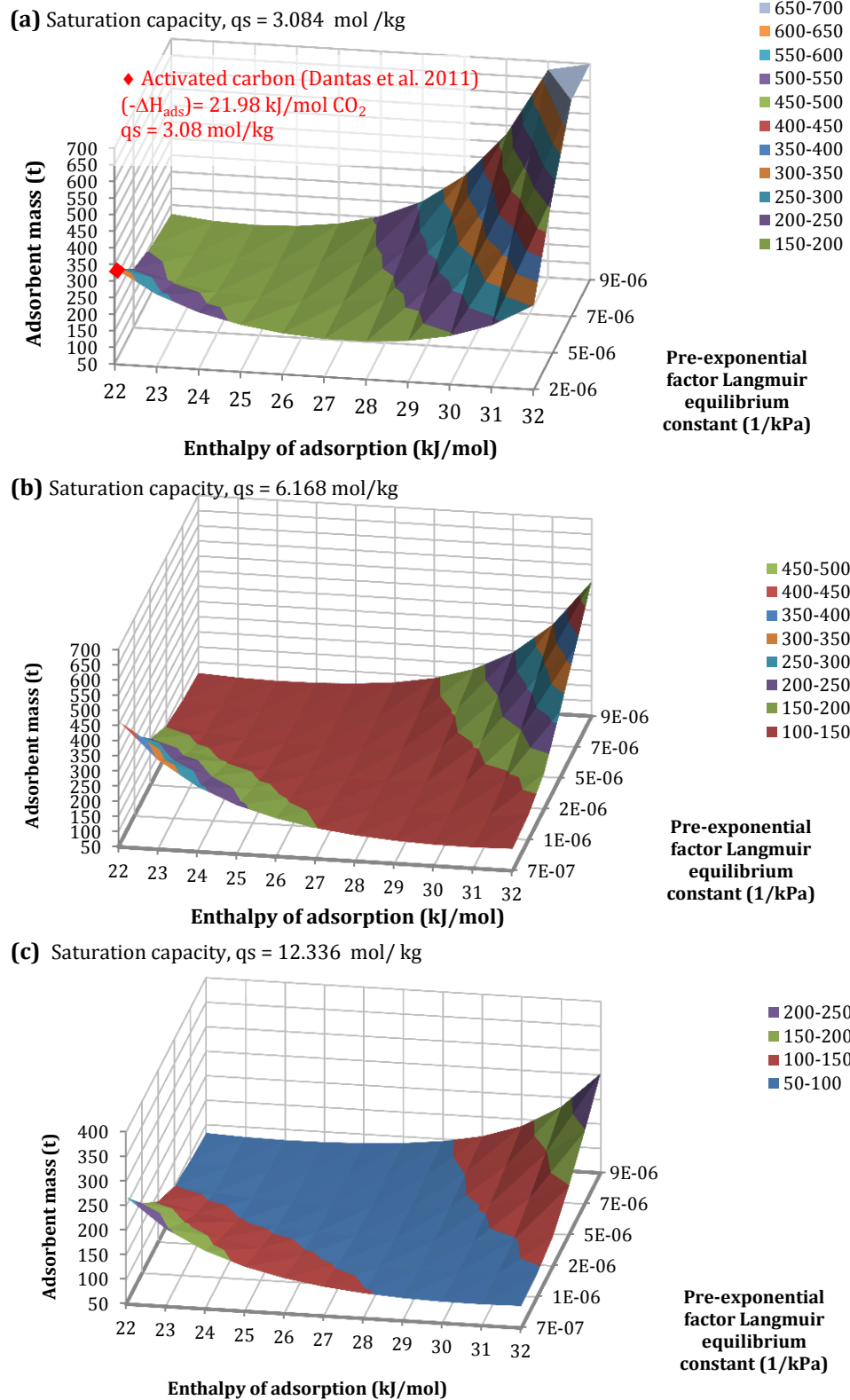
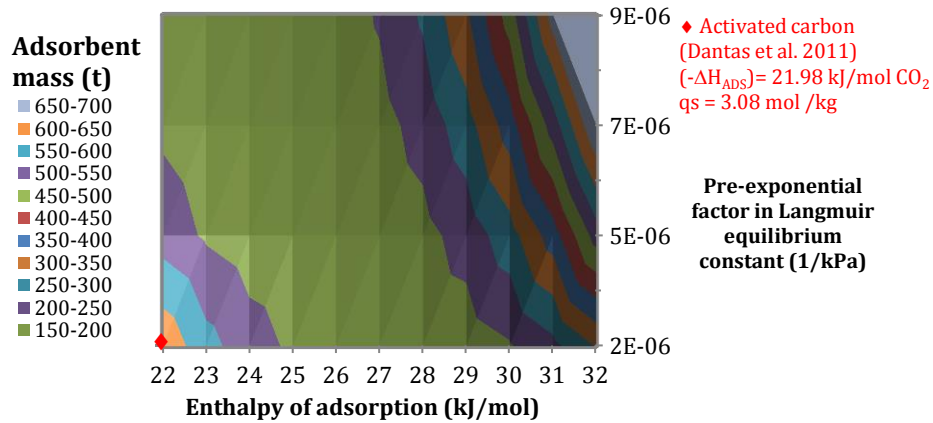
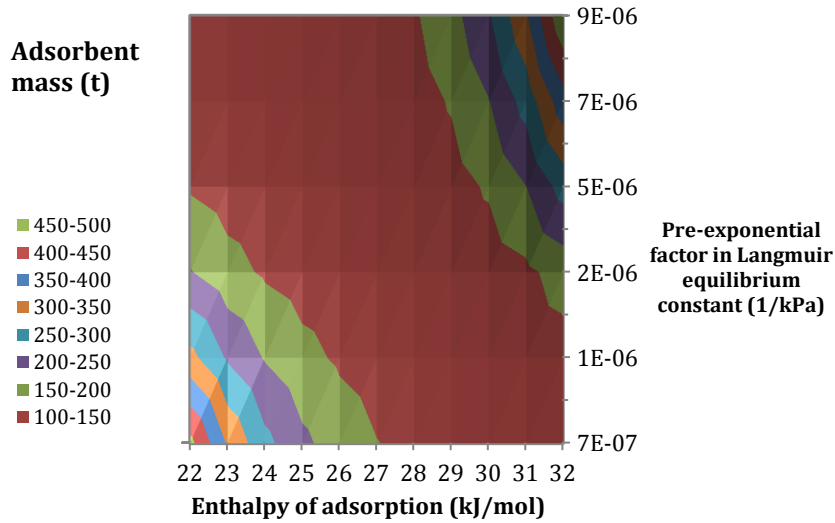


Figure 5.11.- Sensitivity of adsorbent mass to the enthalpy of adsorption and the pre-exponential factor of the equilibrium constant, for a adsorbed saturated capacity of (a) $q_s = 3.08$ mol/kg, (b) $q_s = 6.17$ mol/kg, (c) $q_s = 12.34$ mol/kg. Configuration: S-EGR in parallel at 70% recirculation ratio, 97% selective CO_2 transfer efficiency

(a) Saturation capacity, $q_s = 3.084 \text{ mol/kg}$



(b) Saturation capacity, $q_s = 6.168 \text{ mol/kg}$



(c) Saturation capacity, $q_s = 12.336 \text{ mol/kg}$

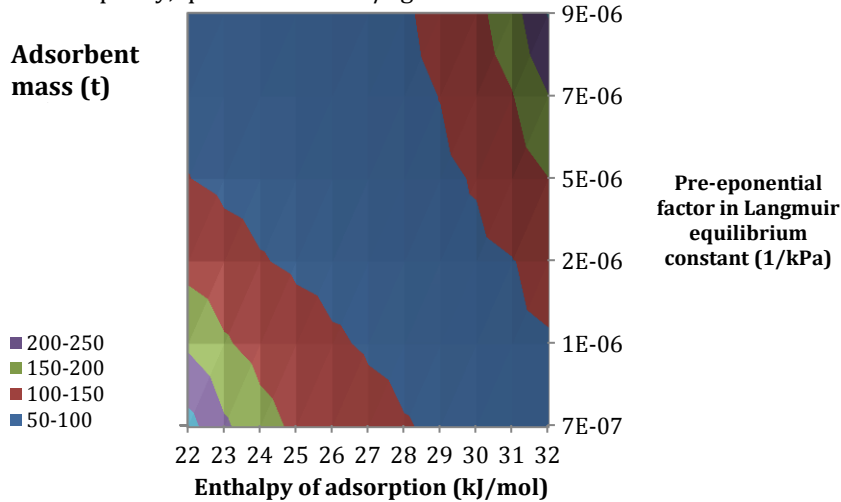


Figure 5.12.- Surface/contours of the sensitivity of adsorbent mass to the enthalpy of adsorption and the pre-exponential factor of the equilibrium constant, for a adsorbed saturated capacity of (a) $q_s = 3.08 \text{ mol/kg}$, (b) $q_s = 6.17 \text{ mol/kg}$, (c) $q_s = 12.34 \text{ mol/kg}$. Configuration: S-EGR in parallel at 70% recirculation ratio, 97% selective CO_2 transfer efficiency.

5.5.2. Sensitivity analysis to the operating conditions

5.5.2.1. Air stream inlet temperature

The effect of increasing the temperature of the air stream for the adsorbent regeneration, e.g. using the available sensible heat in the flue gas leaving the HRSG, on the amount of solid required to achieve 97% CO₂ transfer efficiency is presented in Figure 5.14(b). A 10 °C increase in the temperature of the air stream entering the rotary wheel results in an increase in the amount of solid of approximately 5.5 tonnes. This suggests that a pre-heated air stream does not favour the CO₂ transfer process. The reason is that the cooling capacity of the air stream decreases, despite the fact that a higher temperature favours the CO₂ desorption and regeneration of the solid. The adsorbent enters the adsorption section at a higher temperature than in the base case with air at ambient conditions, as shown in Figure 5.14(a), which is detrimental for the adsorption process. Moreover, the CO₂-enriched air outlet temperature marginally increases by 2 °C for the range of investigated air temperatures, from 17 to 57 °C, derating the gas turbine in approximately 2MW. The small effect of the ambient air temperature is due to the rapid heat transfer in the thermal equilibrium approach.

The effect of a higher ambient temperature on the selective CO₂ transfer efficiency for a fixed amount of solid is also investigated. In the S-EGR in parallel configuration at 70% recirculation ratio, a solvent mass of 326 tonnes was required when the solid material is regenerated with ambient air at 15 °C. An increase in the ambient air temperature of 10 °C results in a 0.5% points reduction of the CO₂ transfer efficiency, as shown in Figure 5.14.

5.5.2.2. Flue gas inlet temperature

A low inlet flue gas temperature thermodynamically enhances the CO₂ adsorption. Although the effect on the amount of solid is marginal, a low temperature is required to minimise the heat transferred into the air stream, so that the temperature of the CO₂-enriched air at the compressor inlet is as low as possible. The lowest flue gas temperature possible at the outlet of the cooling device is however limited by the cooling system of the power plant. The sensitivity analysis is illustrated in Figure 5.15.

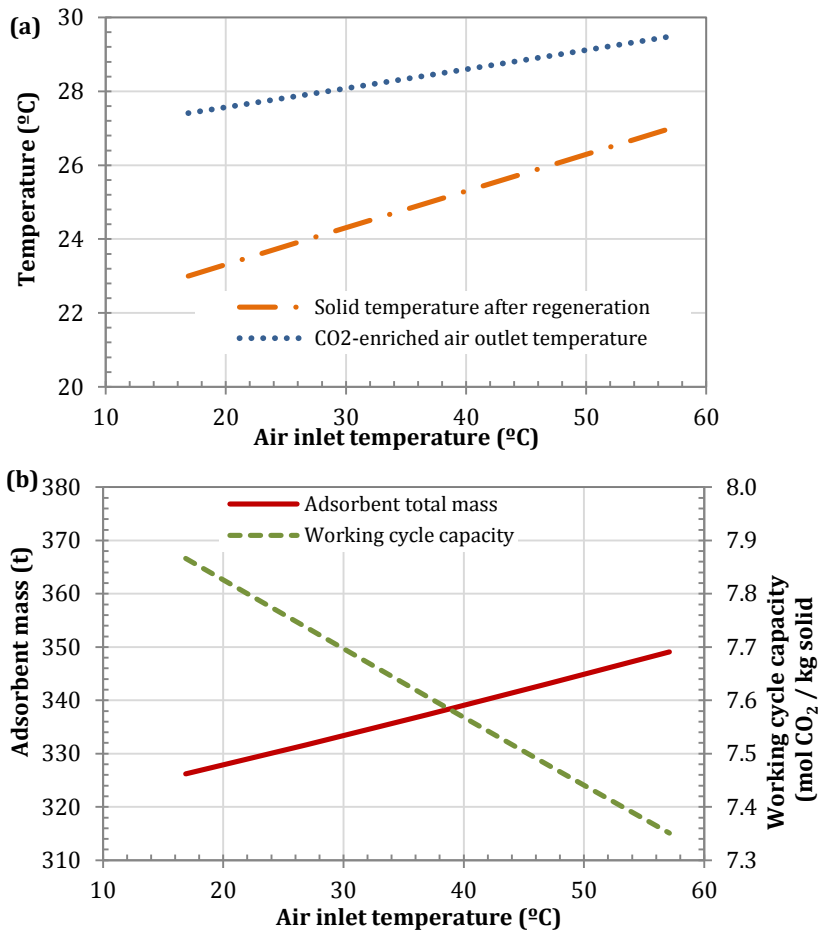


Figure 5.13.- Effect of the air inlet temperature on (a) the CO₂-enriched air and the solid temperatures and (b) the adsorbent mass and the working cycle capacity. Configuration: parallel S-EGR at 70% recirculation ratio.

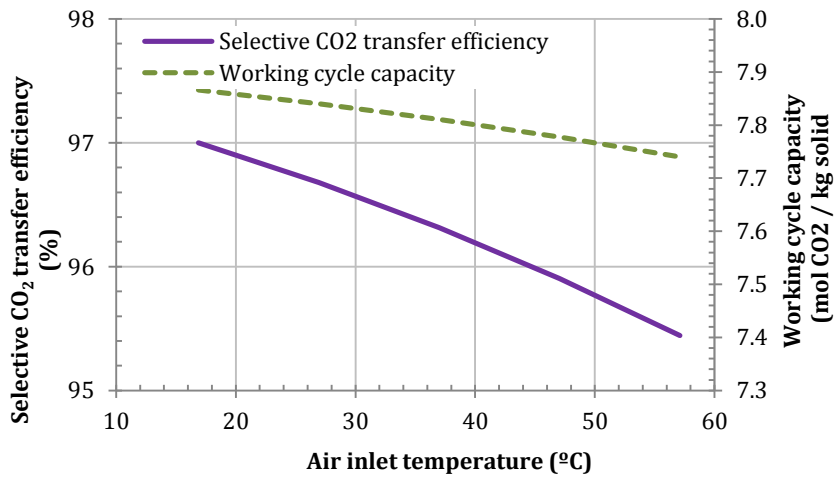


Figure 5.14.- Effect of the air inlet temperature on the selective CO₂ transfer for a given solid mass of 326.21 t. Configuration: parallel S-EGR at 70% recirculation ratio.

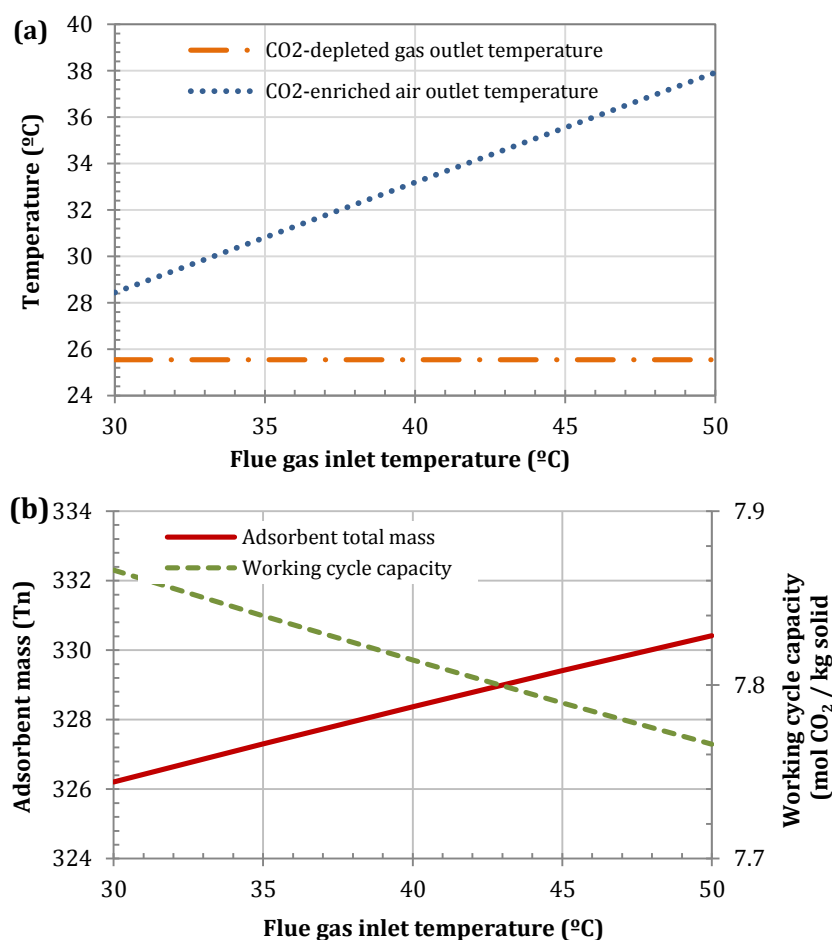


Figure 5.15.- Effect of the flue gas inlet temperature on (a) the air and flue gas outlet temperatures and (b) the adsorbent mass and the working cycle capacity. Configuration: parallel S-EGR at 70% recirculation ratio

5.6. Key findings and recommendations

Chapter 4 shows that the addition of the strategy of S-EGR to a CCGT power plant with aqueous MEA scrubbing technology results in a smaller volume of the absorber packing, compared to a conventional air-combustion CCGT plant with post-combustion capture. The potential benefit in operational and capital costs of adding S-EGR need, however, to be balanced with additional cost and complexity of a system for selective CO₂ transfer. The use of rotary adsorption technology for this application appears to be a promising option with low pressure drop on the basis of the conceptual equilibrium design presented in this Chapter.

The amount of adsorbent is first estimated from process model simulation of activated carbon, used here as reference as it a commercially available hydrophobic material. The use of two rotary devices would be necessary to achieve 97% CO₂ transfer efficiency with a flue gas CO₂ concentration of 14 vol% for the S-EGR in parallel configuration at 70%

recirculation ratio. Two rotary devices would also be necessary to achieve 90 % CO₂ transfer efficiency with a CO₂ concentration of 6 vol% for the configuration with S-EGR in series. A 100% reduction in the amount of solid is possible with Zeolite X13. Its hydrophilic properties are, however, detrimental to capacity and would require to reduce water concentration in the flue gas from 4 vol%, in a water saturated gas at 30 °C, to around 0.1 vol% with the associate increase in the capital and operational cost.

The water content in the flue gas can be reduced, in practical ways, by cooling the flue gas within the limits of the cooling system of the power plant. At 30 °C the water concentration is approximately 4 vol% at the inlet of the rotary wheel. If a lower value is required, e.g. for zeolites, additional equipment upstream of the rotary wheel would be necessary and may significantly add capital cost. The condensed water could be used in the post-combustion capture process to maintain the water balance of the plant.

Alternatively, it could be possible to add a “guard” layer containing a desiccant or a target material which primarily adsorbs water and can subsequently desorb water with ambient air, using the difference in partial pressure between the flue gas and the air. The flue gas enters first into contact with the desiccant and then with the adsorbent selective to CO₂. The effect of increasing the water content in addition to the CO₂ concentration in the compressor inlet stream would have to be further investigated.

Recently, research work has been focused on developing materials with a high affinity for CO₂, which would result in a large equilibrium CO₂ adsorption capacity at a low CO₂ partial pressure. This is, for example, the case of chemical adsorbents for thermal swing adsorption processes proposed for post-combustion CO₂ capture. Physical adsorbents are, however, more suited for selective CO₂ transfer, since the regeneration with an air stream at temperature and pressure near ambient conditions is possible.

The development of new materials for this specific application appears therefore necessary to minimise the amount of solid required and, eventually, the number and the size of the rotary wheel within practical limits.

The optimisation study indicates that increasing the saturation adsorbed capacity from 3 mol/kg, the capacity of activated carbon, up to a value around 10 mol/kg significantly reduces the solid mass requirement. Any further increase then results marginal gain. It also shows that a moderate affinity of the adsorbent material for CO₂ is preferable to maximise the working cycle capacity and minimise the amount of solid. For a saturation adsorbed capacity of 3 mol/kg, an enthalpy of adsorption within a range from 24 to 28 kJ/mol_{CO₂} and pre-exponential factors within a range from $2 \cdot 10^{-6}$ to $9 \cdot 10^{-6}$ kPa⁻¹, results in a solid material

inventory below 200 kg. It is also necessary that the adsorbent presents a hydrophobic behaviour for a range of water concentration in the flue gas up to 10 vol%.

The optimisation of the operating conditions indicates that the temperatures of the flue gas and the air streams have a small effect on the adsorbent mass. Lower flue gas temperature is thermodynamically favourable to the process and enhances CO₂ adsorption under the assumption of equilibrium. It also marginally increases CO₂ concentration in the gas stream due to water condensation, increasing the driving force for mass transfer. The process is also favoured by a temperature of the air stream near ambient conditions. The use of a reheated air stream for solvent regeneration enhances the CO₂ desorption. Yet the cooling capacity decreases and the solid enter the adsorption section at a higher temperature, which is detrimental for the CO₂ adsorption process. Higher air temperature decreases therefore the working cycle capacity. Similarly, a higher ambient air temperature would slightly decrease the CO₂ transfer efficiency by 0.5 %point per 10 °C increase, given a solid mass.

The volume of the rotor section of the wheel containing the adsorbent depends to a great extent on the void fraction of the monolithic structure. Optimisation of the void fraction should provide large surface contact area for a practically possible volume. This is generally achieved with a large number of gas flow channels in parallel with small diameters and small wall thickness.

The dimensions of regenerative rotary heat exchangers have been considered as the maximum diameter for the rotary wheel for this application. Yet, larger diameters could be possible with appropriate structural analysis. The lower density of adsorbent materials, typically 1200 kg/m³, compared to steel used in heat exchanger applications, typically 8000 kg/m³, lead to a lower moment of inertia in the axial direction and lower moment at the wheel diameter. Since adsorption rotary wheels are proposed to operate at atmospheric pressure, space within the power plant layout for the footprint of the rotary wheel and the associated duct work is also an important factor, although it can be expected that this would be of the same order of magnitude as key pieces of equipment of a post-combustion capture process.

Diameter and length in the rotary wheel are selected to provide the volume for the rotor adsorber. The diameter is a trade-off between compact size and flue gas velocity. A larger diameter results in a larger open cross section and a smaller flue gas velocity, which leads to a larger residence time and a smaller pressure drop. The height will result from a trade-off between the residence time and the pressure drop.

For classes of adsorbents within the envelope identified in Section 5.5.1, the next steps for performance assessment would consist of adding the kinetics of the diffusion of CO₂ and N₂ in the porous material (Brandani et al. 2004). Although a monolithic structure offers short diffusion lengths and the kinetics of physisorption are typically fast (Rezaei et al. 2010; Abanades et al. 2015), the solid mass requirements are expected to increase from the equilibrium predictions.

The kinetics of the process will then allow, for each adsorbent, an optimisation of the rotation speed of the rotor section, which defines the rate of adsorbent supply. The faster the rotation speed, the lower the amount of CO₂ to be adsorbed per adsorption/desorption cycle. It is however necessary to allow for a long enough contact time between the solid and the gas phase to approximate to equilibrium.

The flue gas superficial velocity, defined by the open cross section for a given volumetric flow rate, and by extension the rotor diameter, the rotational speed, and the height of the basket containing the adsorbent need to be sized for residence time and a pressure drop.

Options for Heat and Water Management

This chapter is based on:

Herraiz, L., Dougal, H., Cooper, J., Gibbins, J. and Lucquiaud, M. 2015. *Reducing water usage with rotary regenerative gas / gas heat exchangers in natural gas-fired power plants with post-combustion carbon capture*. Energy, vol. 90, pp. 1994–2005.

6.1. Introduction

An additional cooling and process water demand in CCGT power plants when carbon capture technologies are implemented constitutes an important environmental impact and may become a limiting factor for full scale CCS deployment, as introduced in Chapter 1, Section 1.3. The water demand associated to carbon capture systems and the effect on natural water resources have been investigated in literature (Byers et al. 2014, Schakel et al. 2015), yet engineering solutions are necessary to limit the additional water abstraction and water consumption of power plants with CCS, as explained in Chapter 2, Section 2.4. A heat integration option to manage cooling water demand around the post-combustion carbon capture (PCC) process is proposed in this Chapter. It consists on transferring heat from the flue gas stream entering the absorber in the capture unit to the gas stream leaving the absorber, in order to reduce or eliminate the process and cooling water requirements of the direct contact cooler and ensure that the CO₂-depleted gas reaches an appropriate temperature at the stack. This can be achieved with the use of rotary regenerative gas/gas heat exchangers described in Chapter 3, Section 3.4, a technology widely used in coal-fired power plants to increase the thermal efficiency.

An analysis of the thermal performance is conducted for two configurations of a CCGT power plant with PCC systems.

- A conventional (air-based combustion) CCGT plant with PCC.
- A CCGT power plant with PCC and Exhaust Gas Recirculation (EGR).

Hybrid and dry cooling systems are proposed to reduce the size or eliminate the direct contact cooler upstream of the CO₂ capture unit. Different configurations of rotary regenerative gas/gas heat exchangers are examined with respect to water usage, stack

temperature, power requirements and design parameters related to their geometry and operational conditions.

In a CCGT with PCC and EGR, the recirculated gas stream is typically cooled before it is mixed with ambient air, as lower compressor inlet temperature favours the compression and increases the gas turbine power output. In previous work, little consideration has been given to optimising heat and water management of the flue gas loop. The same cooling equipment is typically used for both streams (IEAGHG 2004; Jordal et al. 2012). Recent studies have, however, proposed the recycling of exhaust gas at lower temperatures, with two direct contact coolers introduced to the process (IEAGHG 2012).

The technical assessment conducted in the Chapter considers the flue gas characteristics of a CCGT plant with PCC system described in *Appendix C*.

Section 6.2 describes the configurations of rotary regenerative gas/gas heat exchangers and the thermal performance analysis and the size of the rotary heat exchanger in each configuration is presented in Section 6.3, using a methodology specifically developed for this novel application described in Chapter 3, Section 3.4, which is based on proprietary software developed by Howden Group (Howden 2008). The dimensions and operational parameters results from the dedicated design of the devices to achieve satisfactory outlet temperature of the gas stream at the cold and hot ends. A sensitivity of the performance of the dry cooling system, using ambient air as the cooling fluid, to ambient temperature is reported in Section 6.3.3. Section 6.4 deals with the alternatives for the booster fan location and their implications on the power consumption and on the direction of the leakage flow.

6.2. Novel integration options for heat and water management in CCGT power plant with PCC

Three alternative configurations using rotary heat exchangers are compared to the standard configuration of using exclusively a direct contact cooler (DCC).

- A hybrid cooling system which includes a rotary regenerative gas/gas heat exchanger upstream of a DCC. Heat is transferred from the exhaust flue gas leaving the HRSG into the CO₂-depleted gas stream leaving the absorber to enter the stack.
- A dry air-cooled system which consists of two rotary heat exchangers in series. A rotary air/gas heat exchanger replaces the DCC in the previous configuration, downstream of a rotary regenerative gas/gas heat exchanger.
- A dry air-cooled system with a more compact arrangement to the previous one, which combines the two rotary heat exchangers into a single regenerative rotary gas/gas/air heat exchanger with a trisector configuration.

Block flow diagrams for each configuration in an air combustion CCGT plant and in a CCGT plant with EGR are shown in Figure 6.1 and Figure 6.2, respectively.

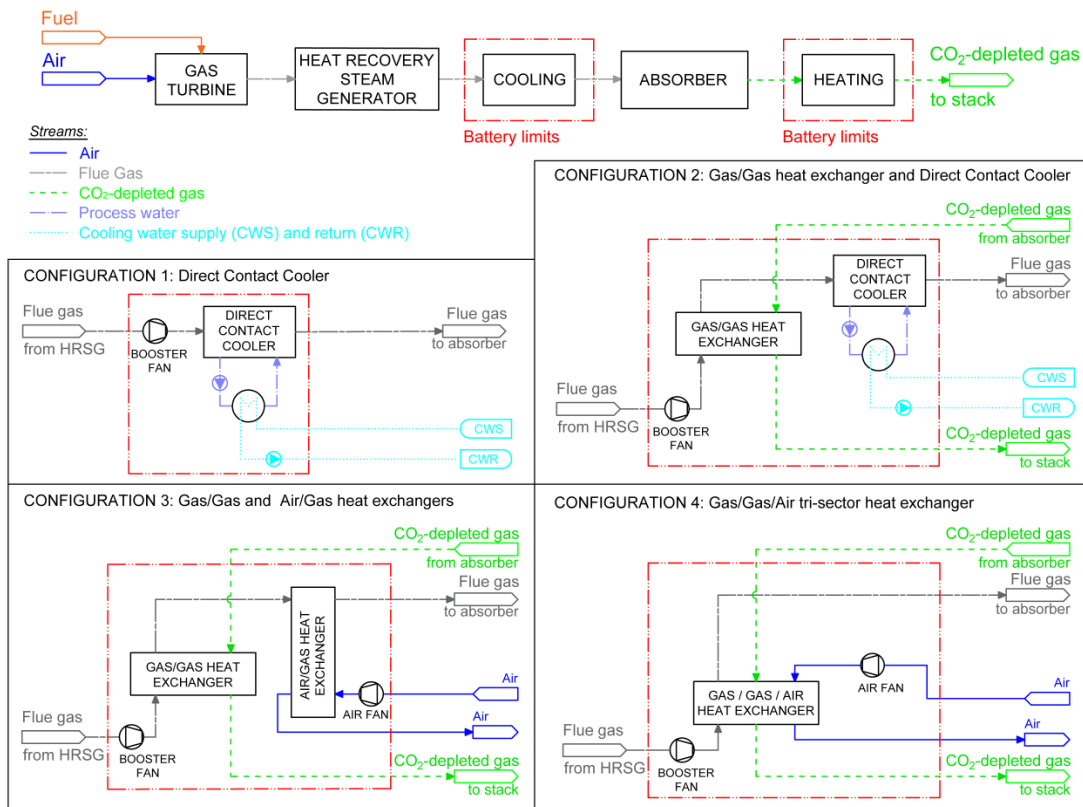


Figure 6.1.- Block flow diagrams of rotary heat exchangers configurations for a conventional (air-based combustion) combined cycle gas turbine plant with post-combustion capture.

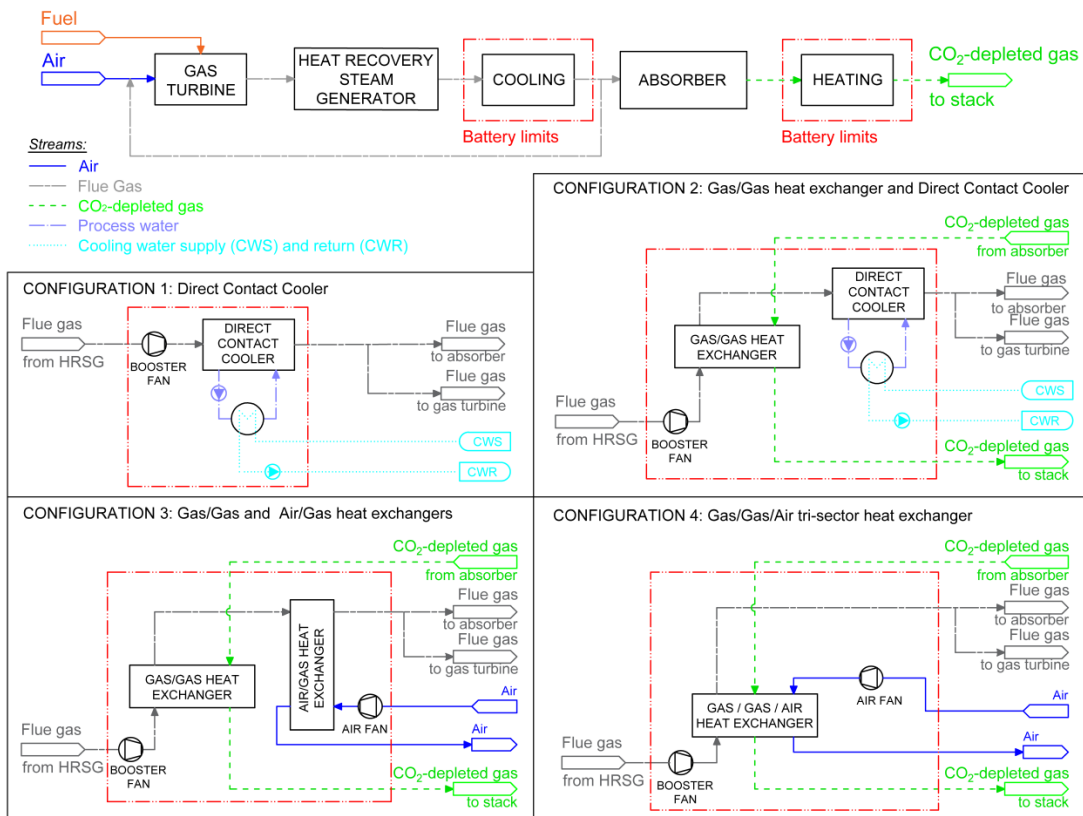


Figure 6.2.- Block flow diagrams of rotary heat exchangers configurations for a combined cycle gas turbine plant with post-combustion carbon capture and exhaust gas recirculation.

6.2.1. Wet cooling system with a direct contact cooler (base case)

The gas is brought into direct contact with process water in a counter current configuration in a packed bed column. The water collected in the cooler sump is passed through a dedicated water-cooled heat exchanger before being returned to the top of the column. Cooling water in the heat exchanger is provided by the primary plant cooling system.

In this work, process water refers to the amount of water used in a recirculating loop to cool down the flue gas by direct contact. There is either consumption or production of process water that needs to be supplied or extracted. The amount depends on the difference between the absolute humidity of the gas at the inlet and at the outlet of the DCC. With appropriate consideration a neutral balance of the circulating loop can be achieved (Kvamsdal et al. 2010). Cooling water for the DCC is taken from the primary cooling system of the power plant and used to cool down the process water. The cooling water is either water abstraction in a once-through cooling system or recirculated water in a recirculating cooling system, contributing then to water consumption in the evaporative cooling towers.

6.2.2. Hybrid system with a gas/gas heat exchangers and a direct contact cooler in series

In the hybrid system, a gas/gas heat exchanger operates upstream of the DCC in a bisector arrangement. The metal elements contained in the baskets of the rotary heat exchanger are continuously heated in contact with the flue gas leaving the HRSG and cooled in contact with the CO₂-depleted gas, transferring sensible heat from the first gas stream into the second gas stream. The CO₂-depleted gas stream reaches the temperature necessary for adequate buoyancy at the inlet of the stack. The typical temperature of 35-45 °C at the carbon capture unit inlet cannot be achieved with the gas/gas heat exchanger alone and further cooling occurs in a direct contact cooler tower with lower process and cooling water requirements.

6.2.3. Dry system with a gas/gas and an air/gas heat exchangers in series

Two consecutive rotary heat exchangers replace the direct contact cooler of the wet cooling system. The first gas/gas heat exchanger transfer sensible heat from the exhaust flue gas stream to the CO₂-depleted gas stream. The gas/gas heat exchanger design is the same as in the previous configuration. In order to reduce further the exhaust flue gas temperature, an additional rotary air/gas heat exchanger using ambient air as the cooling fluid replaces the

smaller direct contact cooler of the hybrid system. A forced draft fan overcomes the pressure drop through the air section of the air/gas heat exchanger.

6.2.4. Dry systems with a trisector gas/gas/air heat exchanger

The two rotary heat exchangers in series of the previous configuration are replaced by a heat exchanger with a tri-sector arrangement with the potential for a large reduction in the overall size, footprint and capital cost. Exhaust flue gas coming from the HRSG flows in a counter current manner to the CO₂-depleted gas stream and to the air stream. The direction of rotation of the heat exchanger is an important consideration so that the baskets turn from the exhaust flue gas section into the absorber outlet gas section and then the air section, as illustrated in Figure 6.3. This allows better heat transfer and a smooth temperature gradient of the elements, as well as an adequate direction of leakage with the appropriate pressure gradient, as discussed in the next section.

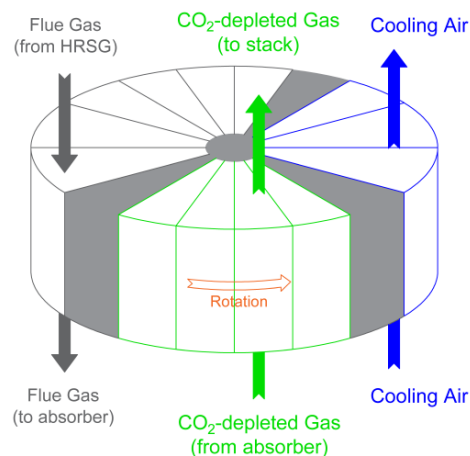


Figure 6.3.- Direction of the flow in a trisector rotary gas/gas/air heat exchanger.

6.3. Thermal performance analysis of the rotary gas/gas heat exchangers

For the reference CCGT power plant described in Appendix C, flue gas leaves the HRSG at 86 °C and 101.3 kPa. The booster fan, located upstream of the direct contact cooler, increases the flue gas pressure by around 10 kPa, resulting in a temperature rise of around 11 °C. Sensible heat is removed by the direct contact cooler and the flue gas enters the absorber saturated in moisture at the dew point approximately 45 °C. The CO₂-depleted gas then leaves the water wash section at the top of the absorber saturated in moisture at a

temperature of 45 °C, in order to maintain a close to neutral water balance in the absorber tower.

For all the configurations the following design criteria have been considered: the gas stream enters the absorber saturated with water at 45 °C and the reheated flue gas enters the stack at a temperature at least higher than 70 °C to ensure thermal buoyancy effect and plume abatement.

The thermal performance analysis of the rotary heat exchangers in each configuration is conducted considering the flue gas flow rate from one train of the reference CCGT power plant with a 2-in-1 configuration (two gas turbines, two HRSGs and one steam cycle). Each flue gas train therefore consists of one gas turbine, one HRSG and one capture unit. Input parameters to the model and main assumptions are summarised in Appendix C and technical operation parameters and key findings are discussed below.

Figure 6.4 summarises the requirements for process water, cooling water and cooling air for each configuration of rotary heat exchangers for air-based combustion and exhaust gas recirculation CCGT plant at 40% recirculation ratio. Table 6.1 includes the dimensions of the heating metal elements assembly in the rotary heat exchangers, the temperatures of gas streams and operational parameters.

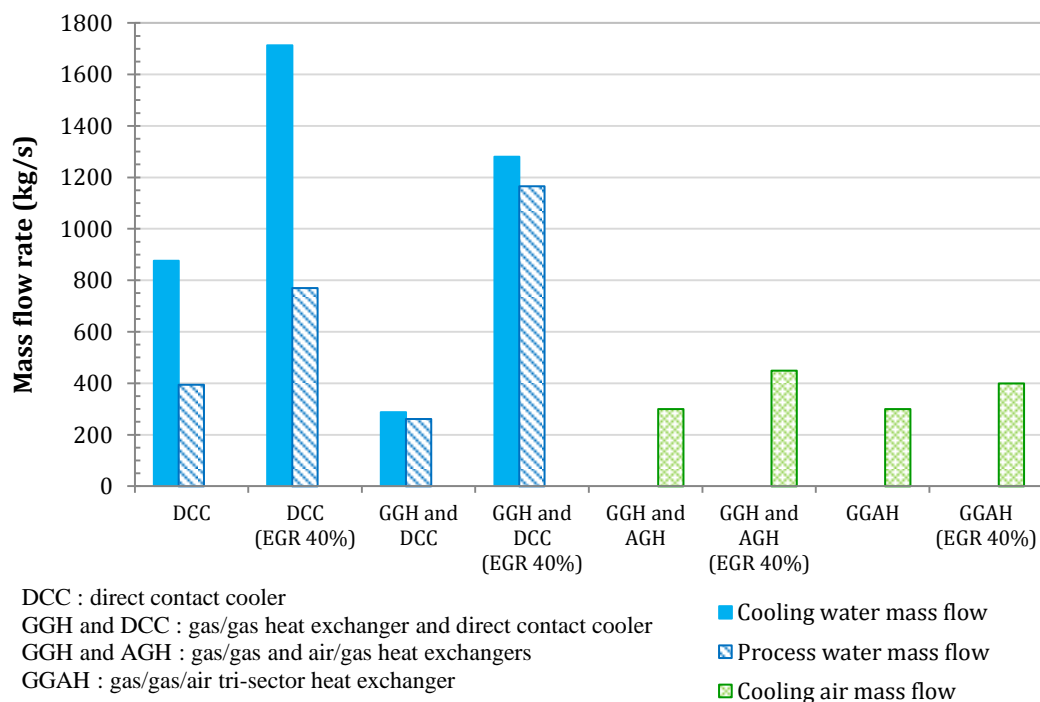


Figure 6.4.- A comparison of the cooling water, recirculating process water and cooling air mass flow rates per gas turbine train in a convectional (air-based combustion) combined cycle gas turbine plant and a plant with an exhaust gas recirculation ratio of 40%, both with post-combustion capture technology.

Table 6.1.- Summary of the results: Rotary heat exchangers basic design and operational parameters (per GT-HSRG-absorber train).

	Gross frontal area m ²	Element depth mm	Heating surface area m ²	Inlet / Outlet temperature °C	Hot End Velocity m/s	Total Pressure drop kPa
<i>Conventional air-based combustion Combined Cycle Gas Turbine plants</i>						
Gas/gas heat exchanger (GGH) (with direct contact cooler)	152 (GGH)	1220 (GGH)	66038	Hot gas 97.5 / 62.6	13.5	Gas ⁽¹⁾ 12.3
				Cold gas 45 / 82.3	12.9	
Gas/gas heat exchanger (GGH) and air/gas heat exchanger (AGH)	152 (GGH)	1220 (GGH)	66038	Hot gas 97.5 / 62.6	13.5	Gas 11.2
				Cold gas 45 / 82.3	12.9	
	124 (AGH)	1000 (AGH)	45868	Hot gas 62.6 / 45	14.6	Air 0.3
Gas/gas/air tri-sector heat exchanger (GGAH)	230	1420	120226	Hot gas 97.5 / 46	11.8	Gas 10.3
				Cold gas 45 / 75.2	11.8	
				Air 15 / 68.3	8.4	Air 0.88
<i>Combined Cycle Gas Turbine plants with 40% Exhaust Gas Recirculation</i>						
Gas/gas heat exchanger (GGH) (with direct contact cooler)	152 (GGH)	1220 (GGH)	66038	Hot gas 97.5 / 73.7	13	Gas 11.7
				Cold gas 45 / 91.6	7.1	
Gas/gas heat exchanger (GGH) and air/gas heat exchanger (AGH)	152 (GGH)	1220 (GGH)	66038	Hot gas 97.5 / 73.7	13	Gas 10.5
				Cold gas 45 / 91.6	7.1	
	124 (AGH)	1000 (AGH)	45868	Cold gas 73.7 / 49.5	14.5	Air 0.65
Gas/gas/air tri-sector heat exchanger (GGAH)	230	1420	120226	Hot gas 97.5 / 46	11.4	Gas 8.9
				Cold gas 45 / 80	7.7	
				Air 15 / 73	11.2	Air 1.2

Note (1): Pressure drop for the gas side includes the absorber, gas ducts and direct contact cooler and/or rotary heat exchanger. Pressure drop through the absorber, gas ducts and direct contact cooler were assumed to be 5, 2.5 and 2.5 kPa respectively [9]. Pressure drop through the rotary heat exchangers are calculated.

6.3.1. CCGT with air-based combustion gas turbine

6.3.1.1. Hybrid cooling systems

In hybrid cooling systems, with a rotary gas/gas heat exchanger and a direct contact cooler in series, heat is transferred in the first device from the gas stream leaving the HRSG to raise the temperature of the gas stream entering the stack above 80 °C, well above the necessary 70 °C to increase buoyancy in the stack. The cooled gas then leaves the gas/gas heat exchanger at a temperature around 62 °C and is further cooled in a direct contact cooler down to a temperature around 45 °C. The lower amount of heat that needs to be removed from the exhaust flue gas in the direct contact cooler results in a significant reduction in process and cooling water demand of 35% and 67% respectively compared to the traditional wet cooling system with a single direct contact cooler. The dimensions of the baskets containing the heating elements are around 1.22 m long and the selected heater size has a front section area of 152 m², which corresponds to a casing diameter of around 14.5 m.

6.3.1.2. Dry cooling systems

In the two dry systems, where air cooling replaces the direct contact cooler, the need for process and cooling water demand for the purpose of cooling the flue gas into the absorber is fully eliminated, contributing to a significant reduction of the overall water usage in the post-combustion capture plant.

In the configuration with two rotary heat exchangers in series, the air/gas heat exchanger operates with mass flow rate of 300 kg/s of ambient air. The air temperature at the hot end reaches 56 °C. If the hot air and the reheated CO₂-depleted gas streams are mixed, the resulting gas stream enters the stack at around 72 °C. The dimensions of the baskets containing the heating elements are around 1 m long and the selected heater size has a front section area of 125 m², which corresponds to a casing diameter of around 13 m.

The trisector gas/gas/air heat exchanger has the potential for a large reduction in the overall size and capital cost. In addition, the pressure drop on the gas side is reduced from 3.4 kPa to 2.8 kPa. An air mass flow rate of 300 kg/s is heated from ambient temperature, 15 °C, up to around 68 °C. The CO₂-depleted gas stream is reheated up to around 75 °C and enters the stack, after being mixed with the hot air, at around 73 °C. The dimensions of the baskets containing the heating elements are around 1.42 m long and the selected heater size has a front section area of 230 m², which corresponds to a casing diameter of around 18 m. When compared to the dimensions for a direct contact cooler treating similar volume of gases

(IEAGHG 2012) of a 10 m x 27 m x 19 m height, this constitute a significant reduction in the overall size.

If a temperature of the gas stream lower than 45 °C at the inlet of the absorber was required, i.e. below the dew point, the temperature difference at the cold end of the rotary regenerative heat exchanger and the driving force for heat transfer would be reduced, leading to an increase in the overall size of the heat transfer surface area. Additional cooling capacity would also be necessary to remove the latent heat of water condensation. This could be achieved either by significantly increasing the heating surface area of the regenerative heater or by operation with larger cooling air flow rates. Water condensation would occur on the heating metal elements in the high temperature gas section and then be transferred to the adjacent section. A large fraction of water droplets could drop by gravity with a carefully selected direction of the gas, and some would evaporate in the air stream. This is illustrated in Figure 6.5.

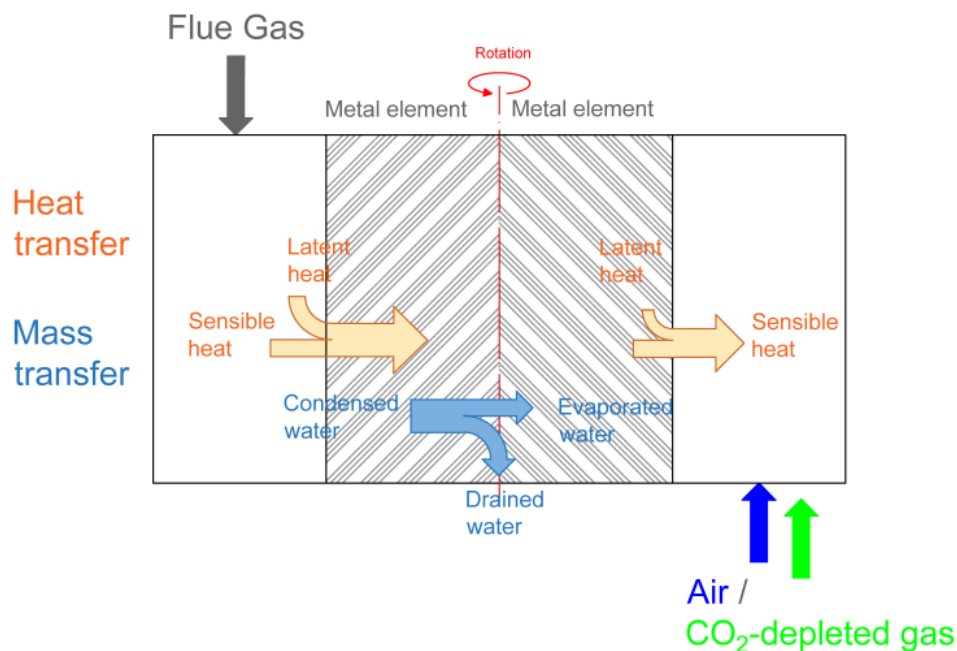


Figure 6.5.- Heat and mass transfer of water for rotary regenerative heat exchangers operated below the dew point.

Ambient air conditions could also play an important part if, for instance, the ambient air temperature was lower than the design temperature of 15 °C. The outlet temperature of the flue gas stream at the cold end would be reduced and water condensation would occur. This could however be managed by adjusting the air flow rate. Enamelled heating elements and appropriate material selection would be applied to mitigate any possible long-term corrosion problems, in a similar manner to FGD GGH applications.

6.3.2. CCGT with EGR: effect of the recirculation ratio

For values of the recirculation ratio comprised from 0 to 40%, water content in the gas stream leaving the HRSG, and the heat transfer duty of the regenerative rotary heat exchangers, increase with the recirculation ratio since the absolute humidity of the recirculated flue gas stream is greater than that of the ambient air used for combustion.

In addition, the total flow rate entering the regenerative rotary heat exchangers is very similar to air-based combustion, whereas the CO₂-depleted gas flow rate is, on the other side of the heat exchanger, reduced by approximately 40%, at that level of exhaust gas recirculation. The lower cooling capacity is then compensated with a larger amount of cooling water or cooling air.

A sensitivity analysis of the recirculation ratio, for the same sizing of the regenerative heat exchangers as for the corresponding configuration of an air-based combustion CCGT plant, shows that the corresponding dew point temperature increases, at constant HRSG outlet temperature for all cases. With 40% EGR, the saturation temperature of the flue gas is around 51 °C, i.e. higher than the 45 °C of a conventional air-based combustion CCGT plant.

One option is to cool the flue gas down to 45 °C to enhance CO₂ removal in the absorber and condense any excess of water. The sensible heat of the gas and latent heat of water have to be removed when the gas is cooled below the dew point. In wet-based and hybrid cooling configurations, process and cooling water flow rates can be increased and excess water is purged from the recirculating process water system. For dry systems with air cooling, water condensation will occur on the heating metal elements of the rotary heat exchangers, as shown in in Figure 6.5. The condensed water that remains over the metal elements will be partially or totally evaporated increasing the absolute humidity of the air and CO₂-depleted gas at the same time as the streams are heated. Excessive condensation in the rotary heat exchangers could be avoided with the gas entering the absorber inlet just above the dew point, at expense of the production of water in the water wash section of the absorber tower and the associated complexity of treating the excess water containing dissolved amines.

6.3.2.1. *Hybrid cooling systems*

In hybrid cooling systems, with a rotary gas/gas heat exchanger and a direct contact cooler in series, the temperature of the gas at the cold end of the gas/gas heat exchanger increases, e.g. from around 62 °C for air-based combustion to 74 °C with 40% EGR. The CO₂-depleted gas outlet temperature entering the stack also increases to 90 °C. This is due to the fact that, as

explained previously, the whole volume of flue gas leaving the HRSG is cooled while only the non-recirculated fraction of the flue gas is reheated on the gas/gas heat exchanger.

The larger amount of specific heat and the latent heat of condensation results in significantly higher water requirements in the direct contact cooler compared to the corresponding configuration in an air-based combustion CCGT plant, as indicated in Figure 6.4. The absolute increase in process water is higher with EGR than with air-based combustion, since additional latent heat of condensation needs to be removed from the flue gas.

6.3.2.2. *Dry cooling systems*

With a gas/gas heat exchanger and an air/gas heat exchanger in series, high levels of EGR lead to higher gas temperature entering the absorber, if the same cooling air flow rate as the air-based combustion case is used. With a cooling air flow rate of 300 kg/s the flue gas is cooled down just above the dew point temperature (around 51 °C) at 40% recirculation ratio. A cooling air flow rate of 450 kg/s is required to further cool the flue gas stream down to 46 °C at the absorber inlet and a temperature of air at the hot end around 57 °C. Figure 6.6 illustrates this effect for a range of recirculation ratios and cooling air mass flow rates for the configuration with two rotary heat exchangers in series.

An increase of the recirculation ratio has a similar effect in the tri-sector gas/gas/air heat exchanger configuration, although to a lower magnitude. The CO₂-depleted gas outlet temperature and the air outlet temperature follow the same trend and increase at larger recirculation ratios, providing a positive effect to enhance stack buoyancy. With an air flow rate of 300 kg/s, at 40% recirculation ratio, the flue gas temperature at the cold end is close to the dew point. A cooling air flow rate of 400 kg/s, as opposed to 450 kg/s, is necessary to cool the flue gas stream down to 46 °C at the absorber inlet. The hot air temperature and the CO₂-depleted gas temperature are respectively 73 °C and 80 °C. Figure 6.7 shows the sensitivity of flue gas and air temperature to the recirculation ratios and the mass flow rate of cooling air.

The increase in cooling air mass flow rate with EGR compared to air-based combustion is smaller in magnitude than the rise in cooling water mass flow rate due to the capacity of the air stream for evaporative cooling. The air gains moisture by evaporating condensed water on the metal elements in the untreated flue gas side. The enthalpy of the air increases due to both the increase in temperature and in absolute humidity.

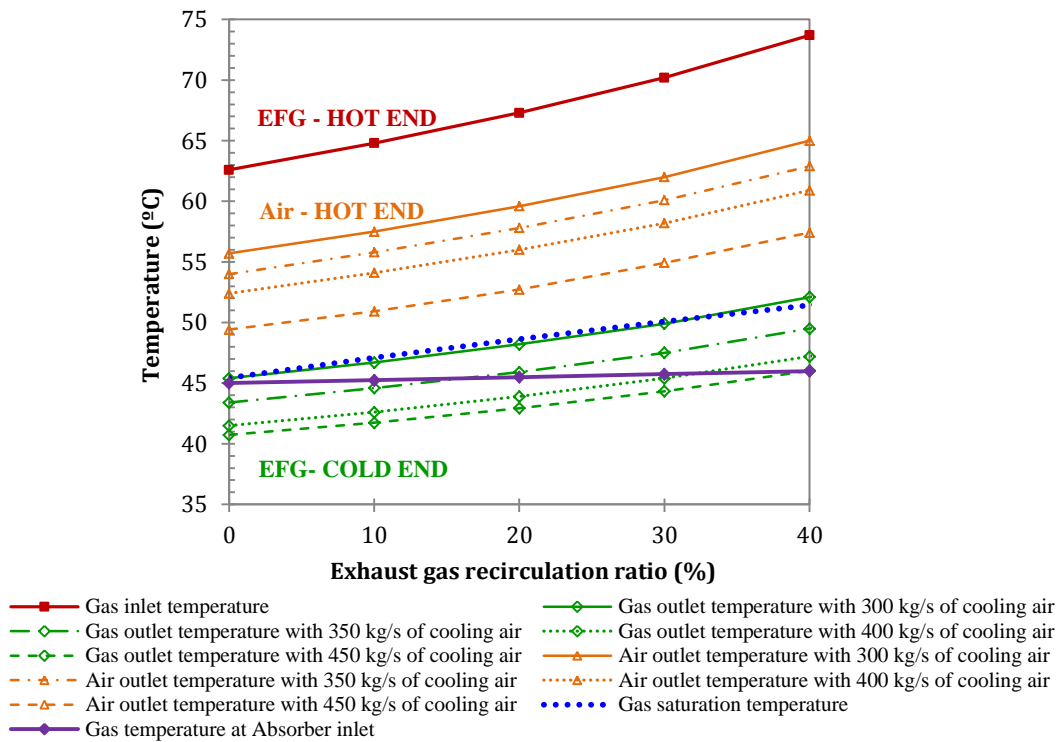


Figure 6.6.- Dry cooling configuration with two rotary heat exchangers in series: Sensitivity analysis of flue gas and air temperature to the recirculation ratio and the mass flow rate of cooling air.

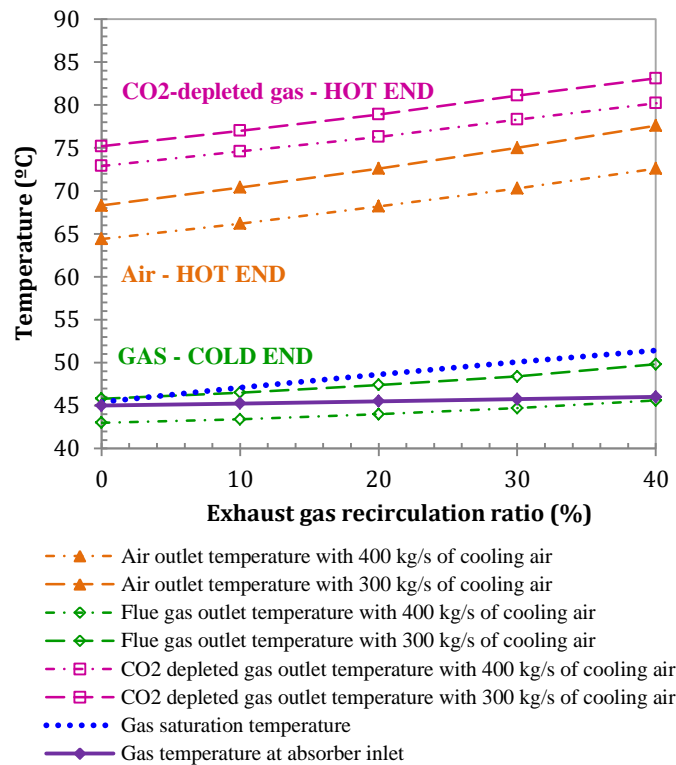


Figure 6.7.- Dry cooling configuration with a trisector gas/gas/air heat exchangers: Sensitivity analysis of flue gas and air temperature to the recirculation ratio and the mass flow rate of cooling air.

6.3.3. Effect of the ambient air temperature on the performance of dry cooling systems

Dry cooling systems are highly dependent on ambient conditions, namely temperature and relative humidity. A sensitivity analysis is shown in Figure 6.8 for a temperature range of ambient air from 10 °C up to 40 °C for the dry air-cooled configuration with two rotary heat exchangers in series, where the air/gas heat exchangers was initially sized for 15 °C, in a conventional CCGT plant without exhaust gas recirculation.

For a given heating surface area, an increase in ambient air temperature results in a lower cooling capacity and, therefore, in higher outlet temperatures for both the exhaust flue gas and the air streams, as illustrated in Figure 6.8. At the design air flow rate, the gas outlet temperature is around 50 °C for an ambient air temperature of 30 °C. This can be brought down to 45 °C, the target gas outlet temperature in this work, by increasing the air flow rate from 300 kg/s to 500 kg/s.

By sizing the blower accordingly, larger cooling air flow rates can compensate, to some extent, for the increase in the flue gas outlet temperature. At ambient temperature above 30 °C, an asymptotic behaviour of the air flow rate to maintain gas outlet temperature at 45 °C is observed. This shows a limitation of this specific configuration designed for 15 °C. Under these conditions, a larger heat exchanger size, combined with a higher cooling air mass flow rate, can be implemented to increase cooling capacity at additional capital costs.

Ultimately, if this technology option was deployed in challenging environments with ambient air temperature much higher than 30 °C, an alternative to augmenting the size of the heat exchanger is to increase the flue gas temperature entering the absorber at the expense of the energetic performance of the post-combustion capture unit. It is worth noting that some wet cooling systems can also be affected by ambient conditions, notably if the evaporative cooling tower supplies water to the direct contact cooler.

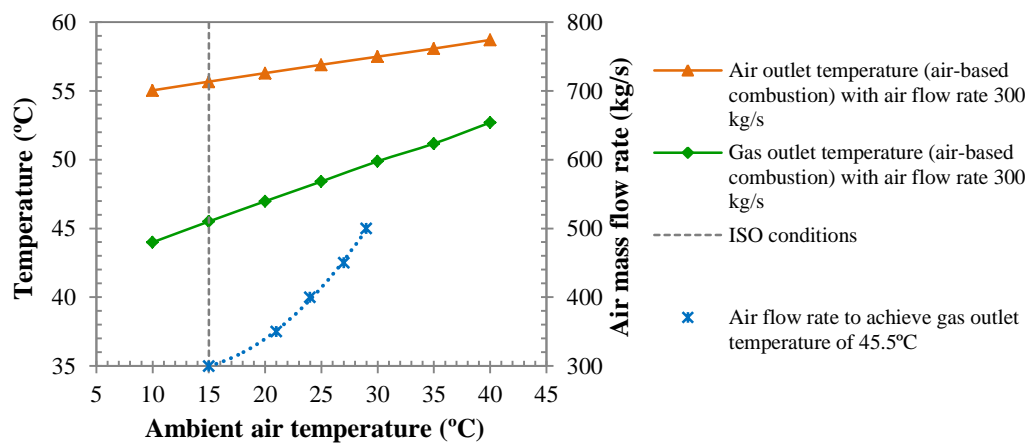


Figure 6.8.- Sensitivity to the ambient air temperature of the performance of a dry cooling configuration with two rotary heat exchangers in series for a conventional CCGT plant (without exhaust gas recirculation). Heating surface area 45868 m².

6.4. Booster fan implications: power requirements and leakage control

An important consideration for this application of rotary heat exchangers is the management of gas leakage between flow streams. Leakage can be mitigated with strategies using proven purge and scavenge systems. Purge and scavenge flows can be extracted from the low-CO₂ reheated flue gas outlet ducting and, via a low leakage fan, passed back, under positive pressure, to specific purge and scavenge slots. The scavenge flow reduces the entrained leakage that is contained in the elements as they rotate, and the purge flow pressurizes the radial and axial seals reducing the amount of direct leakage. Operation at low rotational speed also reduces the entrained leakage (Cooper 1991).

The magnitude and the effects of leakage are highly dependent on the location of the flue gas booster fan required to overcome the additional pressure in the gas pathway (ducts, coolers and the packing of the absorber tower) and, also, avoid any negative effect of increasing the back pressure on the gas turbine exhaust.

In a standard wet cooled configuration, the booster fan can be located upstream of the direct contact cooler for a more accurate control of temperature at the absorber inlet. On the other hand, locating the booster fan downstream of the DCC offers the advantage of a lower temperature and volumetric flow rate at the inlet of the fan, which results in lower fan power consumption (IEAGHG 2012). With rotary heat exchangers, leakage levels, the direction of the leakage flow, the power consumption and the temperature rise due to compression play an important role in the selection of the booster fan location. Locating the fan upstream of the regenerative heat exchanger, as shown in Figure 6.1 and Figure 6.2, is preferable for

carbon capture since the temperature rise due to the compression occurs before the cooling process, resulting in a larger temperature pinch at the cold end of the rotary heat exchangers, reducing the element heating surface and the size of the heat exchanger. This effectively translates into lower pressure drop and lower booster fan power consumption.

Although the pressure differential between the gas streams results in leakage flow from high CO₂ concentration streams to low CO₂ concentration streams (i.e. the gas stream leaving the absorber or the stream of cooling air), and higher leakage levels compared to a configuration with the fan located directly upstream of the absorber tower, the overall magnitude of leakage is, however, very likely to be acceptable. The operating temperature differentials and resulting thermal deformations of the rotor would be significantly lower than power plant air preheaters or FGD gas heaters therefore better sealing can be expected. There is obviously a compromise between leakage and the capital costs of the device. A sensitivity analysis of leakage level on the overall CO₂ removal rate, illustrated in Figure 6.9, shows that, at values lower than 1%, there is a marginal reduction of the overall CO₂ removal rate. The reduction is of the order of 0.45% for a leakage level of 0.5% for an absorber design with a 90% removal rate. It is also worth noting that leakage levels lower than 3% do not have any significant impact on the thermal performance analysis of the different configurations of rotary heat exchangers and results presented.

The total power consumption for each configuration is shown in Figure 6.10 for a convectional CCGT plant and a CCGT plant with 40% EGR. Results include the booster fan, air fan and water pumps power and are reported for one single gas turbine- HRSG- absorber train of the two gas turbines in the reference plant. More details on the power consumption associated with the cooling water pumps of the wet and the hybrid system is provided in Appendix C, Table C.1.

The pressure drop through the gas pathway is of the same order of magnitude in all the configurations and, overall, gas/gas heat exchangers do not introduce additional pressure drops in the system. The trisector gas/gas/air heat exchanger configuration has the smallest overall dimensions and lowest booster fan power consumption.

With exhaust gas recirculation, the reduction in gas flow rates and the pressure drops of the CO₂-depleted gas side lead to a reduction in booster fan power.

Finally, it is worth noting that the power consumption of air fans in the dry cooling systems is considerably smaller than the power of booster fans, and equivalent in magnitude to the power of cooling water pumps in wet and hybrid configurations.

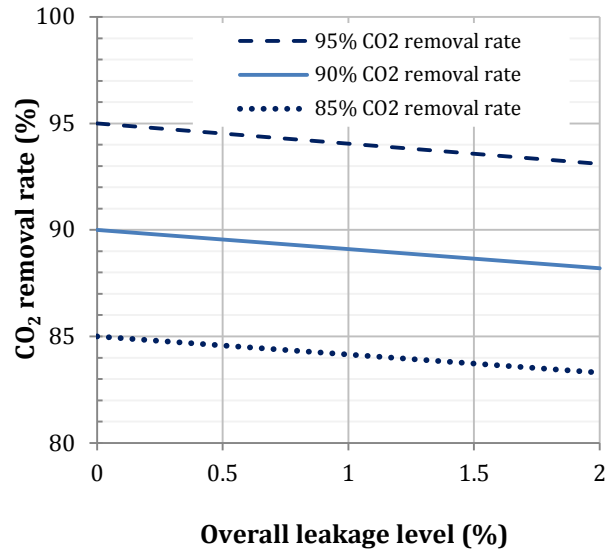


Figure 6.9.- Sensitivity of the overall CO₂ removal ratio to leakage level from the untreated flue gas into the CO₂-depleted gas

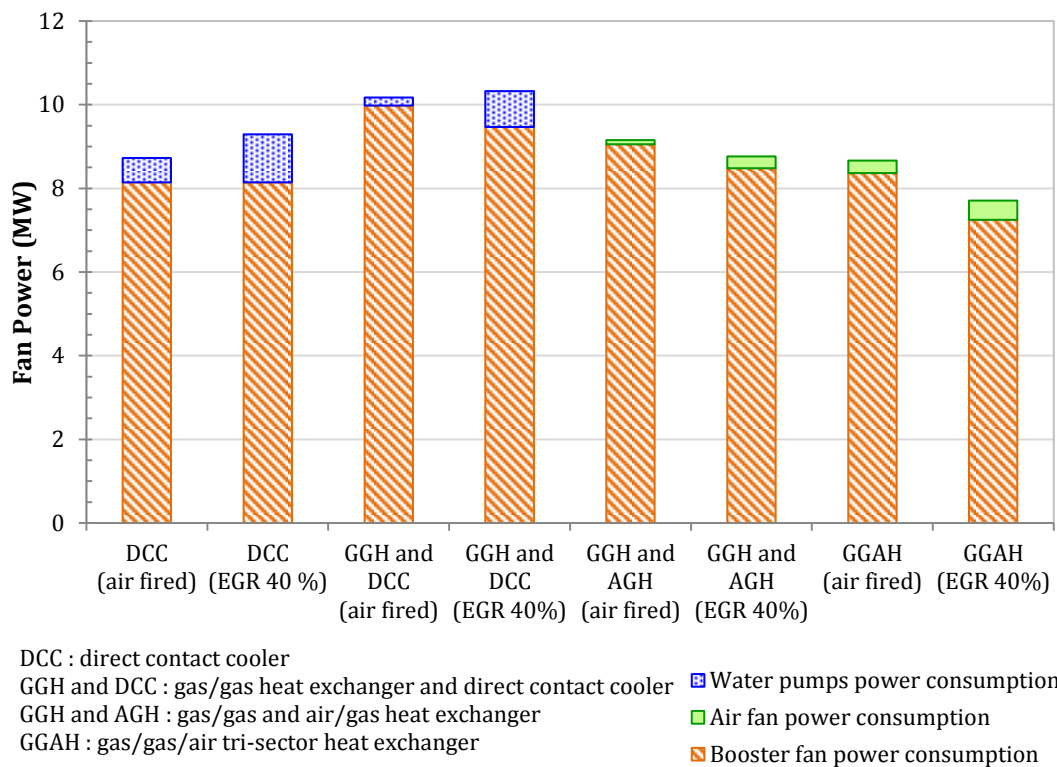


Figure 6.10.- Booster fan, air fan, cooling and process water pumps power consumption per gas turbine train for convectional (air-based combustion) combined cycle gas turbine plant and a plant with 40% exhaust gas recirculation ratio, both with post-combustion capture technology.

7.1. Effect of S-EGR on the CCGT plant with PCC

- S-EGR operated either in parallel or in series with the post-combustion CO₂ capture process significantly increases the CO₂ concentration in the exhaust flue gas of a CCGT power plant, with a relatively small reduction in the oxygen levels in the combustion to approximately 19 vol% from 21 vol% in the ambient air.
 - A CO₂ concentration of 14 vol% is possible at the inlet of the PCC unit with S-EGR in parallel operating at 70% recirculation ratio with 96% PCC efficiency and 97% selective CO₂ transfer efficiency.
 - A CO₂ concentration of 13 vol% is possible at the inlet of the PCC unit with S-EGR in series operating with 95% selective CO₂ transfer efficiency and 31% PCC efficiency.
- The assessment of the compressor and the turbine behaviour of an F-class gas turbine engine, i.e. GE 9F-class, with S-EGR, conducted by evaluating the dimensionless parameters groups that constitute the compressor and the turbine performance curves, indicates that a small deviation from the design operation point, i.e. air-based combustion at ISO ambient conditions, is expected for a range of CO₂ concentration up to 9-10 vol% in the CO₂-enriched air stream fed to the gas turbine compressor. This range is the equivalent to 13-14 vol% CO₂ in the gas turbine exhaust flue gas.
- For both configurations, S-EGR in parallel and S-EGR in series, the gas turbine power output could increase by approximately 15 MW, equivalent to 5% of the gas turbine net power output, as result of the higher density of the CO₂-enriched air compared to ambient air at the same temperature, i.e. 15 °C. Yet, the expected temperature rise through the selective CO₂ transfer system, mainly due to sensible heat transfer from the flue gas to the air, results in a marginal increase in the gas turbine power output with S-EGR in parallel, or even in a reduction in the power output with S-EGR in series, for the operating parameters described above.
- The variation of the thermal and physical properties of the working fluid in the gas turbine, compared to the reference case, is considerably small. Yet, the smaller ratio of specific heats at high CO₂ concentrations leads to a lower compressor outlet

temperature and a higher gas turbine exhaust temperature. The larger amount of heat in the flue gas is used in the bottoming cycle to increase the production of high pressure steam. Consequently, the steam turbine power output increases by approximately 34 MW and 30 MW, and the combined cycle net power output increases by approximately 42 MW and 18 MW, with the S-EGR in parallel configuration and the S-EGR in series configurations described above, respectively. This corresponds to 5.2% and 2.3% of the combined cycle net power output in each configuration. The net increase in the combined cycle power output has been evaluated considering the energy penalty due to steam extraction for the MEA scrubbing process, auxiliary power consumption in the power plant and in the capture plant, and the power consumption for CO₂ compression.

- The increase in the net power output is offset by an increase in the thermal input. A higher natural gas flow rate is required to maintain the turbine inlet temperature at the design value of 1371 °C. The heat input increases by 27 MWth and 8 MWth with S-EGR in parallel and S-EGR in series, respectively and the net thermal efficiency of the combined cycle increases by 0.55 %point and 0.83 %point.
- Regarding the effect on the PCC unit, S-EGR in parallel reduces the flow rate of the flue gas stream entering the absorber, e.g. by 70% at 70% recirculation ratio, in addition to increasing the CO₂ concentration. The PCC efficiency, required to achieve 90% overall CO₂ capture level, exponentially increases with increasing the fraction of the flue gas diverted to the selective CO₂ transfer unit, for a given CO₂ transfer efficiency. The diameter of the absorber column is thus considerably smaller, yet a higher packing section for absorption is necessary, compared to air-based combustion and 35% EGR.
- S-EGR operated in series to the PCC process requires a considerably lower PCC efficiency than 90%, to achieve a 90% overall CO₂ capture level. The total amount of the flue gas generated in the gas turbine is, however, treated and similar diameter of the absorber as in air-based combustion is required. Yet the height of the absorption packing section is considerably smaller compared to air-based combustion and 35% EGR.
- The effect of S-EGR on the PCC process is evaluated in terms of reduction in packing volume and in specific reboiler duty, compared to the reference case with an air-based combustion CCGT power plant with PCC.

- S-EGR in parallel operating at 70% recirculation, 97% selective CO₂ transfer efficiency and 96% PCC efficiency results in a reduction of 46% in packing volume and 5% in specific reboiler duty, compared to air-based combustion, and of 10% in packing volume and 2% in specific reboiler duty, compared to EGR at 35% recirculation ratio.
- S-EGR in series operating at 95% selective CO₂ transfer efficiency and 32% PCC efficiency results in a reduction of 64% in packing volume and 6.6% in specific reboiler duty, compared to air-based configuration, and of 33% in packing volume and 2% in specific reboiler duty, compared to S-EGR in parallel at 70% recirculation ratio for a similar CO₂ concentration in the flue gas of approximately 13-14 vol%.
- Despite of the fact that the largest reduction in absorber packing volume is obtained for S-EGR in series operating at 95% CO₂ transfer efficiency, the design and operation of the selective CO₂ transfer unit to achieve high efficiencies is more challenging than in S-EGR in parallel, since the CO₂ concentration in the flue gas entering this unit is smaller in the former configuration, where the CO₂ is partially removed in the PCC unit.

7.2. Practical feasibility of rotary adsorption for S-EGR

- The conceptual design assessment of the selective CO₂ transfer system with the technology of adsorption in a rotary wheel, conclude that the amount of adsorbent material estimated for activated carbon requires two or more rotary wheels, of approximately 24 m diameter and 2 m long, to achieve the selective CO₂ transfer efficiency specified in the following configurations. It is based on the physical and structured parameters assumed in this work.
 - With S-EGR in parallel, the use of at least two rotary wheels is necessary to achieve 97% CO₂ transfer efficiency from a concentration of 14 vol% in the flue gas entering the system.
 - With S-EGR in series, the use of at least two rotary wheels is necessary to achieve 90 % CO₂ transfer efficiency for a CO₂ concentration of 14 vol% in the flue gas entering the system.
- A 100% reduction in the amount of solid is possible with Zeolite X13. Its hydrophilic properties are, however, detrimental to capacity and would require dehydration to reduce water concentration from 4 vol% in the flue gas leaving the direct contact

cooler saturated in moisture at 30 °C, to around 0.1 vol% with the associate increase in the capital and operational cost.

- The development of new materials for this specific application appears therefore necessary to minimise the amount of solid required and, eventually, the number and the size of the rotary wheels within practical limits.
- The parametric analysis performed in the optimisation study indicates that increasing the adsorbed saturation capacity from 3 mol/ kg, typically the capacity of activated carbon, to approximately 10 mol/ kg significantly reduces the solid mass requirements. Any further increase then results in a marginal gain. It also shows that a moderate affinity of the adsorbent material for CO₂ is preferable to maximise the working capacity and minimise the solid material inventory. For a saturation adsorbed capacity of 3 mol/kg, an enthalpy of adsorption within a range from 24 to 28 kJ/mol_{CO₂} and a pre-exponential factor of the equilibrium constant within a range from $2 \cdot 10^{-6}$ to $9 \cdot 10^{-6}$ kPa⁻¹, would result in a solid material inventory below 200 kg, i.e. approximately the limit for the use of only one rotary wheel system. These are the key parameters indicating the shape of adsorption equilibrium curves and, thus, the affinity of the adsorbent for CO₂ and the temperature dependency. In comparison, the activated carbon considered as reference in this work has an enthalpy of adsorption of 22 kJ/mol_{CO₂} and a pre-exponential factor of $2 \cdot 10^{-6}$ kPa⁻¹.
- It is also necessary that the presence of moisture in the flue gas does not affect the CO₂ adsorption capacity of the adsorbent for a range of water concentrations in the flue gas up to 10 vol%.
- The optimisation of the operating conditions indicates that the temperatures of the flue gas and the air streams entering the system have a small effect on the adsorbent mass, under the assumption of equilibrium. Lower flue gas temperature is thermodynamically favourable to the process and enhances CO₂ adsorption, yet the cooled temperature is limited by the cooling system upstream of the CO₂ transfer system. Higher air temperature, e.g. if a pre-heated air stream is used for regeneration, decreases the working cycle capacity, since the smaller cooling capacity results in a higher temperature of the adsorbent entering the adsorption section in the wheel. The overall adsorption/desorption process is favoured using air at near-ambient temperature. Similarly, a higher ambient air temperature would slightly decrease the CO₂ transfer efficiency by 0.5 %points per 10 °C increase, for a given mass of solid.

7.3. Dry cooling options for CCGT plants with PCC

- Hybrid cooling systems, consisting of a gas/gas heat exchanger and a direct contact cooler, reduce cooling and process water usage by 67% and 35% respectively and ensure that an appropriate stack temperature in excess of 70 °C and an appropriate absorber inlet temperature of approximately 45 °C can be achieved.
- Dry air-cooled systems can be implemented to replace completely the direct contact cooler, eliminating the need for water usage to cool the flue gas prior to the absorber. Water savings with the removal of the direct contact cooler consist of water withdrawal from a fresh water source in a once-through cooling system, and water consumption in a recirculated and hybrid cooling systems with wet cooling towers.
- A configuration with two rotary heat exchangers in series and a configuration with a single gas/gas/air heat exchanger with a trisector arrangement show good thermal performance for an air flow rate of 300 kg/s. A dry cooling system with a trisector configuration reduces complexity, the size and, potentially, the capital cost compared with a configuration with two rotary heat exchangers in series.
- For both configurations, pressure drop in the system is not significantly increased compared to a wet cooling configuration. The power consumption of the air fan is relatively small and equivalent in magnitude to the power of cooling water pumps in wet and hybrid configurations.
- Dry cooling systems are highly dependent on ambient air temperature. For the air/gas heat exchanger design for 15 °C, larger cooling air flow rates can compensate the increase on exhaust flue gas temperature at higher ambient temperatures up to 30 °C. Above this limiting value larger heat exchanger size, combined with a higher cooling air mass flow rate, need to be implemented.
- In CCGT plants with exhaust gas recirculation of 40%, the higher absolute humidity of the exhaust flue gas leaving the heat recovery steam generator results a larger cooling and process water demand to cool the gas down to 45 °C at the absorber inlet, in both wet and hybrid cooling systems. In dry air-cooled systems, the flow rate of the CO₂-depleted gas leaving the absorber decreases, combined with the larger amount of heat that needs to be removed from the gas stream, results in higher cooling air flow rates of 450 kg/s and 400 kg/s for a configuration with two rotary heat exchangers in series and with a gas/gas/air trisector heat exchanger, respectively.

Conclusions of this sections have been presented in Herraiz et al. (2015)

7.4. Limitations and recommendations for future work

The following discusses some of the limitations of the work presented here to recommendation and directions for further research.

- a) The assessment of the gas turbine performance with S-EGR conducted in this thesis considers operation conditions, pressures and temperatures typical of GE F-class gas turbine engines. The effect of S-EGR on the gas turbine and combustion process should be investigated with different operation conditions, e.g. high pressures and temperatures, and/or combustion systems typical of other GTs manufacturers, e.g. H-class gas turbine, reheat combustion system.
- b) Combustion experiments at simulated EGR conditions, conducted in a bench scale lean premixed burner currently used in GE F-class gas turbine technology, suggests a minimum oxygen level of 16-17 vol% in the combustor to ensure flame stability, high combustion efficiency and acceptable levels of CO and unburned hydrocarbons. This oxygen level is achieved at 35% EGR ratio, which corresponds to 2-3 vol% CO₂ in the combustor. The strategy of S-EGR results in higher CO₂ concentrations in the combustor of approximately 9-10 vol%, maintaining oxygen levels at approximately 18-19 vol%. The combustion process at simulated S-EGR conditions needs to be experimentally investigated to evaluate the effect on flame stability, e.g. flash back and blow-off limits, and burner operation, e.g. flame temperature, flame length and CO and unburned hydrocarbons emissions. Combustion tests may define an envelope of possible combinations of CO₂ and oxygen concentrations in the combustor, to eventually identify limits for operation with S-EGR. A deliverable of this thesis consists of the definition of the experimental conditions for further combustion test. Experimental combustion tests will be undertaken in a pre-mixed generic natural gas burner operated at industrial engine representative conditions at Cardiff University's Gas Turbine Research Centre (GTRC) within the scope of the EPSRC project "Selective Exhaust Gas Recirculation for Carbon Capture with Gas Turbines: Integration, Intensification, Scale-up and Optimisation" (SELECT 2014).
- c) This thesis considers new-build CCGT plants with PCC and S-EGR. Yet, the potential of S-EGR to be added to air-based combustion CCGT plants with PCC as a retrofit strategy to decrease the efficiency penalty and/or achieve capture levels in excess of 95% needs further investigation.

-
- d) The effect on the CO₂ capture process of increasing the CO₂ concentration in the flue gas is investigated here for chemical absorption with 30 wt% aqueous MEA solvent. The potential benefit highly depends on thermodynamics, kinetics and mass transfer limitations and, thus, the investigation of the effect using different solvents is recommended. Solvent with slower kinetic reaction rates might benefit to a greater extent of increasing the driving force for mass transfer. Additionally, a significantly higher reduction in the specific reboiler duty might be expected for solvents with a higher CO₂ absorption capacity and/or a smaller enthalpy of absorption. The vapor liquid equilibrium curves should indicate a significant increase in CO₂ loading for the increase in CO₂ partial pressure expected with S-EGR. This may be the case of tertiary amines, e.g. methyldiethanolamine (MDEA), or hindered amines, e.g. 2-amino-2-methyl-1-propanol (AMP).
- e) The conceptual design assessment of the selective CO₂ transfer system is performed for the adsorption/desorption process under equilibrium conditions. For classes of adsorbents with equilibrium parameters and thermodynamic properties within the envelope identified in this thesis, the next steps for performance assessment of the selective CO₂ transfer system would consist of adding the kinetics of the diffusion of CO₂ in the porous material. Structured adsorbents in the form of monoliths offers short diffusion lengths and kinetic of physisorption are typically fast, yet the solid mass requirements are expected to increase from the equilibrium predictions. Adsorption kinetics are necessary in the optimisation of the flue gas surface velocity and the rotation speed, and eventually the diameter and height of the rotary wheel, as these operation and design parameters determine the contact time between the adsorbent and the gas.
- f) Using the guidelines for adsorbent material development provided in this work, a rigorous screening of the literature is a useful step to identify the most promising class of adsorbent for this application. The current literature only focuses on adsorbents for downstream capture systems.
- g) The configuration with S-EGR in parallel with much low volume of flue gas and 14% CO₂ concentration creates opportunities for process intensification of the capture process, in particular the absorber train. In this context, process intensification refers to the development of engineering methods focused on a reduction in the dimensions of CO₂ capture process equipment and capital costs, as an effective way to reduce the cost of electricity of gas CCS.

- h) Rotary adsorption systems for selective CO₂ transfer can potentially be applied to coal-fired power plants and possibly integrated around regenerative rotary gas/gas heat exchangers.
- i) The technical feasibility study of options for water and heat managements was performed for the configurations with an air-based combustion CCGT power plant with PCC and a CCGT power plant with PCC and EGR. This study should be extended to a CCGT with PCC and S-EGR.

7.5. Original contribution addressing knowledge gaps

For the key concepts for CCS on CCGT power plants considered in this thesis, the novelty and contribution to knowledge, as well as recommendation for future work, are summarised in Table 7.1.

Table 7.1.- Key concepts for CCS on CCGT power plants: novelty and contribution to knowledge.

Key concepts for CCS on CCGT power plants	Novelty and contribution to knowledge in this thesis	Recommendations for future work
1.1.- Options for CO₂ enriching flue gas : Exhaust Gas Recirculation		
<i>Integration with the CCGT power plant: effect on the components of the power plant</i>		
<ul style="list-style-type: none"> • Compressor and turbine 	<p>Process model simulations in this thesis reach the same conclusions as in literature for a GE F-class gas turbine (GT) engine.</p> <ul style="list-style-type: none"> ○ Small deviation of the compressor and turbine performance from the design point at 35% and 40% EGR ratio. ○ Gas turbine performance is highly sensitive to the temperature of the recirculated flue gas stream. A higher compressor inlet temperature (> 15°C) results in GT derating. ○ Different working fluid thermodynamic properties (due to a high CO₂ and H₂O concentrations) results in an increase of the GT exhaust temperature. 	<p>Experimental work still required at pilot plant scale (at least)</p>
<ul style="list-style-type: none"> • Combustion 		<p>Experimental work still required at pilot plant scale (at least) for different operating conditions to represent a wider range of GT engines.</p>
<ul style="list-style-type: none"> • Steam cycle 	<p>Process model simulations shows that EGR results in a higher steam mass flow rate in the HRSG and steam turbines (ST) power output [1, 2], due to an increase in the GT exhaust temperature.</p>	
<i>Integration with the steam cycle: thermal energy supply</i>	<p>Similar grade of integration as in an air-based combustion CCGT power plant with PCC (without EGR)</p>	
<i>Effect on post-combustion capture process</i>	<p>Process model simulations performed for 35% EGR ratio results in a smaller reduction in the specific reboiler duty of approx. 3% and similar reduction of the absorber packing volume of approx. 40%. This deviation is due to different operation conditions, e.g. flue gas inlet temperature, solvent lean loading and/or different optimisation procedure.</p>	<p>Common framework to in process model simulation is necessary. Experimental work required in a dedicated pilot plant designed for a typical CO₂ conc. in gas-fired power plants.</p>

Table 7.1.- Key concepts for CCS on CCGT power plants: novelty and contribution to knowledge (cont.)

Key concepts for CCS on CCGT power plants	Novelty and contribution to knowledge in this thesis	Recommendations for future work
1.2.- Options for CO₂ enriching flue gas : Selective Exhaust Gas Recirculation		
<i>Integration with the CCGT power plant: effect on the gas turbine components</i>		
<ul style="list-style-type: none"> • Compressor and turbine performance 	<p>Process simulations of a CCGT with F-class gas turbine technology suggests:</p> <ul style="list-style-type: none"> ○ A minimum deviation of the compressor and turbine operating conditions with S-EGR from the design point. ○ The high CO₂ conc. in the working fluid results in an increase of the GT power output for a compressor inlet temperature of 15 °C (ISO) due to the higher density. ○ Yet the likely increase in the temperature when the air is enriched in CO₂ is detrimental for the compressor performance. 	<p>Effect of S-EGR on compressor and turbine performance requires further investigation in process simulation in a detailed model and experimental texts</p>
<ul style="list-style-type: none"> • Combustion 	<p>Operating conditions in the combustor of the GT with S-EGR are defined in this work to provide the conditions for further experimental investigation within the scope of EPRSC SELECT project</p>	<p>The combustion process with a CO₂-enriched air (approx. 10 vol% CO₂ and 18 vol% O₂) needs to be experimentally investigated at high pressure and temperature</p>
<ul style="list-style-type: none"> • Steam cycle 	<p>Process simulations indicate that the GT exhaust temperature increases at high CO₂ conc. in the working fluid, the high pressure steam production increases and thus the steam turbine power output. No modifications are required in HRSG or steam turbines since the temperature profile does not change significantly.</p>	
<i>Integration with the steam cycle: thermal energy supply</i>	<p>Similar grade of integration as in air-based combustion CCGT power plant with PCC</p>	
<i>Effect on post-combustion capture process</i>	<ul style="list-style-type: none"> ○ S-EGR in parallel with the PCC process reduces the absorber packing volume by 46% and the specific reboiler duty by 5%. ○ S-EGR in series reduces the absorber packing volume by 64% and the specific reboiler duty by 7%, both compared to air-based combustion CCGT with PCC (reference case) 	<p>The benefits of S-EGR on the CO₂ capture process need to be investigated experimentally in a pilot plant designed and optimised for typical CO₂ conc. in gas-fired power plants.</p>
<i>Integration with selective CO₂ transfer system</i>	<p>Design and operating parameters in the S-EGR system with a large effect on the CCGT performance are: pressure drop (low to minimise auxiliary electricity consumption); heat transfer and temperature rise in the air side (low CO₂-enriched air temperature to prevent derating the gas turbine); selectivity to CO₂ over N₂, O₂ and H₂O (high to maintain high oxygen levels in the combustor) and leakage level (low to maintain high oxygen levels in the combustor)</p>	<p>An integrated model is required for a future economic analysis</p>

Table 7.1.- Key concepts for CCS on CCGT power plants: novelty and contribution to knowledge (cont.)

Key concepts for CCS on CCGT power plants	Novelty and contribution to knowledge in this thesis	Recommendations for future work
2.- Technology for Selective CO₂ transfer process		
<i>Selective CO₂ membrane systems</i>	Alternative technologies for S-EGR are possible with a potential reduction in pressure drop, operation and capital costs.	Detailed engineering design is required to investigate the advantages of rotary adsorption over CO ₂ selective membranes.
<i>Physical adsorption in a rotary wheel configuration</i>	<p>The conceptual design assessment of the equilibrium of adsorption/desorption process concludes that</p> <ul style="list-style-type: none"> ○ Physical adsorption in a rotary wheel appears as an option for S-EGR application and allows the regeneration of the solvent with air at near ambient conditions ○ Yet commercially available materials e.g. activated carbon and Zeolites, results in high adsorbent requirements and large size/number of rotary wheel no practically feasible ○ The parametric analysis results in a range of values for saturation capacity, equilibrium constant and enthalpy of adsorption are defined for practical feasibility aiming to provide guidelines for new adsorbent material development. 	A rigorous model including mass transfer resistance / diffusion in the pores and heat transfer resistance is necessary to evaluate the actual solid material inventory and to optimise the rotary speed and flue gas velocity.
3.- Water and heat management in Gas CCS with amine based CO₂ capture systems		
<i>Process water integration options in the CO₂ capture system</i>	Novel options using rotary gas/gas heat exchangers are technically feasible to reduce cooling and process water demand around a CCGT plant equipped with amine-based scrubbing technology.	Further work needs to be done to investigate options to manage cooling and process water demand within the limit of the carbon capture system.
<i>Dry cooling options in power plant</i>	<ul style="list-style-type: none"> ○ Hybrid cooling systems, with a gas/gas heat exchanger and a direct contact cooler, reduce cooling and process water usage by 67% and 35% respectively. ○ Dry cooling systems with gas/gas/air heat exchangers eliminates process and cooling water requirements in the direct contact cooler upstream of the absorber 	Hybrid and Dry –cooling systems has to be investigated for the configurations with S-EGR in parallel and S-EGR in series.
<i>Reheat of the CO₂-depleted gas to the stack</i>	Rotary gas/gas heat exchangers can increase the CO ₂ -depleted gas temperature above 70 °C.	

References

- Abanades, J.C. et al., 2015. Emerging CO₂ capture systems. *International Journal of Greenhouse Gas Control*, 40, pp.126–166.
- Aboudheir, A. & ElMoudir, W., 2009. Performance of formulated solvent in handling of enriched CO₂ flue gas stream. *Energy Procedia*, 1(1), pp.195–204.
- Abu Zahra, M.R.M., 2009. *Carbon Dioxide Capture from Flue Gas - Development and Evaluation of Existing and Novel Process Concepts*. Technische Universiteit Delft. Available at: <http://www.google.com/patents/US20110226010>.
- Akram, M. et al., 2016. Performance evaluation of PACT Pilot-plant for CO₂ capture from gas turbines with Exhaust Gas Recycle. *International Journal of Greenhouse Gas Control*, 47, pp.137–150. Available at: <http://linkinghub.elsevier.com/retrieve/pii/S1750583616300470>.
- Amann, J.M., Kanniche, M. & Bouallou, C., 2009. Natural gas combined cycle power plant modified into an O₂/CO₂ cycle for CO₂ capture. *Energy Conversion and Management*, 50(3), pp.510–521. Available at: <http://dx.doi.org/10.1016/j.enconman.2008.11.012>.
- AMPGas, 2012. Adsorption Materials and Processes for carbon capture from Gas-fired power plants. Available at: [http://gow.epsrc.ac.uk/NGBOViewGranNext Generation CCS Technologyt.aspx?GrantRef=EP/J02077X/1](http://gow.epsrc.ac.uk/NGBOViewGranNextGenerationCCSTechnologyt.aspx?GrantRef=EP/J02077X/1) [Accessed February 2, 2016].
- Aronu, U.E. et al., 2011. Solubility of CO₂ in 15, 30, 45 and 60 mass% MEA from 40 to 120 C and model representation using the extended UNIQUAC framework. *Chemical Engineering Science*, 66(24), pp.6393–6406. Available at: <http://dx.doi.org/10.1016/j.ces.2011.08.042>.
- Aspen Tech, 2016. Aspen Plus V7.0 / Windows. Available at: <http://www.aspentech.com/products/engineering/aspen-plus/>.
- Bai, R. & Yang, R.T., 2001. A Thermodynamically Consistent Langmuir Model for Mixed Gas Adsorption. *Journal of colloid and interface science*, 239(2), pp.296–302. Available at: <http://www.ncbi.nlm.nih.gov/pubmed/11426993>.
- Baker, R.W. et al., 2011. Gas separation process using membranes with permeate sweep to remove CO₂ from combustion gases. *US Patent 7964020B2*.
- Baker, R.W., 2004. *Membrane Technology and Applications* 2nd Editio., John Wiley & Sons.
- Belaissaoui, B. et al., 2013. CO₂ capture for gas turbines: An integrated energy-efficient process combining combustion in oxygen-enriched air, flue gas recirculation, and membrane separation. *Chemical Engineering Science*, 97, pp.256–263. Available at: <http://dx.doi.org/10.1016/j.ces.2013.04.027>.
- Ben-Mansour, R. et al., 2016. Carbon capture by physical adsorption: Materials, experimental investigations and numerical modeling and simulations – A review. *Applied Energy*, 161(JANUARY), pp.225–255. Available at: <http://www.sciencedirect.com/science/article/pii/S0306261915012386>.
- Bhargava, R. et al., 2004. A Feasibility Study of Existing Gas Turbines for Recuperated , Intercooled , and Reheat Cycle. *Journal of Engineering for Gas Turbines and Power*, 126(July), pp.531–544.
- Bianchi, M. et al., 2010. Gas Turbine Power Augmentation Technologies: A Systematic Comparative Evaluation Approach. *Proceedings of ASME Turbo Expo 2010, GT2010-*

- 229, pp.1–9.
- Biliyok, C. & Yeung, H., 2013. Evaluation of natural gas combined cycle power plant for post-combustion CO₂ capture integration. *International Journal of Greenhouse Gas Control*, 19, pp.396–405. Available at: <http://dx.doi.org/10.1016/j.ijggc.2013.10.003>.
- Bolland, O. & Mathieu, P., 1998. Comparison of two CO₂ removal options in combined cycle power plants. *Energy Conversion and Management*, 39(16–18), pp.1653–1663.
- Bolland, O. & Saether, S., 1992. New Concepts for Natural Gas Fired Power Plants. *Energy Conversion and Management*, 33(5), pp.467–475.
- Botero, C. et al., 2009. Redesign, Optimization, and Economic Evaluation of a Natural Gas Combined Cycle with the Best Integrated Technology CO₂ Capture. *Energy Procedia*, 1(1), pp.3835–3842. Available at: <http://dx.doi.org/10.1016/j.egypro.2009.02.185>.
- Boulet, A. & Khiavi, S., 2015. Method of adsorptive gas separation using thermally conductive contactor structure/ US 2015/0068397 A1.
- Boyce, M.P., 2006. *Gas Turbine Engineering Handbook* 3rd Ed., Houston, Texas, USA: Gulf Professional Publishing.
- Brandani, F. et al., 2004. Adsorption Kinetics and Dynamic Behavior of a Carbon Monolith. *Adsorption*, 10, pp.99–109. Available at: <http://link.springer.com/10.1023/B:ADSO.0000039866.37214.6a>.
- Brooks, F.J., 2000. GE Gas Turbine Performance Characteristics. *GE Power Systems*, GER-3567H.
- Bui, M. et al., 2014. Dynamic modelling and optimisation of flexible operation in post-combustion CO₂ capture plants-A review. *Computers and Chemical Engineering*, 61, pp.245–265. Available at: <http://dx.doi.org/10.1016/j.compchemeng.2013.11.015>.
- Burdet, A. et al., 2010. Combustion under Flue Gas Recirculation Conditions in a Gas Turbine Lean Premix Burner. *Proceedings of ASME Turbo Expo 2010, June 14-18, 2010, Glasow, UK*, (GT2010-23396), pp.1–9.
- Byers, E. a, Hall, J.W. & Amezaga, J.M., 2014. Author ' s personal copy Electricity generation and cooling water use : UK pathways to 2050 §. , 25, pp.16–30.
- Chacartegui, R. et al., 2012. SPHERA project: Assessing the use of syngas fuels in gas turbines and combined cycles from a global perspective. *Fuel Processing Technology*, 103, pp.134–145. Available at: <http://dx.doi.org/10.1016/j.fuproc.2011.11.004>.
- Cohen, H., Rogers, C.F.C. & Saravanamuttoo, H.I.H., 1996. *Gas Turbine Theory* 4th Ed., Longman Group Limited.
- Committee on Climate Change, 2015. Sectoral scenarios for the Fifth Carbon Budget. , (November). Available at: <https://d2kx2p8nxa8ft.cloudfront.net/wp-content/uploads/2015/11/Sectoral-scenarios-for-the-fifth-carbon-budget-Committee-on-Climate-Change.pdf>.
- Cooke, D.H., 1985. On Prediction of Off-Design Multistage Turbine Pressures by Stodola's Ellipse. *Journal of Engineering for Gas Turbines and Power*, 107(July 1985), p.596.
- Cooper, J., 1991. Booster Fans and Gas Reheaters for Wet Flue-Gas Desulphurisation Systems, Presented at the International Power Generation Conference. *ASME*, 91–JPGC–Pw.
- Cormos, C.C., Vatopoulos, K. & Tzimas, E., 2013. Assessment of the consumption of water and construction materials in state-of-the-art fossil fuel power generation technologies involving CO₂ capture. *Energy*, 51, pp.37–49. Available at:

- <http://dx.doi.org/10.1016/j.energy.2012.12.050>.
- Dantas, T.L.P. et al., 2011. Carbon dioxide-nitrogen separation through adsorption on activated carbon in a fixed bed. *Chemical Engineering Journal*, 169(1–3), pp.11–19.
- Dantas, T.L.P. et al., 2011. Modeling of the fixed - bed adsorption of carbon dioxide and a carbon dioxide - nitrogen mixture on zeolite 13X. *Brazilian Journal of Chemical Engineering*, 28(3), pp.533–544. Available at: <http://www.scopus.com/inward/record.url?eid=2-s2.0-80052986231&partnerID=tZOtx3y1>.
- Davis, L.B. & Black, S.H., 2000. Dry Low NO_x Combustion Systems for GE Heavy-Duty Gas Turbines. *GE Power Systems*, GER-3568G.
- Delgado, J. a. et al., 2011. Numerical analysis of CO₂ concentration and recovery from flue gas by a novel vacuum swing adsorption cycle. *Computers and Chemical Engineering*, 35, pp.1010–1019.
- Department of Energy and Climate Change and The Rt Hon Amber Rudd MP, 2015. Amber Rudd's speech on a new direction for UK energy policy. Available at: <https://www.gov.uk/government/speeches/amber-rudds-speech-on-a-new-direction-for-uk-energy-policy>.
- Dixon, S.L. & Hall, C.A., 1998. *Fluid mechanics and thermodynamics of turbomachinery* 5th Ed., Elsevier Butterworth-Heinemann.
- Dugas, R.E., 2009. *Carbon Dioxide Absorption , Desorption , and Diffusion in Aqueous Piperazine and Monoethanolamine*.
- EBTF, 2011. European best practice guidelines for assessment of CO₂ capture technologies.
- Eldrid, R., Kaufman, L. & Marks, P., 2001. The 7FB: The Next Evolution of the F Gas Turbine. *GE Power Systems*, GER-4194.
- ElKady, A.M. et al., 2009. Application of Exhaust Gas Recirculation in a DLN F-Class Combustion System for Postcombustion Carbon Capture. *Journal of Engineering for Gas Turbines and Power*, 131(May 2009), p.34505.
- Energy and Climate Change Committee, 2016. Future of carbon capture and storage in the UK - Second Report of Session 2015-2016.
- Energy Technologies Institute, 2015. *Carbon capture and storage: Building the UK carbon capture and storage sector by 2030 - Scenarios and actions*, Available at: <http://www.eti.co.uk/wp-content/uploads/2015/03/CCS-Building-the-UK-carbon-capture-and-storage-sector-by-2013.pdf>.
- ETI (Energy Technologies Institute), 2016. *Reducing the cost of CCS developments in capture plant technology*,
- European Commission, 2014. *A policy framework for climate and energy in the period from 2020 to 2030*,
- European Commission, 2011. *A Roadmap for moving to a competitive low carbon economy in 2050*,
- European Environmental Agency, 2010. Water abstractions for irrigation, manufacturing industry, energy cooling and public water supply (million m³/year) in early 1990s and the period 1997-2007.
- Evulet, A.T. et al., 2009. On the Performance and Operability of GE's Dry Low NO_x Combustors utilizing Exhaust Gas Recirculation for PostCombustion Carbon Capture. *Energy Procedia*, 1(x), pp.3809–3816.

- Fang-Yuan, J., Otto, F.D. & Mather, A.E., 1994. Vapor-Liquid Equilibrium of Carbon Dioxide in Aqueous Mixtures of Monoethanolamine and Methyldiethanolamine. *Industrial & Engineering Chemistry Research*, 33, pp.2002–2005.
- Fernandez, E.S., 2013. *Novel process designs to improve the efficiency of postcombustion carbon dioxide capture*, Available at: <http://homepage.tudelft.nl/v9k6y/thesis-esanchez.pdf>.
- Freguia, S. & Rochelle, G.T., 2003. Modeling of CO₂ capture by aqueous monoethanolamine. *AIChE Journal*, 49(7), pp.1676–1686.
- Ge, T.S. et al., 2008. A review of the mathematical models for predicting rotary desiccant wheel. *Renewable and Sustainable Energy Reviews*, 12(6), pp.1485–1528.
- General Electric Power Generation, 2016. F-class Power Plants. Available at: <https://powergen.gepower.com/products/power-plants/f-class-power-plants.html>.
- General electric thermal power generation, 2016. Steam turbines. Available at: <http://www.ge.com/in/thermal-power/steam-turbine-manufacturers> [Accessed February 2, 2016].
- Gibbins, J. & Chalmers, H., 2008. Carbon capture and storage. *Energy Policy*, 36, pp.4317–4322.
- Gibson, J.A.A. et al., 2016. Adsorption Materials and Processes for Carbon Capture from Gas- Fired Power Plants : AMPGas.
- Global CCS Institute, 2015. The global status of CCS. , pp.1–12.
- Gonzalez Diaz, A. et al., 2014. On the integration of sequential supplementary firing in natural gas combined cycle for CO₂-Enhanced Oil Recovery: A technoeconomic analysis for Mexico. *Energy Procedia*, 63, pp.7558–7567. Available at: <http://dx.doi.org/10.1016/j.egypro.2014.11.791>.
- Grant, P. & Skillings, S., 2009. Decarbonising the GB power sector : evaluating investment pathways , generation patterns and emissions through to 2030. *Redpoint Energy Ltd*, (September).
- Guethe, F. et al., 2011. Flue gas recirculation of the Alstom sequential gas turbine combustor tested at high pressure. *Proceedings of ASME Turbo Expo 2011, June 6-10, 2011, Vancouver, British Columbia, Canada*, (GT2011-45379), pp.1–10.
- Guethe, F., Cruz Garcia, M. & Burdet, A., 2009. Flue Gas Recirculation in Gas Turbine: Investigation of Combustion Reactivity and NO_x emission. *Proceedings of ASME Turbo Expo 2009, June 8-12, 2009, Orlando, Florida, USA*, (GT2009-59221), pp.1–13.
- Gütthe, F., Hellat, J. & Flohr, P., 2009. The Reheat Concept: The Proven Pathway to Ultralow Emissions and High Efficiency and Flexibility. *Journal of Engineering for Gas Turbines and Power*, 131(2), p.021503 1-021503 7.
- Hamborg, E.S. et al., 2014. Results from MEA testing at the CO₂ technology centre mongstad. Part II: Verification of baseline results. *Energy Procedia*, 63, pp.5994–6011. Available at: <http://dx.doi.org/10.1016/j.egypro.2014.11.634>.
- Hasan, M.M.F. et al., 2012. Modeling, Simulation, and Optimization of Postcombustion CO₂Capture for Variable Feed Concentration and Flow Rate. 2. Pressure Swing Adsorption and Vacuum Swing Adsorption Processes. *Industrial & Engineering Chemistry Research*, 51(48), pp.15665–15682.
- Hedin, N. et al., 2013. Adsorbents for the post-combustion capture of CO₂ using rapid temperature swing or vacuum swing adsorption. *Applied Energy*, 104, pp.418–433.

- Available at: <http://dx.doi.org/10.1016/j.apenergy.2012.11.034>.
- Herraiz, L. et al., 2015. Reducing water usage with rotary regenerative gas / gas heat exchangers in natural gas-fired power plants with post-combustion carbon capture. *Energy*, 90, pp.1994–2005. Available at: <http://dx.doi.org/10.1016/j.energy.2015.07.032>.
- Hilliard, M.D., 2008. *A Predictive Thermodynamic Model for an Aqueous Blend of Potassium Carbonate, Piperazine, and Monoethanolamine for Carbon Dioxide Capture from Flue Gas*.
- Hogg, D., 2015. Email from Dougal Hogg, Deputy Chief Engineer - Heater Technology at Howden Group - Howden, on 29th October 2015.
- Howden Group, 2016. No Title. Available at: <http://www.howden.com/products/Pages/ProductSelector.aspx?ProductTypeId=3>.
- Huizeling, E. & Van der Weijde, G., 2011. *ROAD CCS non-confidential FEED study report: special report for the Global Carbon Capture and Storage Institute*,
- Iea, 2013. *Technology Roadmap*, Available at: http://www.springerreference.com/index/doi/10.1007/SpringerReference_7300.
- IEAGHG, 2011. EVALUATION AND ANALYSIS OF WATER USAGE OF POWER PLANTS WITH CO₂ CAPTURE Report : 2010 / 05 March 2011. *Report 2010/05*, (March).
- IGSCC, 2012. Innovative Gas Separation for Carbon Capture. Available at: <http://gow.epsrc.ac.uk/NGBOViewGrant.aspx?GrantRef=EP/G062129/1>.
- International Energy Agency, 2012. *CO₂ capture at gas fired power plants, Report:2012/8*,
- International Energy Agency, 2011. *Cost and Performance of Carbon Dioxide Capture from Power Generation*,
- International Energy Agency, 2004. *Improvement in Power Generation with Post-Combustion Capture of CO₂*, Available at: http://ieaghg.org/docs/General_Docs/Reports/PH4-33 post combustion.pdf.
- International Energy Agency, 2013. *Technology roadmap - Carbon capture and Storage*, Available at: <http://www.iea.org/publications/freepublications/publication/TechnologyRoadmapCarbonCaptureandStorage.pdf>.
- Inventys, 2016. *VeloxoTherm(TM): Breakthrough Carbon Capture Technology*, Available at: <http://www.akercleancarbon.com/section.cfm?path=418,456>.
- Jansohn, P. et al., 2011. Technologies for gas turbine power generation with CO₂ mitigation. *Energy Procedia*, 4(x), pp.1901–1908.
- Jonshagen, K., 2011. *Modern Thermal Power Plants: Aspects on Modelling and Evaluation*.
- Jonshagen, K., Sipöcz, N. & Genrup, M., 2011. A Novel Approach of Retrofitting a Combined Cycle With Post Combustion CO₂ Capture. *Journal of Engineering for Gas Turbines and Power*, 133(1), pp.11703-1–7. Available at: <http://gasturbinespower.asmedigitalcollection.asme.org/article.aspx?articleid=1425741> [Accessed December 1, 2014].
- Jordal, K., Andreas, P., et al., 2012. Design-point and part-load considerations for natural gas combined cycle plants with post combustion capture. *International Journal of Greenhouse Gas Control*, 11, pp.271–282.

- Jordal, K., Ystad, P.A.M., et al., 2012. Design-point and part-load considerations for natural gas combined cycle plants with post combustion capture. *International Journal of Greenhouse Gas Control*, 11, pp.271–282. Available at: <http://linkinghub.elsevier.com/retrieve/pii/S1750583612002198>.
- Kehlhofer, R. et al., 2009. *Combined-Cycle Gas and Steam Turbine Power Plants* 3rd Ed., PennWell. Available at: Online version available at:
- Kitto, J.B. & Stultz, S.C., 1992. *Steam, its generation and use* 41st Ed., The Babcock and Wilcox Company.
- Kodama, A. et al., 2001. The use of psychrometric charts for the optimisation of a thermal swing desiccant wheel. *Applied Thermal Engineering*, 21(16), pp.1657–1674.
- Kutne, P. et al., 2011. Experimental analysis of the combustion behaviour of oxyfuel flames in a gas turbine model combustor. *Proceedings of the Combustion Institute*, 33(2), pp.3383–3390. Available at: <http://dx.doi.org/10.1016/j.proci.2010.07.008>.
- Kvamsdal, H.M. et al., 2010. Maintaining a neutral water balance in a 450 MWe NGCC-CCS power system with post-combustion carbon dioxide capture aimed at offshore operation. *International Journal of Greenhouse Gas Control*, 4(4), pp.613–622.
- Kvamsdal, H.M., Haugen, G. & Svendsen, H.F., 2011. Flue-gas cooling in post-combustion capture plants. *Chemical Engineering Research and Design*, 89(9), pp.1544–1552. Available at: <http://dx.doi.org/10.1016/j.cherd.2011.02.029>.
- Kvamsdal, H.M., Jordal, K. & Bolland, O., 2007. A quantitative comparison of gas turbine cycles with CO₂ capture. *Energy*, 32(1), pp.10–24.
- Li, H., Haugen, G., et al., 2011a. Impacts of exhaust gas recirculation (EGR) on the natural gas combined cycle integrated with chemical absorption CO₂ capture technology. *Energy Procedia*, 4, pp.1411–1418. Available at: <http://dx.doi.org/10.1016/j.egypro.2011.02.006>.
- Li, H., Haugen, G., et al., 2011b. Impacts of exhaust gas recirculation (EGR) on the natural gas combined cycle integrated with chemical absorption CO₂ capture technology. *Energy Procedia*, 4, pp.1411–1418. Available at: <http://linkinghub.elsevier.com/retrieve/pii/S1876610211002037>.
- Li, H., Ditaranto, M. & Berstad, D., 2011a. Technologies for increasing CO₂ concentration in exhaust gas from natural gas-fired power production with post-combustion, amine-based CO₂ capture. *Energy*, 36, pp.1124–1133.
- Li, H., Ditaranto, M. & Berstad, D., 2011b. Technologies for increasing CO₂ concentration in exhaust gas from natural gas-fired power production with post-combustion, amine-based CO₂ capture. *Energy*, 36(2), pp.1124–1133. Available at: <http://dx.doi.org/10.1016/j.energy.2010.11.037>.
- Li, H., Ditaranto, M. & Yan, J., 2012. Carbon capture with low energy penalty: Supplementary fired natural gas combined cycles. *Applied Energy*, 97, pp.164–169. Available at: <http://dx.doi.org/10.1016/j.apenergy.2011.12.034>.
- Li, H. & Yan, J., 2009. Performance Comparison on the Evaporative Gas Turbine Cycles Combined with Different CO₂-Capture Options. *International Journal of Green Energy*, 6(5), pp.512–526. Available at: <http://www.informaworld.com/10.1080/15435070903231369>.
- Liu, F., Guo, H. & Smallwood, G.J., 2003. The chemical effect of CO₂ replacement of N₂ in air on the burning velocity of CH₄ and H₂ premixed flames. *Combustion and Flame*, 133(4), pp.495–497.

- Ma'mun, S. et al., 2005. Solubility of carbon dioxide in 30 mass % monoethanolamine and 50 mass % methyldiethanolamine solutions. *Journal of Chemical and Engineering Data*, 50(2), pp.630–634.
- Macknick, J. et al., 2012. The water implications of generating electricity: water use across the United States based on different electricity pathways through 2050. *Environmental Research Letters*, 7, p.45803. Available at: <http://iopscience.iop.org/1748-9326/7/4/045803/article/>.
- Mangano, E. et al., 2013. Efficient and rapid screening of novel adsorbents for carbon capture in the UK IGSCC project. *Energy Procedia*, 37(0), pp.40–47. Available at: <http://dx.doi.org/10.1016/j.egypro.2013.05.083>.
- Martelli, E., Nord, L.O. & Bolland, O., 2012. Design criteria and optimization of heat recovery steam cycles for integrated reforming combined cycles with CO₂ capture. *Applied Energy*, 92, pp.255–268. Available at: <http://linkinghub.elsevier.com/retrieve/pii/S0306261911007045>.
- Marx, D. et al., 2013. The Role of Water in Adsorption-based CO₂ Capture Systems. *Energy Procedia*, 37, pp.107–114. Available at: <http://www.sciencedirect.com/science/article/pii/S1876610213001008>.
- Masri, a R. & Barlow, R.S., 1992. Chemical Kinetic Effects in Nonpremixed Flames of H₂ / CO₂ Fuel. *Combustion and Flame*, 91(1992), pp.285–309.
- Merkel, T.C. et al., 2013. Selective Exhaust Gas Recycle with Membranes for CO₂ Capture from Natural Gas Combined Cycle Power Plants. *Industrial & Engineering Chemistry Research*, 52, pp.1150–1159. Available at: <http://pubs.acs.org/doi/abs/10.1021/ie302110z>.
- Min, J. et al., 2011. Impact of CO₂, N₂ or Ar diluted in air on the length and lifting behavior of a laminar diffusion flame. *Proceedings of the Combustion Institute*, 33(1), pp.1071–1078.
- National Energy Technology Laboratory - U.S. Department of Energy, 2011. *Carbon Capture Approaches for Natural Gas Combined Cycle Systems*,
- NGCT2, 2016. NGCT2. Available at: <http://www.eti.co.uk/project/ccs-next-generation-gas-capture-technology/>.
- Notz, R., Mangalapally, H.P. & Hasse, H., 2012. Post combustion CO₂ capture by reactive absorption: Pilot plant description and results of systematic studies with MEA. *International Journal of Greenhouse Gas Control*, 6, pp.84–112. Available at: <http://linkinghub.elsevier.com/retrieve/pii/S1750583611002143>.
- Oexmann, J., 2011. *Post - Combustion CO₂ Capture : Energetic Evaluation of Chemical Absorption Processes in Coal - Fired Steam Power Plants*. Technischen Universität Hamburg-Harburg.
- Oexmann, J., Hensel, C. & Kather, A., 2008. Post-combustion CO₂-capture from coal-fired power plants: Preliminary evaluation of an integrated chemical absorption process with piperazine-promoted potassium carbonate. *International Journal of Greenhouse Gas Control*, 2(4), pp.539–552.
- Oexmann, J. & Kather, A., 2009. Post-combustion CO₂ capture in coal-fired power plants: Comparison of integrated chemical absorption processes with piperazine promoted potassium carbonate and MEA. *Energy Procedia*, 1(1), pp.799–806.
- Oxburgh, 2016. *LOWEST COST DECARBONISATION FOR THE UK: THE CRITICAL ROLE OF CCS. Report to the Secretary of State for Business, Energy and Industrial*

- Strategy from the Parliamentary Advisory Group on Carbon Capture and Storage (CCS)*,
- De Paepe, W. et al., 2012. Discussion of the effects of recirculating exhaust air on performance and efficiency of a typical microturbine. *Energy*, 45(1), pp.456–463. Available at: <http://dx.doi.org/10.1016/j.energy.2011.11.060>.
- Pavri, R. & Moore, G.D., 2001. Gas Turbine Emissions and Control. *GE Power Systems*, GER-4211.
- Plaza, J.M., Van Wagener, D. & Rochelle, G.T., 2010. Modeling CO₂ capture with aqueous monoethanolamine. *International Journal of Greenhouse Gas Control*, 4(2), pp.161–166. Available at: <http://dx.doi.org/10.1016/j.egypro.2009.01.154>.
- PSE, 2016. gPROMS ModelBuilder V4.1.0 / Windows. Available at: <http://www.psenterprise.com/modelbuilder.html> [Accessed January 1, 2016].
- Razak, A., 2007. *Industrial Gas Turbines. Performance and Operability* 1st Ed., England: Woodhead publishing limited.
- Razi, N., Svendsen, H.F. & Bolland, O., 2014. Assessment of mass transfer correlations in rate-based modeling of a large-scale CO₂ capture with MEA. *International Journal of Greenhouse Gas Control*, 26, pp.93–108. Available at: <http://dx.doi.org/10.1016/j.ijggc.2014.04.019>.
- Razi, N., Svendsen, H.F. & Bolland, O., 2013. Validation of mass transfer correlations for CO₂ absorption with MEA using pilot data. *International Journal of Greenhouse Gas Control*, 19, pp.478–491. Available at: <http://dx.doi.org/10.1016/j.ijggc.2013.10.006>.
- Rezaei, F. et al., 2010. Comparison of traditional and structured adsorbents for CO₂ separation by vacuum-swing adsorption. *Industrial and Engineering Chemistry Research*, 49(10), pp.4832–4841.
- Rochelle, G.T., 2012. Thermal degradation of amines for CO₂ capture. *Current Opinion in Chemical Engineering*, 1(2), pp.183–190. Available at: <http://dx.doi.org/10.1016/j.coche.2012.02.004>.
- Røkke, P.E. & Hustad, J.E., 2005. Exhaust gas recirculation in gas turbines for reduction of CO₂ emissions; Combustion testing with focus on stability and emissions. *International Journal of Thermodynamics*, 8(4), pp.167–173.
- Ruthven, D.M., 1984. *Principles of Adsorption and Adsorption Processes* Illustrate., John Wiley & Sons.
- Samanta, A. et al., 2012. Post-combustion CO₂ capture using solid sorbents: A review. *Industrial and Engineering Chemistry Research*, 51(4), pp.1438–1463.
- Sánchez, D. et al., 2010. Performance analysis of a heavy duty combined cycle power plant burning various syngas fuels. *International Journal of Hydrogen Energy*, 35, pp.337–345.
- Sanchez Fernandez, E. et al., 2014. Thermodynamic assessment of amine based CO₂ capture technologies in power plants based on European Benchmarking Task Force methodology. *Fuel*, 129, pp.318–329. Available at: <http://dx.doi.org/10.1016/j.apenergy.2014.04.066>.
- Sander, F. et al., 2011. Flue Gas Recirculation in a Gas Turbine: Impact on Performance and Operational Behavior. *Proceedings of ASME Turbo Expo 2011, June 6-10, 2011, Vancouver, British Columbia, Canada*, pp.1–10.
- Saravanamuttoo, H.I.H. & Maclsaac, B.D., 1983. Thermodynamic Models for Pipeline Gas

- Turbine Diagnostics. *Journal of Engineering for Power*, 105, pp.875–884.
- Schakel, W., Pfister, S. & Ramírez, A., 2015. International Journal of Greenhouse Gas Control Exploring the potential impact of implementing carbon capture technologies in fossil fuel power plants on regional European water stress index levels. *International Journal of Greenhouse Gas Control*, 39, pp.318–328. Available at: <http://dx.doi.org/10.1016/j.ijggc.2015.05.031>.
- SELECT, 2014. Selective Exhaust Gas Recirculation for Carbon Capture with Gas Turbines: Integration, Intensification, Scale-up and Optimisation. Available at: <http://gow.epsrc.ac.uk/NGBOViewGrant.aspx?GrantRef=EP/M001482/1>.
- Serna-Guerrero, R., Belmabkhout, Y. & Sayari, A., 2010. Modeling CO₂ adsorption on amine-functionalized mesoporous silica: 1. A semi-empirical equilibrium model. *Chemical Engineering Journal*, 161(1–2), pp.173–181. Available at: <http://dx.doi.org/10.1016/j.cej.2010.04.024>.
- Siemens power generation, 2016. Steam turbines. Available at: <http://www.energy.siemens.com/hq/en/fossil-power-generation/steam-turbines/steam-turbine-products.htm> [Accessed February 2, 2016].
- Sipöcz, N. & Tobiesen, F.A., 2012. Natural gas combined cycle power plants with CO₂ capture – Opportunities to reduce cost. *International Journal of Greenhouse Gas Control*, 7, pp.98–106.
- Spence, B., Horan, D. & Tucker, O., 2014. The peterhead-goldeneye gas post-combustion CCS project. *Energy Procedia*, 63, pp.6258–6266. Available at: <http://dx.doi.org/10.1016/j.egypro.2014.11.657>.
- Stéphenne, K., 2014. Start-up of world's first commercial post-combustion coal fired ccs project: Contribution of shell cansolv to saskpower boundary dam iccs project. *Energy Procedia*, 63, pp.6106–6110. Available at: <http://dx.doi.org/10.1016/j.egypro.2014.11.642>.
- Swisher, J.A. & Bhowan, A.S., 2014. Analysis and optimal design of membrane-based CO₂ capture processes for coal and natural gas-derived flue gas. *Energy Procedia*, 63, pp.225–234. Available at: <http://dx.doi.org/10.1016/j.egypro.2014.11.024>.
- THE INTERGOVERNMENTAL PANEL ON CLIMATE CHANGE (IPCC), 2014. *Climate Change 2014: Synthesis Report. Contribution of Working Groups I, II and III to the Fifth Assessment Report of the Intergovernmental Panel on Climate Change*,
- Thimsen, D. et al., 2014. Results from MEA testing at the CO₂ Technology Centre Mongstad. Part I: Post-Combustion CO₂ capture testing methodology. *Energy Procedia*, 63, pp.5938–5958. Available at: <http://linkinghub.elsevier.com/retrieve/pii/S187661021402445X>.
- UK Government, 2008. *Climate Change Act 2008 - Chapter 27*,
- Vaccarelli, M., Carapellucci, R. & Giordano, L., 2014. Energy and economic analysis of the CO₂ capture from flue gas of combined cycle power plants. *Energy Procedia*, 45, pp.1165–1174. Available at: <http://dx.doi.org/10.1016/j.egypro.2014.01.122>.
- Veneman, R. et al., 2012. Continuous CO₂ capture in a circulating fluidized bed using supported amine sorbents. *Chemical Engineering Journal*, 207–208, pp.18–26.
- Voleno, A. et al., 2014. Post-combustion CO₂ capture from natural gas combined cycles by solvent supported membranes. *Energy Procedia*, 63, pp.7389–7397. Available at: <http://dx.doi.org/10.1016/j.egypro.2014.11.775>.

- Walsh, P.P. & Fletcher, P., 2004. *Gas Turbine Performance* 2nd Ed., John Wiley & Sons.
- Walters, M.S. et al., 2016. Control Relevant Model of Amine Scrubbing for CO₂ Capture from Power Plants.
- Wijmans, J.G., Merkel, T.C., Baker, R.W., et al., 2012a. Power generation process with partial recycle of carbon dioxide. *US Patent 8220247B2*, 2(12).
- Wijmans, J.G., Merkel, T.C., Baker, R.W., et al., 2012b. Power Generation process with partial recycle of carbon dioxide. *US Patent 8220248B2*.
- Wijmans, J.G., Merkel, T.C. & Baker, R.W., 2012. Gas separation process using membranes with permeate sweep to remove CO₂ from gaseous fuel combustion exhaust. *US Patent 8177885B2*.
- Wijmans, J.G., Merkel, T.C. & Baker, R.W., 2011. Process for separating Carbon Dioxide from flue gas using parallel carbon dioxide capture and sweep-based membrane separation steps. *US Patent 80257515B2*.
- Xiao, P. et al., 2008. Capture of CO₂ from flue gas streams with zeolite 13X by vacuum-pressure swing adsorption. *Adsorption*, 14, pp.575–582. Available at: <http://link.springer.com/10.1007/s10450-008-9128-7>.
- Xu, D. et al., 2013. Effects of water vapour on CO₂ capture with vacuum swing adsorption using activated carbon. *Chemical Engineering Journal*, 230, pp.64–72. Available at: <http://www.sciencedirect.com/science/article/pii/S1385894713008619>.
- Yamauchi, H. et al., 2007. Performance of VOC abatement by thermal swing honeycomb rotor adsorbers. *Industrial and Engineering Chemistry Research*, 46(12), pp.4316–4322.
- Zhai, H. & Rubin, E.S., 2010. Performance and cost of wet and dry cooling systems for pulverized coal power plants with and without carbon capture and storage. *Energy Policy*, 38, pp.5653–5660.
- Zhai, H., Rubin, E.S. & Versteeg, P.L., 2011. Water use at pulverized coal power plants with postcombustion carbon capture and storage. *Environmental science & technology*, 45, pp.2479–2485.
- Zhang, Y. et al., 2016. Absorber modeling for NGCC carbon capture with aqueous piperazine. *The Royal Society of Chemistry. faraday Discussion*.

Technical data of the Reference Power Plant.

Appendix A contains the technical data of the reference case with an air-based combustion CCGT power plant with post-combustion capture considered in this thesis to perform the work presented in Chapter 4 and Chapter 5. Technical data are based on the EBTF common framework document (EBTF 2011) and the International Energy Agency report of 2012 (IEA 2012).

A.1. Ambient conditions

Table A.1.- Ambient conditions

Pressure (ISO)	kPa	101.325
Temperature (ISO)	°C	15
Relative humidity, ϕ	%	60
<i>Composition, dry molar fraction (%)</i>		
N ₂	% vol	78.08
CO ₂	% vol	0.03
H ₂ O	% vol	0.00
Ar	% vol	0.94
O ₂	% vol	20.95
Molar Mass	g/mol	28.86

A.2. Natural gas

Table A.2.- Natural gas supply specifications

Fuel type	Natural Gas	
Supply temperature	°C	10
Supply pressure	MPa	7
<i>Composition, molar fraction (%)</i>		
CH ₄	% vol	89
C ₂ H ₆	% vol	7
C ₃ H ₈	% vol	1
C ₄ H ₁₀	% vol	0.11
N ₂	% vol	0.89
CO ₂	% vol	2
S	ppm	<5
Molar mass	g/mol	17.84
CO ₂ emissions	g/kWh LHV	208.00
<i>Heating values</i>		
Low heat value (LHV)		
@ 25 °C	MJ/kg	46.94
High heat value (HHV)		
@ 25 °C	MJ/kg	51.58

A.3 Technical parameters for the combined cycle gas turbine power plant

Table A.3.- Technical parameters for the steam cycle of the CCGT plant

<i>Heat recovery steam generator parameters</i>		
HRSG efficiency	%	99.7
<i>Temperature differences</i>		
ΔT approach main steam	$^{\circ}\text{C}$	42
ΔT approach hot reheated steam	$^{\circ}\text{C}$	34
ΔT pinch gas boiling - liquid in evaporator	$^{\circ}\text{C}$	10
ΔT subcooling economiser	$^{\circ}\text{C}$	3
<i>Pressure losses</i>		
ΔP gas side	kPa	2.6
ΔP HP SH	%	3.5
ΔP HP ECO	%	2.6
ΔP IP RH	%	3
ΔP IP SH	%	2
ΔP IP ECO	%	3
ΔP LP SH	%	2
ΔP LP ECO	%	1.3
ΔP system - LIVE STEAM	%	9
ΔP system - COLD RH	%	7
ΔP system- HOT RH	%	9
ΔP system - LP STEAM	%	9
<i>Temperature losses</i>		
From superheater / reheater to turbine (approximately 0.5 K)	kJ/kg	1
<i>Condenser</i>		
P condenser	kPa	4.814
Saturation temperature	$^{\circ}\text{C}$	32.20
Temperature pinch	$^{\circ}\text{C}$	3.2
Feed water temperature (after feed water pump)	$^{\circ}\text{C}$	32.2
Cooling water supply (CWS) temperature	$^{\circ}\text{C}$	18
Cooling water return (CWR) temperature	$^{\circ}\text{C}$	29
Condenser duty	MW	224.3
Power to thermal duty (Electric consumption for heat rejection of rejected thermal power)	%	0.8
<i>Feed water pumps</i>		
Pump efficiency	%	70
Generator efficiency	%	98.5

Table A.4.- Technical parameters for the steam cycle of the CCGT plant (cont.)

<i>Steam turbines</i>		
<i>HP STEAM TURBINE</i>		
Pressure inlet	bar	170
Inlet temperature	°C	600
Isentropic efficiency	%	88.15%
<i>IP STEAM TURBINE</i>		
Inlet Pressure	bar	40
Inlet Temperature	°C	600
Isentropic efficiency	%	92.40%
<i>LP STEAM TURBINE</i>		
Inlet Pressure	bar	3.75
Inlet Temperature	°C	266.93
Isentropic efficiency	%	88.00%
<i>Fuel heater</i>		
Fuel Inlet Temperature	°C	9.00
Fuel Outlet Temperature	°C	117.00
IP water inlet temperature	°C	252.85
Temperature pinch	°C	26.98
<i>Efficiency calculations</i>		
Mechanical efficiency	%	99.6
Generator efficiency	%	98.5

A.4 Technical parameters for the capture plant

Table A.4.- Technical parameters for the CO₂ capture plant and compression train

<i>Flue gas conditioning system</i>		
Booster fan pressure ratio	bar	0.1
Booster fan isentropic efficiency	%	85
Booster fan mechanical efficiency	%	95
Direct contact cooler flue gas outlet temperature	°C	45
Direct contact cooler + rotary heat exchanger pressure drop	bar	0.05
<i>Absorber</i>		
Solvent		MEA
Concentration	% wt.	30
Lean solvent temperature	°C	40
Flue gas inlet temperature	°C	45
Flue gas temperature water wash outlet	°C	45
Absorber column pressure	bar	1.1
Flooding factor	%	80
Packing		Mellapak 250 Y
Absorber column pressure drop	mbar	50
<i>Lean/rich heat exchanger</i>		
Lean/rich heat exchanger DT min	°C	8
Lean/rich stream heat exchanger pressure drop	kPa	20
Rich pump outlet pressure	bar	
<i>Stripper</i>		
Stripper column pressure drop	mbar	300
Stripper column number of stages	--	8
Flooding factor	%	80
<i>Reboiler</i>		
Reboiler pressure / saturated	bar	3
Saturated steam inlet temperature	°C	133
Lean solvent outlet temperature	°C	120
Pinch temperature	°C	13
<i>Lean/ Rich solvent pumps</i>		
Pumps hydraulic efficiency	%	75
Pumps driver efficiency	%	95
<i>CO₂ compression plant</i>		
Final delivery pressure	bar	110
CO ₂ purity	%	99.8
Compression stages pressure ratios	--	4.3 / 4.3 / 3.7
Compressor isentropic efficiency	%	85
Compressor mechanical efficiency	%	95
Intercooler stages	--	3
Intercoolers outlet temperature	°C	28
Pump efficiency	%	75
Pump delivery pressure	bar	110

Process Flow Diagrams

Appendix B presents the process flow diagrams of the configuration consisting of a Combined Cycle Gas Turbine Power Plant equipped with post-combustion carbon capture systems.

Figure B.1- Process flow diagram for an air-based combustion Combined Cycle Gas Turbine plant with Post-combustion CO₂ Capture.

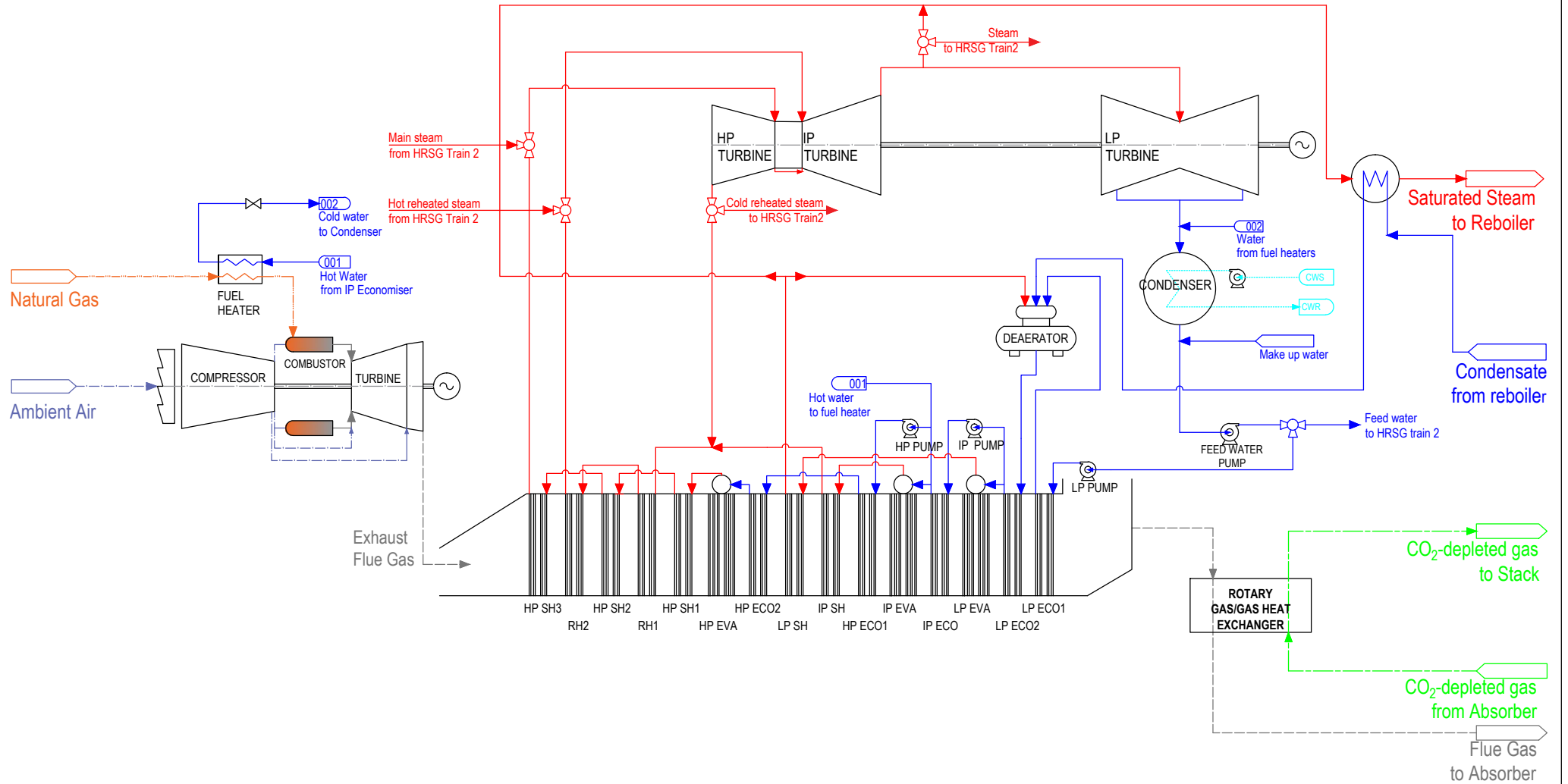
Figure B.2- Process flow diagram for a Combined Cycle Gas Turbine plant with Exhaust Gas Recirculation and Post-combustion CO₂ Capture.

Figure B.3- Process flow diagram for a Combined Cycle Gas Turbine power plant with Selective Exhaust Gas Recirculation in parallel to the Post-combustion CO₂ Capture process.

Figure B.4- Process flow diagram for a Combined Cycle Gas Turbine power plant with Selective Exhaust Gas Recirculation in series to the Post-combustion CO₂ Capture process.


Figure B.5- Process flow diagram for the post-combustion CO₂ capture plant with aqueous monoethanolamine scrubbing technology and the CO₂ compression train.

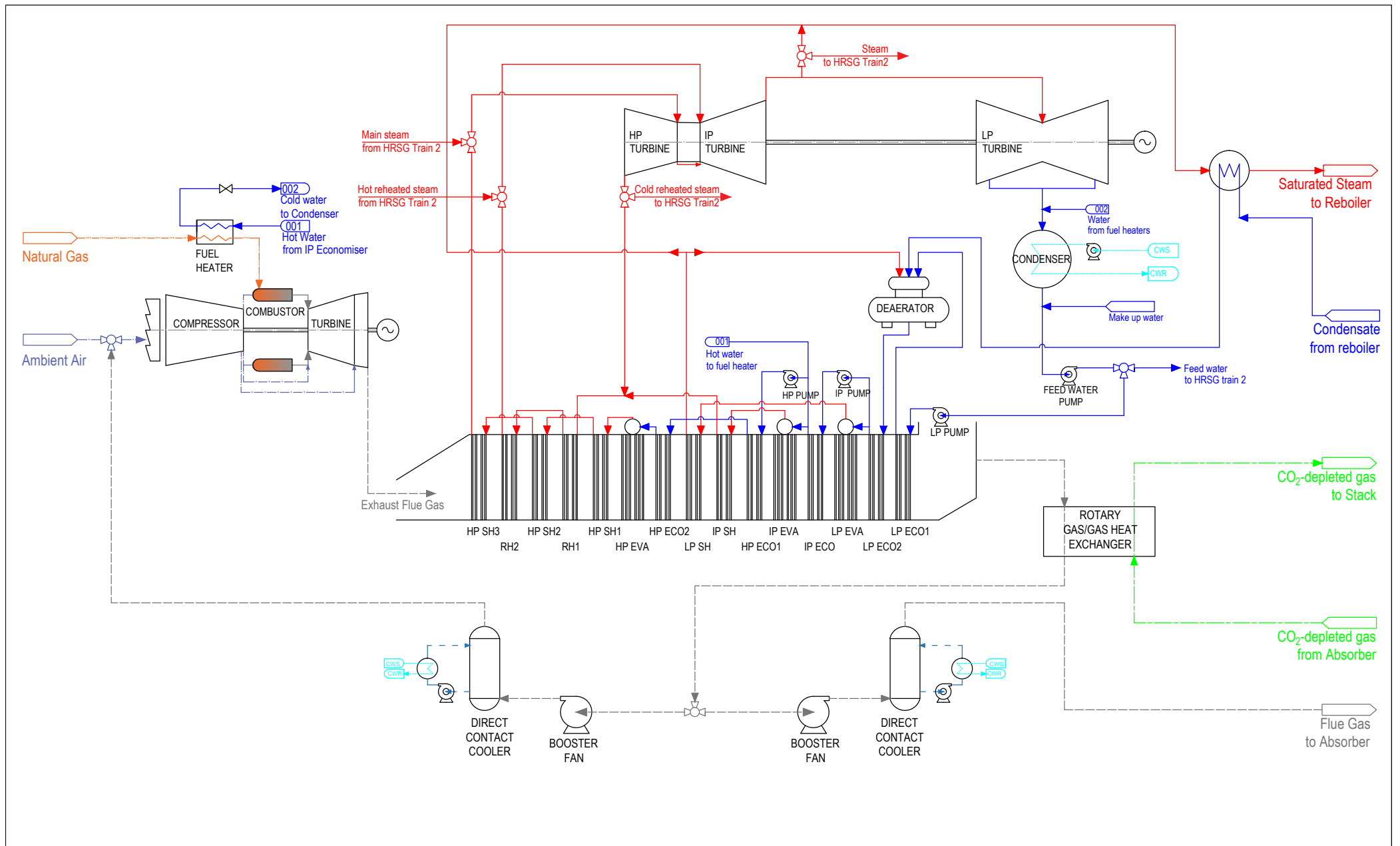
Figure B.6- Block diagram for process model simulations: gPROMS and Aspen Plus linked model.



LEGEND:


--- Ambient Air	— Water (steam cycle)
--- Flue Gas	— Steam (steam cycle)
--- CO ₂ -depleted flue gas	--- Process water
--- Fuel / Natural Gas	--- Cooling water

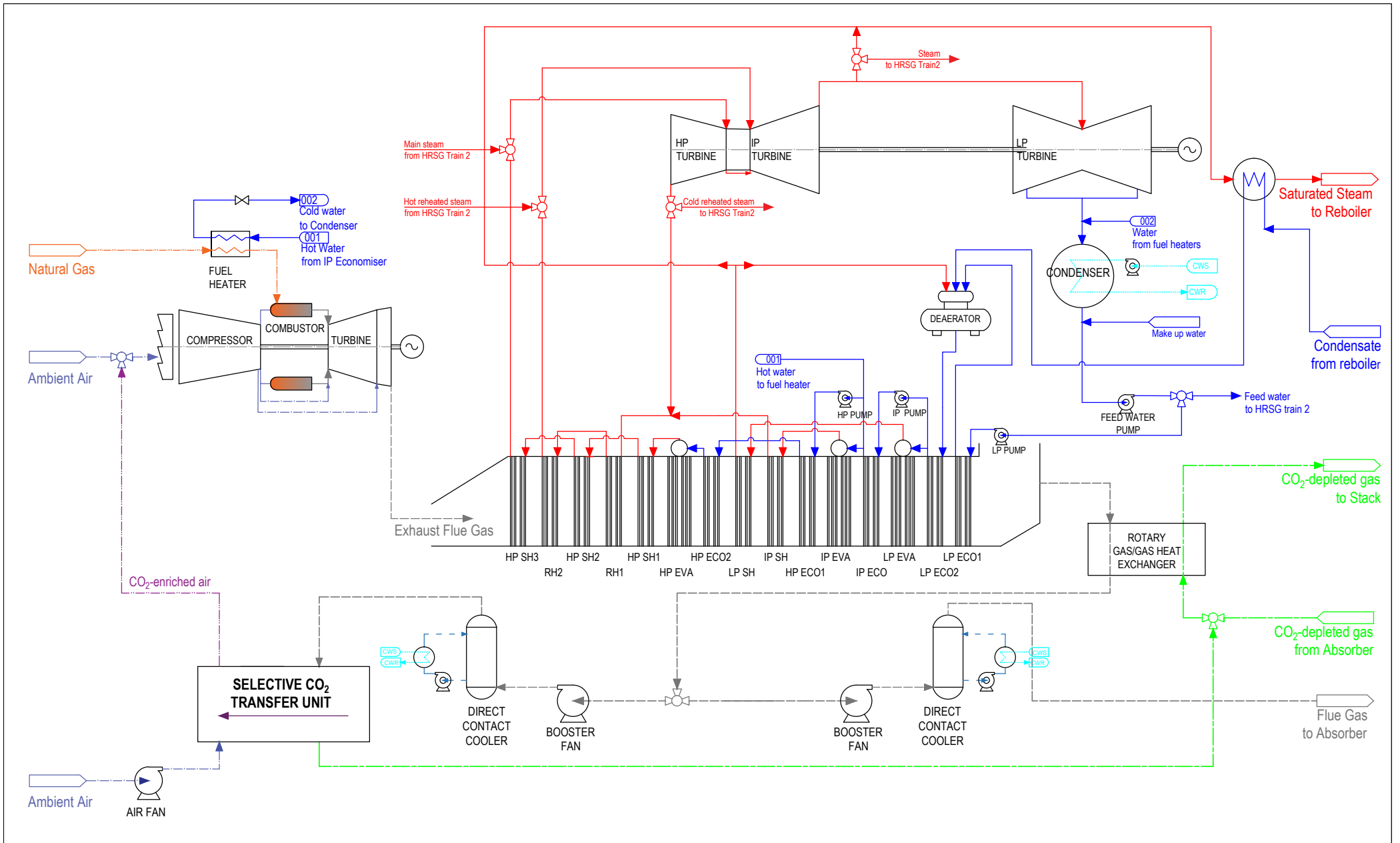
 THE UNIVERSITY of EDINBURGH	Process Flow Diagram CCGT plant with CO ₂ CAPTURE	
	Drawn by: Laura Herraiz	Date: 1/05/2016
	Reviewed by: E. Sánchez Fernández	Date: 1/05/2016
	University of Edinburgh	Revision: 1



LEGEND:


- Ambient Air
- Water (steam cycle)
- Flue Gas
- Steam (steam cycle)
- CO₂-depleted flue gas
- Process water
- Fuel / Natural Gas
- Cooling water

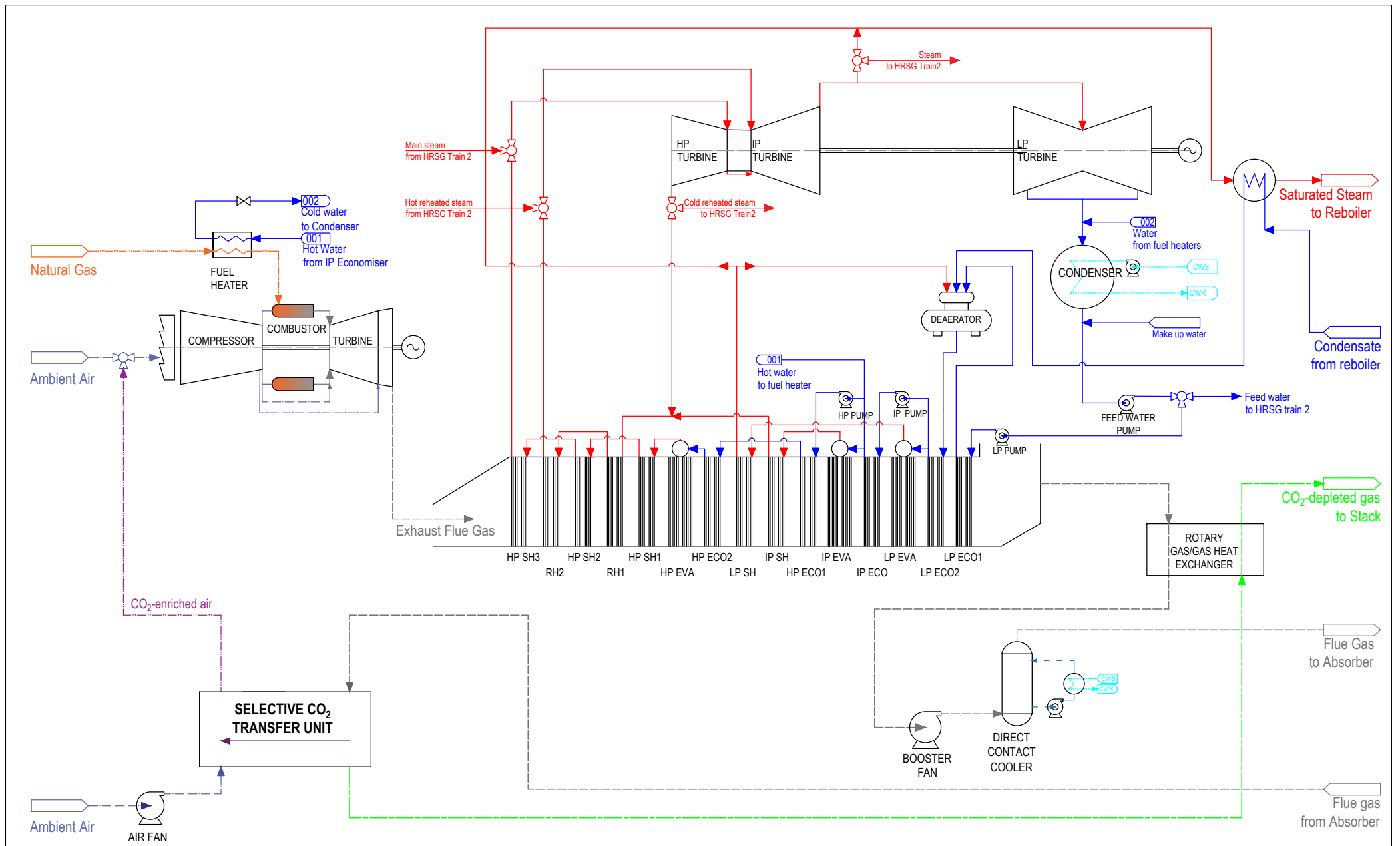
 THE UNIVERSITY OF EDINBURGH		Process Flow Diagram CCGT plant with CO ₂ CAPTURE and EGR	
Drawn by: Laura Herraiz		Date: 1/05/2016	
Reviewed by: E. Sánchez Fernández		Date: 1/05/2016	
University of Edinburgh		Revision: 1	



LEGEND:

— Ambient Air	— Water (steam cycle)
- - - CO ₂ -enriched air	— Steam (steam cycle)
- - - Flue Gas	- - - Process water
- - - CO ₂ -depleted flue gas	- - - Cooling water
- - - Fuel / Natural Gas	

 THE UNIVERSITY OF EDINBURGH	Process Flow Diagram CCGT with CO ₂ CAPTURE and S-EGR Parallel	
	Drawn by: Laura Herraiz	Date: 1/05/2016
	Reviewed by: E. Sánchez Fernández	Date: 1/05/2016
	University of Edinburgh	Revision: 1



LEGEND:

- Ambient Air
- - - CO₂-enriched air
- - - Flue Gas
- - - CO₂-depleted flue gas
- - - Fuel / Natural Gas
- Water (steam cycle)
- Steam (steam cycle)
- - - Process water
- - - Cooling water

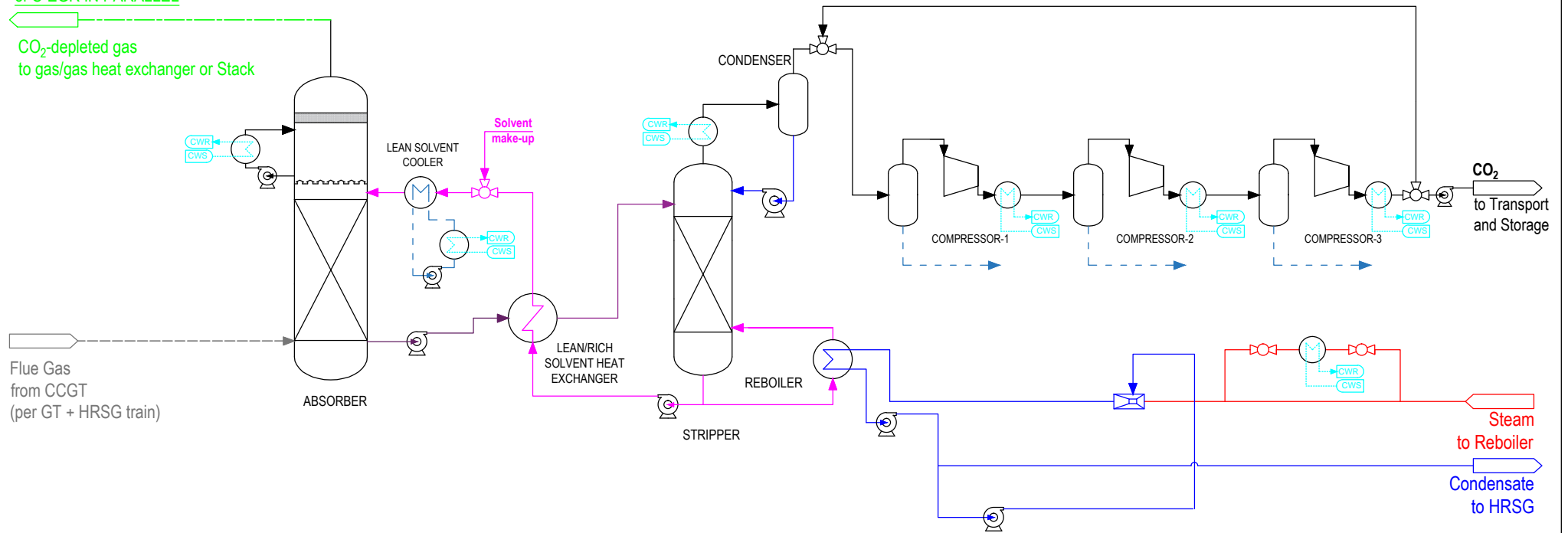
THE UNIVERSITY OF EDINBURGH		Process Flow Diagram CCGT with CO₂ CAPTURE and S-EGR Series	
Drawn by: Laura Herraiz		Date: 1/05/2016	
Reviewed by: E. Sánchez Fernández		Date: 1/05/2016	
University of Edinburgh		Revision: 1	

Configuration: S-EGR IN SERIES

Flue gas
to selective CO₂ transfer device

Configuration: air-based combustion, EGR
or S-EGR IN PARALLEL

CO₂-depleted gas
to gas/gas heat exchanger or Stack



LEGEND:


- Flue Gas
- CO₂-depleted flue gas
- CO₂
- Rich solvent
- Lean solvent
- Water (steam cycle)
- Steam (steam cycle)
- Process water
- Cooling water

AIR-COMBUSTION (1 PCC UNIT per GT-HRSG train with 2 absorbers)

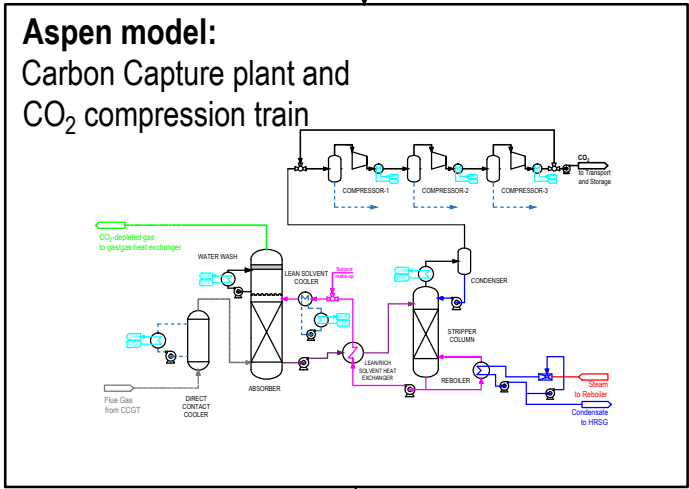
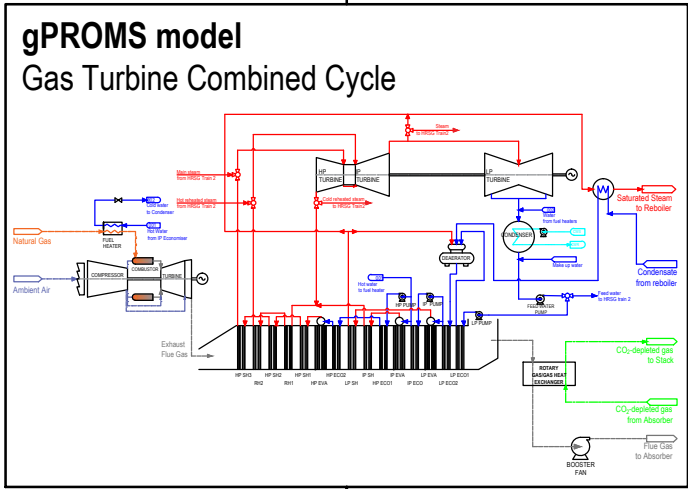
EGR (1 PCC UNIT per GT-HRSG train with 1 absorber)

S-EGR IN PARALLEL (1 PCC UNIT per GT-HRSG train with 1 absorber)

S-EGR IN SERIES (1 PCC UNIT per GT-HRSG train with 2 absorbers)

 THE UNIVERSITY of EDINBURGH	Process Flow Diagram POST-COMBUSTION CO ₂ CAPTURE PLANT	
	Drawn by: Laura Herraiz	Date: 1/05/2016
Reviewed by: E. Sánchez Fernández	Date: 1/05/2016	
University of Edinburgh	Revision: 1	

Flue gas stream
 - Composition
 - Flow rate
 - Temperature
 - Pressure



<u>CO₂-depleted gas stream</u> - Composition - Flow rate - Temperature - Pressure	<u>Superheated low pressure steam</u> - Flow rate - Pressure - Temperature	<u>Cooling water</u> - Cooling duty - Flow rate
--	---	---

Power
 - Compression work
 - Auxiliary power consumption (solvent pumps, booster fan)

CCGT power plant with CO₂ capture systems
 - Net power output
 - Net thermal efficiency

Technical data for the reference CCGT plant for water management assessment

Appendix C contains the technical and operation data and stream variables of the CCGT power plant with PCC with and without EGR, as well as the main assumption considered to perform the heat and water management technical assessment in Chapter 6.

C.1. Reference natural gas combined cycle power plant

The reference plant is an 800 MWe air-fired natural gas combined cycle (NGCC) with a 2-on-1 configuration: two GE937IFB gas turbines with the flue gas exiting into two HRSGs, which jointly supply steam to a subcritical triple pressure steam cycle. The gas turbine operates at a turbine inlet temperature (TIT) of 1371 °C and air fuel ratio (AFR) of 40.5 on mass basis, at ISO atmospheric conditions and 100% load, with a power output at coupling of 285 MWe. In a combined cycle, the remaining heat contained in the exhaust flue gas is partially recovered to generate steam at three pressure levels. In this work, the flue gas is assumed to leave the HRSG at a temperature of 86 °C (IEA 2012) Two post-combustion capture units with primary amine-base solvent technology are implemented at the tail-end, one per each gas turbine - HRSG train. In each train, flue gas is cooled down before entering the absorber. The gas composition at the outlet is then calculated assuming a removal ratio of CO₂ of 90% and that gas leaves the water wash section saturated at a temperature of 45°C. Stream variables are shown in Table C.1 and Table C.2 for a single gas turbine – heat recovery steam generator – absorber unit train. The electricity output penalty of capture and compression in the air-fired CCGT and the CCGT with EGR is not considered in the scope of this work.

Table C.1.- Exhaust flue gas stream information at HRSG outlet at different recirculation ratios (per GT-HSRG-absorber train).

EGR ratio		0	10	20	30	40
Temperature	°C	86	86	86	86	86
Pressure (HRSG outlet)	kPa	101.3	101.3	101.3	101.3	101.3
Dew Temperature (HRSG outlet)	°C	43.6	45.3	46.8	48.2	49.6
Pressure (fan outlet)	kPa	111.3	111.3	111.3	111.3	111.3
Dew Temperature (fan outlet)	°C	45.4	47.1	48.6	50.1	51.4
Mass flow rate	kg/s	670	662	655	648	643
Molar flow rate	mol/s	2353	2329	2305	2284	2263
Molar mass	g/mol	28.48	28.44	28.41	28.39	28.4
<i>Composition</i>						
CO ₂	% vol	4.15%	4.62%	5.21%	5.97%	6.99%
H ₂ O	% vol	8.79%	9.57%	10.35%	11.12%	11.89%
N ₂	% vol	74.26%	74.00%	73.82%	73.78%	73.93%
O ₂	% vol	11.90%	10.92%	9.74%	8.25%	6.30%
Ar	% vol	0.89%	0.89%	0.88%	0.88%	0.89%

Table C.2.- CO₂-depleted gas stream information at absorber outlet, at different recirculation ratios (per GT-HSRG- absorber train).

EGR ratio		0	10	20	30	40
Temperature	°C	45	45	45	45	45
Pressure	kPa	106.3	106.3	106.3	106.3	106.3
Mass flow rate	kg/s	633	556	482	410	340.
Molar flow rate	mol/s	2264	1990	1726	1471	1225
Molar mass	g/mol	27.97	27.94	27.9	27.85	27.79
<i>Composition</i>						
CO ₂	% vol	0.43%	0.48%	0.55%	0.65%	0.77%
H ₂ O	% vol	9.52%	9.56%	9.62%	9.70%	9.80%
N ₂	% vol	76.82%	77.57%	78.53%	79.78%	81.51%
O ₂	% vol	12.31%	11.45%	10.36%	8.92%	6.94%
Ar	% vol	0.92%	0.93%	0.94%	0.96%	0.98%

C.2. Assumptions

Table C.3.- Assumptions

AMBIENT AIR ISO CONDITIONS		
Temperature	°C	15
Pressure	bar	1.013
Relative humidity	%	60
DIRECT CONTACT COOLER		
Approach temperature between ambient wet bulb temperature and cooling water supply (IEA 2012)	°C	7
Cooling water supply temperature	°C	15
DCC Bottom temperature differential with air cooling (IEA 2012)	°C	46
DCC Bottom temperature differential with EGR	°C	23
DCC Cooler temperature pinch (IEA 2012)	°C	7
Cooling water temperature rise (IEA 2012)	°C	10
PUMPS		
Efficiency (EBTF 2011)	%	75
Process water pump head (Huizeling and Van der Weijde 2010, EBTF 2011)	m	57
Cooling water pump head (Huizeling and Van der Weijde 2010, EBTF 2011)	m	26
Pump electric power to cooling duty ratio	%	0.8
FANS		
Efficiency	%	85
PRESSURE DROP		
Absorber pressure drop (IEA 2012, Sanchez Fernandez et al 2014)	kPa	5
Ducts pressure drop	kPa	2.5
Direct contact cooler pressure drop (IEA 2012, Sanchez Fernandez et al 2014)	kPa	3
ROTARY HEAT EXCHANGERS (Howden 2008)		
Rotational speed	rpm	0.75 - 1
Element metal thickness	mm	0.75
Enamel total thickness	mm	0.3